Simulating Electronically Nonadiabatic Dynamics via the Generalized Quantum Master Equation

by

Ellen Mulvihill

A dissertation submitted in partial fulfillment
of the requirements for the degree of
Doctor of Philosophy
(Chemistry and Scientific Computing)
in The University of Michigan
2021

Doctoral Committee:

Professor Eitan Geva, Chair
Professor Kevin Kubarych
Professor Jennifer Ogilvie
Associate Professor Dominika Zgid

Ellen Mulvihill
emulvi@umich.edu
ORCID iD: 0000-0002-4233-2869

DEDICATION

To my family, for their love and support.

ACKNOWLEDGMENTS

This dissertation would not be possible without the help of many people. First and foremost, I would like to thank my advisor Eitan Geva for all of his support throughout my degree. His mentorship has been invaluable throughout my time at Michigan, allowing me the independence in pursuing my research to help me grow as a scientist and providing help when I inevitably needed it. His support in both my academic and career pursuits has helped me to better understand my goals and to work towards them. Pursuing a PhD is a long and difficult process, with times where research can come relatively easily to times where getting results seems impossible and I don't think I can thank Eitan enough for helping to make this process as smooth and happy as possible. I would also like to thank my committee, Dominika Zgid, Kevin Kubarych, and Jennifer Ogilvie, who have provided helpful insight into projects and career advice along with many interesting conversations about their research which has been inspiring for my own.

I would like to thank my labmates both past and present: Alex Schubert, Xiang Sun, Kyle Williams, Yifan Lai, Kristina Lenn, Xing Gao, Yudan Liu, and Max Saller. Much of this work would not have been possible without Alex's help with understanding and exploring the GQME when I first started graduate school. Xiang was an important part of the Ehrenfest work along with helping me to learn how to program algorithms from scratch. I worked with Kyle on the Compute-to-Learn chemistry education project, where he laid a lot of the foundation. I have enjoyed working with Yifan, who is only one year younger in the program so we've overlapped for several years, on the Compute-to-Learn chemistry education project along with the many helpful and interesting conversations about research over the past few years. I've worked with Kristina on expanding the Ehrenfest with GQME project to multi-state systems, which has been

critical for moving beyond simple systems. Xing has been a lot of help with understanding the QC/MH methods and the FMO system. Yudan has always been a happy and hardworking presence in the lab and I've enjoyed working with her on various projects while she was visiting as an undergraduate and now as a graduate student in the group. Though our overlapping time has been brief, Max has been a huge help with understanding some of the more advanced QC/MH methods along with providing invaluable help on my defense presentation.

I would like to thank my friends, who have provided support and a break from chemistry when I needed it. This includes my friends in the pchem cluster with whom I have spent many late nights working on problem sets or celebrating our progress in chemistry. To the friends I have made through CGSC and GSSPC, who I am fortunate to have met within the department. For the many friends I have made in the computational chemistry room whose conversations have been all the more missed recently, including my cubiclemates Alan Chien and Hanjie Jiang, who have gone down many internet rabbit holes when we got sidetracked from work. For Janelle Kirsch, Brandon Lee, and Sahil Chhabra, for their equal willingness to play every intramural under the sun. To Lindsay Michocki, Mark Mantell, and Audrey Tolbert, whose friendship since the beginning of our PhD journey has provided much support and happiness throughout. To Blair Winograd, who I have been fortunate to have worked on several projects with and whose friendship and understanding I am so thankful to have. To Michael and Allison Roessler, with whom I have literally expanded my understanding of the world through our exploration of Ann Arbor, Michigan, Chicago, and Europe and whose friendship has been invaluable in this stage of my life and I'm sure will continue to be throughout the rest of my life. Allison has been a constant friend throughout our time at Michigan to the point where we were often mistaken for each other and I will miss being only a cubicle wall away from her most days but am forever grateful to have made a lifelong friendship as wonderful as hers. To my friends from Glen Ellyn and Chicago, particularly Ashley Stone, Erin Loftus, Caitlyn Chomyok, Charlotte Caffrey, Emily Becker, Dayle Comerford, and Kim Albrecht, whose entertaining and supportive messages have provided helpful diversions from chemistry and a forum to vent any frustrations.

To my extended family, who has always been supportive and curious about my research, even when I definitely did not understand it well enough to make sense in explaining what I was doing. And to my immediate family, whose love and support throughout my life has made it possible for me to complete this dissertation. To my mom, for her unwavering belief in my abilities, helping me to appreciate the beauty in everything, and showing me the importance of kindness. To my sister Ruth, who has listened to my many ramblings, answered my many questions from the serious to the very random, and has long been the person whose support I turned to when I needed it most. To my brother Daniel, whose creativity has inspired me to think in different ways and whose humor has helped me to laugh especially in times when I needed it most. And to my dad, who taught me algebra on napkins, inspiring my pursuit of math and science; encouraged and pushed me to strive toward my interests; and who I know continues to watch over me.

TABLE OF CONTENTS

LIST OF FIGURES

LIST OF TABLES

LIST OF APPENDICES

ABSTRACT

One of the greatest challenges facing computational chemistry is the simulation of electronically nonadiabatic dynamics. While there are several reduced dynamics methods for doing so, they often rely on restrictive assumptions such as weak coupling between the electronic and nuclear degrees of freedom (DOF) or between electronic states. An alternative approach for simulating nonadiabatic dynamics is via mixed quantum-classical (MQC) and quasiclassical (QC) methods which can handle strong coupling but their reliability and computational feasibility decrease with increasing simulation time. In comparison, the generalized quantum master equation (GQME) requires no approximation in its derivation and scales favorably with increasing simulation time.

In the first chapter of this dissertation, two previous approaches to the GQME will be examined and a modified approach to the GQME (M-GQME) will be introduced. The two previous approaches are reliant on splitting the Hamiltonian into system, bath, and system-bath coupling terms which is neither natural nor convenient for simulating nonadiabatic dynamics. In comparison, the M-GQME is optimized for simulating nonadiabatic dynamics. Within the M-GQME, new protocols will be introduced for calculating the memory kernel via different MQC and QC methods. Through the application of the M-GQME to a spin-boson model with the memory kernel obtained via the Ehrenfest method, it will be shown that the M-GQME is more stable and robust compared to the previous approaches and that limiting the use of Ehrenfest to calculating the memory kernel enhances its accuracy in comparison to using it to directly simulate the system's dynamics.

In the second chapter, two mapping Hamiltonian (MH) approaches with a QC approximation will be outlined and utilized to calculate the memory kernel of the M-GQME. These QC/MH methods have several advantages over the Ehrenfest method, including describing both the electronic and nuclear degrees of freedom as classical-like quantities and the ability to have non-Hermitian initial electronic states. By combining the QC/MH methods with the M-GQME on the spin-boson model, it will be shown that the M-GQME with the QC/MH methods outperforms both the M-GQME with Ehrenfest and the direct application of the QC/MH methods.

In the third chapter, forty-four different methods for obtaining the memory kernel of the GQME are systematically explained and explored, including the three approaches previously discussed. The ability to calculate the memory kernel of the GQME is relatively new and a thorough examination of the different ways of obtaining the memory kernel has not been done. Through the study of these many approaches on the spin-boson model, the impact of the different approaches will be described and the benefits of the M-GQME compared to other approaches further solidified.

In the fourth and fifth chapters, the M-GQME will be applied to models of the Fenna-Matthews-Olson (FMO) complex, a photosynthetic system, and the 2,6,-bis(methylene) adamantyl (BMA) radical cation, which contains a conical intersection. These two systems represent areas of considerable interest, given the prevalence of photosynthesis and conical intersections in biologically- and technologically-relevant systems. As will be shown, the success of the M-GQME with FMO and preliminary failure with BMA illuminates future areas where the M-GQME is expected to succeed along with the limitations of its application.

CHAPTER I

Introduction

I.1 Motivation and Methods for Simulating Electronically Nonadiabatic Dynamics

Broadly defined, chemical dynamics is the study of processes that involve mass, charge, and energy transfer in molecular systems. Such processes can be reactive (i.e., involving breaking and forming chemical bonds) or non-reactive (e.g., charge and energy transfer). Examples include vibrational and electronic relaxation and oxidation-reduction reactions which are pertinent to many technologically- and biologically-relevant processes, such as photovoltaics and photosynthesis. Quantum dynamical effects often play a central role in these important processes, including when they take place in the condensed phase.[1–3] As a result, the simulation of quantum dynamics in condensed-phase systems remains one of the most important challenges facing computational chemistry. In principle, quantum dynamics in such systems can be simulated by numerically solving the Schrödinger equation. However, the exponential scaling of the computational cost with system dimensionality makes the numerically exact simulation of quantum dynamics in complex molecular systems non-feasible, with the important exception of a subclass of model Hamiltonians whose form makes such an exact simulation possible.[4–10] Because of this, many methods involving approximations have been proposed to simulate quantum dynamics in the condensed phase.

Nonadiabatic molecular dynamics corresponds to an important class of inherently quantum-mechanical dynamical processes. Commonly-used approaches for modeling the nonadiabatic

molecular dynamics are based on Marcus theory,[1,11] Fermi's golden rule (FGR),[1,12–18] or the Redfield quantum master equation.[1,19–25] However, these approaches are based on multiple restrictive assumptions (see Table I.1). In particular, these approaches are perturbative in nature and assume weak coupling between the electronic and nuclear degrees of freedom (DOF) or between electronic states. An alternative approach for simulating nonadiabatic dynamics is via mixed quantum-classical (MQC) and quasiclassical (QC) methods. These methods can handle strong coupling but their reliability and computational feasibility decrease with increasing simulation time.

In this dissertation, an approach for simulating nonadiabatic molecular dynamics is pursued that is based on the generalized quantum master equation (GQME). Importantly, the GQME describes the quantum-mechanically exact dynamics of the electronic DOF and as such is not subject to the restrictive assumptions underlying the above-mentioned perturbative methods. The GQME is arguably the most general framework for simulating electronically nonadiabatic reduced dynamics, as it requires no approximations in its derivation and has the ability to capture the full electronic density matrix.[26–35] Within the GQME, the memory kernel is the key quantity, as it both gives the correlation between molecular structure and electronic dynamics and is the most difficult quantity to calculate. The memory kernel can be calculated from projection-free inputs[28] obtained via MQC and QC methods, which are known to become inaccurate and/or expensive with increasing simulation time. The memory kernel is often short-lived in comparison to the lifetime of the system, allowing one to restrict the dynamical input to short times. Thus, restricting the use of MQC and QC methods to calculating the short-lived memory kernel is an important advantage of the GQME. For example, the Ehrenfest method[36] is feasible for complex systems but known to become increasingly inaccurate with increasing simulation time. Thus, restricting its use to a short-time learning period circumvents the need to address its inaccuracy at longer times. Another example is the mixed quantum-classical Liouville method,[37–43] which is a robust and accurate mixed quantum-classical method whose computational cost rapidly increases with increasing simulation time. Once again, restricting its use to a short-time learning period needed for calculating the memory kernel allows one to extend the applicability of the mixed quantum-classical Liouville

method to arbitrarily long times.

	Marcus	equilibrium FGR	nonequilibrium FGR	Redfield	GQME
Quantum nuclear effects	-	+	+	+	+
Dynamical nuclear effects	-	+	+	+	+
Non-Condon effects	-	+	+	+	+
Non-Gaussian statistics	-	+	+	+	+
Nonequilibrium initial state	-	-	+	+	+
Coherence dynamics	-	-	-	+	+
Non-perturbative	-	-	-	-	+

Table I.1: Hierarchy of Reduced Dynamics Methods

Direct application of GQME approaches is relatively new, with the first method introduced in 2003[28] and much of the further expansion and study occurring within the last five years.[32,35,44–46] As such, deeper understanding of the approaches and the aspects that lead to better results is yet to be fully determined. An in-depth review of the various GQME approaches would help with determining the optimal approach to use in different applications along with identifying features of the system and approaches that are most impactful. Since the GQME approaches can also be used with a variety of input methods, creating a framework that can be used with one's choice of input MQC or QC method is essential, as different methods offer either greater efficiency or greater applicability and the choice of method depends on the system being tested.

It is also important for the GQME framework, with all of its options, to be extendable to any application involving complex molecular systems. Being able to do so will allow for direct insight into the molecular picture underlying electronically nonadiabatic dynamics, to suggest ways for improving the efficiency of systems and technologies based on nonadiabatic dynamics.

The GQME-based methodology fills a gap which is not addressed by currently available methods for simulating electronically nonadiabatic dynamics. Methods based on FGR or the Redfield equation require assuming weak electronic coupling between electronic states or electronic and nuclear DOF while direct application of MQC and QC methods that can handle strong coupling often have decreasing reliability and/or computational feasibility with increasing simulation time. The GQME-based methodology allows one to restrict the dynamical input to short times while providing a unified framework that can describe a wide range of coupling strengths. As such,

it capitalizes on the advantages of both alternative approaches without suffering from the corresponding disadvantages.

I.2 Wave Function v. Density Operator Formalisms

Many formulations of quantum dynamics, including the Schrödinger equation, describe the state of a system using a time-dependent wave function $\Psi(r,t)$. However, wave functions can only describe the state of isolated, or "closed," quantum systems. A different description of the quantum state is needed when dealing with an open system that constitutes a subsystem of an extended quantum systems. The density operator offers this necessary flexibility, as it is able to describe the state of both open and closed quantum systems.

While wave functions represent ket vectors, $|\Psi(t)\rangle$, in Hilbert space, the density operator is represented by a matrix in the same space. Generally speaking, the density operator is given by $\hat{\rho}(t) = \sum_k p_k(t)|\psi_k(t)\rangle\langle\psi_k(t)|$, where $\{p_k(t)\}$ are real, non-negative numbers that satisfy $\sum_k p_k(t) = 1$ and $\{|\psi_k(t)\rangle\}$ are kets in the Hilbert space of the system. The case where the sum has only one term corresponds to a pure state while the case where it has two or more terms corresponds to a mixed state. The density operator has several important properties, including that it is Hermitian [i.e., $\hat{\rho}(t) = \hat{\rho}^\dagger(t)$]; the diagonal elements of the density matrix are non-negative and have a trace of 1; the trace of the density operator squared is bound by $\mathrm{Tr}\{\hat{\rho}^2(t)\} \leq 1$, with equality iff the system is in a pure state; and the density matrix elements must satisfy the Schwartz inequality, $\langle j|\hat{\rho}(t)|j\rangle\langle k|\hat{\rho}(t)|k\rangle \geq \left|\langle k|\hat{\rho}(t)|j\rangle\right|^2$.

For a closed system, the density operator often starts out in a pure state, given by $\hat{\rho}(t) = |\Psi(t)\rangle\langle\Psi(t)|$. Furthermore, the state maintains its purity upon time evolution. The equation of motion for the density operator of a closed system can then be derived using the time-dependent

Schrödinger equation:

$$\begin{aligned}\frac{d}{dt}\rho(t) &= \frac{d}{dt}\Big(|\Psi(t)\rangle\langle\Psi(t)|\Big) = \left(\frac{d}{dt}|\Psi(t)\rangle\right)\langle\Psi(t)| + |\Psi(t)\rangle\left(\frac{d}{dt}\langle\Psi(t)|\right) \\ &= -\frac{i}{\hbar}\hat{H}|\Psi(t)\rangle\langle\Psi(t)| + \frac{i}{\hbar}|\Psi(t)\rangle\langle\Psi(t)|\hat{H} \\ \frac{d}{dt}\rho(t) &= -\frac{i}{\hbar}\Big[\hat{H},\hat{\rho}(t)\Big] \equiv -\frac{i}{\hbar}\mathcal{L}\hat{\rho}(t) \end{aligned} \tag{I.1}$$

where $\mathcal{L} \equiv [\hat{H},\cdot]$ is the quantum Liouville superoperator. Eq. (I.1) is known as the quantum Liouville equation and describes the dynamics of a closed system when described by the density operator $\hat{\rho}(t)$.

I.3 Nakajima-Zwanzig Generalized Quantum Master Equation

In the case of a subsystem of an extended quantum system, the extended system can often be assumed to be a closed system. Therefore, the dynamics of the extended system can be described by the quantum Liouville equation, Eq. (I.1). Similar to the Schrödinger equation, a numerically exact solution of the quantum Liouville equation scales unfavorably with system size and is computationally unfeasible for most systems of practical interest, particularly condensed-phase systems. A reduced dynamics approach takes advantage of the fact that in many cases, only a few DOF are of interest and the rest of the DOF only matter insofar as their impact on the dynamics of the DOF of interest. Mathematically, one can focus on the subsystem of interest by using projection operator techniques. A projection superoperator $\mathcal{P}$ is defined by the idempotence property $\mathcal{P}^2 = \mathcal{P}$ and has a complimentary projection superoperator $\mathcal{Q} = 1 - \mathcal{P}$. The Nakajima-Zwanzig GQME describes the dynamics of the projected density operator $\mathcal{P}\hat{\rho}(t)$:

$$\frac{d}{dt}\mathcal{P}\hat{\rho}(t) = -i\mathcal{P}\mathcal{L}\mathcal{P}\hat{\rho}(t) - \int_{t_0}^{t} d\tau \mathcal{P}\mathcal{L}e^{-i\mathcal{Q}\mathcal{L}(t-\tau)}\mathcal{Q}\mathcal{L}\mathcal{P}\hat{\rho}(\tau) - i\mathcal{P}\mathcal{L}e^{-i\mathcal{Q}\mathcal{L}(t-t_0)}\mathcal{Q}\hat{\rho}(t_0) \quad . \tag{I.2}$$

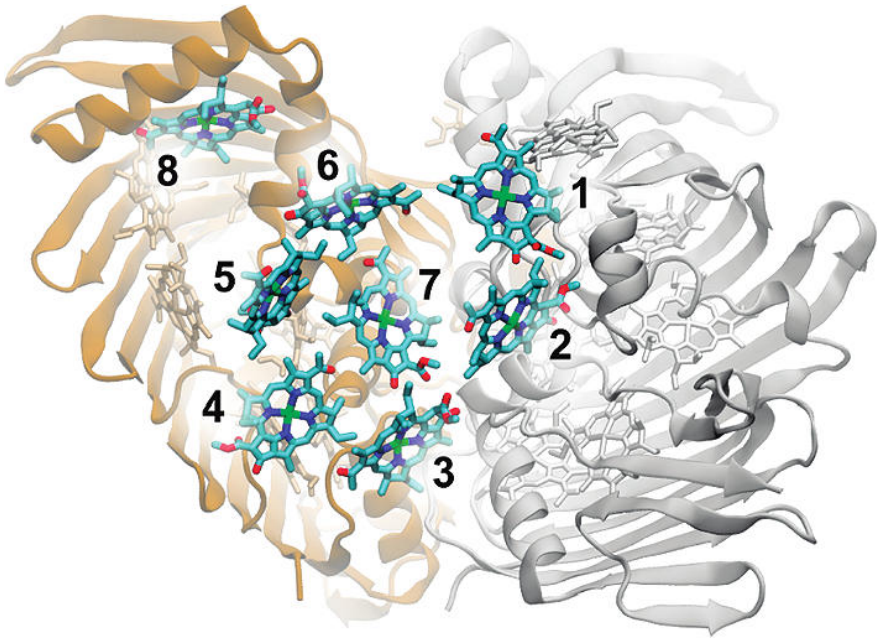

Figure I.1: Fenna-Matthews-Olson (FMO) Complex showing the eight electronic states on one of the trimers.

The reader is referred to Section 10.4.2 of Ref. 1 for the derivation of this equation. It is important to note that the general Nakajima-Zwanzig GQME given in Eq. (I.2) is an exact equation of motion with no approximations made during the derivation.

I.4 Systems of Interest for the GQME

An important attribute of the GQME methodology is its applicability, by design, for simulating nonadiabatic dynamics in truly complex molecular systems. Many condensed-phase molecular systems of technological or biological importance are known to have quantum effects that are not being fully captured by current methods used to study their dynamics. Systems of particular interest include organic donor-acceptor dyads and donor-bridge-acceptor triads in liquid solution,[47] organic photovoltaic materials,[48] and photosynthetic systems such as the Fenna-Matthews-Olson (FMO) complex[49] (Fig. I.1)[50] and Photosystem II.[51]

These systems can be described by an overall Hamiltonian with the following general form:

$$\hat{H} = \sum_{j=1}^{N_e} \hat{H}_j |j\rangle\langle j| + \sum_{\substack{j,k=1 \\ k\neq j}}^{N_e} \hat{V}_{jk} |j\rangle\langle k| \quad . \tag{I.3}$$

Here, $\hat{H}_j = \hat{\mathbf{P}}/2 + V_j\left(\hat{\mathbf{R}}\right)$ is the nuclear Hamiltonian when the system is in the electronic state $|j\rangle$, $\hat{\mathbf{R}} = \left(\hat{R}_1, ..., \hat{R}_{N_n}\right)$ and $\hat{\mathbf{P}} = \left(\hat{P}_1, ..., \hat{P}_{N_n}\right)$ are the mass-weighted position and momentum operators of the N_n nuclear DOF, and $\left\{\hat{V}_{jk} = V_{jk}\left(\hat{\mathbf{R}}\right)\right\}$ couple electronic states to each other. Throughout this dissertation, boldfaced variables, e.g., $\mathbf{A}$, indicate vector quantities; a hat over a variable, e.g., $\hat{B}$, indicates an operator quantity; and calligraphic font, e.g., $\mathcal{C}$, indicates a super-operator.

It should be noted that the electronic states, $\{|j\rangle\}$, are assumed to be independent of $\hat{\mathbf{R}}$ (i.e., the so-called crude adiabatic basis[52]). The index j in Eq. (I.3) runs over the N_e electronic states. For example, a two-state donor-acceptor system would correspond to $N_e = 2$. Many processes involving nonadiabatic dynamics in condensed phase systems are described in terms of a Hamiltonian of the form of Eq. (I.3). Furthermore, describing nonadiabatic dynamics in terms of a crude adiabatic representation, rather than in terms of Born-Oppenheimer representation, is not an approximation since the dynamics is independent of the representation employed.[52]

Importantly, $\{\hat{\mathbf{R}}, \hat{\mathbf{P}}\}$ are meant to correspond to the Cartesian positions and momenta of the individual atoms in a complex molecular system that would typically consist of a large number ($> 10^2$) of atoms. Thus, $V_j\left(\hat{\mathbf{R}}\right)$ would typically correspond to the electronic-state-specific potential energy surface (PES) that describes the interaction between the atoms in electronic state $|j\rangle$. The electronic coupling terms, $\left\{V_{jk}\left(\hat{\mathbf{R}}\right)\right\}$, can be $\hat{\mathbf{R}}$-dependent, with the assumption that they are $\hat{\mathbf{R}}$-independent corresponding to the Condon approximation. Our working hypothesis is that $\left\{V_j\left(\hat{\mathbf{R}}\right)\right\}$ and $\left\{V_{jk}\left(\hat{\mathbf{R}}\right)\right\}$ can be obtained from on-the-fly electronic structure calculations and/or semi-empirical force fields (e.g., see Ref. 18).

In most cases of practical importance, the initial state of the overall (nuclear + electronic)

system would be given by a density operator of the following form:

$$\hat{\rho}(0) = \hat{\rho}_n(0) \otimes \hat{\sigma}(0) \ . \tag{I.4}$$

Here, $\hat{\rho}_n(0) = \text{Tr}_e\{\hat{\rho}(0)\}$ is the reduced density operator that describes the initial state of the nuclear DOF, where $\text{Tr}_e\{\cdot\}$ stands for partially tracing over the electronic Hilbert space. Similarly, the reduced density operator that describes the initial state of the electronic DOF is obtained by partially tracing over the nuclear Hilbert space:

$$\hat{\sigma}(0) = \text{Tr}_n\{\hat{\rho}(0)\} = \sum_{j,k=1}^{N_e} \sigma_{jk}(0)|j\rangle\langle k| \ . \tag{I.5}$$

The state of the overall system at a later time t would then be given by:

$$\hat{\rho}(t) = e^{-i\hat{H}t/\hbar}\hat{\rho}_n(0) \otimes \hat{\sigma}(0)e^{i\hat{H}t/\hbar} \equiv e^{-i\mathcal{L}t/\hbar}\hat{\rho}_n(0) \otimes \hat{\sigma}(0) \ . \tag{I.6}$$

Here, $\hat{H}$ is the overall Hamiltonian, Eq. (I.3), and $\mathcal{L}(\cdot) = [\hat{H}, \cdot]$ is the corresponding Liouvillian.

The nuclear and electronic states at time t are described by the corresponding reduced density operators,

$$\begin{aligned} \hat{\rho}_n(t) &= \text{Tr}_e\{\hat{\rho}(t)\} \ , \\ \hat{\sigma}(t) &= \text{Tr}_n\{\hat{\rho}(t)\} = \sum_{j,k=1}^{N_e} \sigma_{jk}(t)|j\rangle\langle k| \ . \end{aligned} \tag{I.7}$$

Importantly, knowledge of $\hat{\sigma}(t)$ would allow for the evaluation of both the electronic populations, $\{\sigma_{jj}(t) = \langle j|\hat{\sigma}(t)|j\rangle\}$, and coherences, $\{\sigma_{jk}(t) = \langle j|\hat{\sigma}(t)|k\rangle|j \neq k\}$. The electronic density matrix element at time t can be written in terms of overall system quantum correlation functions

of the form $\langle \hat{A}\hat{B}(t)\rangle = \mathrm{Tr}\left\{\hat{A}e^{i\hat{H}t/\hbar}\hat{B}e^{-i\hat{H}t/\hbar}\right\}$:

$$\sigma_{jk}(t) = \sum_{u,v=1}^{N_e} \sigma_{uv}(0)\,\mathrm{Tr}\Big\{\hat{\rho}_n(0)|u\rangle\langle v|e^{i\hat{H}t/\hbar}|k\rangle\langle j|e^{-i\hat{H}t/\hbar}\Big\}\ . \tag{I.8}$$

Here, $\mathrm{Tr} \equiv \mathrm{Tr}_e\mathrm{Tr}_n$ is the trace over the electronic and nuclear Hilbert spaces.

I.5 Overview of The Dissertation

The rest of this dissertation will be organized as follows. In Chapter II, the previous approaches to the GQME will be outlined and a modified approach introduced with results provided comparing these approaches on the spin-boson model with the Ehrenfest method as input. In Chapter III, two mapping Hamiltonian (MH) methods combined with a quasiclassical (QC) approximation will be introduced and their results as input methods for the modified approach to the GQME (M-GQME) will be compared with the Ehrenfest method on the spin-boson model. An exploration of the various approaches to the memory kernel of the GQME will be outlined in Chapter IV along with the information gleaned from applying these methods to a spin-boson model. In Chapter V, the Fenna-Matthews-Olson (FMO) complex, a photosynthetic complex with long-lived quantum coherences, will be introduced and the results from applying the M-GQME to FMO will be provided and discussed. Another molecular system, the non-Condon 2,6-bis(methylene) adamantyl (BMA) radical cation will be introduced in Chapter VI along with two other systems of interest for future work and preliminary results from the application of M-GQME to BMA will be provided. A short summary of the dissertation and outlook for future projects with the M-GQME will be given in Chapter VII. Mathematical proofs of equations and additional results for the spin-boson model from Chapter IV are provided in Appendices A and B, respectively.

CHAPTER II

Modified Approach to the Generalized Quantum Master Equation

II.1 Introduction

The modified generalized quantum master equation (M-GQME) scheme presented herein builds upon, but is distinctly different from, previously proposed schemes[28,29,53] based on the Nakajima-Zwanzig GQME (NZ-GQME) given in Eq. (I.2).[3,26–28,54–61] These previous approaches are built by first dividing the overall Hamiltonian into a system-bath form,

$$\hat{H} = \hat{H}_S + \hat{H}_B + \hat{H}_{BS} \ . \tag{II.1}$$

Here, $\hat{H}_S$ is the system Hamiltonian, $\hat{H}_B$ is the bath Hamiltonian, and $\hat{H}_{BS}$ is the coupling between system and bath. While casting the overall Hamiltonian in the system-bath form has proven to be extremely useful in many other contexts, it is neither natural nor convenient when dealing with an overall Hamiltonian of the form of Eq. (I.3). This is because the first term in Eq. (I.3), $\sum_{j=1}^{N_e} \hat{H}_j |j\rangle\langle j|$, associates a *different* nuclear Hamiltonian, $\hat{H}_j$, with each electronic state, $|j\rangle$, thereby making it impossible to come up with a uniquely defined bath Hamiltonian, $\hat{H}_B$. It should be noted that while it is in principle possible to cast the Hamiltonian in Eq. (I.3) in the form of Eq. (II.1), the fact that there is no one unique way of accomplishing this can complicate the implementation of a GQME-based approach which is based on the system-bath form in a number of ways:

(i) First, when using an approximate method to evaluate the memory kernel, different choices of $\hat{H}_B$, $\hat{H}_S$, and $\hat{H}_{BS}$ may lead to different results without a clear criterion for choosing between them.

(ii) Second, the nuclear DOF are often assumed to start out at equilibrium with respect to $\hat{H}_B$, such that $\hat{\rho}_n(0) = \hat{\rho}_B^{\text{eq}} = \exp\Big[-\beta\hat{H}_B\Big]/Z_B$ where Z_B is the canonical partition function to $\hat{H}_B$, which means that the definition of $\hat{H}_B$ needs to change whenever the nuclear initial conditions, i.e., $\hat{\rho}_n(0)$, does.

(iii) Third, the system-bath coupling, $\hat{H}_{BS}$, is often defined so that $\text{Tr}_B\{\hat{H}_{BS}\hat{\rho}_B^{\text{eq}}\} = 0$, which implies that the definition of $\hat{H}_{BS}$ will also be dependent on the choice of $\hat{H}_B$.

(iv) Fourth, the projection operator used to derive the GQME is often defined as $\mathcal{P}(\cdot) = \hat{\rho}_B^{\text{eq}} \otimes \text{Tr}_B\{\cdot\}$, and would also need to be modified when the definition of $\hat{H}_B$ changes.

(v) Fifth, the second term in Eq. (I.3), $\sum_{\substack{j,k=1 \\ k\neq j}}^{N_e} \hat{V}_{jk}|j\rangle\langle k|$, is purely electronic in the Condon approximation, $\hat{V}_{jk} \to V_{jk}$, and therefore part of the system Hamiltonian. However, this term becomes a system-bath coupling term in the non-Condon case, thereby making it difficult to create a unified computational framework that can treat both Condon and non-Condon cases.

Therefore, the development of the *modified GQME (M-GQME)* approach that avoids casting the Hamiltonian in the system-bath form given in Eq. (II.1) is an improvement over the previous approaches.

The rest of this chapter is organized as follows. Previous approaches to the GQME that are based on the system-bath splitting of the Hamiltonian given in Eq. (II.1) are described in Sec. II.2. The modified approach to the GQME is outlined in Sec. II.3. The method of obtaining the memory kernel via projection-free inputs is described in Sec. II.4. The procedure for calculating these projection-free inputs with the Ehrenfest method is outlined in Sec. II.5. The results obtained by applying the Ehrenfest method with the GQME to a spin-boson model and the discussion of these results are reported in Sec. II.6. Concluding remarks are given in Sec. II.7.

II.2 Previous Approaches to the GQME

In previous approaches to the GQME, that Hamiltonian is in system-bath form as given in Eq. (II.1) and the initial nuclear density matrix in Eq. (I.4) is often given by $\hat{\rho}_n(0) = \hat{\rho}_B^{\text{eq}} = e^{-\beta\hat{H}_B}\Big/\text{Tr}_B\Big\{e^{-\beta\hat{H}_B}\Big\}$. It is also often assumed, without loss of generality, that $\hat{H}_{BS}$ is defined such that $\langle\hat{H}_{BS}\rangle_B^{\text{eq}} \equiv \text{Tr}_B\Big\{\hat{\rho}_B^{\text{eq}}\hat{H}_{BS}\Big\} = 0$. As described in Sec. I.3, the dynamics of the projected state, $\mathcal{P}\hat{\rho}(t)$ is given by the NZ-GQME given in Eq. (I.2).[1,2,62,63] Using a projection operator of the form $\mathcal{P}(\cdot) = \hat{\rho}_B^{\text{eq}} \otimes \text{Tr}_B\{\cdot\}$, substituting it into Eq. (I.2), and tracing over the bath Hilbert space then leads to the quantum-mechanically exact dynamics of the reduced system density operator, given by a GQME of the following form:

$$\frac{d}{dt}\hat{\sigma}(t) = -\frac{i}{\hbar}\mathcal{L}_S\hat{\sigma}(t) - \int_0^t d\tau\mathcal{K}(\tau)\hat{\sigma}(t-\tau) \quad . \tag{II.2}$$

Here, $-i\mathcal{L}_S\hat{\sigma}(t)/\hbar = -i[\hat{H}_S,\hat{\sigma}(t)]/\hbar$ and $-\int_0^t d\tau\mathcal{K}(\tau)\hat{\sigma}(t-\tau)$ correspond to the bath-free and bath-induced contributions to the system's reduced dynamics, respectively.

The bath-induced component is dictated by the memory kernel superoperator, $\mathcal{K}(\tau)$, which, under the above mentioned conditions, can be written in a variety of different, yet equivalent, forms:

$$\begin{aligned}
\mathcal{K}(\tau) &= \frac{1}{\hbar^2}\text{Tr}_B\Big\{\mathcal{L}_{BS}e^{-i\mathcal{Q}\mathcal{L}\tau/\hbar}\mathcal{Q}\mathcal{L}\hat{\rho}_B^{\text{eq}}\Big\} \\
&= \frac{1}{\hbar^2}\text{Tr}_B\Big\{\mathcal{L}_{BS}e^{-i\mathcal{Q}\mathcal{L}\tau/\hbar}\mathcal{Q}\mathcal{L}_{BS}\hat{\rho}_B^{\text{eq}}\Big\} \\
&= \frac{1}{\hbar^2}\text{Tr}_B\Big\{\mathcal{L}_{BS}e^{-i\mathcal{Q}\mathcal{L}\tau/\hbar}\mathcal{L}_{BS}\hat{\rho}_B^{\text{eq}}\Big\} \\
&= \frac{1}{\hbar^2}\text{Tr}_B\Big\{\mathcal{L}_{BS}e^{-i\mathcal{Q}\mathcal{L}\mathcal{Q}\tau/\hbar}\mathcal{L}_{BS}\hat{\rho}_B^{\text{eq}}\Big\} \\
&= \frac{1}{\hbar^2}\text{Tr}_B\Big\{\mathcal{L}_{BS}\mathcal{Q}e^{-i\mathcal{L}\mathcal{Q}\tau/\hbar}\mathcal{L}_{BS}\hat{\rho}_B^{\text{eq}}\Big\} \\
&= \frac{1}{\hbar^2}\text{Tr}_B\Big\{\mathcal{L}_{BS}e^{-i\mathcal{L}\mathcal{Q}\tau/\hbar}\mathcal{L}_{BS}\hat{\rho}_B^{\text{eq}}\Big\} \\
&= \frac{1}{\hbar^2}\text{Tr}_B\Big\{\mathcal{L}_{BS}e^{-i(\mathcal{L}-\mathcal{L}_{BS}\mathcal{P})\tau/\hbar}\mathcal{L}_{BS}\hat{\rho}_B^{\text{eq}}\Big\} \quad .
\end{aligned} \tag{II.3}$$

Here, $\mathcal{L}_{BS}(\cdot) = [\hat{H}_{BS}, \cdot]$ and $\mathcal{Q} = 1 - \mathcal{P}$. The memory kernel $\mathcal{K}(\tau)$ typically vanishes at $\tau > \tau_c$, where τ_c is the characteristic finite correlation or memory time of the system.

Simulating the dynamics of the system DOF based on Eq. (II.2) requires knowledge of $\mathcal{L}_S$ and $\mathcal{K}(\tau)$. Obtaining $\mathcal{L}_S$ is straightforward given knowledge of the Hamiltonian, making the memory kernel the key quantity needed for simulating the dynamics of the electronic DOF based on Eq. (II.2). However, the evaluation of $\mathcal{K}(\tau)$ is made challenging by the fact that it is time-dependent and the time dependence of $\mathcal{K}(\tau)$ is nontrivial because it is dictated by the projection-dependent propagator, $e^{-i\mathcal{Q}\mathcal{L}\tau/\hbar}$, rather than by the projection-independent propagator, $e^{-i\mathcal{L}\tau/\hbar}$. One strategy for overcoming the latter difficulty is by using a scheme for evaluating $\mathcal{K}(\tau)$ from projection-free inputs, i.e., inputs that involve $e^{-i\mathcal{L}\tau/\hbar}$ rather than $e^{-i\mathcal{Q}\mathcal{L}\tau/\hbar}$. Combined with exact or approximate methods for evaluating those projection-free inputs can then lead to a methodology that can be applied to complex molecular systems.

The following subsections outline two of the previously proposed schemes for calculating $\mathcal{K}(\tau)$ from projection-free inputs. The differences between the schemes can be generally traced back to which of the forms of the memory kernel, Eq. (II.3), is chosen as the starting point. Each of these approaches then uses the following general operator identity to determine a scheme for evaluating $\mathcal{K}(\tau)$ from projection-free inputs:[28,29]

$$e^{-i\mathcal{B}\tau/\hbar} = e^{-i\mathcal{A}\tau/\hbar} - \frac{i}{\hbar}\int_0^\tau d\tau' e^{-i\mathcal{A}(\tau-\tau')/\hbar}(\mathcal{B}-\mathcal{A})e^{-i\mathcal{B}\tau'/\hbar} \quad . \tag{II.4}$$

II.2.1 Shi-Geva Approach

The original scheme for calculating the memory kernel of the GQME[28] was based on the following expression for the memory kernel [see Eq. (II.3)]:

$$\mathcal{K}(\tau) = \frac{1}{\hbar^2}\mathrm{Tr}_B\left\{\mathcal{L}_{BS}e^{-i(\mathcal{L}-\mathcal{L}_{BS}\mathcal{P})\tau/\hbar}\mathcal{L}_{BS}\hat{\rho}_B^{\mathrm{eq}}\right\} \quad . \tag{II.5}$$

Substituting $\mathcal{A} = \mathcal{L}$ and $\mathcal{B} = \mathcal{L} - \mathcal{L}_{BS}\mathcal{P}$ into the operator identity in Eq. (II.4), one can then obtain

$$e^{-i(\mathcal{L}-\mathcal{L}_{BS}\mathcal{P})\tau/\hbar} = e^{-i\mathcal{L}\tau/\hbar} + \frac{i}{\hbar}\int_0^\tau d\tau' e^{-i\mathcal{L}(\tau-\tau')/\hbar}\mathcal{L}_{BS}\mathcal{P}e^{-i(\mathcal{L}-\mathcal{L}_{BS}\mathcal{P})\tau'/\hbar} \quad . \tag{II.6}$$

Substituting Eq. (II.6) into Eq. (II.5) leads to the following expression for the memory kernel:

$$\mathcal{K}(\tau) = \mathcal{K}_1(\tau) + i\int_0^\tau \mathcal{K}_1(\tau-\tau')\mathcal{K}_2(\tau') \quad . \tag{II.7}$$

Here,

$$\mathcal{K}_1(\tau) = \frac{1}{\hbar^2}\mathrm{Tr}_B\Big\{\mathcal{L}_{BS}e^{-i\mathcal{L}\tau/\hbar}\mathcal{L}_{BS}\hat{\rho}_B^{\mathrm{eq}}\Big\} \tag{II.8}$$

and

$$\mathcal{K}_2(\tau) = \frac{1}{\hbar}\mathrm{Tr}_B\Big\{e^{-i(\mathcal{L}-\mathcal{L}_{BS}\mathcal{P})\tau/\hbar}\mathcal{L}_{BS}\hat{\rho}_B^{\mathrm{eq}}\Big\} \tag{II.9}$$

are auxiliary kernels that are needed in order to calculate the memory kernel.

It should be noted that unlike $\mathcal{K}_1(\tau)$, which is projection-free, $\mathcal{K}_2(\tau)$ is projection-dependent. As such, calculating $\mathcal{K}_2(\tau)$ involves a similar challenge to that of calculating $\mathcal{K}(\tau)$. However, $\mathcal{K}_2(\tau)$ can be evaluated from the following Volterra equation, obtained by substituting Eq. (II.6) into Eq. (II.9):

$$\mathcal{K}_2(\tau) = \mathcal{K}_3(\tau) + i\int_0^\tau d\tau' \mathcal{K}_3(\tau-\tau')\mathcal{K}_2(\tau') \quad . \tag{II.10}$$

Here,

$$\mathcal{K}_3(\tau) = \frac{1}{\hbar}\mathrm{Tr}_B\Big\{e^{-i\mathcal{L}\tau/\hbar}\mathcal{L}_{BS}\hat{\rho}_B^{\mathrm{eq}}\Big\} \tag{II.11}$$

is a projection-free auxiliary kernel. Thus, given the projection-free inputs $\mathcal{K}_1(\tau)$ and $\mathcal{K}_3(\tau)$, the memory kernel, $\mathcal{K}(\tau)$, can be obtained with the Shi-Geva (SG-NZ) approach via the two coupled equations, Eqs. (II.7) and (II.10).

II.2.2 Zhang-Ka-Geva Approach

An alternative scheme for calculating the memory kernel of the GQME[29] was based on writing the memory kernel in the following form [see Eq. (II.3)]:

$$\mathcal{K}(\tau) = \frac{1}{\hbar^2}\mathrm{Tr}_B\Big\{\mathcal{L}_{BS}e^{-i\mathcal{Q}\mathcal{L}\tau/\hbar}\mathcal{Q}\mathcal{L}\hat{\rho}_B^{\mathrm{eq}}\Big\} \quad . \tag{II.12}$$

Substituting $\mathcal{A} = \mathcal{L}$ and $\mathcal{B} = \mathcal{Q}\mathcal{L}$ into Eq. (II.4) and plugging that into Eq. (II.12) then leads to the following Volterra equation for $\mathcal{K}(\tau)$:

$$\mathcal{K}(\tau) = \dot{\Phi}(\tau) + \frac{i}{\hbar}\Phi(\tau)\mathcal{L}_S + \int_0^\tau d\tau'\Phi(\tau-\tau')\mathcal{K}(\tau') \quad . \tag{II.13}$$

Here, $\Phi(\tau)$ is a projection-free input:

$$\Phi(\tau) = \frac{i}{\hbar}\mathrm{Tr}_B\Big\{\mathcal{L}_{BS}e^{-i\mathcal{L}\tau/\hbar}\hat{\rho}_B^{\mathrm{eq}}\Big\} \quad . \tag{II.14}$$

Therefore, the memory kernel can be obtained with the Zhang-Ka-Geva (ZKG-NZ) approach by first calculating $\Phi(\tau)$ and $\dot{\Phi}(\tau)$ and then calculating the memory kernel via Eq. (II.13).

II.3 The Modified Approach to the GQME

The modified approach starts with a system whose overall Hamiltonian is given by Eq. (I.3), rather than by Eq. (II.1). As described in Sec. I.3, the dynamics of the projected state, $\mathcal{P}\hat{\rho}(t)$ is given by the NZ-GQME given in Eq. (I.2).[1,2,62,63] Next, the projection operator is explicitly defined as follows:

$$\mathcal{P}(\cdot) = \hat{\rho}_n^{\mathrm{ref}} \otimes \mathrm{Tr}_n\{\cdot\} \quad . \tag{II.15}$$

Here, $\hat{\rho}_n^{\mathrm{ref}}$ is a reference nuclear density operator of one's choice (as long as $\mathrm{Tr}_n\left\{\hat{\rho}_n^{\mathrm{ref}}\right\} = 1$, which is required for $\mathcal{P}^2 = \mathcal{P}$). Substituting the projection operator in Eq. (II.15) into Eq. (I.2) and

tracing over the nuclear Hilbert space then leads to the following GQME for the reduced electronic density operator $\hat{\sigma}(t)$:

$$\frac{d}{dt}\hat{\sigma}(t) = -\frac{i}{\hbar}\langle\mathcal{L}\rangle_n^{\text{ref}}\hat{\sigma}(t) - \int_0^t d\tau\ \mathcal{K}(\tau)\hat{\sigma}(t-\tau) + \mathcal{I}(t)\ . \tag{II.16}$$

Here,

$$\langle\mathcal{L}\rangle_n^{\text{ref}} = \text{Tr}_n\left\{\mathcal{L}\hat{\rho}_n^{\text{ref}}\right\} \tag{II.17}$$

accounts for the Hamiltonian and Markovian dynamics generated by the Hamiltonian $\langle\hat{H}\rangle_n^{\text{ref}} = \text{Tr}_n\left\{\hat{H}\hat{\rho}_n^{\text{ref}}\right\}$, while the remaining two terms on the R.H.S. account for the non-Hamiltonian and non-Markovian dynamics generated by the coupling between the electronic and nuclear DOF. More specifically, the memory kernel, $\mathcal{K}(\tau)$, which accounts for the effect of the nuclear DOF within the time interval $(0,t)$ on the electronic DOF at time t, is given by

$$\mathcal{K}(\tau) = \frac{1}{\hbar^2}\text{Tr}_n\Big\{\mathcal{L}\,e^{-i\mathcal{Q}\mathcal{L}\tau/\hbar}\mathcal{Q}\mathcal{L}\hat{\rho}_n^{\text{ref}}\Big\} \tag{II.18}$$

and the inhomogeneous term, $\hat{I}(t)$, which accounts for the effect of the initial state of the nuclear DOF on the electronic DOF at time t, is given by

$$\hat{I}(t) = -\frac{i}{\hbar}\text{Tr}_n\Big\{\mathcal{L}e^{-i\mathcal{Q}\mathcal{L}t/\hbar}\mathcal{Q}\hat{\rho}_n(0)\Big\}\ . \tag{II.19}$$

It should be noted that both $\mathcal{K}(\tau)$ and $\hat{I}(t)$ would typically vanish at $\tau, t > \tau_c$, where τ_c is the characteristic finite correlation or memory time of the electronic DOF.

As is well known, there is no one unique choice of $\hat{\rho}_n^{\text{ref}}$ in Eq. (II.15) and the specific choice is dictated by the questions one is asking and convenience.[29,64,65] As a result, different choices of $\hat{\rho}_n^{\text{ref}}$ would lead to different versions of the GQME. In this sense, the equation of motion that governs the dynamics of the electronic DOF is not unique, although the different equations of motion must all reproduce the same electronic dynamics (as long as the quantum-mechanically exact memory kernel and inhomogeneous term can be obtained). In practice, it is convenient to choose $\hat{\rho}_n^{\text{ref}}$ in a

manner that will simplify the resulting GQME. The assignment $\hat{\rho}_n^{\text{ref}} = \hat{\rho}_n(0)$ (the initial state of the nuclear DOF) is such a convenient choice and leads to the following definition of the projection operator:

$$\mathcal{P}(\cdot) = \hat{\rho}_n(0) \otimes \text{Tr}_n\{\cdot\} \ . \tag{II.20}$$

This choice is convenient because it leads to the elimination of the inhomogeneous term from the GQME.[29] However, it should be noted that this choice also implies that the memory kernel will be explicitly dependent on the initial state of the nuclear DOF. In other words, changing the state of the nuclear DOF at the initial time $t = 0$ [$\hat{\rho}_n(0)$] would alter the equation of motion [see Eq. (II.21)] that dictates the dynamics of the electronic DOF at later times $t > 0$. It should also be noted that the specific form of $\hat{\rho}_n(0)$ is dictated by how the system is prepared, which is ultimately dependent on the experimental setup. Importantly, $\hat{\rho}_n(0)$ need not be of the form $\hat{\rho}_B^{\text{eq}} = Z_B^{-1} e^{-\beta \hat{H}_B}$. It should be noted that this is also not required within the ZKG-NZ scheme (see Sec. II.2.2).[29]

Substituting the projection operator in Eq. (II.20) into Eq. (II.16) leads to the following GQME for the electronic reduced density operator, $\hat{\sigma}(t)$:

$$\frac{d}{dt}\hat{\sigma}(t) = -\frac{i}{\hbar}\langle \mathcal{L} \rangle_n^0 \hat{\sigma}(t) - \int_0^t d\tau \mathcal{K}(\tau)\hat{\sigma}(t-\tau) \ . \tag{II.21}$$

Here, $\langle \mathcal{L} \rangle_n^0$ (the overall Liouvillian averaged over the initial state of the nuclear DOF, resulting in a superoperator in the electronic Liouville-subspace) and $\mathcal{K}(\tau)$ (the memory kernel superoperator) are given by:

$$\begin{aligned} \langle \mathcal{L} \rangle_n^0 (\cdot) &\equiv \text{Tr}_n \left\{ \hat{\rho}_n(0) \mathcal{L} \right\} (\cdot) \\ &= \left[\sum_{j=1}^{N_e} \langle \hat{H}_j \rangle_n^0 |j\rangle\langle j| + \sum_{\substack{j,k=1 \\ k \neq j}}^{N_e} \langle \hat{V}_{jk} \rangle_n^0 |j\rangle\langle k|, \cdot \right] \ , \end{aligned} \tag{II.22}$$

and

$$\mathcal{K}(\tau) = \frac{1}{\hbar^2} \text{Tr}_n \Big\{ \mathcal{L} e^{-i\mathcal{Q}\mathcal{L}\tau/\hbar} \mathcal{Q}\mathcal{L}\hat{\rho}_n(0) \Big\} \ , \tag{II.23}$$

respectively.

Importantly, evaluation of the Liouvillian and memory kernel terms in Eqs. (II.22) and (II.23), respectively, does not require casting the Hamiltonian in system-bath form or that the initial state of the nuclear DOF corresponds to thermal equilibrium with respect to the bath Hamiltonian. In what follows, Eq. (II.21) is referred to as the *modified GQME (M-GQME)*, in order to distinguish it from versions of the GQME which are based on casting the overall Hamiltonian in system-bath form and assuming that the initial state of the nuclear DOF corresponds to equilibrium with respect to the bath Hamiltonian (see Sec. II.2).

It should be noted that the expression for the memory kernel, Eq. (II.23), can be further simplified by introducing the Condon approximation, $\hat{V}_{jk} \to V_{jk}$, leading to the following equation for the memory kernel:

$$\mathcal{K}(\tau) = \frac{1}{\hbar^2}\mathrm{Tr}_n\Big\{\mathcal{L}_{\text{zero}}\, e^{-i\mathcal{Q}\mathcal{L}\tau/\hbar}\mathcal{Q}\mathcal{L}_{\text{zero}}\hat{\rho}_n(0)\Big\} \quad . \tag{II.24}$$

To prove this, let $\mathcal{L} = \mathcal{L}_{\text{zero}} + \mathcal{L}_{\text{int}}$, where

$$\begin{aligned}
\mathcal{L}_{\text{zero}}(\cdot) &= [\hat{H}_{\text{zero}}, \cdot] = \left[\sum_{j=1}^{N_e} \hat{H}_j |j\rangle\langle j|, \cdot\right] \quad , \\
\mathcal{L}_{\text{int}}(\cdot) &= [\hat{H}_{\text{int}}, \cdot] = \left[\sum_{\substack{j,k=1 \\ k\neq j}}^{N_e} \hat{V}_{jk} |j\rangle\langle k|, \cdot\right] \quad ,
\end{aligned} \tag{II.25}$$

[see Eq. (I.3)] and note that $\mathcal{L}_{\text{int}}$ becomes a purely electronic superoperator in the Condon approx-

imation. As a result:

$$
\begin{aligned}
&\mathrm{Tr}_n\left\{\mathcal{L}_{\text{int}}e^{-i\mathcal{Q}\mathcal{L}\tau/\hbar}\mathcal{Q}\hat{A}\right\} \\
&\quad=\mathcal{L}_{\text{int}}\mathrm{Tr}_n\left\{e^{-i\mathcal{Q}\mathcal{L}\tau/\hbar}\mathcal{Q}\hat{A}\right\} \\
&\quad=\mathcal{L}_{\text{int}}\mathrm{Tr}_n\left\{\left[1-\frac{i}{\hbar}\mathcal{Q}\mathcal{L}\tau+\frac{1}{2}\left(-\frac{i}{\hbar}\right)^2\mathcal{Q}\mathcal{L}\mathcal{Q}\mathcal{L}\tau^2+\ldots\right]\mathcal{Q}\hat{A}\right\} \\
&\quad=\mathcal{L}_{\text{int}}\mathrm{Tr}_n\left\{\left[\mathcal{Q}-\frac{i}{\hbar}\mathcal{Q}\mathcal{L}\mathcal{Q}\tau+\frac{1}{2}\left(-\frac{i}{\hbar}\right)^2\mathcal{Q}\mathcal{L}\mathcal{Q}\mathcal{L}\mathcal{Q}\tau^2+\ldots\right]\hat{A}\right\} \\
&\quad=\mathcal{L}_{\text{int}}\mathrm{Tr}_n\left\{\mathcal{Q}[\ldots]\right\}=\mathcal{L}_{\text{int}}\left(\mathrm{Tr}_n\left\{[\ldots]\right\}-\mathrm{Tr}_n\left\{\mathcal{P}[\ldots]\right\}\right) \\
&\quad=\mathcal{L}_{\text{int}}\left(\mathrm{Tr}_n\left\{[\ldots]\right\}-\mathrm{Tr}_n\left\{[\ldots]\right\}\right)=0 \quad .
\end{aligned}
\tag{II.26}
$$

This implies that one can replace $\mathcal{L}$ by $\mathcal{L}_{\text{zero}}$ on the left side of the exponent in Eq. (II.23).

$\mathcal{L}$ can also be replaced by $\mathcal{L}_{\text{zero}}$ on the right side of the exponent in Eq. (II.23), since

$$
\begin{aligned}
\mathcal{Q}\mathcal{L}_{\text{int}}\hat{\rho}_n(0)\hat{\sigma}(t)&=\mathcal{L}_{\text{int}}\mathcal{Q}\hat{\rho}_n(0)\hat{\sigma}(t)=\mathcal{L}_{\text{int}}\left[\hat{\rho}_n(0)\hat{\sigma}(t)-\mathcal{P}\hat{\rho}_n(0)\hat{\sigma}(t)\right] \\
&=\mathcal{L}_{\text{int}}\left[\hat{\rho}_n(0)\hat{\sigma}(t)-\hat{\rho}_n(0)\hat{\sigma}(t)\right]=0 \quad .
\end{aligned}
\tag{II.27}
$$

Therefore, in the Condon limit,

$$
\mathcal{K}(\tau)=\frac{1}{\hbar^2}\mathrm{Tr}_n\Big\{\mathcal{L}_{\text{zero}}e^{-i\mathcal{Q}\mathcal{L}\tau/\hbar}\mathcal{Q}\mathcal{L}_{\text{zero}}\hat{\rho}_n(0)\Big\} \quad . \tag{II.28}
$$

II.4 M-GQME Memory Kernel and Projection-Free Inputs

Simulating the dynamics of the electronic DOF based on Eq. (II.21) requires knowledge of $\langle\mathcal{L}\rangle_n^0$ and $\mathcal{K}(\tau)$. Obtaining $\langle\mathcal{L}\rangle_n^0$ requires the evaluation of the time-independent averages over the nuclear DOF at the initial time, $\langle\hat{H}_j\rangle_n^0$ and $\langle\hat{V}_{jk}\rangle_n^0$, which are relatively straightforward to calculate, either fully quantum-mechanically, semiclassically, or fully classically.[66]

Assuming that $\langle\mathcal{L}\rangle_n^0$ can be obtained, the memory kernel of the M-GQME, Eq. (II.23), is the key quantity needed for simulating the dynamics of the electronic DOF based on Eq. (II.21). However,

unlike $\langle\mathcal{L}\rangle_n^0$, the evaluation of $\mathcal{K}(\tau)$ is made challenging by the fact that it is time-dependent. Furthermore, the time-dependence of $\mathcal{K}(\tau)$ is nontrivial because it is dictated by the projection-dependent propagator, $e^{-i\mathcal{Q}\mathcal{L}\tau/\hbar}$, rather than by the projection-independent propagator, $e^{-i\mathcal{L}\tau/\hbar}$. One strategy for overcoming the latter difficulty is by using a scheme for evaluating $\mathcal{K}(\tau)$ from projection-free inputs, i.e., inputs that involve $e^{-i\mathcal{L}\tau/\hbar}$ rather than $e^{-i\mathcal{Q}\mathcal{L}\tau/\hbar}$. Combined with exact or approximate methods for evaluating those projection-free inputs can then lead to a methodology that can be applied to complex molecular systems.

Substituting $\mathcal{A} = \mathcal{L}$ and $\mathcal{B} = \mathcal{Q}\mathcal{L}$ into Eq. (II.4) results in

$$e^{-i\mathcal{Q}\mathcal{L}\tau/\hbar} = e^{-i\mathcal{L}\tau/\hbar} + \frac{i}{\hbar}\int_0^\tau d\tau' e^{-i\mathcal{L}(\tau-\tau')/\hbar}\mathcal{P}\mathcal{L}e^{-i\mathcal{Q}\mathcal{L}\tau'/\hbar} \quad . \tag{II.29}$$

Substituting Eq. (II.29) into Eq. (II.23) then leads the following Volterra equation of the second-kind for $\mathcal{K}(\tau)$:

$$\mathcal{K}(\tau) = i\dot{\mathcal{F}}(\tau) - \frac{1}{\hbar}\mathcal{F}(\tau)\langle\mathcal{L}\rangle_n^0 + i\int_0^\tau d\tau' \mathcal{F}(\tau-\tau')\mathcal{K}(\tau') \quad . \tag{II.30}$$

Here,

$$\mathcal{F}(\tau) = \frac{1}{\hbar}\mathrm{Tr}_n\Big\{\mathcal{L}e^{-i\mathcal{L}\tau/\hbar}\hat{\rho}_n(0)\Big\} \quad . \tag{II.31}$$

Thus, given the projection-free quantity $\mathcal{F}(\tau)$, Eq. (II.30) can be solved numerically for the projection-dependent $\mathcal{K}(\tau)$ (see Sec. II.4.1). In the Condon case, substituting Eq. (II.29) into Eq. (II.28) leads to the following Volterra equation of the second-kind for $\mathcal{K}(\tau)$ in the Condon limit:

$$\mathcal{K}(\tau) = \mathcal{F}_1(\tau) - \frac{1}{\hbar}\mathcal{F}_2(\tau)\langle\mathcal{L}_{\text{zero}}\rangle_n^0 + i\int_0^\tau d\tau' \, \mathcal{F}_2(\tau-\tau')\mathcal{K}(\tau') \quad . \tag{II.32}$$

Here,

$$\mathcal{F}_1(\tau) = \frac{1}{\hbar^2}\mathrm{Tr}_n\Big\{\mathcal{L}_{\text{zero}}e^{-i\mathcal{L}\tau/\hbar}\mathcal{L}_{\text{zero}}\hat{\rho}_n(0)\Big\} \quad , \tag{II.33}$$

$$\mathcal{F}_2(\tau) = \frac{1}{\hbar}\mathrm{Tr}_n\Big\{\mathcal{L}_{\text{zero}}e^{-i\mathcal{L}\tau/\hbar}\hat{\rho}_n(0)\Big\} \quad . \tag{II.34}$$

In contrast to the memory kernel, $\mathcal{F}(\tau)$, $\mathcal{F}_1(\tau)$, and $\mathcal{F}_2(\tau)$ are not required to have finite lifetimes. Hence, the problem of calculating $\mathcal{K}(\tau)$ translates into that of calculating $\mathcal{F}(\tau)$ and $\dot{\mathcal{F}}(\tau)$ in the non-Condon case and $\mathcal{F}_1(\tau)$ and $\mathcal{F}_2(\tau)$ in the Condon case.

In practice, $\mathcal{K}(\tau)$, $\mathcal{F}(\tau)$, $\mathcal{F}_1(\tau)$, and $\mathcal{F}_2(\tau)$ are each represented by $N_e^2 \times N_e^2$ matrices in terms of the electronic basis $\{|j\rangle|j = 1, \ldots, N_e\}$ (e.g. 4×4 matrices in the case of a system with two electronic states). The corresponding matrix elements of $\mathcal{F}(\tau)$ are given by:

$$\begin{aligned}
\mathcal{F}_{jkuv}(\tau) &= \frac{1}{\hbar}\mathrm{Tr}\Big\{(|j\rangle\langle k|)^\dagger \mathcal{L} e^{-i\mathcal{L}\tau/\hbar}\hat{\rho}_n(0)|u\rangle\langle v|\Big\} \\
&= \frac{1}{\hbar}\mathrm{Tr}\left\{\hat{\rho}_n(0)|u\rangle\langle v|e^{i\hat{H}\tau/\hbar}[|k\rangle\langle j|, \hat{H}]e^{-i\hat{H}\tau/\hbar}\right\} \\
&= \frac{1}{\hbar}\mathrm{Tr}\Big\{\hat{\rho}_n(0)|u\rangle\langle v|e^{i\hat{H}\tau/\hbar}\left[\hat{H}_j - \hat{H}_k\right]|k\rangle\langle j|e^{-i\hat{H}\tau/\hbar}\Big\} \\
&\quad + \frac{1}{\hbar}\sum_{l=1}^{N_e}\mathrm{Tr}\Big\{\hat{\rho}_n(0)|u\rangle\langle v|e^{i\hat{H}\tau/\hbar}\left[\hat{V}_{jl}|k\rangle\langle l| - \hat{V}_{lk}|l\rangle\langle j|\right]e^{-i\hat{H}\tau/\hbar}\Big\}
\end{aligned} \tag{II.35}$$

Performing similar derivations, the matrix elements of $\mathcal{F}_1(\tau)$ are given by

$$\mathcal{F}_{1,jkuv}(\tau) = \frac{1}{\hbar^2}\,\mathrm{Tr}\left\{\left[\hat{H}_u\hat{\rho}_n(0) - \hat{\rho}_n(0)\hat{H}_v\right]|u\rangle\langle v|e^{i\hat{H}\tau/\hbar}|b\rangle\langle a|\Big(\hat{H}_a - \hat{H}_b\Big)e^{-i\hat{H}\tau/\hbar}\right\} \tag{II.36}$$

and the matrix elements of $\mathcal{F}_2(\tau)$ are given by

$$\mathcal{F}_{2,jkuv}(\tau) = \frac{1}{\hbar}\,\mathrm{Tr}\left\{\hat{\rho}_n(0)|u\rangle\langle v|e^{i\hat{H}\tau/\hbar}|b\rangle\langle a|\Big(\hat{H}_a - \hat{H}_b\Big)e^{-i\hat{H}\tau/\hbar}\right\} \tag{II.37}$$

Thus, $\mathcal{F}_{jkuv}(\tau)$, $\mathcal{F}_{1,jkuv}(\tau)$, and $\mathcal{F}_{2,jkuv}(\tau)$ can be given in terms of expressions of the form:

$$\mathrm{Tr}\left\{\hat{\Omega}\,|u\rangle\langle v|e^{i\hat{H}\tau/\hbar}\,\hat{\Gamma}\,|b\rangle\langle a|e^{-i\hat{H}\tau/\hbar}\right\} \quad . \tag{II.38}$$

Here, the nuclear operator $\hat{\Omega}$ is $\hat{\rho}_n(0)$ for $\mathcal{F}_{jkuv}(\tau)$ and $\mathcal{F}_{2,jkuv}(\tau)$ and $\left[\hat{H}_u\hat{\rho}_n(0) - \hat{\rho}_n(0)\hat{H}_v\right]$ for $\mathcal{F}_{1,jkuv}(\tau)$ while the nuclear operator $\hat{\Gamma} = \Gamma(\hat{\mathbf{R}})$ is either

(i) $V_j\left(\hat{\mathbf{R}}\right) - V_k\left(\hat{\mathbf{R}}\right)$ with $a = j$ and $b = k$,

(ii) $V_{ja}\left(\hat{\mathbf{R}}\right)$ with $a \neq j$ and $b = k$, or

(iii) $V_{bk}\left(\hat{\mathbf{R}}\right)$ with $a = j$ and $b \neq k$

and terms with $a \neq j$ and $b \neq k$ do not occur and options (ii) and (iii) do not occur for $\mathcal{F}_{1,jkuv}(\tau)$ and $\mathcal{F}_{2,jkuv}(\tau)$.

The number of quantities of the form of Eq. (II.38) that needs to be calculated scales rather favorably with the dimensionality of the electronic Hilbert space ($\sim N_e^4$). It should be noted that those quantities only need to be calculated once for a given initial state, and that they can be calculated independently in a trivially parallelized manner.

II.4.1 Numerical Solution of the Memory Kernel Volterra Equation

In this section, the iterative algorithm used for solving Eqs. (II.30) and (II.32) numerically is outlined. It should be noted that these equations are Volterra equations of the second kind, and as such have the following general form:

$$f(t) = \int_{t_0}^{t} ds\; h(t,s)f(s) + g(t) \;\; . \tag{II.39}$$

Given that $h(t,s)$ and $g(t)$ are known, this equation is solved for $f(t)$. Comparing Eq. (II.39) with Eqs. (II.30) and (II.32) shows that in our case this is an operator equation with $t_0 \to 0$, $t \to \tau$, $s \to \tau'$, and $f(t) \to \mathcal{K}(\tau)$ in both the Condon and non-Condon cases and $h(t,s) \to i\mathcal{F}(\tau - \tau')$ and $g(t) = i\dot{\mathcal{F}}(\tau) - \frac{1}{\hbar}\mathcal{F}(\tau)\langle\mathcal{L}\rangle_n^0$ for a non-Condon system and $h(t,s) \to i\mathcal{F}_2(\tau - \tau')$ and $g(t) = \mathcal{F}_1(\tau) - \frac{1}{\hbar}\mathcal{F}_2(\tau)\langle\mathcal{L}_{\text{zero}}\rangle_n^0$ for a Condon system.

The iterative algorithm starts out with $f(t) = g(t)$ as the initial guess. Substituting this initial guess into Eq. (II.39) generates another estimator of $f(t)$, which is then substituted back into Eq. (II.39). This procedure is repeated until convergence, where the estimators obtained in two subsequent steps are indistinguishable within a prescribed tolerance.

In practice, $f(t)$ is a matrix and time is discretized, $t_n = n\Delta t$ with $n = 0, 1, 2, ..., N_{\text{max}}$. Let

$f^i_{jk}(n\Delta t)$ be the value of (j,k)-th matrix element of f after the i-th iteration:

$$f^i_{jk}(n\Delta t) = \int_0^{n\Delta t} ds \sum_{l=1}^{N_e} h_{jl}(n\Delta t, s) f^{i-1}_{lk}(s) + g_{jk}(n\Delta t) \tag{II.40}$$

The time integral in Eq. (II.40) is calculated via the extended trapezoidal rule. The results reported in this paper were obtained using the following criterion for convergence: $\left| f^i_{jk}(n\Delta t) - f^{i-1}_{jk}(n\Delta t) \right| \leq 10^{-10}$ (for all time steps n and matrix elements jk). For the applications reported in this chapter, the typical number of iterations necessary for obtaining converged results was 4-16.

II.5 Ehrenfest Method for Obtaining the Projection-Free Inputs

The methodology outlined in Sec. II.4 is general and can be used for calculating the memory kernel of the M-GQME via any exact or approximate method of one's choice.[29,32,44,65,67] In this section, a protocol is outlined for calculating the projection-free inputs $\mathcal{F}_{jkuv}(\tau)$, $\mathcal{F}_{1,jkuv}(\tau)$, and $\mathcal{F}_{2,jkuv}(\tau)$ via the Ehrenfest method. This starts by noting that they can be given in terms of expressions of the form of Eq. (II.38). The expression in Eq. (II.38) can be interpreted as the expectation value of $\hat{\Gamma}\,|b\rangle\langle a|$ at time t when the initial state is given by $\hat{\Omega}\,|u\rangle\langle v|$ and the dynamics is dictated by the overall Hamiltonian, $\hat{H}$ [see Eq. (I.3)]. However, while $\hat{\Omega}$ always contains $\hat{\rho}_n(0)$, which is by definition a legitimate nuclear density operator, associating $|u\rangle\langle v|$ with an initial electronic density operator, $\hat{\sigma}(0)$, is not possible when $u \neq v$ since in this case $|u\rangle\langle v|$ is not Hermitian, has zero trace, and does not satisfy the Schwarz inequality [$|\sigma_{jk}| \leq (\sigma_{jj}\sigma_{kk})^{1/2}$].

The fact that $|u\rangle\langle v|$ is not a legitimate density operator when $u \neq v$ can become an obstacle when one attempts to evaluate Eq. (II.38) via semiclassical or mixed quantum-classical methods. In this section, this point is demonstrated in the context of the Ehrenfest method. Within this method, the nuclear DOF are treated classically, the electronic DOF are treated quantum-mechanically, and the impact of the electronic DOF on the nuclear DOF is treated in a mean-field manner. In practice,

initial positions and momenta of the nuclear DOF are sampled based on the Wigner transform of $\hat{\rho}_n(0)$, $\rho_{n,W}(\mathbf{R},\mathbf{P};t=0)$, or its classical limit, and expectation values are obtained by averaging over the corresponding ensemble of classical trajectories. The effect of the nuclear DOF on the electronic DOF is accounted for by the fact that each classical trajectory of the nuclear DOF, $\mathbf{R}(t)$, corresponds to a different realization of a time-dependent Hamiltonian that govern the dynamics of the electronic density operator,

$$\hat{H}_{\text{el}}(t) = \sum_{j=1}^{N_e} V_j[\mathbf{R}(t)]|j\rangle\langle j| + \sum_{\substack{j,k=1 \\ k\neq j}}^{N_e} V_{jk}[\mathbf{R}(t)]|j\rangle\langle k| \quad . \tag{II.41}$$

The effect of the electronic DOF on the nuclear DOF is accounted for by propagating the nuclear DOF on the mean-field PES:

$$V_{\text{mf}}(\mathbf{R}) = \sum_{j=1}^{N_e} \sigma_{jj}(t) V_j(\mathbf{R}) + \sum_{\substack{j,k=1 \\ k\neq j}}^{N_e} \sigma_{kj}(t) V_{jk}(\mathbf{R}) \quad . \tag{II.42}$$

Attempting to use the Ehrenfest method when the initial electronic density operator is non-Hermitian, e.g., $\hat{\sigma}(0) = |u\rangle\langle v|$ when $u \neq v$, results in a complex mean-field PES, which in turn leads to nonphysical complex classical positions and momenta of the nuclear DOF. This problem can be bypassed by switching to a basis of the electronic Liouville space consisting of operators that satisfy the conditions for a density operator. The choice of basis is not unique but a relatively unbiased choice that satisfies hermiticity, trace one, and Schwarz inequality corresponds to:

$$\begin{aligned} \hat{X}_{uv} &= \frac{1}{2}\Big[|u\rangle\langle u| + |v\rangle\langle v| + |u\rangle\langle v| + |v\rangle\langle u|\Big] \quad , \\ \hat{Y}_{uv} &= \frac{1}{2}\Big[|u\rangle\langle u| + |v\rangle\langle v| - i|u\rangle\langle v| + i|v\rangle\langle u|\Big] \quad . \end{aligned} \tag{II.43}$$

The results reported in this chapter were obtained based on this choice. It should be noted that Montoya-Castillo and Reichman[32] proposed an alternative approach for resolving the above mentioned discrepancies which is based on the identity $|u\rangle\langle v| + |v\rangle\langle u| = \sum_k \lambda_k |\lambda_k\rangle\langle\lambda_k|$ and sep-

arately simulating Ehrenfest dynamics for each $|\lambda_k\rangle\langle\lambda_k|$ (here, $\{|\lambda_k\rangle\}$ are the eigenfunctions of $|u\rangle\langle v| + |v\rangle\langle u|$ and $\{\lambda_k\}$ are the corresponding eigenvalues).

In practice, one starts with $\hat{X}_{uv}$ and $\hat{Y}_{uv}$ instead of $|u\rangle\langle v|$ and $|v\rangle\langle u|$ as initial electronic states, to obtain the Ehrenfest approximations of

$$\begin{aligned} &\mathrm{Tr}\left\{\hat{\Omega}\,\hat{X}_{uv}e^{i\hat{H}\tau/\hbar}\,\Gamma(\hat{\mathbf{R}})|b\rangle\langle a|e^{-i\hat{H}\tau/\hbar}\right\} \quad , \\ &\mathrm{Tr}\left\{\hat{\Omega}\,\hat{Y}_{uv}e^{i\hat{H}\tau/\hbar}\,\Gamma(\hat{\mathbf{R}})|b\rangle\langle a|e^{-i\hat{H}\tau/\hbar}\right\} \quad . \end{aligned} \tag{II.44}$$

The corresponding results for $|u\rangle\langle v|$ and $|v\rangle\langle u|$ as the initial electronic states can then be expressed as linear combinations of the results in Eq. (II.44). For example:

$$\begin{aligned} &\mathrm{Tr}\left\{\hat{\Omega}\,|u\rangle\langle v|e^{i\hat{H}\tau/\hbar}\,\Gamma(\hat{\mathbf{R}})|b\rangle\langle a|e^{-i\hat{H}\tau/\hbar}\right\} \\ &\quad= \mathrm{Tr}\left\{\hat{\Omega}\,\hat{X}_{uv}e^{i\hat{H}\tau/\hbar}\,\Gamma(\hat{\mathbf{R}})|b\rangle\langle a|e^{-i\hat{H}\tau/\hbar}\right\} \\ &\qquad+ i\mathrm{Tr}\left\{\hat{\Omega}\,\hat{Y}_{uv}e^{i\hat{H}\tau/\hbar}\,\Gamma(\hat{\mathbf{R}})|b\rangle\langle a|e^{-i\hat{H}\tau/\hbar}\right\} \\ &\qquad- \frac{1}{2}(1+i)\mathrm{Tr}\left\{\hat{\Omega}\,|u\rangle\langle u|e^{i\hat{H}\tau/\hbar}\,\Gamma(\hat{\mathbf{R}})|b\rangle\langle a|e^{-i\hat{H}\tau/\hbar}\right\} \\ &\qquad- \frac{1}{2}(1+i)\mathrm{Tr}\left\{\hat{\Omega}\,|v\rangle\langle v|e^{i\hat{H}\tau/\hbar}\,\Gamma(\hat{\mathbf{R}})|b\rangle\langle a|e^{-i\hat{H}\tau/\hbar}\right\} \quad . \end{aligned} \tag{II.45}$$

II.6 Results for a Spin-Boson Model

In this section, the applicability and robustness of the M-GQME is demonstrated by obtaining the memory kernel via Ehrenfest-based projection-free inputs and applying the M-GQME to a spin-boson model system with two electronic states [donor (D) and acceptor (A)], harmonic electronic PESs which are shifted in equilibrium energy and geometry, and an electronic coupling coefficient which is assumed to be constant (Condon approximation). The overall Hamiltonian is given by:

$$\hat{H} = \hat{H}_D|D\rangle\langle D| + \hat{H}_A|A\rangle\langle A| + V_{DA}|D\rangle\langle A| + V_{AD}|A\rangle\langle D| \ , \tag{II.46}$$

where

$$\begin{aligned}
\hat{H}_D &= \epsilon + \sum_{i=1}^{N_n} \left[\frac{\hat{P}_i^2}{2} + \frac{1}{2}\omega_i^2 \hat{R}_i^2 - c_i \hat{R}_i \right] \quad , \\
\hat{H}_A &= -\epsilon + \sum_{i=1}^{N_n} \left[\frac{\hat{P}_i^2}{2} + \frac{1}{2}\omega_i^2 \hat{R}_i^2 + c_i \hat{R}_i \right] \quad , \\
V_{DA} &= V_{AD} = \Gamma \quad .
\end{aligned} \tag{II.47}$$

Here, Γ is a positive constant, 2ϵ is the shift in equilibrium energy between the donor and acceptor states ($\epsilon = 0$ and $\epsilon \neq 0$ correspond to the unbiased and biased cases, respectively) and $2c_i/\omega_i^2$ is the corresponding shift in equilibrium geometry along the i-th mode coordinate. Since this system satisfies the Condon approximation, the projection-free inputs $\mathcal{F}_1(\tau)$ and $\mathcal{F}_2(\tau)$ are used to obtain the memory kernel as shown in Sec. II.4.

Also compared are the results obtained based on the M-GQME scheme to those obtained from GQME-based schemes that start out with the overall Hamiltonian in a system-bath form. The schemes used are the Shi-Geva[28] (SG-NZ) and Zhang-Ka-Geva[29] (ZKG-NZ) system-bath-based schemes (see Sec. II.2), that have the form of Eq. (II.1) with the system, bath, and system-bath terms given by:

$$\begin{aligned}
\hat{H}_S &= \epsilon \left[|D\rangle\langle D| - |A\rangle\langle A| \right] + \Gamma \left[|D\rangle\langle A| + |A\rangle\langle D| \right] \quad , \\
\hat{H}_B &= \frac{1}{2}\left[\hat{H}_D + \hat{H}_A \right] = \sum_{i=1}^{N_n} \frac{\hat{P}_i^2}{2} + \frac{1}{2}\omega_i^2 \hat{R}_i^2 \quad , \\
\hat{H}_{BS} &= -\sum_{i=1}^{N_n} c_i R_i \left[|D\rangle\langle D| - |A\rangle\langle A| \right] \quad .
\end{aligned} \tag{II.48}$$

The values of $\{\omega_i\}$ and $\{c_i\}$ ($i = 1, ..., N_n$) are obtained based on an Ohmic spectral density with exponential cutoff:

$$J(\omega) = \frac{\pi}{2} \sum_{i=1}^{N_n} \frac{c_i^2}{\omega_i} \delta(\omega - \omega_i) \overset{N_n \to \infty}{\longrightarrow} \frac{\pi\hbar}{2} \xi \omega e^{-\omega/\omega_c} \tag{II.49}$$

Here, ξ is the Kondo parameter (a measure of the shift in equilibrium geometry) and ω_c is the cutoff frequency. The discrete set of N_n nuclear mode frequencies, $\{\omega_1, ..., \omega_{N_n}\}$, and coupling coefficients, $\{c_1, ..., c_{N_n}\}$, for the Ohmic spectral density with exponential cutoff, Eq. (III.25), were obtained following the procedure described in Ref. 68:

$$\omega_i = -\omega_c \ln\left(1 - i\frac{\omega_0}{\omega_c}\right) \tag{II.50}$$

$$c_i = \sqrt{\xi\hbar\omega_0}\omega_i \ . \tag{II.51}$$

Here, the i in Eq. (II.50) refers to the number of the mode (rather than the imaginary unit) and

$$\omega_0 = \frac{\omega_c}{N_n}\left(1 - e^{-\omega_{\text{max}}/\omega_c}\right) \ , \tag{II.52}$$

where $\omega_{N_n} = \omega_{\text{max}}$ is the frequency of the highest frequency mode.

The value of ω_{max} is determined using the following procedure. First the parameter α is defined as

$$\alpha = \frac{\int_0^{\omega_{\text{max}}} d\omega J(\omega)}{\int_0^{\infty} d\omega J(\omega)} = 1 - e^{-\omega_{\text{max}}/\omega_c}\left(\frac{\omega_{\text{max}}}{\omega_c} + 1\right) \ . \tag{II.53}$$

The parameter α controls the discretized spectral density. A value close to one yields a spectral density that covers high frequencies but at the cost of an overall coarse-grained frequency distribution. This could be compensated by an increased number of modes at the expense of increased computational costs. In practice, the actual value of α is determined in a manner that balances accuracy with cost. For the calculations reported in this paper, the value of α was set to 0.95.

Given the value of α, ω_{max} can be determined from Eq. (II.53),

$$\omega_{\text{max}} = -\left[W\left(\frac{1-\alpha}{e}\right) - 1\right]\omega_c \ , \tag{II.54}$$

where $W(x)$ is the Lambert W function, $W(xe^x) = x$. $W(x)$ was calculated numerically using the python library function $scipy.special.lambertw(x, i, tol)$ with $x = (\alpha - 1)/e$, $\alpha = 0.95$, $i = -1$,

and $tol = 10^{-6}$, with the result rounded to the next whole integer for ω_{max}.

The initial state of the nuclear DOF was chosen as:

$$\hat{\rho}_n(0) = \frac{e^{-\beta \hat{H}_B}}{\text{Tr}_n\left\{e^{-\beta \hat{H}_B}\right\}} \ , \tag{II.55}$$

where $\hat{H}_B$ is as in Eq. (II.48) and the initial nuclear position and momenta are sampled based on the Wigner transform of Eq. (III.26),

$$\rho_{n,W}(\mathbf{R},\mathbf{P};0) = \prod_{i=1}^{N_n} \frac{\tanh(\beta\hbar\omega_i/2)}{\pi\hbar} \exp\left[-\frac{2\tanh(\beta\hbar\omega_i/2)}{\hbar\omega_i}\left(\frac{P_i^2}{2}+\frac{1}{2}\omega_i^2 R_i^2\right)\right] \ . \tag{II.56}$$

It should be noted that this particular choice is dictated by our desire to compare the M-GQME scheme with the SG-NZ and ZKG-NZ schemes, which require that the initial nuclear state corresponds to thermal equilibrium with respect to the bath Hamiltonian, by definition and to eliminate the inhomogeneous term, respectively. At the same time, it is also important to emphasize that the M-GQME is designed to accommodate arbitrary initial nuclear states of one's choice.

Calculations were carried out for five different sets of parameter values (see Table III.1) averaged over 10^5 trajectories. The memory kernel and projection-free inputs elements were found to have the following properties:

(i) $\mathcal{K}_{jjuv}(\tau) = \mathcal{F}_{1,jjuv}(\tau) = \mathcal{F}_{2,jjuv}(\tau) = 0$,

(ii) and $\mathcal{K}_{jkuv}(\tau) = \mathcal{K}^*_{kjvu}(\tau)$; $\mathcal{F}_{1,jkuv}(\tau) = \mathcal{F}^*_{1,kjvu}(\tau)$; $\mathcal{F}_{2,jkuv}(\tau) = -\mathcal{F}^*_{2,kjvu}(\tau)$.

The nonvanishing matrix elements of the memory kernel superoperators, which were calculated using the Ehrenfest method and the population difference between donor and acceptor states, which corresponds to the expectation value of $\hat{\sigma}_z(t) = |D\rangle\langle D|(t) - |A\rangle\langle A|(t)$, for models #1-5 are shown in Figs. II.1-II.5, respectively. Exact results were adopted from Ref. 44 for models #1-4 and from Ref. 69 for model #5. The nonvanishing matrix elements of the projection-free input superoperators $\mathcal{F}_1(\tau)$ and $\mathcal{F}_2(\tau)$ for models #2 and #3 are given in Figs. II.8-II.9 .

Table II.1: Model and simulation parameters

	model parameters					numerical parameters		
Model #	ϵ	Γ	β	ξ	ω_c	ω_{max}	N_n	Δt
1	1.0	1.0	5.0	0.1	1.0	5	400	0.02
2	1.0	1.0	5.0	0.1	2.0	10	400	0.02
3	1.0	1.0	5.0	0.1	7.5	36	400	0.02
4	1.0	1.0	5.0	0.4	2.0	10	400	0.02
5	0.0	$0.\overline{33}$	3.0	0.1	1.0	5	200	0.02

One observation that can be gleamed from Figs. II.1-II.5 is that the M-GQME and ZKG-NZ schemes produce memory kernels that are better behaved at long time than those produced by the SG-NZ scheme. More specifically, with the exception of model #1, the memory kernels obtained via the SG-NZ scheme are observed to oscillate asymptotically, rather than vanish.

The instabilities of the Ehrenfest-based SG-NZ memory kernels have been reported in previous studies.[32,44] In one previous study,[44] these instabilities were dealt with by truncating the memory kernel at short times. This indeed reproduces the population dynamics reported in Ref. 44, which also happens to be in excellent agreement with the exact result (see Fig. II.6). For example, in the case of model #4, this meant truncating the memory kernel at $t_{\text{mem}} = 1.5\,\Gamma^{-1}$.[44] However, truncating the memory kernel at $t_{\text{mem}} = 1.5\,\Gamma^{-1}$ also causes the M-GQME and ZKG-NZ to disagree with the exact result. A closer inspection of Fig. II.4 reveals that the memory kernel is actually longer lived and that truncating it at $t_{\text{mem}} = 10.0\,\Gamma^{-1}$ would be more reasonable.[70] Indeed, truncating the memory kernel at $t_{\text{mem}} = 10.0\,\Gamma^{-1}$ rather than at $t_{\text{mem}} = 1.5\,\Gamma^{-1}$ significantly improves the agreement between the population dynamics produced by M-GQME and ZKG-NZ and the exact result (see Fig. II.4). At the same time, it also causes the population dynamics produced by the SG-NZ to oscillate asymptotically around the exact result, which is consistent with a similar observation made in Ref. 44. In another previous study,[32] the memory time was determined by a "plateau of stability" found in the $\sigma_z(t)$ dynamics with respect to the memory time. However, as shown in Fig. II.7 and acknowledged in Ref. 32, this plateau can be short-lived or nonexistent. Additionally, determination of the plateau of stability without knowledge of the exact results can be challenging.

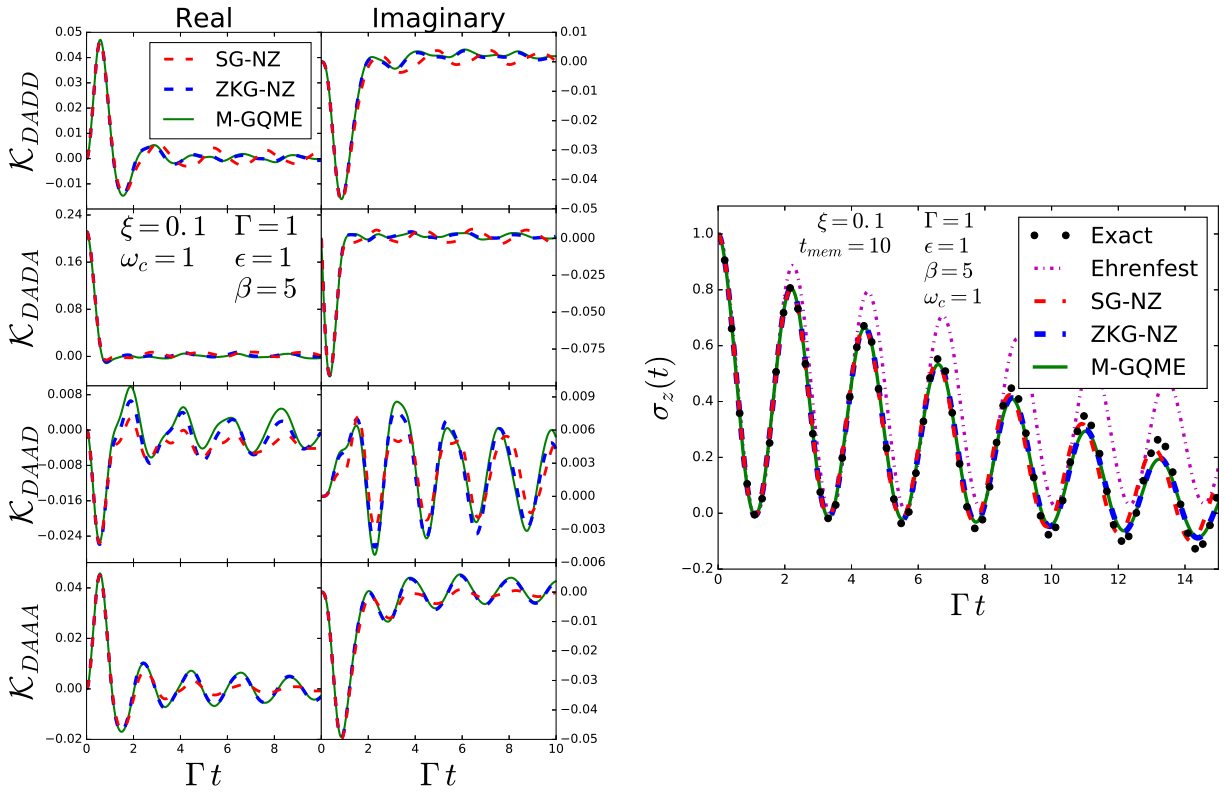

Figure II.1: On the left are the real and imaginary parts of the nonvanishing matrix elements of the memory kernel for model #1 in Table III.1. Shown are memory kernels obtained via the SG-NZ (dashed red), ZKG-NZ (dashed blue), and M-GQME (solid green) schemes. The memory kernels of all three schemes perform similarly for this set of parameters, with all elements having finite lifetimes.
On the right is the electronic population difference as a function of time for model #1 in Table III.1. Shown are the exact result as well as the results obtained via direct application of the Ehrenfest method and via SG-NZ, ZKG-NZ, and M-GQME with memory kernel calculated via the Ehrenfest method. Notably, the direct application of Ehrenfest yields worse results than any of the GQME approaches that use Ehrenfest as input.

In comparison, $\sigma_z(t)$ dynamics within the M-GQME and ZKG-NZ schemes converge smoothly, as seen in Fig. II.7, which makes finding a plateau of stability unnecessary. The M-GQME and ZKG-NZ convergence are obtained with a memory time equal to the lifetime of the memory kernel, e.g., $t_{\text{mem}} = 10.0\,\Gamma^{-1}$ in the case of model #4.

Another observation is that the population dynamics produced by M-GQME, ZKG-NZ, and SG-NZ with memory kernels obtained via the Ehrenfest method are in much better agreement with the exact result than the population dynamics obtained via direct application of the Ehrenfest

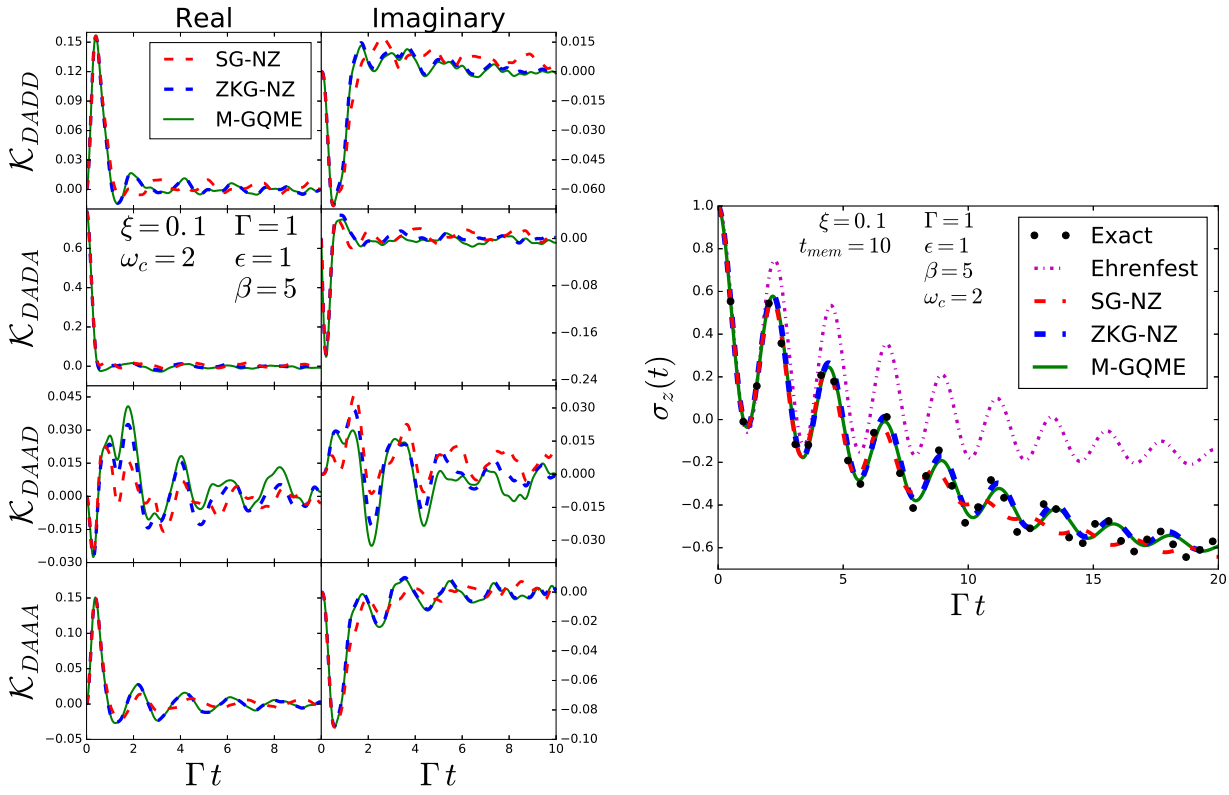

Figure II.2: On the left are the real and imaginary parts of the nonvanishing matrix elements of the memory kernel for model #2 in Table III.1. Shown are memory kernels obtained via the SG-NZ (dashed red), ZKG-NZ (dashed blue), and M-GQME (solid green) schemes. The memory kernels of all three schemes perform similarly for this set of parameters, with some elements having slightly more erratic behavior than seen in the model #1 memory kernels given in Fig. II.1.
On the right is the electronic population difference as a function of time for model #2 in Table III.1. Shown are the exact result as well as the results obtained via direct application of the Ehrenfest method and via SG-NZ, ZKG-NZ, and M-GQME with memory kernel calculated via the Ehrenfest method. While still showing markedly better results than the direct application of Ehrenfest, the SG-NZ GQME approach deviates from the exact results at longer times more so than the ZKG-NZ and M-GQME approaches.

method. At first sight, this is somewhat surprising, given that the memory time, $t_{\text{mem}} = 10.0\,\Gamma^{-1}$, is comparable to the population relaxation time scale. However, it should be noted that within the GQME, the effect of the density operator at time $t - \tau$ on its dynamics at time t decreases with increasing τ due to the finite lifetime of the memory kernel. Thus, as the Ehrenfest method becomes less accurate with increasing time, its contribution to the dynamics through $\mathcal{K}(\tau)$ diminishes as well. As a result, using the Ehrenfest method to calculate the memory kernel leads to

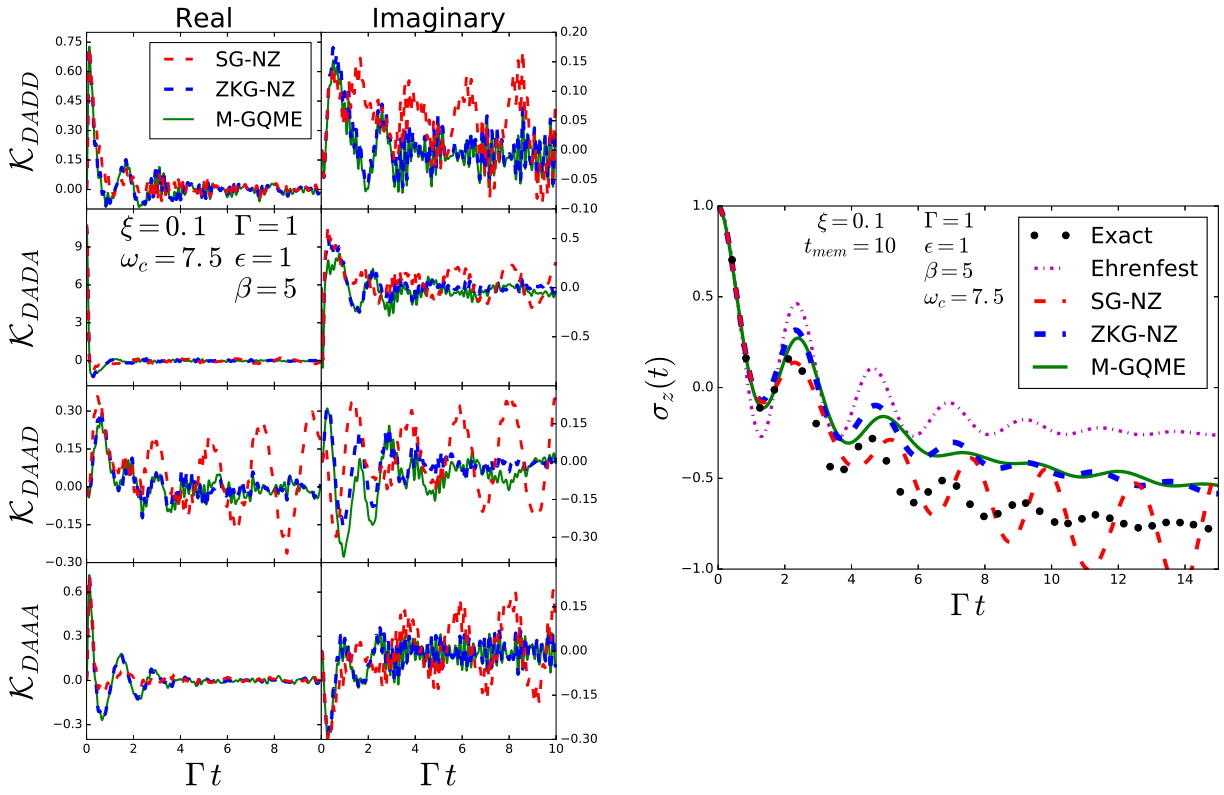

Figure II.3: On the left are the real and imaginary parts of the nonvanishing matrix elements of the memory kernel for model #3 in Table III.1. The SG-NZ memory kernel (dashed red) has long-time oscillations not seen in the M-GQME memory kernel (solid green) and ZKG-NZ memory kernel (dashed blue). All three memory kernels show higher instability compared to the memory kernels of models #1 and #2, shown in Figs. II.1 and II.2.
On the right is the electronic population difference as a function of time for model #3 in Table III.1. Shown are the exact result as well as the results obtained via direct application of the Ehrenfest method and via SG-NZ, ZKG-NZ, and M-GQME with memory kernel calculated via the Ehrenfest method. While still performing better than the direct application of Ehrenfest, the GQME approaches show significant departure from the exact results. The reason for this can be traced to the breakdown of the validity of the treatment of the nuclear DOF as classical within the Ehrenfest method when the frequency of the nuclear modes increases.

significantly more accurate results than using the Ehrenfest method to calculate the population dynamics directly. It should be noted that the authors of Ref. 32 also argued that the improvement of the GQME over direct Ehrenfest could be due to the additional information about the electronic-nuclear coupling gained through the sampling of nuclear operators within the inputs for the memory kernel.

Yet another interesting observation is the loss of accuracy and stability of the memory kernels

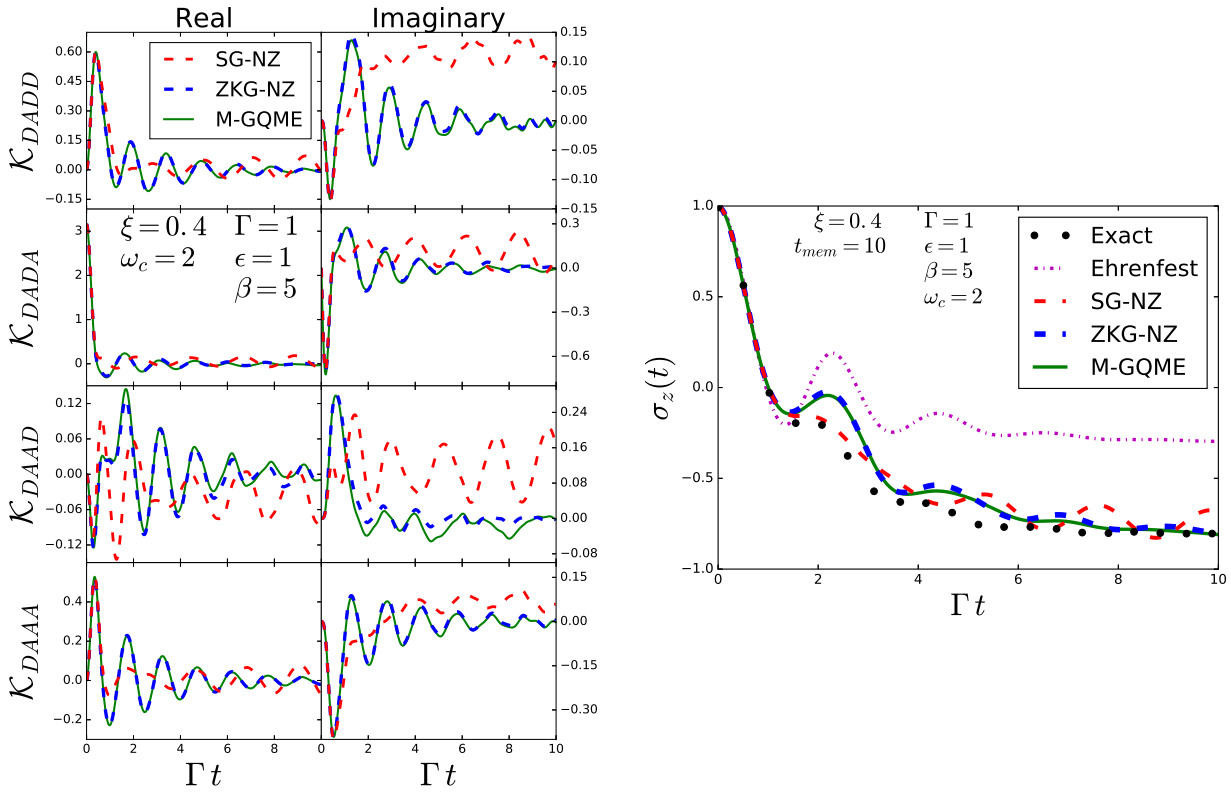

Figure II.4: On the left are the real and imaginary parts of the nonvanishing matrix elements of the memory kernel for model #4 in Table III.1. The SG-NZ memory kernel (dashed red) has long-time oscillations not seen in the M-GQME memory kernel (solid green) and ZKG-NZ memory kernel (dashed blue), with some elements of the SG-NZ memory kernel oscillating around values other than zero. This behavior leads to varying electronic population difference dynamics for the SG-NZ scheme with different memory times as shown in the graph on the right and in Fig. II.6. On the right is the electronic population difference as a function of time for model #4 in Table III.1. Shown are the exact result as well as the results obtained via direct application of the Ehrenfest method and via SG-NZ, ZKG-NZ, and M-GQME with memory kernel calculated via the Ehrenfest method. While initially closer to the exact results, the SG-NZ GQME approach shows asymptotic oscillations at longer times which are not seen in the ZKG-NZ and M-GQME approaches.

with increasing cutoff frequency, ω_c (see Figs. II.1-II.3). This can be traced back to the treatment of the nuclear DOF as classical within the Ehrenfest method. More specifically, increasing ω_c corresponds to increasing the frequency of the nuclear modes and thereby making the assumption that they can be treated as classical less valid. Along with the increasing instability, another trend seen in Figs. II.1-II.3 is that with the increasing cutoff frequency, the scale of the memory kernels also increases.

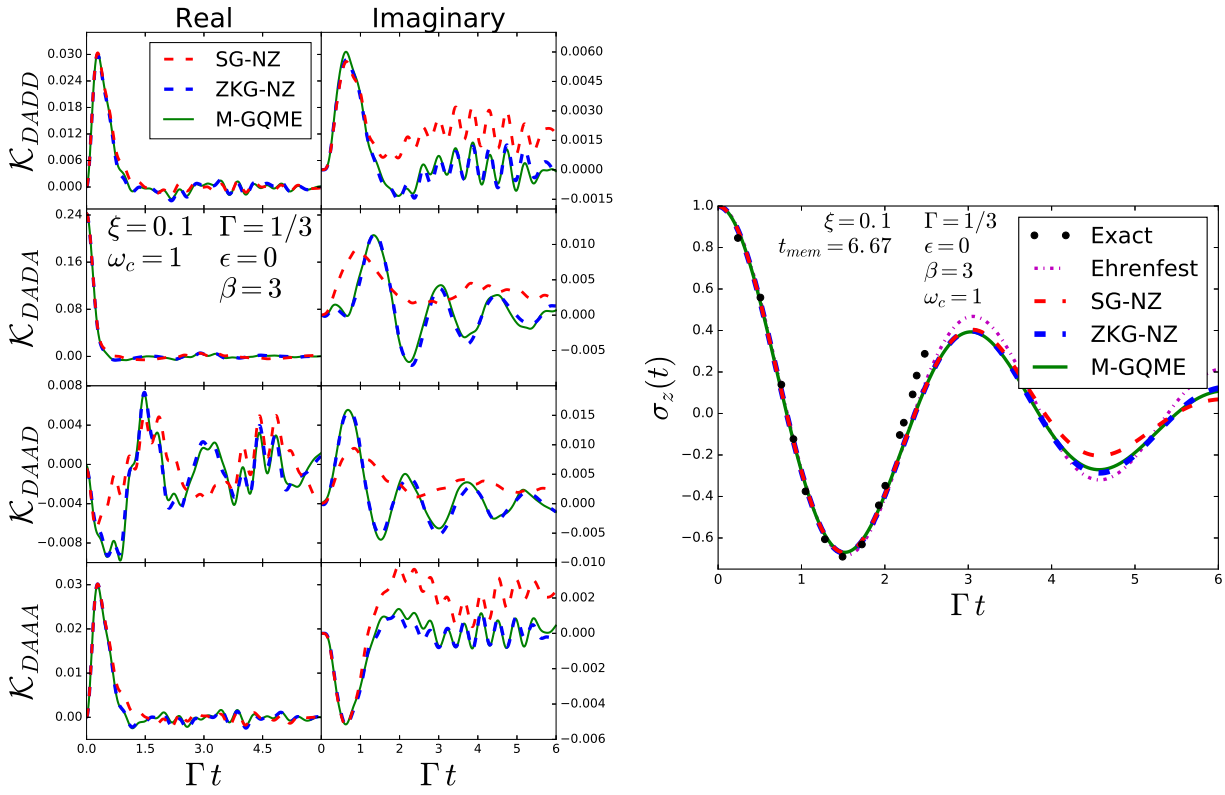

Figure II.5: On the left are the real and imaginary parts of the nonvanishing matrix elements of the memory kernel for model #5 in Table III.1. The ZKG-NZ memory kernel (dashed blue) and M-GQME memory kernel (solid green) perform similarly while the SG-NZ memory kernel (dashed red) displays different behavior, with some elements not converging to zero.
On the right is the electronic population difference as a function of time for model #5 in Table III.1. Shown are the exact result as well as the results obtained via direct application of the Ehrenfest method and via SG-NZ, ZKG-NZ, and M-GQME with memory kernel calculated via the Ehrenfest method. For the unbiased case, good agreement is seen between all approaches and the exact results. This is a notable deviation from the biased cases, where direct application of Ehrenfest is unable to capture the exact dynamics while the GQME approaches give significantly more accurate results, particularly for the ZKG-NZ and M-GQME approaches.

Finally, it is interesting to contrast the biased case ($\epsilon \neq 0$, Figs. II.1-II.4), with the unbiased case ($\epsilon = 0$, Fig. II.5). While direct application of the Ehrenfest method appears to produce rather accurate results in the unbiased case, it is observed to lead to significant deviations in the biased case. This can be traced back to the Ehrenfest method's failure to capture detailed balance. Interestingly, restricting the use of the Ehrenfest method to calculating the memory kernel and simulating the electronic dynamics through the GQME gives rise to significantly more accurate results

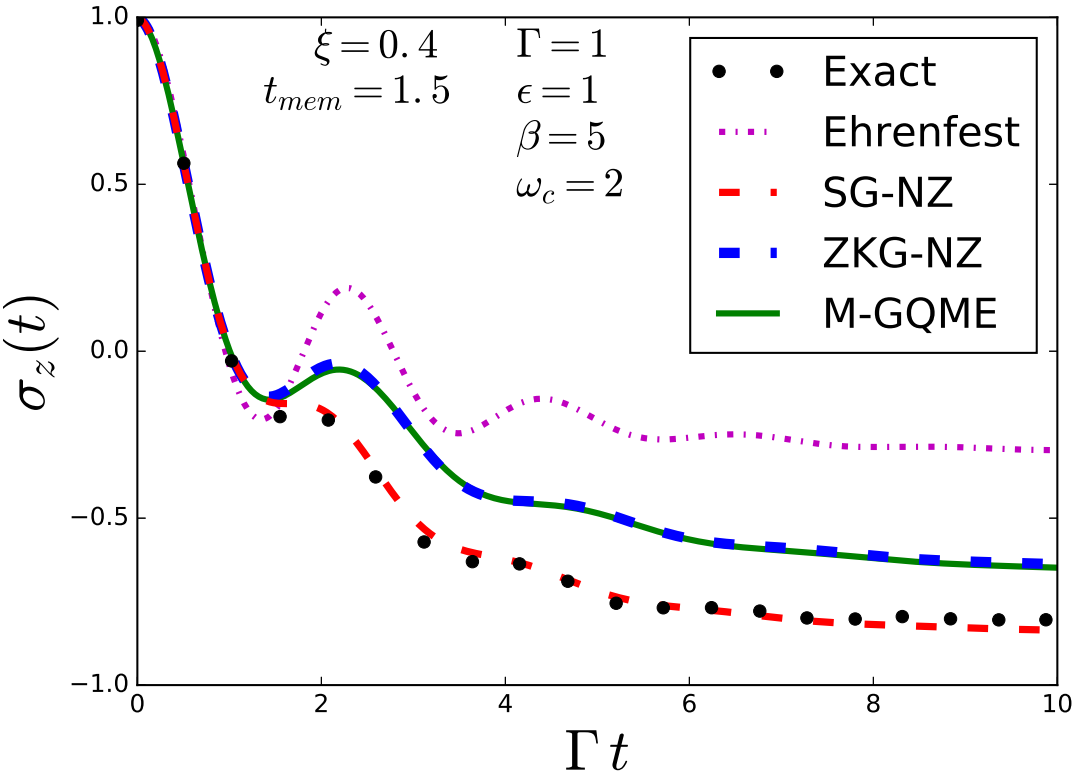

Figure II.6: Electronic population difference as a function of time for model #4 in Table III.1 with the memory truncated at $t_{\text{mem}} = 1.5\,\Gamma^{-1}$. Shown are the exact result as well as the results obtained via direct application of the Ehrenfest method and via SG-NZ, ZKG-NZ, and M-GQME with memory kernel calculated via the Ehrenfest method. Here, the SG-NZ GQME approach achieves good agreement with the exact results while the ZKG-NZ and M-GQME approaches show significant differences. However, as seen in Fig. II.4, a memory time of $t_{\text{mem}} = 10.0\,\Gamma^{-1}$ is more reasonable than $t_{\text{mem}} = 1.5\,\Gamma^{-1}$; this leads to the results shown in Fig. II.4, where the ZKG-NZ and M-GQME approaches obtain better agreement with the exact results than the SG-NZ approach.

in the biased case. It should be noted that given the quantum-mechanically exact memory kernel, the GQME is guaranteed to satisfy detailed balance since it corresponds to the exact equation of motion of the electronic DOF. The fact that it still does rather well even when the memory kernel is calculated via the Ehrenfest method should be considered as yet another advantage of the GQME approach.

II.7 Concluding Remarks

Although the system-bath paradigm has been a central theme in the study of quantum open systems, there are cases where it is not desirable to cast the overall Hamiltonian in system-bath form, Eq. (II.1). A prime example is nonadiabatic dynamics, where it is neither natural nor convenient to cast the Hamiltonian in terms of a system Hamiltonian, which only depends on the electronic DOF, a bath Hamiltonian, which only depends on the nuclear DOF, and a system-bath interaction term, which couples them. This is because the overall Hamiltonian underlying nonadiabatic dynamics associates a *different* nuclear Hamiltonian with each electronic state, thereby making the definition of a single bath Hamiltonian non-unique and essentially arbitrary. The lack of a unique system-bath Hamiltonian can be particularly problematic when approximate methods are used to evaluate the memory kernel, as would often be the case when dealing with realistic molecular models, since different choices of bath Hamiltonian may lead to different results without a clear criterion for choosing between them.

This chapter utilized the fact that the GQME, which represents the exact equation of motion of the electronic DOF during nonadiabatic dynamics, does not in fact need to be based on casting the overall Hamiltonian in system-bath form.[32,65,71] This form of the GQME is referred to as the M-GQME. Also presented is a practical scheme for calculating the memory kernel of the M-GQME, either exactly or approximately, that does not rely on the system-bath form. In doing so, we end up with a natural and convenient GQME-based approach for simulating the dynamics of the electronic DOF during nonadiabatic dynamics.

It should be noted that unlike other methods for simulating nonadiabatic dynamics, such as Ehrenfest, surface hopping, MQCL, and SQC, the approach based on the M-GQME is focused on the dynamics of the electronic DOF. The dynamics of the nuclear DOF is only captured to the extent that it impacts the electronic DOF. The memory kernel represents the minimum input of the nuclear DOF that is required in order to account for their effect on the dynamics of the electronic DOF. In this respect, the GQME can be thought of as going beyond approaches based on FGR,

where the coupling between the electronic and nuclear DOF is assumed weak and the impact of the nuclear DOF on the electronic DOF is captured by the two-time autocorrelation function of the coupling between nuclear and electronic DOF.[1,12–18] Unlike FGR-based approaches, the GQME does not require assuming weak coupling between electronic states and describes the electronic dynamics in terms of the full electronic density matrix, rather than in terms of the electronic populations, which correspond to its diagonal elements.

On the one hand, the loss of more detailed information on the dynamics of the nuclear DOF may be viewed as a disadvantage of the GQME-based approach to nonadiabatic dynamics. On the other hand, focusing on the memory kernel rather than on a complete description of the nuclear DOF, offers several important advantages. First, it is often the case that the only interesting aspect of the nuclear dynamics is its impact on the electronic dynamics. Thus, the compactness of the memory kernel provides an elegant way for focusing on this aspect without needing to figure out whether or not a given detail of the nuclear dynamics impacts the electronic DOF. Second, the compactness of the memory kernel and its finite memory time also implies that calculating it via a given method, either exact or approximate, can be more cost-effective and/or lead to more accurate results than a direct application of the same method. Third, it should be remembered that most useful approximate methods describe nuclear dynamics in terms of an ensemble of classical-like trajectories, and are constructed in such a way that only the ensemble average, rather than individual trajectories, can be related to physically meaningful measurable quantities like electronic populations and coherences. The fact that the memory kernel is defined in terms of a trace over the nuclear DOF implies that it incorporates this ensemble-averaging automatically and is therefore directly related to the only relevant measurable quantities.

In summary, the M-GQME provides a rigorous and general approach for simulating electronically nonadiabatic dynamics. Within this approach, the memory kernel superoperator is the key quantity which dictates how the electronic dynamics is impacted by the nuclear DOF, regardless of the strength or type of coupling. What makes this approach particularly appealing is the fact that calculating the memory kernel via exact or approximate methods can be more cost-effective and/or

accurate than direct application of those methods. Given the non-uniqueness associated with the choice of basis in Eq. (II.43), which appears to be inherent to the Ehrenfest method, it would also be highly desirable to explore calculating the memory kernel via approximate methods other than the Ehrenfest method. The following chapter will explore two different mapping Hamiltonian methods with a quasiclassical approximation that do not require the Eq. (II.43) and compare their results as input methods for the GQME to Ehrenfest.

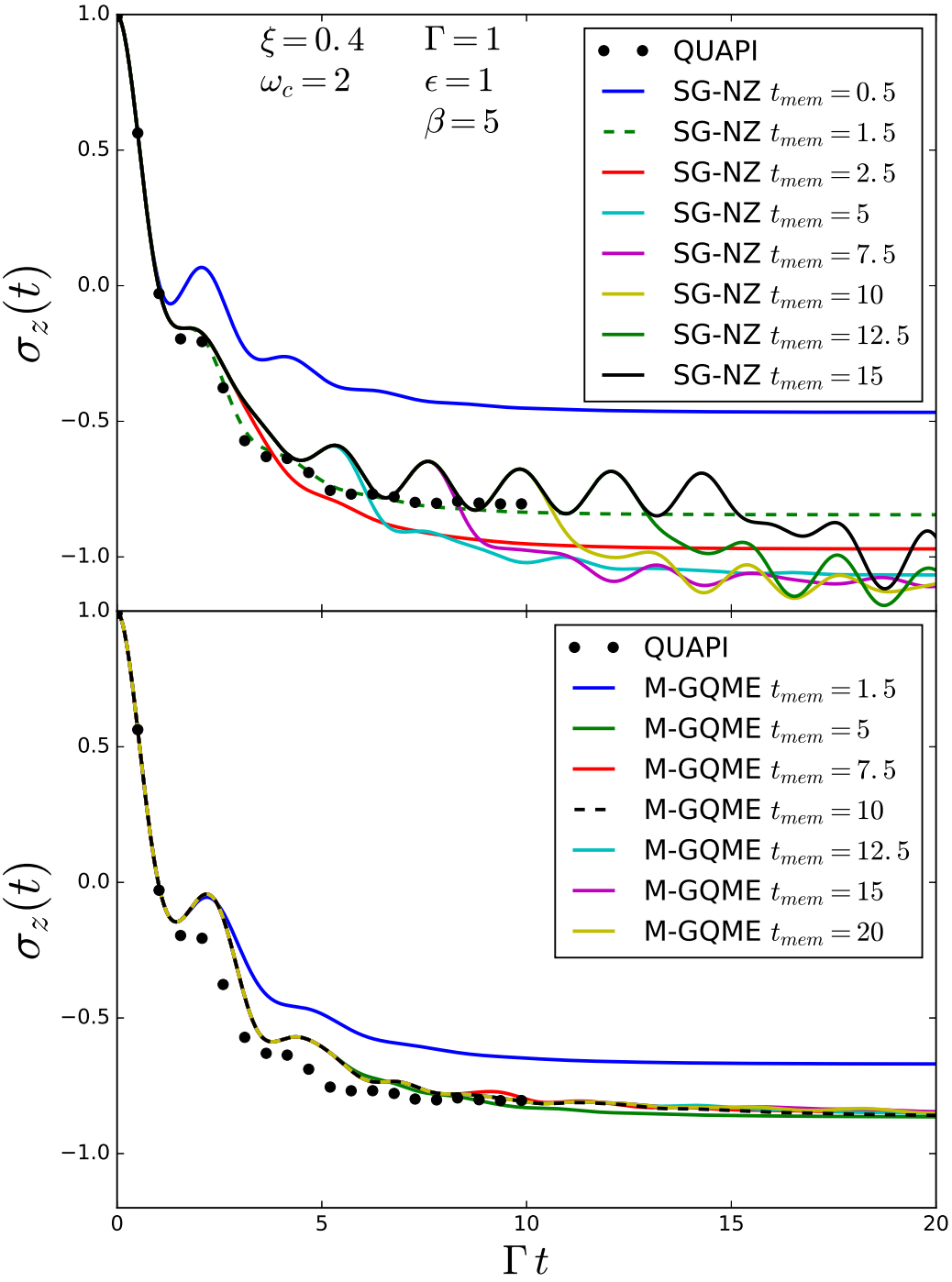

Figure II.7: Electronic population difference as a function of time for model #4 in Table III.1 with varying memory times for the SG-NZ method and the M-GQME method in the top graph and bottom graph, respectively. The SG-NZ method shows changing dynamics with differing memory time while the M-GQME converges to dynamics that do not change with increasing memory time. The dashed line in the top graph indicates the memory time used by Kelly et. al. (see Fig. II.6) and the dashed line in the bottom graph indicates the memory time used in this paper (see Fig. II.4).

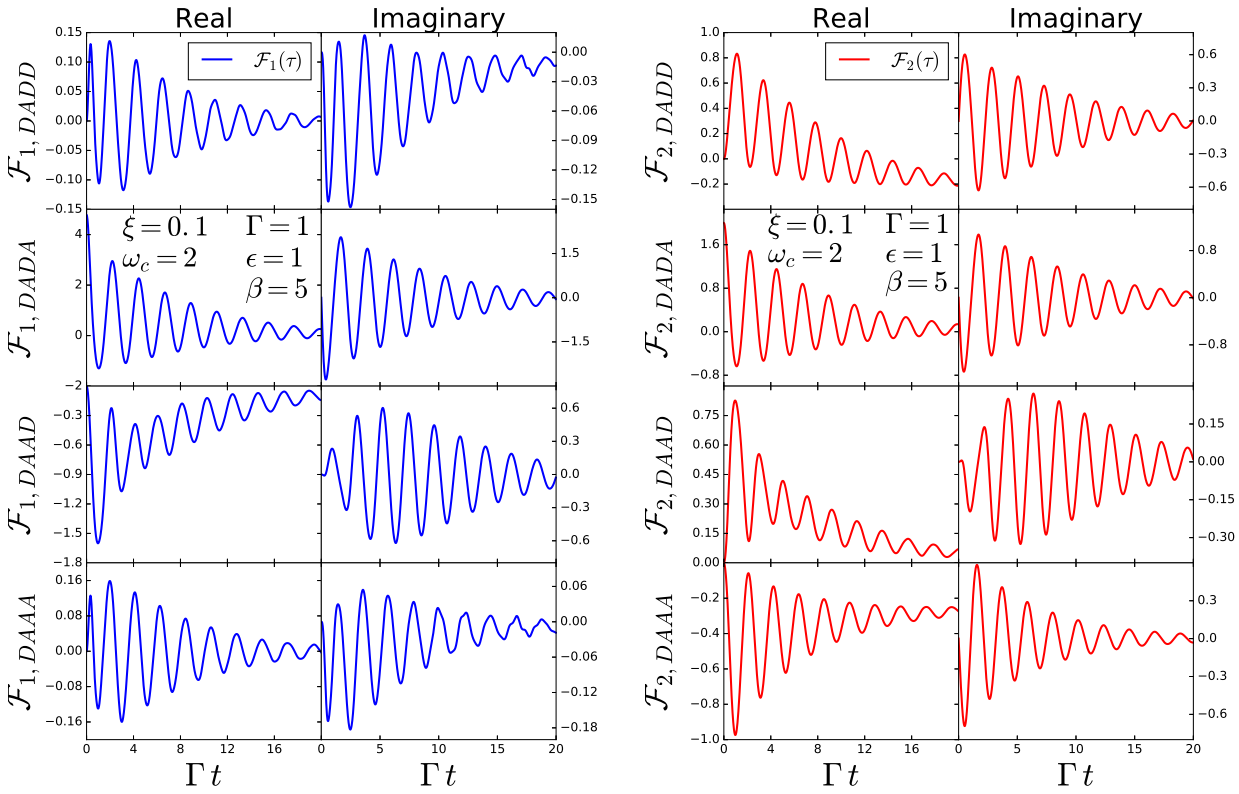

Figure II.8: The real and imaginary parts of the nonvanishing matrix elements of the projection-free input $\mathcal{F}_1(\tau)$ for model #2 in Table III.1. The lifetimes of the projection-free input $\mathcal{F}_1(\tau)$ and $\mathcal{F}_2(\tau)$ are more than double the lifetime of the M-GQME memory kernel for the same set of parameters, as shown in Fig. II.2. Also, the $DADD$ imaginary and $DAAD$ real elements for $\mathcal{F}_1(\tau)$ and the $DADD$ real, $DAAD$ real, and $DAAA$ real elements for $\mathcal{F}_2(\tau)$ appear to be converging to values other than zero.

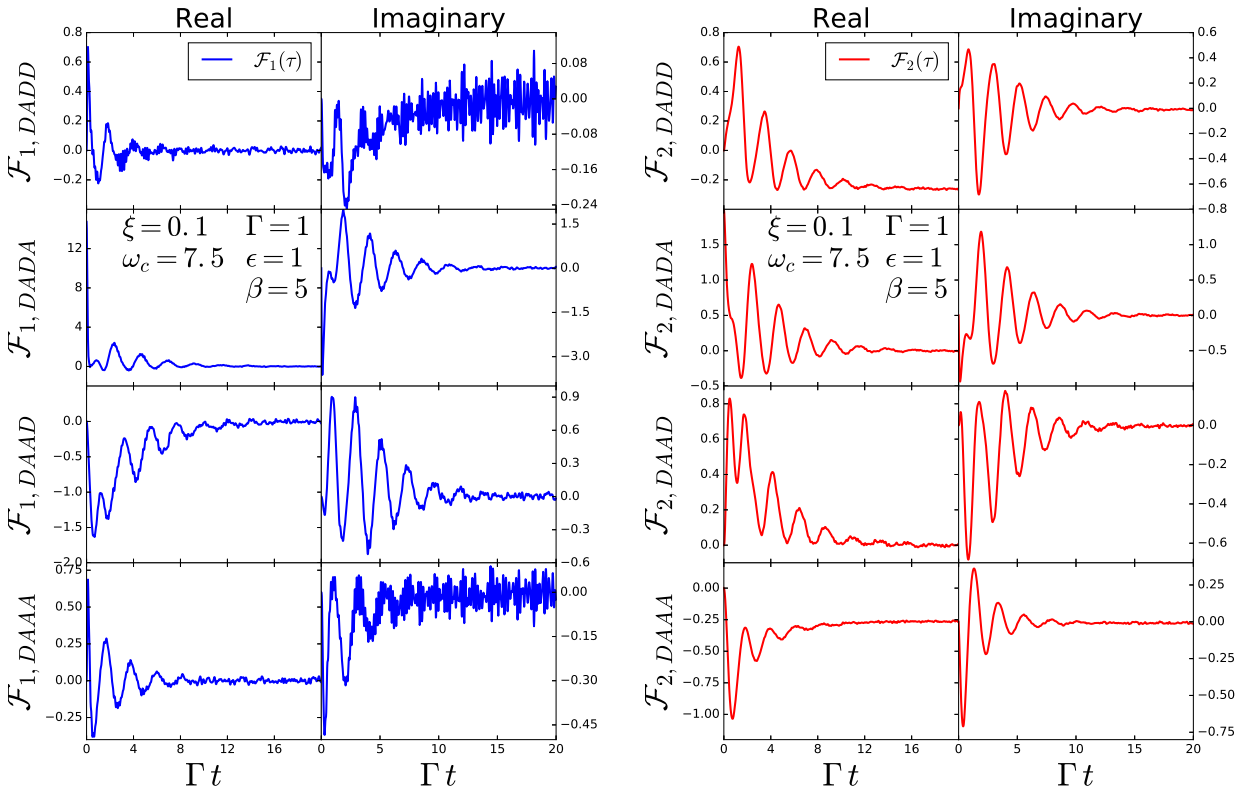

Figure II.9: The real and imaginary parts of the nonvanishing matrix elements of the projection-free input $\mathcal{F}_1(\tau)$ and $\mathcal{F}_2(\tau)$ for model #3 in Table III.1. The instability seen within the M-GQME memory kernel for this set of parameters (Fig. II.3) can also be seen in the projection-free input $\mathcal{F}_1(\tau)$. The lifetimes of the projection-free input $\mathcal{F}_1(\tau)$ and $\mathcal{F}_2(\tau)$ are closer to the lifetime of the corresponding memory kernel (Fig. II.3) compared to $\mathcal{F}_1(\tau)$, $\mathcal{F}_2(\tau)$, and $\mathcal{K}(\tau)$ of model #2, as seen in Figs. II.8 and II.2.

CHAPTER III

Mapping Hamiltonian + Quasiclassical Approximation Methods with the M-GQME

III.1 Introduction

The central quantity within the GQME framework is the memory kernel superoperator. The compact nature of the memory kernel (a $N_e^2 \times N_e^2$ matrix, where N_e is the number of electronic states involved) and the fact that it contains all the information needed to account for the effect of the nuclear DOF on the electronic DOF makes it a key quantity when it comes to determining the correlation between molecular structure and electronic dynamics. The memory kernel is often found to be short-lived compared to the time scale of the electronic dynamics it impacts, which suggests that the ability to accurately capture the electronic dynamics can be enhanced by restricting the use of approximate methods to calculating the memory kernel.[53] This is because the accuracy of the approximate methods often deteriorates with increasing time while the GQME is exact beyond the approximate method used to capture the short-lived memory kernel.

Several recent studies have pursued such a strategy with the Ehrenfest method as the approximate method of choice for calculating the memory kernel, including the one shown in Chapter II.[30,32,35] The Ehrenfest-based approach has met with considerable success for the benchmark models it was applied to (see Sec. II.6). However, there are several reasons for why extending the range of approximate methods used for calculating the memory kernel beyond the Ehrenfest method is desirable. First, being able to choose from different approximate methods can be beneficial, given

that the suitability of the approximate method can often be informed by the system and process it is applied to. Second, the requirement that the electronic density matrix be Hermitian in order for the mean force experienced by the nuclear DOF within the Ehrenfest method to be real has led to multiple protocols for calculating the memory kernel, which can give different answers, without a clear criterion for choosing between them.[32,35] Third, as a mixed quantum-classical method, the Ehrenfest method treats the dynamics of the electronic and nuclear DOF in terms of rather different quantities (a wave function or density matrix and phase-space variables, respectively). Treating both electronic and nuclear DOF as classical-like[72] could therefore make it easier to incorporate the method into existing classical molecular dynamics (MD) codes.

Approximate methods that seem to overcome some of these potential shortcomings of the Ehrenfest method can be obtained by combining the mapping Hamiltonian (MH) approach[72–80] with quasiclassical (QC) approximations, including the linearized semiclassical (LSC) approximation.[41,53,81–90] Within the resulting QC/MH methods, the electronic DOF are mapped onto classical-like variables, so that the dynamics of the overall system (electronic DOF + nuclear DOF) can be described in terms of classical-like trajectories. In addition, within LSC, the force on the nuclear DOF is real even when the initial electronic state is non-Hermitian.

Previous to the research outlined in this chapter, there was one other preliminary study that used a QC/MH approach for calculating the memory kernel;[53] the work presented herein extends upon it in several ways. First, two different ways of using a QC/MH method to calculate the memory kernel of the GQME are tested and compared. Second, the implementation is done within the framework of the recently introduced GQME formalism outlined in Sec. II.3, which is geared towards simulating electronically nonadiabatic dynamics.[35] Third, the accuracy of the QC/MH-based approaches are tested and compared to the Ehrenfest-based approach on a wider range of parameter space.

The remainder of this chapter is organized as follows. Two different versions of the QC/MH method are described in Sec. III.2. The calculation of the GQME memory kernel from projection-free inputs obtained via the QC/MH method is described in Sec. III.3. The utility and accuracy of

combining QC/MH with GQME are demonstrated on a benchmark model in Sec. III.4. Concluding remarks are offered in Sec. III.5.

III.2 The Mapping Hamiltonian (MH) Approach and Linearized Semiclassical (LSC) approximation

The MH approach is based on casting the complete set of purely electronic operators, $\{|j\rangle\langle k|\}$, onto an isomorphic set of operators, $\{M_{jk}\left(\hat{\mathbf{q}},\hat{\mathbf{p}}\right)\}$, that satisfy the same commutation relations:[72,73,91–98]

$$|j\rangle\langle k| \mapsto M_{jk}\left(\hat{\mathbf{q}},\hat{\mathbf{p}}\right) \quad . \tag{III.1}$$

Here, $\{\hat{\mathbf{q}},\hat{\mathbf{p}}\}$ represents a set of auxiliary Cartesian coordinate and momentum operators associated with the mapping (not to be confused with the coordinate and momentum operators of the actual electrons). The motivation for replacing the original set of electronic operators with the mapping operators can be traced back to the fact that unlike $\{|j\rangle\langle k|\}$, $\{M_{jk}\left(\hat{\mathbf{q}},\hat{\mathbf{p}}\right)\}$ have classical-like analogues. As a result, classical-like approximations can be constructed.

Within the MH approach, $|u\rangle\langle v|$ and $|k\rangle\langle j|$ in Eq. (I.8) are replaced by $M_{uv}\left(\hat{\mathbf{q}},\hat{\mathbf{p}}\right)$ and $M_{kj}\left(\hat{\mathbf{q}},\hat{\mathbf{p}}\right)$, respectively, so that:

$$\sigma_{jk}(t) = \sum_{u,v=1}^{N_e} \sigma_{uv}(0)\,\mathrm{Tr}\left\{\hat{\rho}_n(0) M_{uv}\left(\hat{\mathbf{q}},\hat{\mathbf{p}}\right) e^{i\hat{H}t/\hbar} M_{kj}\left(\hat{\mathbf{q}},\hat{\mathbf{p}}\right) e^{-i\hat{H}t/\hbar}\right\} \quad . \tag{III.2}$$

Applying the LSC approximation to Eq. (III.2), we obtain the following approximate expression for $\sigma_{jk}(t)$:[53,83]

$$\begin{aligned}\sigma_{jk}^{\mathrm{LSC}}(t) = &\left(\frac{1}{2\pi\hbar}\right)^N \sum_{u,v=1}^{N_e} \sigma_{uv}(0) \\ &\times \int \mathbf{dR}_0 \int \mathbf{dP}_0 \int \mathbf{dq}_0 \int \mathbf{dp}_0 \left[\hat{\rho}_n(0)\right]_W \left(\mathbf{R}_0,\mathbf{P}_0\right) [M_{uv}]_W \left(\mathbf{q}_0,\mathbf{p}_0\right) [M_{kj}]_W \left(\mathbf{q}_t,\mathbf{p}_t\right) \quad ,\end{aligned} \tag{III.3}$$

where $N = N_e + N_n$ is the total number of DOF of the overall system. The W subscripts in Eq. (III.3) denote the corresponding Wigner transforms,

$$\begin{aligned}
[M_{uv}]_W(\mathbf{q},\mathbf{p}) &= \int \mathbf{dz}\, e^{-i\mathbf{zp}/\hbar} \left\langle \mathbf{q}+\frac{\mathbf{z}}{2}\middle| M_{uv}(\hat{\mathbf{q}},\hat{\mathbf{p}}) \middle|\mathbf{q}-\frac{\mathbf{z}}{2}\right\rangle \quad , \\
[\hat{\rho}_n(0)]_W(\mathbf{R},\mathbf{P}) &= \int \mathbf{dZ}\, e^{-i\mathbf{ZP}/\hbar} \left\langle \mathbf{R}+\frac{\mathbf{Z}}{2}\middle| \hat{\rho}_n(0) \middle|\mathbf{R}-\frac{\mathbf{Z}}{2}\right\rangle \quad .
\end{aligned} \tag{III.4}$$

Importantly, $\{\mathbf{R}_t, \mathbf{P}_t, \mathbf{q}_t, \mathbf{p}_t\}$ are obtained by starting at the initial state $\{\mathbf{R}_0, \mathbf{P}_0, \mathbf{q}_0, \mathbf{p}_0\}$ and solving the classical Hamilton equations based on the following classical-like Hamiltonian:

$$H(\mathbf{R},\mathbf{P},\mathbf{q},\mathbf{p}) = \sum_{j=1}^{N_e} H_j(\mathbf{R},\mathbf{P})[M_{jj}]_W(\mathbf{q},\mathbf{p}) + \sum_{\substack{j,k=1 \\ k\neq j}}^{N_e} V_{jk}(\mathbf{R})[M_{jk}]_W(\mathbf{q},\mathbf{p}) \quad . \tag{III.5}$$

The above-mentioned QC/MH approach has several attractive features:

- **Advantageous computational cost:** The computational cost of calculating $\sigma_{jk}^{\mathrm{LSC}}(t)$ is the same as that of a classical MD simulation of a classical system with N DOF.

- **Captures feedback between nuclear and electronic dynamics:** The classical-like Hamiltonian in Eq. (III.5) couples $(\mathbf{R},\mathbf{P})$ and $(\mathbf{q},\mathbf{p})$. As a result, the electronic dynamics is affected by the nuclear dynamics and vice versa. Thus, feedback between the nuclear and electronic DOF, which is the central feature of electronically nonadiabatic dynamics, is captured by QC/MH.

- **Goes beyond Ehrenfest:** The initial electronic state is mapped onto $\sum_{j,k=1}^{N_e} \sigma_{jk}(0)[M_{uv}]_W(\mathbf{q}_0,\mathbf{p}_0)$, which implies a distribution over the initial conditions, $(\mathbf{q}_0,\mathbf{p}_0)$. This distribution arises from two sources: (i) $[M_{uv}]_W(\mathbf{q}_0,\mathbf{p}_0)$ is typically not a localized function of $(\mathbf{q}_0,\mathbf{p}_0)$ and thereby calls for sampling different initial $(\mathbf{q}_0,\mathbf{p}_0)$ and (ii) unless the system starts in one of the basis states, $\hat{\sigma}(0) = |j\rangle\langle j|$, different electronic density matrix elements will give rise to different $(\mathbf{q}_0,\mathbf{p}_0)$ distributions. Importantly, $(\mathbf{q}_t,\mathbf{p}_t)$ depend on $(\mathbf{q}_0,\mathbf{p}_0)$ and will differ from one choice of $(\mathbf{q}_0,\mathbf{p}_0)$ to another. Furthermore,

the dynamics of the nuclear DOF takes place on a PES which is explicitly dependent on $(\mathbf{q}_t, \mathbf{p}_t)$:

$$V(\mathbf{R}, t) = \sum_{j=1}^{N_e} [M_{jj}]_W(\mathbf{q}_t, \mathbf{p}_t) V_j(\mathbf{R}) + \sum_{\substack{j,k=1 \\ k \neq j}}^{N_e} [M_{jk}]_W(\mathbf{q}_t, \mathbf{p}_t) V_{jk}(\mathbf{R}) \quad . \tag{III.6}$$

Thus, the same choice of $(\mathbf{R}_0, \mathbf{P}_0)$ can lead to multiple $(\mathbf{R}_t, \mathbf{P}_t)$ since different choices of $(\mathbf{q}_0, \mathbf{p}_0)$ would lead to different $(\mathbf{q}_t, \mathbf{p}_t)$ and thereby different forces that the nuclear DOF are subject to. This is similar to surface hopping methods (although in this case, the force terms change continuously) but should be contrasted with the Ehrenfest method, where the force on the nuclear DOF is obtained by averaging over the entire instantaneous electronic state and thereby does not allow for such multiplicity of nuclear trajectories to emerge.

- **Treats electronic populations and coherences on equal footing:** Populations and coherences have their own mapping variables $\{[M_{jj}]_W(\mathbf{q}, \mathbf{p})$ for populations and $[M_{jk}]_W(\mathbf{q}, \mathbf{p})$, with $j \neq k$, for coherences$\}$. This should be contrasted with the Ehrenfest method, where states with non-zero coherences can give rise to complex forces on the nuclear DOF, and with surface hopping methods, which is focused on population transfer between electronic states and underestimates decoherence.[99,100]

The actual choice of mapping variables is not unique and multiple choices of mapping variables have been proposed and employed.[95–98] This can be considered an advantage due to the flexibility it allows for choosing a mapping approach which would be best suited to the problem at hand. The research presented in this chapter adopted the widely used choice proposed by Stock and Thoss (ST)[74] (sometimes also referred to in the literature as the Meyer-Miller mapping, due to its similarity to the mapping proposed earlier by Meyer and Miller[73]).

Within the ST mapping, each electronic state is associated with a different quantum harmonic oscillator. The creation and annihilation operators of these independent harmonic oscillators, $\left\{\hat{a}_j, \hat{a}_j^\dagger \middle| j = 1, ..., N_e\right\}$, satisfy the following commutation relations: $\left[\hat{a}_j, \hat{a}_j^\dagger\right] = \delta_{jk}$. The elec-

tronic operators, $\{|j\rangle\langle k|\}$, are then mapped onto harmonic oscillator operators[74]

$$|j\rangle\langle k| \mapsto \hat{a}_j^\dagger \hat{a}_k \quad . \tag{III.7}$$

The mapping in Eq. (III.7) is justified by the fact that $\{|j\rangle\langle k|\}$ and $\{\hat{a}_j^\dagger \hat{a}_k\}$ satisfy the same commutation relations among themselves. Using Eq. (III.7), the Hamiltonian in Eq. (I.3) can also be cast in terms of $\{\hat{a}_j, \hat{a}_j^\dagger\}$:

$$\hat{H} = \sum_{j=1}^{N_e} \hat{H}_j \hat{a}_j^\dagger \hat{a}_j + \sum_{\substack{j,k=1 \\ k\neq j}}^{N_e} \hat{V}_{jk} \hat{a}_j^\dagger \hat{a}_k \quad . \tag{III.8}$$

It should be noted that the electronic closure relation, $\sum_{j=1}^{N_e} |j\rangle\langle j| = \hat{1}$, maps onto $\sum_{j=1}^{N_e} \hat{a}_j^\dagger \hat{a}_j = \hat{1}$. While the latter identity is clearly not generally true for the sum of number operators of a system consisting of multiple harmonic oscillators, the fact that $\sum_{j=1}^{N_e} \hat{a}_j^\dagger \hat{a}_j$ commutes with the overall Hamiltonian in the ST representation, Eq. (III.8), implies that it is a constant of the motion. This means that the quantum dynamics in terms of the ST mapping variables is restricted to the subspace spanned by the singly-excited states of the overall Hilbert space of a system that consists of N_e harmonic oscillators,

$$\{|1_1\rangle = |1, 0, \ldots, 0, 0\rangle, \ldots, |1_{N_e}\rangle = |0, 0, \ldots, 0, 1\rangle\} \quad . \tag{III.9}$$

Within this subspace, $\hat{a}_j^\dagger \hat{a}_k = |1_j\rangle\langle 1_k|$. Thus, mapping $|j\rangle\langle k|$ onto $|1_j\rangle\langle 1_k|$ is equivalent to mapping it onto $\hat{a}_j^\dagger \hat{a}_k$, and guaranteed to give the same results as long as those operators are treated fully quantum mechanically. However, this is no longer the case when the LSC approximation is applied, which leads to the two different versions of the LSC approximation described below.

One version of the MH approach can be obtained by expressing $\hat{a}_j^\dagger$ and $\hat{a}_j$ in terms of Cartesian

coordinates and momenta $\{\hat{q}_j, \hat{p}_j\}$, as follows:

$$\begin{aligned} \hat{a}_j^\dagger &= \frac{1}{\sqrt{2\hbar}}\Big(\hat{q}_j - i\hat{p}_j\Big) \quad , \\ \hat{a}_j &= \frac{1}{\sqrt{2\hbar}}\Big(\hat{q}_j + i\hat{p}_j\Big) \quad . \end{aligned} \tag{III.10}$$

Combining the mapping in Eq. (III.7) with Eq. (III.10) then yields

$$\begin{aligned} |\lambda\rangle\langle\lambda| \mapsto \hat{M}^{(1)}_{\lambda\lambda}(\hat{\mathbf{q}}, \hat{\mathbf{p}}) &= \frac{1}{2\hbar}\Big(\hat{q}_\lambda^2 + \hat{p}_\lambda^2 - \hbar\Big) \quad , \\ |\lambda\rangle\langle\gamma| \mapsto \hat{M}^{(1)}_{\lambda\gamma}(\hat{\mathbf{q}}, \hat{\mathbf{p}}) &= \frac{1}{2\hbar}\Big(\hat{q}_\lambda\hat{q}_\gamma + \hat{p}_\lambda\hat{p}_\gamma + i\hat{q}_\lambda\hat{p}_\gamma - i\hat{p}_\lambda\hat{q}_\gamma\Big) \quad , \end{aligned} \tag{III.11}$$

where $\lambda \neq \gamma$ and the indices λ and γ will be used consistently throughout this chapter to indicate indices that are always not equal. This is opposed to all other indices, e.g., j and k, which can be equal unless specifically denoted otherwise. The corresponding Wigner transforms are then given by

$$\begin{aligned} \Big[M^{(1)}_{\lambda\lambda}\Big]_W(\mathbf{q}, \mathbf{p}) &= \frac{1}{2\hbar}\Big(q_\lambda^2 + p_\lambda^2 - \hbar\Big) \quad , \\ \Big[M^{(1)}_{\lambda\gamma}\Big]_W(\mathbf{q}, \mathbf{p}) &= \frac{1}{2\hbar}\Big(q_\lambda q_\gamma + p_\lambda p_\gamma + iq_\lambda p_\gamma - ip_\lambda q_\gamma\Big) \quad . \end{aligned} \tag{III.12}$$

Another version of the MH approach can be obtained based on mapping $|j\rangle\langle k|$ onto $|1_j\rangle\langle 1_k|$ [see Eq. (III.9)]. The corresponding Wigner transforms are then given by (see Sec. III.2.1)

$$\begin{aligned} \Big[M^{(2)}_{\lambda\lambda}\Big]_W(\mathbf{q}, \mathbf{p}) &= G(\mathbf{q}, \mathbf{p})\left(q_\lambda^2 + p_\lambda^2 - \frac{\hbar}{2}\right) \quad , \\ \Big[M^{(2)}_{\lambda\gamma}\Big]_W(\mathbf{q}, \mathbf{p}) &= G(\mathbf{q}, \mathbf{p})\Big(q_\lambda q_\gamma + p_\lambda p_\gamma + iq_\lambda p_\gamma - ip_\lambda q_\gamma\Big) \quad , \end{aligned} \tag{III.13}$$

where $G(\mathbf{q}, \mathbf{p})$ is a phase-space Gaussian function,

$$G(\mathbf{q}, \mathbf{p}) = \frac{2^{N_e+1}}{\hbar}\exp\left[-\frac{1}{\hbar}\sum_{l=1}^{N_e}\Big(q_l^2 + p_l^2\Big)\right] \quad . \tag{III.14}$$

Importantly, according to Eq. (III.3), calculating $\sigma_{jk}^{\mathrm{LSC}}(t)$ calls for integrating over the initial

conditions, $\{\mathbf{R}_0, \mathbf{P}_0\}$ and $\{\mathbf{q}_0, \mathbf{p}_0\}$. In practice, this requires being able to sample $\{\mathbf{R}_0, \mathbf{P}_0\}$ and $\{\mathbf{q}_0, \mathbf{p}_0\}$ based on well-behaved probability densities. While $[\hat{\rho}_n(0)]_W(\mathbf{R}_0, \mathbf{P}_0)$ typically provides such a well behaved probability density for $\{\mathbf{R}_0, \mathbf{P}_0\}$, this is not the case for $\{\mathbf{q}_0, \mathbf{p}_0\}$ within LSCI. This is because $\left[M^{(1)}_{\lambda\lambda}\right]_W(\mathbf{q}, \mathbf{p}) = \frac{1}{2\hbar}\Big(q_\lambda^2 + p_\lambda^2 - \hbar\Big)$ and $\left[M^{(1)}_{\lambda\gamma}\right]_W(\mathbf{q}, \mathbf{p}) = \frac{1}{2\hbar}\Big(q_\lambda q_\gamma + p_\lambda p_\gamma + i q_\lambda p_\gamma - i p_\lambda q_\gamma\Big)$ are not bounded functions of $\{\mathbf{q}, \mathbf{p}\}$. Attempting to determine $\{\mathbf{q}_0, \mathbf{p}_0\}$ by requiring that $\left[M^{(1)}_{jk}\right]_W(\mathbf{q}_0, \mathbf{p}_0) = \sigma_{jk}(0)$ reveals that it is not possible to find a specific set of values of $\{\mathbf{q}_0, \mathbf{p}_0\}$ that satisfy this equation (see Sec. III.2.2). This implies that there needs to be a distribution over $\{\mathbf{q}_0, \mathbf{p}_0\}$, such that the above-mentioned condition is satisfied on average, $\left\langle \left[M^{(1)}_{jk}\right]_W(\mathbf{q}_0, \mathbf{p}_0) \right\rangle = \sigma_{jk}(0)$. However, requiring that this condition is satisfied on average does not uniquely determine the underlying distribution over $\{\mathbf{q}_0, \mathbf{p}_0\}$ (see Sec. III.2.2).

On the other hand, the phase-space Gaussian function $G(\mathbf{q}, \mathbf{p})$ in $\left[M^{(2)}_{jk}\right]_W(\mathbf{q}, \mathbf{p})$ [see Eq. (III.13)] provides a natural and unique choice of a probability density. Thus, in what follows, we choose to use Eq. (III.13) at the initial time. However, this still leaves one with a choice of which of the two mappings to use when evaluating $[M_{kj}]_W(\mathbf{q}_t, \mathbf{p}_t)$. This in turn leads to two different versions of LSC, which we refer to as LSCI and LSCII. More specifically [see Eq. (III.3)]:

$$\sigma_{jk}^{\text{LSCI/II}}(t) = \left(\frac{1}{2\pi\hbar}\right)^N \sum_{u,v=1}^{N_e} \sigma_{uv}(0) \times \int \mathbf{dR}_0 \int \mathbf{dP}_0 \int \mathbf{dq}_0 \int \mathbf{dp}_0 \, [\hat{\rho}_n(0)]_W(\mathbf{R}_0, \mathbf{P}_0) \left[M^{(2)}_{uv}\right]_W(\mathbf{q}_0, \mathbf{p}_0) \left[M^{(1)/(2)}_{kj}\right]_W(\mathbf{q}_t, \mathbf{p}_t) \quad , \tag{III.15}$$

where $(1)/(2)$ corresponds to the choice between Eq. (III.12)/(III.13) for $[M_{kj}]_W(\mathbf{q}_t, \mathbf{p}_t)$. Therefore, the difference between the QC/MH methods is that LSCI uses $\left[M^{(2)}_{uv}\right]_W(\mathbf{q}_0, \mathbf{p}_0)$ for initial electronic sampling and $\left[M^{(1)}_{uv}\right]_W(\mathbf{q}_0, \mathbf{p}_0)$ for the electronic dynamics at time t while LSCII uses $\left[M^{(2)}_{uv}\right]_W(\mathbf{q}_0, \mathbf{p}_0)$ for both initial electronic sampling and the electronic dynamics at time t. It should be noted that in the literature, LSCI has also been referred as the Poisson-bracket mapping equation (PBME)[101] and LSCII has also been referred as the linearized semiclassical initial value representation (LSC-IVR).[102]

III.2.1 Derivation of LSCII mapping variables

This section details the derivation of the mapping variables for the electronic populations and coherences within LSCII, Eq. (III.13). To this end, the harmonic oscillator ground and first excited state wavefunctions in the position representation are used, given by

$$\begin{aligned}\varphi_0(q_j) &= \left(\frac{1}{\pi\hbar}\right)^{1/4} e^{-q_j^2/2\hbar} \quad , \\ \varphi_1(q_j) &= \left(\frac{4}{\pi\hbar^3}\right)^{1/4} q_j e^{-q_j^2/2\hbar} \quad .\end{aligned} \tag{III.16}$$

Using Eq. (III.16), the mapping variables of the electronic populations are given by:

$$\begin{aligned}\left[M^{(2)}_{\lambda\lambda}\right]_W(\mathbf{q},\mathbf{p}) &= \int d\mathbf{z} e^{-i\mathbf{z}\mathbf{p}/\hbar}\left\langle \mathbf{q}+\frac{\mathbf{z}}{2}\middle|1_\lambda\right\rangle\left\langle 1_\lambda\middle|\mathbf{q}-\frac{\mathbf{z}}{2}\right\rangle \\ &= \int dz_\lambda e^{-iz_\lambda p_\lambda/\hbar}\varphi_1\left(q_\lambda+\frac{z_\lambda}{2}\right)\varphi_1\left(q_\lambda-\frac{z_\lambda}{2}\right) \\ &\qquad \times\prod_{\substack{l=1\\ l\neq\lambda}}^{N_e}\int dz_l e^{-iz_l p_l/\hbar}\varphi_0\left(q_l+\frac{z_l}{2}\right)\varphi_0\left(q_l-\frac{z_l}{2}\right) \\ &= \frac{2^2}{\hbar}\left(q_\lambda^2+p_\lambda^2-\frac{\hbar}{2}\right)e^{-(q_\lambda^2+p_\lambda^2)/\hbar}\prod_{\substack{l=1\\ l\neq\lambda}}^{N_e}2e^{-(q_l^2+p_l^2)/\hbar} \\ &= \frac{2^{N_e+1}}{\hbar}\left(q_\lambda^2+p_\lambda^2-\frac{\hbar}{2}\right)\exp\left[-\frac{1}{\hbar}\sum_{l=1}^{N_e}\left(q_l^2+p_l^2\right)\right] \quad .\end{aligned} \tag{III.17}$$

Similarly, the mapping variables of the electronic coherences are given by:

$$\begin{aligned}
\Big[M^{(2)}_{\lambda\gamma}\Big]_W(\mathbf{q},\mathbf{p})\Big[|1_\lambda\rangle\langle 1_\gamma|\Big]_W(\mathbf{q},\mathbf{p}) &= \int d\mathbf{z} e^{-i\mathbf{z}\mathbf{p}/\hbar}\Big\langle \mathbf{q}+\frac{\mathbf{z}}{2}\Big|1_\lambda\Big\rangle\Big\langle 1_\gamma\Big|\mathbf{q}-\frac{\mathbf{z}}{2}\Big\rangle \\
&= \int dz_\lambda e^{-iz_\lambda p_\lambda/\hbar}\varphi_1\Big(q_\lambda+\frac{z_\lambda}{2}\Big)\varphi_0\Big(q_\lambda-\frac{z_\lambda}{2}\Big)\int dz_\gamma e^{-iz_\gamma p_\gamma/\hbar}\varphi_0\Big(q_\gamma+\frac{z_\gamma}{2}\Big)\varphi_1\Big(q_\gamma-\frac{z_\gamma}{2}\Big) \\
&\quad\times\prod_{\substack{l=1\\ l\neq\lambda,\gamma}}^{N_e}\int dz_l e^{-iz_l p_l/\hbar}\varphi_0\Big(q_l+\frac{z_l}{2}\Big)\varphi_0\Big(q_l-\frac{z_l}{2}\Big) \\
&= \sqrt{\frac{2^3}{\hbar}}(q_\lambda-ip_\lambda)e^{-(q_\lambda^2+p_\lambda^2)/\hbar}\sqrt{\frac{2^3}{\hbar}}(q_\gamma+ip_\gamma)e^{-(q_\gamma^2+p_\gamma^2)/\hbar}\prod_{\substack{l=1\\ l\neq\lambda,\gamma}}^{N_e}2e^{-(q_l^2+p_l^2)/\hbar} \\
&= \frac{2^{N_e+1}}{\hbar}(q_\lambda-ip_\lambda)(q_\gamma+ip_\gamma)\exp\Bigg[-\frac{1}{\hbar}\sum_{l=1}^{N_e}\Big(q_l^2+p_l^2\Big)\Bigg] \quad .
\end{aligned} \tag{III.18}$$

III.2.2 Initial conditions within LSCI

In this section, we discuss determining $\{\mathbf{q}_0,\mathbf{p}_0\}$ within LSCI by requiring that $\Big[M^{(1)}_{jk}\Big]_W(\mathbf{q}_0,\mathbf{p}_0) = \sigma_{jk}(0)$. To this end, we consider a system with two electronic states, $\{|D\rangle,|A\rangle\}$, whose initial state is given by $\hat{\sigma}(0) = |D\rangle\langle D|$. Requiring that $\Big[M^{(1)}_{jk}\Big]_W(\mathbf{q}_0,\mathbf{p}_0) = \sigma_{jk}(0)$ then leads to the following set of four coupled equations for $\{q_{D,0},p_{D,0},q_{A,0},p_{A,0}\}$:

$$\begin{aligned}
\frac{1}{2\hbar}\Big(q_{D,0}^2+p_{D,0}^2-\hbar\Big) &= 1 \ , \\
\frac{1}{2\hbar}\Big(q_{A,0}^2+p_{A,0}^2-\hbar\Big) &= 0 \ , \\
\frac{1}{2\hbar}\Big(q_{D,0}q_{A,0}+p_{D,0}p_{A,0}\Big) &= 0 \ , \\
\frac{1}{2\hbar}\Big(q_{D,0}p_{A,0}-p_{D,0}q_{A,0}\Big) &= 0 \ .
\end{aligned} \tag{III.19}$$

However, those four equations are inconsistent and therefore cannot be solved by a unique choice of $\{q_{D,0},p_{D,0},q_{A,0},p_{A,0}\}$. Thus, it appears that the only way to simultaneously satisfy those four equations is by imposing a distribution over $\{q_{D,0},p_{D,0},q_{A,0},p_{A,0}\}$ and requiring that the equations

are satisfied on average.

For example, expressing Eq. (III.20) in terms of action-angle variables $\{n_{D,0}, u_{D,0}, n_{A,0}, u_{A,0}\}$, defined by

$$\begin{aligned} q_{j,0} &= \sqrt{2\hbar(n_{j,0}+1/2)}\cos(u_{j,0}) \quad , \\ p_{j,0} &= -\sqrt{2\hbar(n_{j,0}+1/2)}\sin(u_{j,0}) \quad , \end{aligned} \tag{III.20}$$

yields:

$$n_{D,0} = 1 \quad , \quad n_{A,0} = 0 \quad , \quad \sqrt{n_{D,0}n_{A,0}}e^{i(u_{A,0}-u_{D,0})} = 0 \ , \tag{III.21}$$

which can be satisfied on average by allowing $u_{A,0} - u_{D,0}$ to be uniformly distributed between $(0, 2\pi)$, such that $\langle e^{i(u_{A,0}-u_{D,0})}\rangle = 0$. However, this choice is not unique. As an example, one can add a distribution over the action variables, $n_{D,0}$ and $n_{A,0}$, such that $\langle n_{D,0}\rangle = 1$ and $\langle n_{A,0}\rangle = 0$. The recently introduced symmetrical quasi-classical method (SQC) of Cotton and Miller is based on such an assumption, where the shape and width of the distribution over $n_{D,0}$ and $n_{A,0}$ are picked so as to maximize efficiency and accuracy.[75–80]

III.3 QC/MH Methods and the GQME

Previously in Sec. II.5, the procedure for using the Ehrenfest method to obtain the projection-free inputs, through which the memory kernel and subsequently the reduced dynamics can be calculated, was outlined. A similar procedure can be used to determine how to calculate the projection-free inputs using QC/MH methods. The projection-free inputs are built by correlation functions of the form given in Eq. (II.38). Within the QC/MH methods, these correlation functions are approx-

imated by [see Eq. (III.15)]:

$$\mathrm{Tr}\left\{\hat{\Omega}|u\rangle\langle v|e^{i\hat{H}\tau/\hbar}\,\Gamma(\hat{\mathbf{R}})|b\rangle\langle a|e^{-i\hat{H}\tau/\hbar}\right\} \approx \frac{1}{(2\pi\hbar)^N}\int d\mathbf{R}_0\int d\mathbf{P}_0\,\Omega_W(\mathbf{R}_0,\mathbf{P}_0)\left[M_{uv}^{(2)}\right]_W(\mathbf{q}_0,\mathbf{p}_0)\,\Gamma_W(\mathbf{R}_\tau)\left[M_{ba}^{(1)/(2)}\right]_W(\mathbf{q}_\tau,\mathbf{p}_\tau) \quad . \tag{III.22}$$

As noted previously in this section, the QC/MH methods differ from the Ehrenfest method in that the electronic populations and coherences are treated on equal footing and the initial electronic state contains a distribution function. This means that QC/MH methods do not need to use linear combinations when starting in electronic states $|u\rangle\langle v|$ with $u \neq v$ and can instead directly calculate the correlation functions given in Eq. (III.22), even for non-Hermitian initial electronic states.

III.4 Illustrative applications

In this section, we demonstrate the feasibility and accuracy of calculating the memory kernel of the GQME via the two versions of the QC/MH method outlined in Sec. III.2. We do so by applying the method to the spin-boson model and comparing to the quantum-mechanically exact results.[44,69] We also compare to results based on calculating the memory kernel of the GQME via the Ehrenfest method, shown previously in Sec. II.6, and results obtained by direct application of the two QC/MH methods and the Ehrenfest method.

The spin-boson Hamiltonian is put in the form of Eq. (I.3):

$$\hat{H} = \hat{H}_D|D\rangle\langle D| + \hat{H}_A|A\rangle\langle A| + V_{DA}|D\rangle\langle A| + V_{AD}|A\rangle\langle D| \quad , \tag{III.23}$$

where

$$\begin{aligned}
\hat{H}_D &= \epsilon + \sum_{i=1}^{N_n} \left[\frac{\hat{P}_i^2}{2} + \frac{1}{2}\omega_i^2 \hat{R}_i^2 - c_i \hat{R}_i \right] \quad , \\
\hat{H}_A &= -\epsilon + \sum_{i=1}^{N_n} \left[\frac{\hat{P}_i^2}{2} + \frac{1}{2}\omega_i^2 \hat{R}_i^2 + c_i \hat{R}_i \right] \quad , \\
V_{DA} &= V_{AD} = \Gamma \quad .
\end{aligned} \tag{III.24}$$

Here, 2ϵ is the shift in equilibrium energy between the donor (D) and acceptor (A) states and Γ is a positive constant describing the electronic coupling between the donor and acceptor states. Since Γ is a constant, this system satisfies the Condon approximation and therefore we will use the projection-free inputs $\mathcal{F}_1(\tau)$ and $\mathcal{F}_2(\tau)$ to obtain the memory kernel [see Eqs. (II.33) and (II.34)].

The same as in Sec. II.6, the spectral density is assumed Ohmic with exponential cutoff:

$$J(\omega) = \frac{\pi}{2} \sum_{i=1}^{N_n} \frac{c_i^2}{\omega_i} \delta(\omega - \omega_i) \overset{N_n \to \infty}{\longrightarrow} \frac{\pi\hbar}{2} \xi \omega e^{-\omega/\omega_c} \quad . \tag{III.25}$$

where ξ is the Kondo parameter and ω_c is the cutoff frequency. The discretization procedure to obtain the N_n nuclear mode frequencies and coupling coefficients is given in Sec. II.6. The initial state of the nuclear DOF was chosen as:

$$\hat{\rho}_n(0) = \frac{e^{-\beta(\hat{H}_D + \hat{H}_A)/2}}{\mathrm{Tr}_n \left\{ e^{-\beta(\hat{H}_D + \hat{H}_A)/2} \right\}} \quad , \tag{III.26}$$

and the initial nuclear positions and momenta are sampled based on the Wigner transform of Eq. (III.26),

$$\rho_{n,W}(\mathbf{R}, \mathbf{P}; t=0) = \prod_{i=1}^{N_n} \frac{\tanh(\beta\hbar\omega_i/2)}{\pi\hbar} \exp\left[-\frac{2\tanh(\beta\hbar\omega_i/2)}{\hbar\omega_i} \left(\frac{P_i^2}{2} + \frac{1}{2}\omega_i^2 R_i^2 \right) \right] \quad . \tag{III.27}$$

Calculations were carried out for the five different sets of parameter values studied previously in Sec. II.6 and copied below in Table III.1, with the sole difference being a time step of $\Delta t =$

$0.01\,\Gamma^{-1}$ as opposed to $\Delta t = 0.02\,\Gamma^{-1}$. Models 1-3 differ only in increasing cutoff frequency, model 4 represents a high-friction case, and model 5 corresponds to an unbiased, weakly-coupled system at higher finite temperature.

The numerical integration scheme was adopted from Ref. 72 with some differences. We start out by writing the overall system Hamiltonian operator, Eq. (I.3), in the following form

$$\hat{H} = \frac{\hat{\mathbf{P}}^2}{2} + \sum_{j=1}^{N_e} V_j(\hat{\mathbf{R}})|j\rangle\langle j| + \sum_{\substack{j,k=1 \\ k\neq j}}^{N_e} V_{jk}(\hat{\mathbf{R}})|j\rangle\langle k| = \hat{H}_1 + \hat{H}_2 \quad . \tag{III.28}$$

Here,

$$\begin{aligned}
\hat{H}_1 &= \frac{\hat{\mathbf{P}}^2}{2} \quad , \\
\hat{H}_2 &= V_0(\hat{\mathbf{R}}) \sum_{j=1}^{N_e} |j\rangle\langle j| + \sum_{j,k=1}^{N_e} \bar{h}_{jk}(\hat{\mathbf{R}})|j\rangle\langle k| \quad , \\
V_0(\hat{\mathbf{R}}) &= \frac{\sum_{j=1}^{N_e} V_j(\hat{\mathbf{R}})}{N_e} \quad , \\
\bar{h}_{jk}(\hat{\mathbf{R}}) &= \Big[V_j(\hat{\mathbf{R}}) - V_0(\hat{\mathbf{R}})\Big]\,\delta(j,k) + V_{jk}(\hat{\mathbf{R}})(1-\delta_{j,k}) \quad .
\end{aligned} \tag{III.29}$$

Within QC/MH, the dynamics is governed by the corresponding classical-like mapping Hamiltonians [see Eqs. (III.12) and (III.13)]:

$$\begin{aligned}
\hat{H}_1 &= \frac{\mathbf{P}^2}{2} \quad , \\
\hat{H}_2 &= V_0(\mathbf{R}) + \frac{1}{2\hbar} \sum_{j,k=1}^{N_e} \bar{h}_{jk}(\mathbf{R})(q_j q_k + p_j p_k) \quad .
\end{aligned} \tag{III.30}$$

In the next step, $\bar{h}_{jk}(\mathbf{R})$ is diagonalized:

$$\bar{h}_{jk}(\mathbf{R}) = C_{jl}(\mathbf{R}) E_l(\mathbf{R}) C^{-1}_{lk}(\mathbf{R}) \quad . \tag{III.31}$$

Here, $\{E_l(\mathbf{R})\}$ and $\{C_{jl}(\mathbf{R})\}$ are the eigenvalues and eigenvectors of $\bar{h}_{jk}(\mathbf{R})$, respectively. The

latter can be obtained in closed form for the two-state system used in this paper defined in Eq. (III.24):[103]

$$
\begin{aligned}
E_1(\mathbf{R}) &= \sqrt{\bar{h}_{12}^2 + \bar{h}_{11}^2(\mathbf{R})} = -E_2(\mathbf{R}) \quad , \\
C_{11}(\mathbf{R}) &= C_{22}(\mathbf{R}) = \frac{\bar{h}_{12}}{\sqrt{[E_1(\mathbf{R}) - \bar{h}_{11}(\mathbf{R})]^2 + \bar{h}_{12}^2}} \quad , \\
C_{12}(\mathbf{R}) &= -C_{21}(\mathbf{R}) = \frac{\bar{h}_{11}(\mathbf{R}) - E_1(\mathbf{R})}{\sqrt{[E_1(\mathbf{R}) - \bar{h}_{11}(\mathbf{R})]^2 + \bar{h}_{12}^2}} \quad .
\end{aligned}
\tag{III.32}
$$

The propagation of $\{\mathbf{q}_t, \mathbf{p}_t, \mathbf{R}_t, \mathbf{P}_t\}$ from time τ to time $\tau + \Delta\tau$ is carried out in three steps:

1. Propagate $\mathbf{R}$ by half time step from τ to $\tau + \Delta\tau/2$, based on H_1:

$$
R_i\left(\tau + \frac{\Delta\tau}{2}\right) = R_i(\tau) + P_i(\tau)\frac{\Delta\tau}{2} \quad . \tag{III.33}
$$

2. Propagate $\{\mathbf{q}, \mathbf{p}, \mathbf{P}\}$ by one time step, from τ to $\tau + \Delta\tau$:

$$
\begin{aligned}
q_j(\tau + \Delta\tau) &= C_{jl}(\mathbf{R})C_{lk}^{-1}(\mathbf{R}) \\
&\quad \times \left[\cos\left(\frac{E_l(\mathbf{R})\Delta\tau}{\hbar}\right) q_k(\tau) + \sin\left(\frac{E_l(\mathbf{R})\Delta\tau}{\hbar}\right) p_k(\tau)\right] \quad ,
\end{aligned}
\tag{III.34}
$$

$$
\begin{aligned}
p_j(\tau + \Delta\tau) &= C_{jl}(\mathbf{R})C_{lk}^{-1}(\mathbf{R}) \\
&\quad \times \left[\cos\left(\frac{E_l(\mathbf{R})\Delta\tau}{\hbar}\right) p_k(\tau) - \sin\left(\frac{E_l(\mathbf{R})\Delta\tau}{\hbar}\right) q_k(\tau)\right] \quad ,
\end{aligned}
\tag{III.35}
$$

$$
\begin{aligned}
P_i(\tau + \Delta\tau) &= P_i(\tau) - \frac{\partial V_0(R_i)}{\partial R_i}\Delta\tau \\
&\quad - \frac{1}{2\hbar}\sum_{j,k=1}^{N_e} \frac{\partial \bar{h}_{jk}(R_i)}{\partial R_i} \int_\tau^{\tau+\Delta\tau} dt \Big[q_j(t)q_k(t) + p_j(t)p_k(t)\Big] \quad .
\end{aligned}
\tag{III.36}
$$

For the spin-boson model used in this paper, Eq. (III.36) can be put in the following form:

$$P_i(\tau+\Delta\tau) = P_i(\tau) - \frac{\partial V_0(R_i)}{\partial R_i}\Delta\tau \qquad \text{(III.37)}$$
$$- \frac{1}{2\hbar}\sum_{j=1}^{2}\frac{\partial E_j(R_i)}{\partial R_i}\left\{\tilde{q}_j^2(\tau)+\tilde{p}_j^2(\tau) - \frac{\bar{h}_{12}}{\bar{h}_{jj}(R)}\Big[\tilde{q}_j(\tau)\tilde{q}_k(\tau)+\tilde{p}_j(\tau)\tilde{p}_k(\tau)\Big]\right\} \ ,$$

where,

$$\tilde{q}_j(t) = \sum_{\mu=1}^{N_e} C_{j\mu}^{-1}(\mathbf{R})q_\mu(t) \quad , \quad \tilde{p}_j(t) = \sum_{\mu=1}^{N_e} C_{j\mu}^{-1}(\mathbf{R})p_\mu(t) \quad . \qquad \text{(III.38)}$$

Notably, Eq. (III.37) has an additional term on the R.H.S. which is not included in Eq. (C19) of Ref. 72. The accuracy of Eq. (III.37) with the above mentioned extra term was verified numerically by comparing to results obtained by calculating the integral in Eq. (III.36) with the extended trapezoid method.

3. Propagate $\mathbf{R}$ by half time step from $\tau+\Delta\tau/2$ to $\tau+\Delta\tau$, based on H_1:

$$R_i(\tau+\Delta\tau) = R_i\left(\tau+\frac{\Delta\tau}{2}\right) + P_i(\tau+\Delta\tau)\frac{\Delta\tau}{2} \quad . \qquad \text{(III.39)}$$

The results reported in this paper were obtained by averaging over 200,000 trajectories for each model and choice of dynamical method. Figs. III.1-III.5 give the nonvanishing matrix elements of the memory kernel superoperators and the population difference between donor and acceptor states, which corresponds to the expectation value of $\hat{\sigma}_z(t) = |D\rangle\langle D|(t) - |A\rangle\langle A|(t)$, for models 1-5, respectively. Exact results were adopted from Ref. 44 for models 1-4 and from Ref. 69 for model 5.

Inspection of the results in Figs. III.1-III.5 gives rise to the following noteworthy observations:

- **Direct application fails to capture dynamics at long times:** For all the models considered, simulation of the electronic dynamics by direct application of either LSCI, LSCII, or Ehrenfest methods gives rise to qualitatively different results that become increasingly less accurate with increasing time (see Figs. III.1-III.5). More specifically, while direct applica-

Table III.1: Model and simulation parameters

	model parameters					numerical parameters		
Model #	ϵ	Γ	β	ξ	ω_c	$\omega_{\max}$	N_n	Δt
1	1.0	1.0	5.0	0.1	1.0	5	400	0.01
2	1.0	1.0	5.0	0.1	2.0	10	400	0.01
3	1.0	1.0	5.0	0.1	7.5	36	400	0.01
4	1.0	1.0	5.0	0.4	2.0	10	400	0.01
5	0.0	$0.\overline{333}$	3.0	0.1	1.0	5	200	0.01

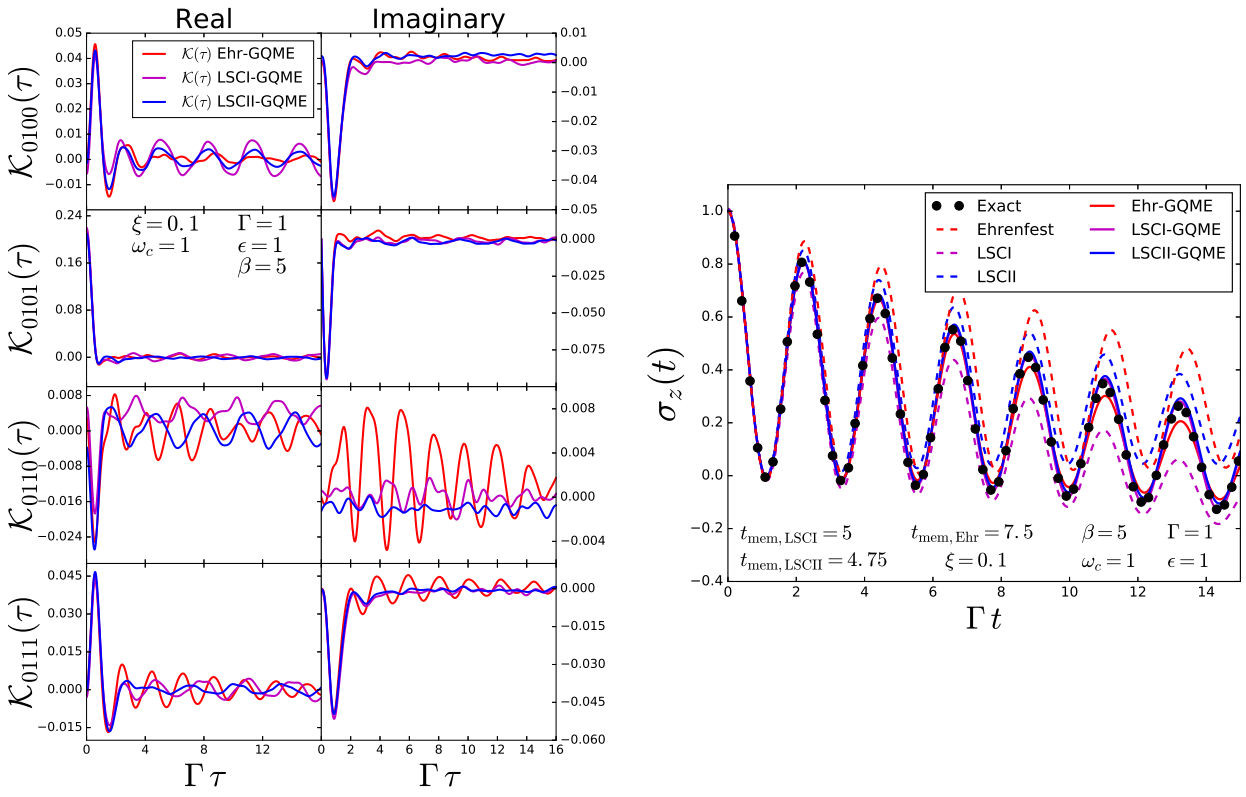

Figure III.1: On the left are the real and imaginary parts of the nonvanishing matrix elements of the memory kernel for model 1 in Table III.1. Shown are memory kernels obtained via the Ehrenfest (red), LSCI (magenta), and LSCII (blue) methods.
On the right is the electronic population difference, $\sigma_z(t) = \sigma_{DD}(t) - \sigma_{AA}(t)$, as a function of time for model 1 in Table III.1. Shown are the exact result (black circles), the results obtained via direct application of the Ehrenfest (dashed red), LSCI (dashed magenta), and LSCII (dashed blue) methods and results obtained based on the GQME with the memory kernel calculated via the Ehrenfest (Ehr-GQME, solid red), LSCI (LSCI-GQME, solid magenta), and LSCII (LSCII-GQME, solid blue) methods.

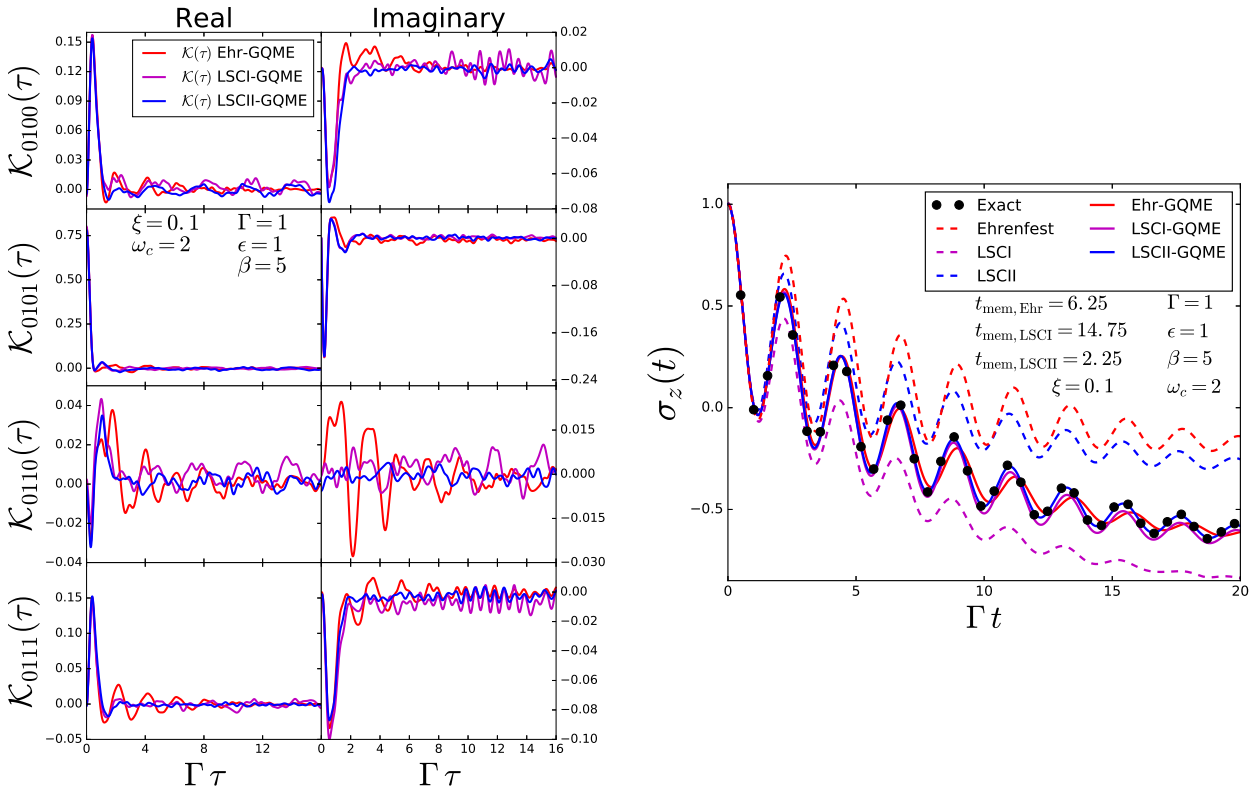

Figure III.2: On the left are the real and imaginary parts of the nonvanishing matrix elements of the memory kernel for model 2 in Table III.1. Shown are memory kernels obtained via the Ehrenfest (red), LSCI (magenta), and LSCII (blue) methods.
On the right is the electronic population difference, $\sigma_z(t) = \sigma_{DD}(t) - \sigma_{AA}(t)$, as a function of time for model 2 in Table III.1. Shown are the exact result (black circles), the results obtained via direct application of the Ehrenfest (dashed red), LSCI (dashed magenta), and LSCII (dashed blue) methods and results obtained based on the GQME with the memory kernel calculated via the Ehrenfest (Ehr-GQME, solid red), LSCI (LSCI-GQME, solid magenta), and LSCII (LSCII-GQME, solid blue) methods.

tion of LSCI is typically observed to produce a faster relaxation and too small asymptotic values of $\sigma_z(t)$ compared to the exact results, LSCII and Ehrenfest are observed to produce slower relaxation and larger asymptotic values of $\sigma_z(t)$ compared to the exact results (although LSCII is observed to be in somewhat better agreement with the exact results than Ehrenfest). LSCI and LSCII are also seen to damp the oscillatory behavior of $\sigma_z(t)$ more strongly compared to Ehrenfest.

- **Improvement over direct application with the GQME for all methods:** Remarkably,

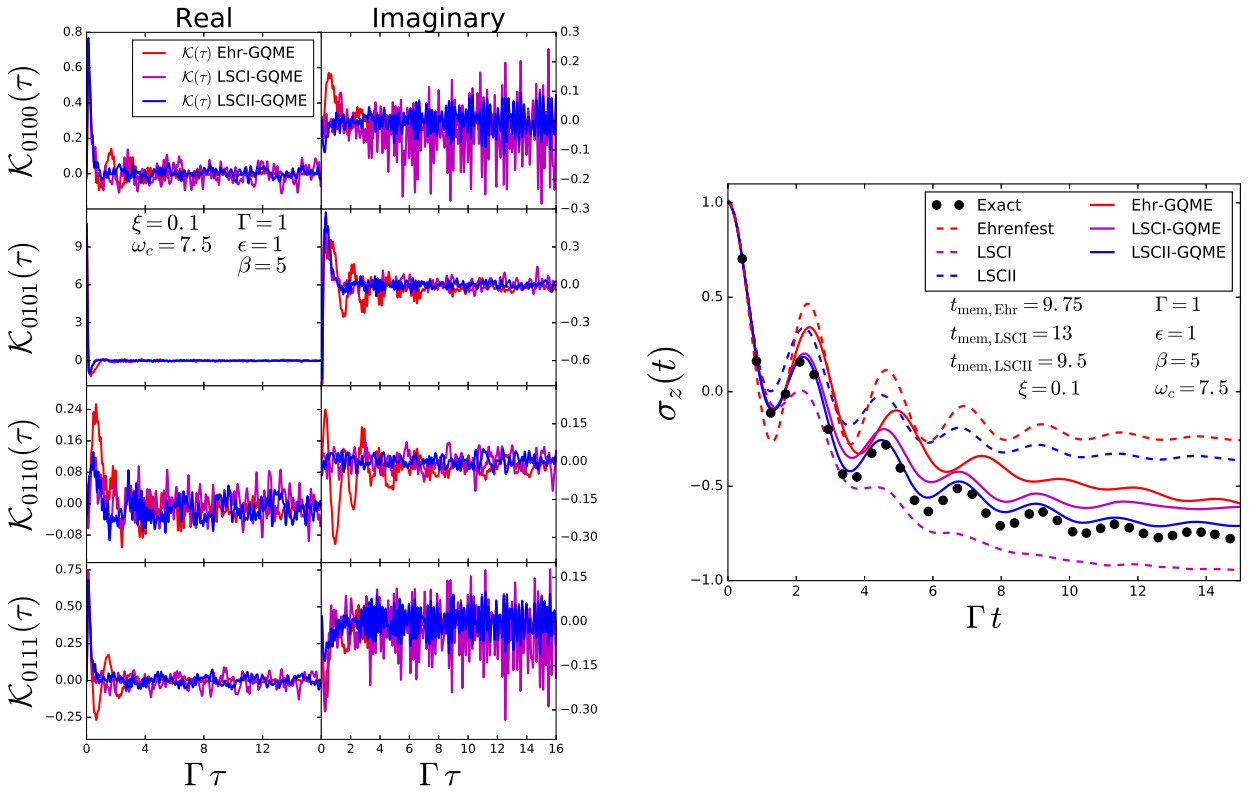

Figure III.3: On the left are the real and imaginary parts of the nonvanishing matrix elements of the memory kernel for model 3 in Table III.1. Shown are memory kernels obtained via the Ehrenfest (red), LSCI (magenta), and LSCII (blue) methods.
On the right is the electronic population difference, $\sigma_z(t) = \sigma_{DD}(t) - \sigma_{AA}(t)$, as a function of time for model 3 in Table III.1. Shown are the exact result (black circles), the results obtained via direct application of the Ehrenfest (dashed red), LSCI (dashed magenta), and LSCII (dashed blue) methods and results obtained based on the GQME with the memory kernel calculated via the Ehrenfest (Ehr-GQME, solid red), LSCI (LSCI-GQME, solid magenta), and LSCII (LSCII-GQME, solid blue) methods.

despite the rather inaccurate and qualitatively different behavior of the three methods, they produce similar, and rather accurate, results when their use is restricted to calculating the memory kernel of the GQME, with LSCII typically leading to the most accurate results, Ehrenfest to the least accurate results, and LSCI's accuracy intermediate between them.

- **Computational benefit of shorter memory time needed for LSCII-GQME:** The memory kernels produced by LSCI and LSCII tend to have a less oscillatory behavior at longer times than those produced by the Ehrenfest method, with LSCII producing the most stable

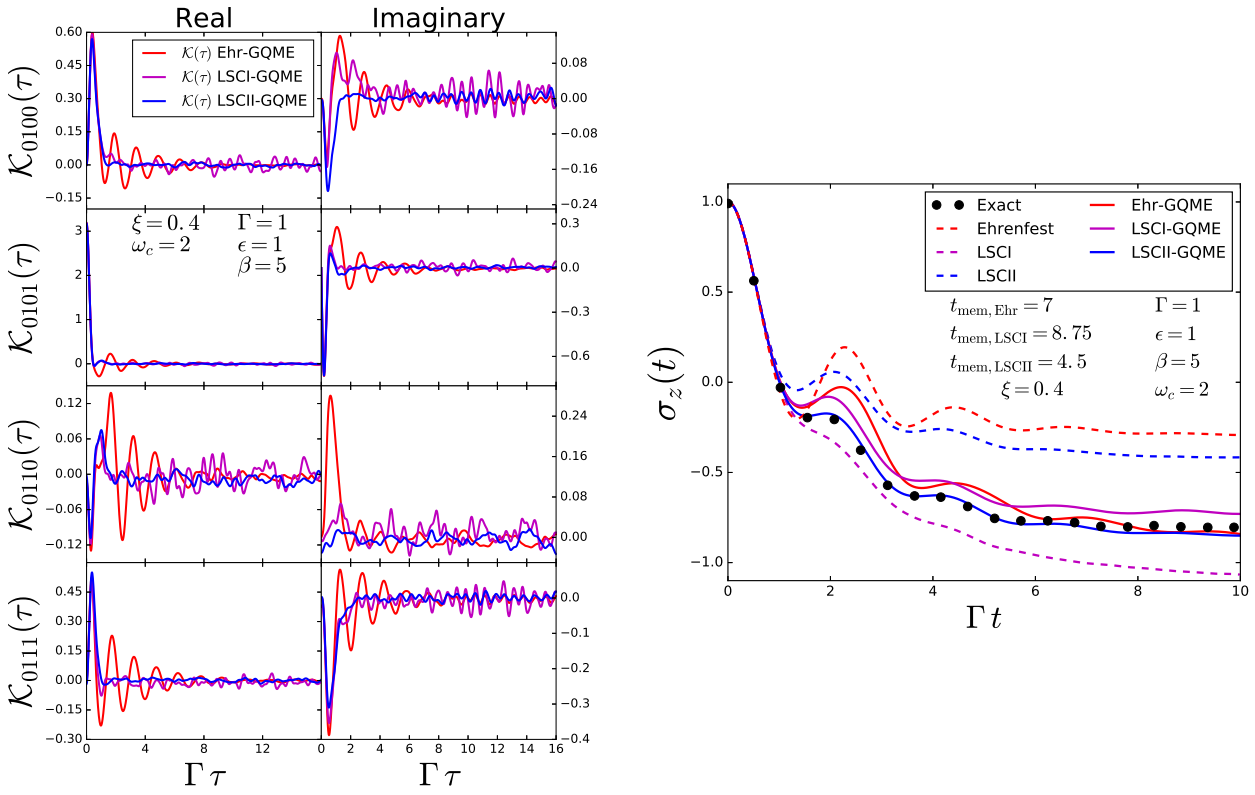

Figure III.4: On the left are the real and imaginary parts of the nonvanishing matrix elements of the memory kernel for model 4 in Table III.1. Shown are memory kernels obtained via the Ehrenfest (red), LSCI (magenta), and LSCII (blue) methods.
On the right is the electronic population difference, $\sigma_z(t) = \sigma_{DD}(t) - \sigma_{AA}(t)$, as a function of time for model 4 in Table III.1. Shown are the exact result (black circles), the results obtained via direct application of the Ehrenfest (dashed red), LSCI (dashed magenta), and LSCII (dashed blue) methods and results obtained based on the GQME with the memory kernel calculated via the Ehrenfest (Ehr-GQME, solid red), LSCI (LSCI-GQME, solid magenta), and LSCII (LSCII-GQME, solid blue) methods.

kernels (see Figs. III.1-III.5). As a result, in all five sets of model parameters under consideration, it was possible to obtain converged electronic dynamics via LSCII-based memory kernels using a memory time which is shorter compared to that used to obtain the LSCI- and Ehrenfest-based memory kernels (see Figs. III.1-III.5), including twice by more than a factor of 2 compared to Ehrenfest (see Figs. III.2 and III.5). Memory times were determined by the algorithm outlined in Sec. III.4.1. Given that the calculation of the projection-free inputs and the subsequent calculation of the memory kernel are the most costly parts of a GQME-based simulation, being able to cut the memory time corresponds to a significant

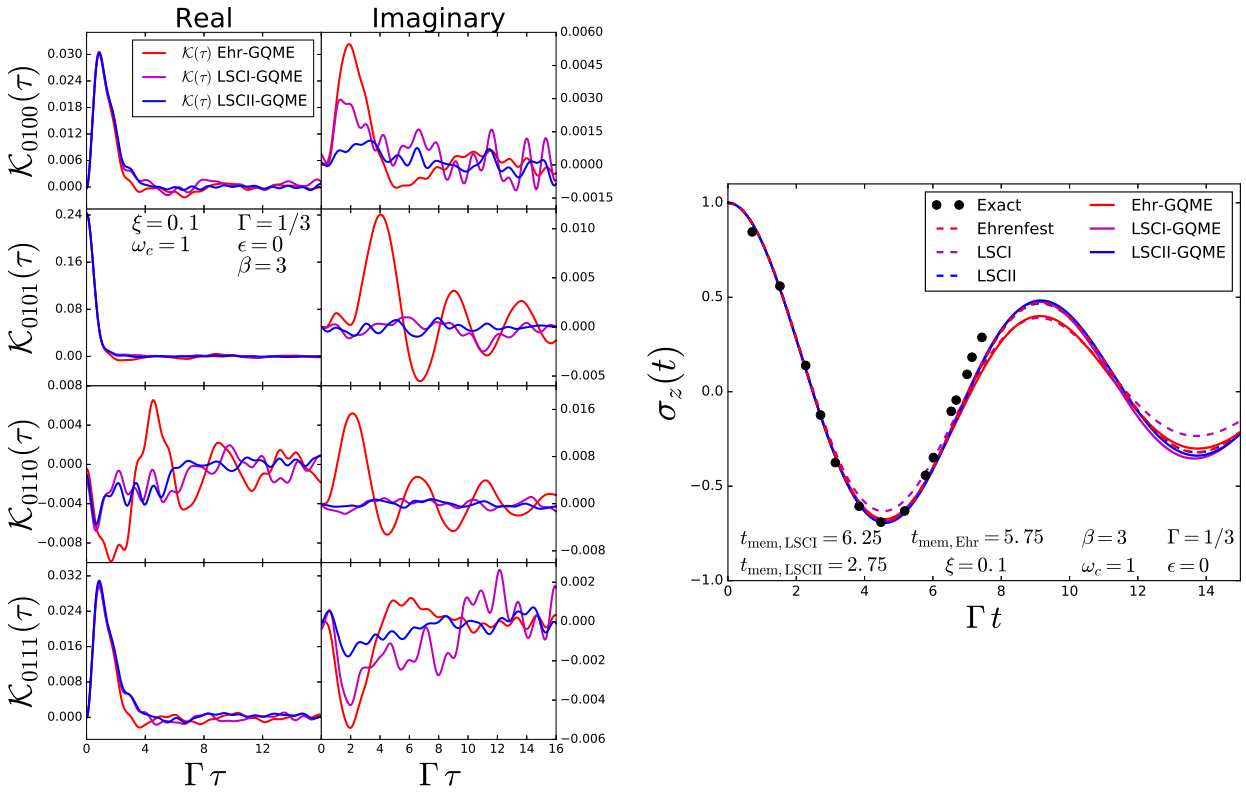

Figure III.5: On the left are the real and imaginary parts of the nonvanishing matrix elements of the memory kernel for model 5 in Table III.1. Shown are memory kernels obtained via the Ehrenfest (red), LSCI (magenta), and LSCII (blue) methods.
On the right is the electronic population difference, $\sigma_z(t) = \sigma_{DD}(t) - \sigma_{AA}(t)$, as a function of time for model 5 in Table III.1. Shown are the exact result (black circles), the results obtained via direct application of the Ehrenfest (dashed red), LSCI (dashed magenta), and LSCII (dashed blue) methods and results obtained based on the GQME with the memory kernel calculated via the Ehrenfest (Ehr-GQME, solid red), LSCI (LSCI-GQME, solid magenta), and LSCII (LSCII-GQME, solid blue) methods.

reduction in computational cost.

- **Improvement in results for least-classical set of parameters:** The QC/MH approach involves the approximation that the nuclear DOF can be treated classically, which is not always valid. The high cutoff frequency of model 3 (see Fig. III.3) implies that treating the nuclear DOF as classical may be the least justifiable for this model. Indeed, the Ehrenfest method was shown in Sec. II.6 to deviate significantly from the exact result in this case (see Figs. II.3 and III.3).[35] Interestingly, while LSCII is also observed to deviate from the exact result in

this case, it is also seen to significantly outperform Ehrenfest (see Fig. III.3). Since both Ehrenfest and LSCII treat the nuclear DOF classically, this difference seems to suggest that the inferior performance of Ehrenfest is partially due to the mean field approximation underlying it.

III.4.1 Memory time convergence algorithm

In this section, we outline the algorithm used to obtain the memory time for the dynamics of the electronic population difference, $\sigma_z(t) = \sigma_{DD}(t) - \sigma_{AA}(t)$. For each step, convergence is defined as

$$|\sigma_z(n\Delta t) - \sigma_{z,\text{max}}(n\Delta t)| \leq 0.02 \tag{III.40}$$

for all $n = 0, 1, 2, ..., N_{\text{max}}$, where $N_{\text{max}}\Delta t$ is equal to the chosen maximum value of t and $\sigma_{z,\text{max}}(n\Delta t)$ is the electronic population difference for a memory time $t_{\text{mem, max}} = N_{\text{max}}\Delta t$. The convergence parameter of 0.02 was chosen as it is $1/100$th of the maximum range of the $\sigma_z(t)$ values, from -1 to 1.

For the spin-boson model in this paper with parameters given in Table III.1, $t_{\text{mem, max}} = 15\,\Gamma t$ for models 1, 3, and 5; $t_{\text{mem, max}} = 20\,\Gamma t$ for model 2; and $t_{\text{mem, max}} = 10\,\Gamma t$ for model 4. For models 1-4, $t_{\text{mem, max}}$ is equivalent to the maximum time of the exact results while a longer time was chosen for model 5 because the maximum time of the exact results was shorter than one full oscillation.

The memory time convergence algorithm is as follows:

1. Calculate $\sigma_{z,\text{max}}(t)$ with a memory time equal to the maximum value of Γt in Figs. III.1 - III.5.

2. Calculate $\sigma_z(t)$ with a memory time equal to half the maximum value of Γt. There are two possible scenarios:

- If Eq. (III.40) is satisfied, the memory time is decreased by 2.5 and a boolean, α, is set to `true` to denote that the first instance of convergence has been reached.

- If Eq. (III.40) is not satisfied, the memory time is increased by 2.5 and $\alpha = \texttt{false}$. While $\alpha = \texttt{false}$, continue to calculate $\sigma_z(t)$ with the memory time increasing by 2.5 for each loop until Eq. (III.40) is satisfied and $\alpha = \texttt{true}$.

3. Once $\alpha = \texttt{true}$, the memory time is decreased by 2.5 and $\sigma_z(t)$ recalculated in a loop until Eq. (III.40) is no longer satisfied, with $\sigma_z(t)$ stored as $\sigma_{z,\text{prev}}(t)$ each time the loop restarts. A boolean, η, is then set to $\texttt{true}$ to indicate that non-convergence has occurred after convergence had been reached previously.

4. Once $\eta = \texttt{true}$, the memory time is increased by 2.5 then decreased by 0.25 in a loop while the recalculated $\sigma_z(t)$ satisfies Eq. (III.40), with $\sigma_z(t)$ stored as $\sigma_{z,\text{prev}}(t)$ each time the loop restarts. If Eq. (III.40) is no longer satisfied, $\sigma_{z,\text{prev}}(t)$ is determined as the converged $\sigma_z(t)$ at the lowest possible memory time (by steps of 0.25).

III.5 Concluding remarks

This chapter introduced two different ways of using the QC/MH method to calculate the memory kernel of the GQME. The two QC/MH-based approaches were benchmarked against a spin-boson model, for which the exact results are known, and compared with a previously proposed Ehrenfest-based approach.

There are several reasons why the QC/MH method can be the method of choice for calculating the memory kernel of the GQME. First, due to the requirement that the electronic density matrix be Hermitian in order for the mean force experienced by the nuclear DOF within the Ehrenfest method to be real, there are multiple protocols for calculating the memory kernel that can give different answers, without a clear criterion for choosing between them.[35] In contrast, within both LSCI and LSCII, the force experienced by the nuclear DOF is always real regardless of whether or not the initial electronic state is described by a Hermitian operator. Second, the fact that LSC treats both electronic and nuclear DOF on the same footing in terms of classical-like phase-space variables should make it easier to incorporate into existing classical MD codes.

The results reported in this chapter demonstrate that LSC provides a useful route for calculating GQME memory kernels. LSCII in particular seems to produce asymptotically better behaved memory kernels that lead to both computational cost reduction and more accurate electronic dynamics in comparison to both Ehrenfest and LSCI. Further study of the accuracy and computational cost of combining QC/MH, as well as other approximate and exact methods, with the GQME approach would be highly desirable. For example, Saller, Kelly, and Richardson have recently introduced a new QC/MH-based method that shows great improvement over LSCI and LSCII.[104,105] Using their approach for calculating the memory kernel, which would be desirable in cases where it is seen to be less accurate on its own, can be achieved following the procedure proposed in this paper. Several other recently proposed methods[106,107] aimed at simulating the dynamics of systems described by the Hamiltonian in Eq. (I.3) may also benefit from being combined with the GQME approach. Along with exploring other input methods, research into extending the range of applications to models with more than two states, anharmonic PESs, and non-Condon electronic coupling is also of great interest.

CHAPTER IV

Exploration of the Various Approaches to Obtain the Memory Kernel of the GQME

IV.1 Introduction

In Chapter II, the Shi-Geva, Zhang-Ka-Geva, and modified approach to the GQME were introduced. Due to the many variations of the memory kernel, partially introduced in Eq. (II.3), and the manipulability of the general identity given in Eq. (II.4), these three approaches are only three of many. Additionally, as introduced in Ref. 32, the projection-free inputs can be calculated various ways, by calculating the correlation functions (CFs) in the form given in Eq. (II.38) (i) directly or (ii) following one of three types of expansions involving time-derivatives of other projection-free inputs or of the time propagation superoperator for the reduced electronic density matrix, $\mathcal{U}(\tau) = \mathrm{Tr}_n\{e^{-i\mathcal{L}\tau/\hbar}\hat{\rho}_n(0)\}$.

In this chapter, the methods studied include four system-bath approaches and three modified approaches with Condon and non-Condon variations along with the four possible expansions for obtaining the projection-free inputs for each, leading to forty-four different methods of obtaining the GQME. It should be noted that these forty-four different methods are obtained with no approximations, meaning that if an exact input method is used, they would give the same result. However, with approximate input methods, these different methods could and are expected to give different results. This thorough investigation of the GQME helps to understand the impact of the different components of the projection-free inputs and the form of the Volterra equations on the results,

allowing better selection of the approach to use for future systems and input methods of interest.

In this chapter, the eleven different approaches (the four system-bath approaches and three modified approaches with Condon and non-Condon variations, with one having two different Condon variations) will be introduced in Sec. IV.2. The four expansions possible for each of the eleven approaches will be outlined Sec. IV.3. The results for these methods on the spin-boson model with the two QC/MH input methods from Chapter III will be outlined in Sec. IV.4. A discussion of these results is given in Sec. IV.5. Concluding remarks are given in Sec. IV.6. Additional results are included in Appendix B.

IV.2 Approaches for obtaining the memory kernel

In this section, the eleven different approaches for obtaining the memory kernel will be discussed in further detail. The eleven approaches can first be divided into whether they are based on the system-bath splitting of the Hamiltonian detailed in Sec. II.2 or if they are based on the modified form of the GQME outlined in Sec. II.3. This distinction will be noted in differentiating the approaches by including either *System-Bath* for the former or *Modified* for the latter in the approaches' titles.

The approaches can further be divided based on the number of equations needed to obtain the memory kernel. Four approaches, one with the system-bath form and three with the modified form, have two equations to obtain the memory kernel: the first equation is a Volterra integral equation of the second type to obtain an intermediary projection-dependent input and the second is an equation to obtain the memory kernel from the projection-free and projection-dependent inputs. These four approaches are designated by including *Two-Equation* in their titles and *TE* in their abbreviations.

The remaining seven approaches all have only one Volterra equation to obtain the memory kernel directly from the projection-free inputs. These seven approaches can be divided based on the form of the memory kernel the approach begins with; more distinctly, based on the form of the exponential within the memory kernel. For the approaches explored in this chapter, the relevant

forms of the system-bath memory kernel are

$$\mathcal{K}(\tau) = \frac{1}{\hbar^2}\mathrm{Tr}_B\Big\{\mathcal{L}_{BS}e^{-i(\mathcal{L}-\mathcal{L}_{BS}\mathcal{P})\tau/\hbar}\mathcal{L}_{BS}\hat{\rho}_B^{\mathrm{eq}}\Big\} \quad , \tag{IV.1}$$

$$= \frac{1}{\hbar^2}\mathrm{Tr}_B\Big\{\mathcal{L}_{BS}e^{-i\mathcal{Q}\mathcal{L}\tau/\hbar}\mathcal{Q}\mathcal{L}\hat{\rho}_B^{\mathrm{eq}}\Big\} \quad , \tag{IV.2}$$

$$= \frac{1}{\hbar^2}\mathrm{Tr}_B\Big\{\mathcal{L}_{BS}e^{-i\mathcal{Q}\mathcal{L}\tau/\hbar}\mathcal{Q}\mathcal{L}_{BS}\hat{\rho}_B^{\mathrm{eq}}\Big\} \quad , \tag{IV.3}$$

$$= \frac{1}{\hbar^2}\mathrm{Tr}_B\Big\{\mathcal{L}_{BS}\mathcal{Q}e^{-i\mathcal{L}\mathcal{Q}\tau/\hbar}\mathcal{L}_{BS}\hat{\rho}_B^{\mathrm{eq}}\Big\} \quad ; \tag{IV.4}$$

the relevant forms of the modified non-Condon memory kernel are

$$\mathcal{K}(\tau) = \frac{1}{\hbar^2}\mathrm{Tr}_n\Big\{\mathcal{L}\,e^{-i\mathcal{Q}\mathcal{L}\tau/\hbar}\mathcal{Q}\mathcal{L}\hat{\rho}_n(0)\Big\} \quad , \tag{IV.5}$$

$$= \frac{1}{\hbar^2}\mathrm{Tr}_n\Big\{\mathcal{L}\mathcal{Q}\,e^{-i\mathcal{L}\mathcal{Q}\tau/\hbar}\mathcal{L}\hat{\rho}_n(0)\Big\} \quad ; \tag{IV.6}$$

and the relevant forms of the modified Condon memory kernel are

$$\mathcal{K}(\tau) = \frac{1}{\hbar^2}\mathrm{Tr}_n\Big\{\mathcal{L}_{\mathrm{zero}}\,e^{-i\mathcal{Q}\mathcal{L}\tau/\hbar}\mathcal{Q}\mathcal{L}_{\mathrm{zero}}\hat{\rho}_n(0)\Big\} \quad , \tag{IV.7}$$

$$= \frac{1}{\hbar^2}\mathrm{Tr}_n\Big\{\mathcal{L}_{\mathrm{zero}}\mathcal{Q}\,e^{-i\mathcal{L}\mathcal{Q}\tau/\hbar}\mathcal{L}_{\mathrm{zero}}\hat{\rho}_n(0)\Big\} \quad . \tag{IV.8}$$

Looking at the memory kernel forms given in Eqs. (IV.2), (IV.3), (IV.5), and (IV.7), the exponent has the projection superoperator $\mathcal{Q}$ first and the Liouvillian superoperator $\mathcal{L}$ second. In comparison, Eqs. (IV.4), (IV.6), and (IV.8) have the projection superoperator $\mathcal{Q}$ second and the Liouvillian superoperator $\mathcal{L}$ first in the exponent. For this reason, the four approaches that have memory kernels of the forms given in Eqs. (IV.2), (IV.3), (IV.5), and (IV.7) are designated as *Projection-First (PF)* and the three approaches that have memory kernels of the forms given in Eqs. (IV.4), (IV.6), and (IV.8) are designated as *Projection-Second (PS)*.

The two-equation, projection-first, and projection-second approaches that use the modified form of the GQME have both non-Condon and Condon versions, leading to six different approaches. Additionally, the modified two-equation approach has two different Condon versions,

giving a total of seven different approaches that use the modified form of the GQME. Combined with the four approaches that use the system-bath form of the GQME, this gives the eleven different approaches for obtaining the memory kernel. The list of titles and abbreviations of these approaches is:

- *System-Bath Two-Equation (SB-TE)*;
- *System-Bath Projection-First, Version 1 (SB-PF1)*;
- *System-Bath Projection-First, Version 2 (SB-PF2)*;
- *System-Bath Projection-Second (SB-PS)*;
- *Modified Two-Equation Non-Condon (M-TE-NC)*;
- *Modified Two-Equation Condon, Version 1 (M-TE-C1)*;
- *Modified Two-Equation Condon, Version 2 (M-TE-C2)*;
- *Modified Projection-First Non-Condon (M-PF-NC)*;
- *Modified Projection-First Condon (M-PF-C)*;
- *Modified Projection-Second Non-Condon (M-PS-NC)*;
- *Modified Projection-Second Condon (M-PS-C)*;

and can be visualized using the titles-only tree diagram shown in Fig. IV.1. These eleven approaches are further detailed in the following subsections and a more detailed tree diagram is given at the end of this section in Figs. IV.2.

The identities used by the approaches to obtain projection-free inputs have one of the following general forms:[28,29,62,108]

$$e^{-i\mathcal{B}\tau/\hbar} = e^{-i\mathcal{A}\tau/\hbar} - \frac{i}{\hbar}\int_0^\tau d\tau'\, e^{-i\mathcal{A}(\tau-\tau')/\hbar}(\mathcal{B}-\mathcal{A})e^{-i\mathcal{B}\tau'/\hbar} \quad , \tag{IV.9}$$

$$e^{-i\mathcal{B}\tau/\hbar} = e^{-i\mathcal{A}\tau/\hbar} - \frac{i}{\hbar}\int_0^\tau d\tau'\, e^{-i\mathcal{A}\tau'/\hbar}(\mathcal{B}-\mathcal{A})e^{-i\mathcal{B}(\tau-\tau')/\hbar} \quad , \tag{IV.10}$$

where the first equation was given previously in Eq. (II.4). Additionally, the different approaches use Liouvillian superoperators based on the splitting of the Hamiltonian. The system-bath Hamiltonian is given by $\hat{H} = \hat{H}_S + \hat{H}_B + \hat{H}_{BS}$ [see Eq. (II.1)] and each term has a matching Liouvillian operator; e.g., $\mathcal{L}_S = [\hat{H}_S, \cdot\,]$, $\mathcal{L}_B = [\hat{H}_B, \cdot\,]$, and $\mathcal{L}_{BS} = [\hat{H}_{BS}, \cdot\,]$, respectively. The modified Hamiltonian can be split into two terms $\hat{H} = \hat{H}_{\text{zero}} + \hat{H}_{\text{int}}$ given by $\hat{H}_{\text{zero}} = \sum_{j=1}^{N_e} \hat{H}_j |j\rangle\langle j|$

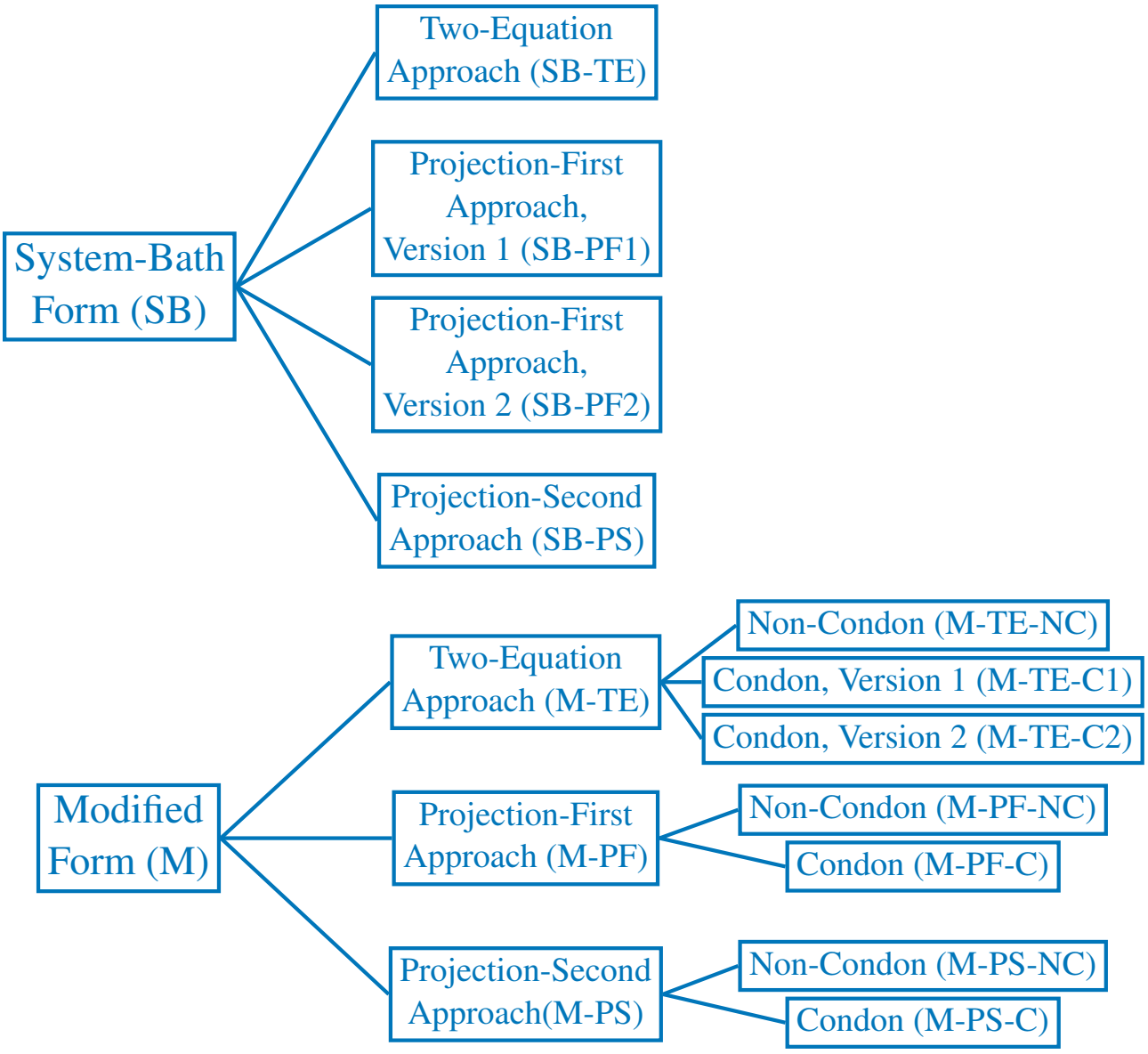

Figure IV.1: Tree diagram of the titles for the eleven approaches to obtaining the memory kernel explored in this chapter.

and $\hat{H}_{\text{int}} = \sum_{\substack{j,k=1 \\ k\neq j}}^{N_e} \hat{V}_{jk}|j\rangle\langle k|$. Each term has a matching Liouvillian operator as well, given by $\mathcal{L}_{\text{zero}}(\cdot) = [\hat{H}_{\text{zero}}, \cdot\,]$ and $\mathcal{L}_{\text{int}}(\cdot) = [\hat{H}_{\text{int}}, \cdot\,]$, respectively [see Eq. (II.25)].

IV.2.1 System-Bath Two-Equation Approach (SB-TE)

The system-bath two-equation approach (SB-TE) is the same as the Shi-Geva approach introduced in Sec. II.2.1. While more details are given in Sec. II.2.1, some details are copied below that are important for understanding the expansions of the projection-free inputs given in Sec. IV.3 and for comparing to the other methods. The SB-TE approach uses a memory kernel of the form given in Eq. (II.5):

$$\mathcal{K}(\tau) = \frac{1}{\hbar^2}\mathrm{Tr}_B\Big\{\mathcal{L}_{BS}\, e^{-i(\mathcal{L}-\mathcal{L}_{BS}\mathcal{P})\tau/\hbar}\mathcal{L}_{BS}\hat{\rho}_B^{\mathrm{eq}}\Big\} \quad .$$

Substituting $\mathcal{A} = \mathcal{L}$ and $\mathcal{B} = \mathcal{L} - \mathcal{L}_{BS}\mathcal{P}$ into the operator identity in Eq. (IV.9) and plugging into the memory kernel above gives the following expression for the memory kernel [Eq. (II.7)]

$$\mathcal{K}(\tau) = \mathcal{K}_1(\tau) + i\int_0^\tau \mathcal{K}_1(\tau-\tau')\mathcal{K}_2(\tau') \quad ,$$

where [see Eqs. (II.8) and (II.9)]

$$\mathcal{K}_1(\tau) = \frac{1}{\hbar^2}\,\mathrm{Tr}_B\left\{\mathcal{L}_{BS}e^{-i\mathcal{L}\tau/\hbar}\mathcal{L}_{BS}\,\hat{\rho}_B^{\mathrm{eq}}\right\} \quad ,$$
$$\mathcal{K}_2(\tau) = \frac{1}{\hbar}\,\mathrm{Tr}_B\left\{e^{-i(\mathcal{L}-\mathcal{L}_{BS}\mathcal{P})\tau/\hbar}\mathcal{L}_{BS}\,\hat{\rho}_B^{\mathrm{eq}}\right\} \quad .$$

Repeating the process for $\mathcal{K}_2(\tau)$, since it is projection-dependent, leads to the Volterra equation [see Eq. (II.10)]

$$\mathcal{K}_2(\tau) = \mathcal{K}_3(\tau) + i\int_0^\tau d\tau'\,\mathcal{K}_3(\tau-\tau')\mathcal{K}_2(\tau') \quad ,$$

where [see Eq. (II.11)]

$$\mathcal{K}_3(\tau) = \frac{1}{\hbar}\,\mathrm{Tr}_B\left\{e^{-i\mathcal{L}\tau/\hbar}\mathcal{L}_{BS}\,\hat{\rho}_B^{\mathrm{eq}}\right\} \quad .$$

Therefore, obtaining the memory kernel via the SB-TE approach requires first calculating $\mathcal{K}_1(\tau)$ and $\mathcal{K}_3(\tau)$, then calculating $\mathcal{K}_2(\tau)$ through Eq. (II.10), and finally calculating $\mathcal{K}(\tau)$ via Eq. (II.7).

IV.2.2 System-Bath Projection-First Approach, Version 1 (SB-PF1)

The system-bath projection-first approach, version 1 (SB-PF1) is the same as the Zhang-Ka-Geva approach introduced in Sec. II.2.2. While more details are given in Sec. II.2.2, some details are copied below. The SB-PF1 approach uses a memory kernel of the form given in Eq. (II.12):

$$\mathcal{K}(\tau) = \frac{1}{\hbar^2}\mathrm{Tr}_B\Big\{\mathcal{L}_{BS}e^{-i\mathcal{Q}\mathcal{L}\tau/\hbar}\mathcal{Q}\mathcal{L}\hat{\rho}_B^{\mathrm{eq}}\Big\} \quad .$$

Substituting $\mathcal{A} = \mathcal{L}$ and $\mathcal{B} = \mathcal{Q}\mathcal{L}$ into Eq. (IV.9) and plugging that into the memory kernel above leads to the following Volterra equation for $\mathcal{K}(\tau)$ [see Eq. (II.13)]:

$$\mathcal{K}(\tau) = \dot{\Phi}(\tau) + \frac{i}{\hbar}\Phi(\tau)\mathcal{L}_S + \int_0^\tau d\tau' \Phi(\tau-\tau')\mathcal{K}(\tau') \quad ,$$

where $\Phi(\tau)$ and $\dot{\Phi}(\tau)$ are the projection-free inputs [see Eq. (II.14)]

$$\begin{aligned}
\Phi(\tau) &= \frac{i}{\hbar}\mathrm{Tr}_B\Big\{\mathcal{L}_{BS}e^{-i\mathcal{L}\tau/\hbar}\hat{\rho}_B^{\mathrm{eq}}\Big\} \quad , \\
\dot{\Phi}(\tau) &= \frac{1}{\hbar^2}\mathrm{Tr}_B\Big\{\mathcal{L}_{BS}e^{-i\mathcal{L}\tau/\hbar}\mathcal{L}\hat{\rho}_B^{\mathrm{eq}}\Big\} \quad .
\end{aligned} \tag{IV.11}$$

Therefore, obtaining the memory kernel via the SB-PF1 approach requires first calculating $\Phi(\tau)$ and $\dot{\Phi}(\tau)$ and then calculating the memory kernel via Eq. (II.13).

IV.2.3 System-Bath Projection-First Approach, Version 2 (SB-PF2)

The system-bath projection-first approach, version 2 (SB-PF2) was previously introduced in Ref. 32. In the SB-PF2 approach, the memory kernel has the form

$$\mathcal{K}(\tau) = \frac{1}{\hbar^2}\mathrm{Tr}_B\Big\{\mathcal{L}_{BS}e^{-i\mathcal{Q}\mathcal{L}\tau/\hbar}\mathcal{Q}\mathcal{L}_{BS}\hat{\rho}_B^{\mathrm{eq}}\Big\} \quad . \tag{IV.12}$$

Substituting $\mathcal{A} = \mathcal{L}$ and $\mathcal{B} = \mathcal{QL}$ into Eq. (IV.9) and plugging that into Eq. (IV.12) leads to a Volterra equation of the form

$$\mathcal{K}(\tau) = \mathcal{K}_1(\tau) + \int_0^\tau d\tau' \, \Phi(\tau - \tau')\mathcal{K}(\tau') \quad , \tag{IV.13}$$

where $\mathcal{K}_1(\tau)$ is as given in Eq. (II.8) and copied above in Sec. IV.2.1 and $\Phi(\tau)$ is as given in Eq. (II.14) and copied above in Sec. IV.2.2. Therefore, obtaining the memory kernel via the SB-PF1 approach requires first calculating $\mathcal{K}_1(\tau)$ and $\Phi(\tau)$ and then calculating the memory kernel via Eq. (IV.13). Notably, this approach has projection-free inputs that are also used in the SB-TE and SB-PF1 approaches, which will help narrow down the effect of the form of the projection-free inputs and the equations for the memory kernel.

IV.2.4 System-Bath Projection-Second Approach (SB-PS)

The system-bath projection-second approach (SB-PS) was previously introduced in Ref. 32. In the SB-PS approach, the memory kernel has the form

$$\mathcal{K}(\tau) = \frac{1}{\hbar^2}\mathrm{Tr}_B\Big\{\mathcal{L}_{BS}\mathcal{Q}e^{-i\mathcal{L}\mathcal{Q}\tau/\hbar}\mathcal{L}_{BS}\hat{\rho}_B^{\mathrm{eq}}\Big\} \quad . \tag{IV.14}$$

Substituting $\mathcal{A} = \mathcal{LQ}$ and $\mathcal{B} = \mathcal{L}$ into Eq. (IV.10) and plugging that into Eq. (IV.14) leads to a Volterra equation of the form

$$\mathcal{K}(\tau) = \mathcal{K}_1(\tau) + \int_0^\tau d\tau' \, \mathcal{K}(\tau - \tau')\mathcal{K}_3(\tau') \quad , \tag{IV.15}$$

where $\mathcal{K}_1(\tau)$ is as given in Eq. (II.8), $\mathcal{K}_3(\tau)$ is as given in Eq. (II.11), and both are copied above in Sec. IV.2.1. Therefore, obtaining the memory kernel via the SB-PF1 approach requires first calculating $\mathcal{K}_1(\tau)$ and $\mathcal{K}_3(\tau)$ and then calculating the memory kernel via Eq. (IV.15). Notably, this approach uses the same projection-free inputs as the SB-TE approach but only a single Volterra equation is needed to obtain the memory kernel, rather than two coupled equations. Additionally,

the memory kernel is the first superoperator in the integral whereas in the Volterra equations in the SB-PF1 and SB-PF2 approaches, it is the second superoperator.

IV.2.5 Modified Two-Equation Approach (M-TE)

IV.2.5.1 Non-Condon Variation (M-TE-NC)

The non-Condon modified two-equation approach (M-TE-NC) starts from a memory kernel of the form:

$$\mathcal{K}(\tau) = \frac{1}{\hbar^2}\mathrm{Tr}_n\Big\{\mathcal{L}\mathcal{Q}\, e^{-i\mathcal{L}\mathcal{Q}\tau/\hbar}\mathcal{L}\hat{\rho}_n(0)\Big\} \quad . \tag{IV.16}$$

Substituting $\mathcal{A} = \mathcal{L}$ and $\mathcal{B} = \mathcal{L}\mathcal{Q}$ into the operator identity in Eq. (IV.9) and plugging into Eq. (IV.16) above gives the following expressions for the memory kernel

$$\mathcal{K}(\tau) = i\dot{\mathcal{F}}(\tau) - \frac{1}{\hbar}\langle\mathcal{L}\rangle_n^0\mathcal{G}(\tau) + i\int_0^\tau d\tau'\left[i\dot{\mathcal{F}}(\tau-\tau') - \frac{1}{\hbar}\langle\mathcal{L}\rangle_n^0\mathcal{G}(\tau-\tau')\right]\mathcal{G}_2(\tau') \quad , \tag{IV.17}$$

where $\dot{\mathcal{F}}(\tau)$ is the time-derivative of $\mathcal{F}(\tau)$ given in Eq. (II.31), which is equivalent to

$$\dot{\mathcal{F}}_1(\tau) = -\frac{i}{\hbar^2}\,\mathrm{Tr}_n\left\{\mathcal{L}e^{-i\mathcal{L}\tau/\hbar}\mathcal{L}\,\hat{\rho}_n(0)\right\} \quad , \tag{IV.18}$$

and $\mathcal{G}(\tau)$ and $\mathcal{G}_2(\tau)$ are given by

$$\mathcal{G}(\tau) = \frac{1}{\hbar}\,\mathrm{Tr}_n\left\{e^{-i\mathcal{L}\tau/\hbar}\mathcal{L}\hat{\rho}_n(0)\right\} \tag{IV.19}$$

$$\mathcal{G}_2(\tau) = \frac{1}{\hbar}\,\mathrm{Tr}_n\left\{e^{-i\mathcal{L}\mathcal{Q}\tau/\hbar}\mathcal{L}\hat{\rho}_n(0)\right\} \tag{IV.20}$$

Repeating the process for $\mathcal{G}_2(\tau)$, since it is projection-dependent, leads to the Volterra equation

$$\mathcal{G}_2(\tau) = \mathcal{G}(\tau) + i\int_0^\tau d\tau'\mathcal{G}(\tau-\tau')\mathcal{G}_2(\tau') \quad . \tag{IV.21}$$

Therefore, the process of obtaining the memory kernel via the non-Condon M-TE approach (M-TE-NC) requires first calculating $\dot{\mathcal{F}}(\tau)$ and $\mathcal{G}(\tau)$, then calculating $\mathcal{G}_2(\tau)$ through Eq. (IV.21), and finally calculating $\mathcal{K}(\tau)$ via Eq. (IV.17).

IV.2.5.2 Condon Variation, Version 1 (M-TE-C1)

The Condon modified two-equation approach, version 1 (M-TE-C1) starts from a memory kernel of the form:

$$\mathcal{K}(\tau) = \frac{1}{\hbar^2}\mathrm{Tr}_n\Big\{\mathcal{L}_{\text{zero}}\mathcal{Q}\, e^{-i\mathcal{L}\mathcal{Q}\tau/\hbar}\mathcal{L}_{\text{zero}}\hat{\rho}_n(0)\Big\} \quad . \tag{IV.22}$$

Substituting $\mathcal{A} = \mathcal{L}$ and $\mathcal{B} = \mathcal{L}\mathcal{Q}$ into the operator identity in Eq. (IV.9) and plugging into Eq. (IV.22) above results in the following derivation

$$\begin{aligned}
\mathcal{K}(\tau) &= \frac{1}{\hbar^2}\mathrm{Tr}_n\Big\{\mathcal{L}_{\text{zero}}\mathcal{Q}\Big[e^{-i\mathcal{L}\tau/\hbar} + \frac{i}{\hbar}\int_0^\tau d\tau'\, e^{-i\mathcal{L}(\tau-\tau')/\hbar}\mathcal{L}\mathcal{P}e^{-i\mathcal{L}\mathcal{Q}\tau'/\hbar}\Big]\mathcal{L}_{\text{zero}}\hat{\rho}_n(0)\Big\} \\
&= \frac{1}{\hbar^2}\mathrm{Tr}_n\Big\{\mathcal{L}_{\text{zero}}\mathcal{Q}e^{-i\mathcal{L}\tau/\hbar}\mathcal{L}_{\text{zero}}\hat{\rho}_n(0)\Big\} \\
&\quad + \frac{i}{\hbar}\int_0^\tau d\tau'\,\frac{1}{\hbar^2}\mathrm{Tr}_n\Big\{\mathcal{L}_{\text{zero}}\mathcal{Q}e^{-i\mathcal{L}(\tau-\tau')/\hbar}\mathcal{L}\hat{\rho}_n(0)\Big\}\,\mathrm{Tr}_n\Big\{e^{-i\mathcal{L}\mathcal{Q}\tau'/\hbar}\mathcal{L}_{\text{zero}}\hat{\rho}_n(0)\Big\} \\
&= \frac{1}{\hbar^2}\mathrm{Tr}_n\Big\{\mathcal{L}_{\text{zero}}\, e^{-i\mathcal{L}\tau/\hbar}\mathcal{L}_{\text{zero}}\hat{\rho}_n(0)\Big\} - \frac{1}{\hbar^2}\mathrm{Tr}_n\Big\{\mathcal{L}_{\text{zero}}\hat{\rho}_n(0)\Big\}\,\mathrm{Tr}_n\Big\{e^{-i\mathcal{L}\tau/\hbar}\mathcal{L}_{\text{zero}}\hat{\rho}_n(0)\Big\} \\
&\quad + i\int_0^\tau d\tau'\,\Big[\frac{1}{\hbar^2}\mathrm{Tr}_n\Big\{\mathcal{L}_{\text{zero}}e^{-i\mathcal{L}(\tau-\tau')/\hbar}\Big(\mathcal{L}_{\text{zero}}+\mathcal{L}_{\text{int}}\Big)\hat{\rho}_n(0)\Big\} \\
&\qquad - \frac{1}{\hbar^2}\mathrm{Tr}_n\Big\{\mathcal{L}_{\text{zero}}\hat{\rho}_n(0)\Big\}\,\mathrm{Tr}_n\Big\{e^{-i\mathcal{L}(\tau-\tau')/\hbar}\Big(\mathcal{L}_{\text{zero}}+\mathcal{L}_{\text{int}}\Big)\hat{\rho}_n(0)\Big\}\Big]\frac{1}{\hbar}\,\mathrm{Tr}_n\Big\{e^{-i\mathcal{L}\mathcal{Q}\tau'/\hbar}\mathcal{L}_{\text{zero}}\hat{\rho}_n(0)\Big\} \\
&= \mathcal{F}_1(\tau) - \frac{1}{\hbar}\langle\mathcal{L}_{\text{zero}}\rangle_n^0\,\mathcal{F}_2(\tau) + i\int_0^\tau d\tau'\,\Big[\frac{1}{\hbar^2}\mathrm{Tr}_n\Big\{\mathcal{L}_{\text{zero}}e^{-i\mathcal{L}(\tau-\tau')/\hbar}\mathcal{L}_{\text{zero}}\hat{\rho}_n(0)\Big\} \\
&\quad + \frac{1}{\hbar^2}\mathrm{Tr}_n\Big\{\mathcal{L}_{\text{zero}}e^{-i\mathcal{L}(\tau-\tau')/\hbar}\hat{\rho}_n(0)\Big\}\mathcal{L}_{\text{int}} - \frac{1}{\hbar^2}\langle\mathcal{L}_{\text{zero}}\rangle_n^0\,\mathrm{Tr}_n\Big\{e^{-i\mathcal{L}(\tau-\tau')/\hbar}\mathcal{L}_{\text{zero}}\hat{\rho}_n(0)\Big\} \\
&\qquad + \frac{1}{\hbar^2}\langle\mathcal{L}_{\text{zero}}\rangle_n^0\,\mathrm{Tr}_n\Big\{e^{-i\mathcal{L}(\tau-\tau')/\hbar}\hat{\rho}_n(0)\Big\}\mathcal{L}_{\text{int}}\Big]\mathcal{G}_{2,\text{zero}}(\tau')
\end{aligned} \tag{IV.23}$$

$$\begin{aligned}
\mathcal{K}(\tau) = \mathcal{F}_1(\tau) - \frac{1}{\hbar}\langle\mathcal{L}_{\text{zero}}\rangle_n^0\mathcal{G}_{\text{zero}}(\tau) + i\int_0^\tau d\tau'\,\Big[&\mathcal{F}_1(\tau-\tau') + \frac{1}{\hbar}\mathcal{F}_2(\tau-\tau')\mathcal{L}_{\text{int}} \\
&- \frac{1}{\hbar}\langle\mathcal{L}_{\text{zero}}\rangle_n^0\mathcal{G}_{\text{zero}}(\tau-\tau') - \frac{1}{\hbar^2}\langle\mathcal{L}_{\text{zero}}\rangle_n^0\,\mathcal{U}_{\text{M}}(\tau-\tau')\mathcal{L}_{\text{int}}\Big]\mathcal{G}_{2,\text{zero}}(\tau') \quad ,
\end{aligned} \tag{IV.24}$$

where $\mathcal{L}_{\text{int}}$ is able to commute with $\hat{\rho}_n(0)$ and move outside of the trace over the nuclear DOF because it is a purely electronic superoperator in the Condon approximation. $\mathcal{F}_1(\tau)$ is as given in Eq. (II.33),

$$\mathcal{F}_1(\tau) = -\frac{i}{\hbar^2}\,\mathrm{Tr}_n\left\{\mathcal{L}_{\text{zero}} e^{-i\mathcal{L}\tau/\hbar}\mathcal{L}_{\text{zero}}\,\hat{\rho}_n(0)\right\} \quad , \tag{IV.25}$$

and $\mathcal{G}_{\text{zero}}(\tau)$ and $\mathcal{G}_{2,\text{zero}}(\tau)$ are given by

$$\mathcal{G}_{\text{zero}}(\tau) = \frac{1}{\hbar}\,\mathrm{Tr}_n\left\{e^{-i\mathcal{L}\tau/\hbar}\mathcal{L}_{\text{zero}}\hat{\rho}_n(0)\right\} \quad , \tag{IV.26}$$

$$\mathcal{G}_{2,\text{zero}}(\tau) = \frac{1}{\hbar}\,\mathrm{Tr}_n\left\{e^{-i\mathcal{L}\mathcal{Q}\tau/\hbar}\mathcal{L}_{\text{zero}}\hat{\rho}_n(0)\right\} \quad . \tag{IV.27}$$

Repeating the process for $\mathcal{G}_{2,\text{zero}}(\tau)$, since it is projection-dependent, results in the following derivation of the Volterra equation

$$\begin{aligned}
\mathcal{G}_{2,\text{zero}}(\tau) &= \frac{1}{\hbar}\,\mathrm{Tr}_n\left\{\left[e^{-i\mathcal{L}\tau/\hbar} + \frac{i}{\hbar}\int_0^\tau d\tau'\, e^{-i\mathcal{L}(\tau-\tau')/\hbar}\mathcal{L}\mathcal{P}e^{-i\mathcal{L}\mathcal{Q}\tau'/\hbar}\right]\mathcal{L}_{\text{zero}}\hat{\rho}_n(0)\right\} \\
&= \frac{1}{\hbar}\,\mathrm{Tr}_n\left\{e^{-i\mathcal{L}\tau/\hbar}\mathcal{L}_{\text{zero}}\hat{\rho}_n(0)\right\} \\
&\quad + \frac{i}{\hbar}\int_0^\tau d\tau'\,\frac{1}{\hbar}\,\mathrm{Tr}_n\left\{e^{-i\mathcal{L}(\tau-\tau')/\hbar}\mathcal{L}\hat{\rho}_n(0)\right\}\mathrm{Tr}_n\left\{e^{-i\mathcal{L}\mathcal{Q}\tau'/\hbar}\mathcal{L}_{\text{zero}}\hat{\rho}_n(0)\right\} \\
&= \mathcal{G}_{\text{zero}}(\tau) + i\int_0^\tau d\tau'\left[\frac{1}{\hbar}\,\mathrm{Tr}_n\left\{e^{-i\mathcal{L}(\tau-\tau')/\hbar}\mathcal{L}_{\text{zero}}\hat{\rho}_n(0)\right\}\right. \\
&\quad \left. + \frac{1}{\hbar}\,\mathrm{Tr}_n\left\{e^{-i\mathcal{L}(\tau-\tau')/\hbar}\hat{\rho}_n(0)\right\}\mathcal{L}_{\text{int}}\right] \times \frac{1}{\hbar}\,\mathrm{Tr}_n\left\{e^{-i\mathcal{L}\mathcal{Q}\tau'/\hbar}\mathcal{L}_{\text{zero}}\hat{\rho}_n(0)\right\}
\end{aligned} \tag{IV.28}$$

$$\mathcal{G}_{2,\text{zero}}(\tau) = \mathcal{G}_{\text{zero}}(\tau) + i\int_0^\tau d\tau'\left[\mathcal{G}_{\text{zero}}(\tau-\tau') + \frac{1}{\hbar}\mathcal{U}_{\text{M}}(\tau-\tau')\mathcal{L}_{\text{int}}\right]\mathcal{G}_{2,\text{zero}}(\tau') \quad . \tag{IV.29}$$

Therefore, the process of obtaining the memory kernel via the Condon M-TE approach, version 1 (M-TE-C1) requires first calculating $\mathcal{F}_1(\tau)$ and $\mathcal{G}_{\text{zero}}(\tau)$, then calculating $\mathcal{G}_{2,\text{zero}}(\tau)$ through Eq. (IV.29), and finally calculating $\mathcal{K}(\tau)$ via Eq. (IV.24).

IV.2.5.3 Condon Variation, Version 2 (M-TE-C2)

The Condon modified two-equation approach, version 2 (M-TE-C2) starts from the same memory kernel as M-TE-C1, Eq. (IV.22), and uses the same identity expression. The difference begins

in the derivation of the Volterra equation, starting from Eq. (IV.23):

$$\begin{aligned}
\mathcal{K}(\tau) &= \frac{1}{\hbar^2}\mathrm{Tr}_n\Big\{\mathcal{L}_{\text{zero}}\mathcal{Q}e^{-i\mathcal{L}\tau/\hbar}\mathcal{L}_{\text{zero}}\hat{\rho}_n(0)\Big\} \\
&\quad + \frac{i}{\hbar}\int_0^\tau d\tau' \, \frac{1}{\hbar^2}\,\mathrm{Tr}_n\Big\{\mathcal{L}_{\text{zero}}\mathcal{Q}e^{-i\mathcal{L}(\tau-\tau')/\hbar}\mathcal{L}\hat{\rho}_n(0)\Big\}\,\mathrm{Tr}_n\Big\{e^{-i\mathcal{L}\mathcal{Q}\tau'/\hbar}\mathcal{L}_{\text{zero}}\hat{\rho}_n(0)\Big\} \\
&= \frac{1}{\hbar^2}\mathrm{Tr}_n\Big\{\mathcal{L}_{\text{zero}}e^{-i\mathcal{L}\tau/\hbar}\mathcal{L}_{\text{zero}}\hat{\rho}_n(0)\Big\} - \frac{1}{\hbar^2}\mathrm{Tr}_n\Big\{\mathcal{L}_{\text{zero}}\hat{\rho}_n(0)\Big\}\,\mathrm{Tr}_n\Big\{e^{-i\mathcal{L}\tau/\hbar}\mathcal{L}_{\text{zero}}\hat{\rho}_n(0)\Big\} \\
&\quad + \frac{i}{\hbar}\int_0^\tau d\tau' \, \frac{1}{\hbar^2}\mathrm{Tr}_n\Big\{\mathcal{L}\mathcal{Q}e^{-i\mathcal{L}(\tau-\tau')/\hbar}\mathcal{L}\hat{\rho}_n(0)\Big\}\,\mathrm{Tr}_n\Big\{e^{-i\mathcal{L}\mathcal{Q}\tau'/\hbar}\mathcal{L}_{\text{zero}}\hat{\rho}_n(0)\Big\} \\
&= \frac{1}{\hbar^2}\mathrm{Tr}_n\Big\{\mathcal{L}_{\text{zero}}e^{-i\mathcal{L}\tau/\hbar}\mathcal{L}_{\text{zero}}\hat{\rho}_n(0)\Big\} - \frac{1}{\hbar^2}\mathrm{Tr}_n\Big\{\mathcal{L}_{\text{zero}}\hat{\rho}_n(0)\Big\}\,\mathrm{Tr}_n\Big\{e^{-i\mathcal{L}\tau/\hbar}\mathcal{L}_{\text{zero}}\hat{\rho}_n(0)\Big\} \\
&\quad + \frac{i}{\hbar}\int_0^\tau d\tau' \left[\frac{1}{\hbar^2}\mathrm{Tr}_n\Big\{\mathcal{L}e^{-i\mathcal{L}(\tau-\tau')/\hbar}\mathcal{L}\hat{\rho}_n(0)\Big\}\right. \\
&\qquad \left. - \frac{1}{\hbar^2}\mathrm{Tr}_n\Big\{\mathcal{L}\hat{\rho}_n(0)\Big\}\,\mathrm{Tr}_n\Big\{e^{-i\mathcal{L}(\tau-\tau')/\hbar}\mathcal{L}\hat{\rho}_n(0)\Big\}\right]\mathrm{Tr}_n\Big\{e^{-i\mathcal{L}\mathcal{Q}\tau'/\hbar}\mathcal{L}_{\text{zero}}\hat{\rho}_n(0)\Big\} \\
\mathcal{K}(\tau) &= \mathcal{F}_1(\tau) - \frac{1}{\hbar}\langle\mathcal{L}_{\text{zero}}\rangle_n^0\mathcal{G}_{\text{zero}}(\tau) + i\int_0^\tau d\tau'\left[i\dot{\mathcal{F}}(\tau-\tau') - \frac{1}{\hbar}\langle\mathcal{L}\rangle_n^0\mathcal{G}(\tau-\tau')\right]\mathcal{G}_{2,\text{zero}}(\tau')
\end{aligned} \tag{IV.30}$$

where $\mathcal{F}_1(\tau)$ is as given in Eq. (II.33) and copied in Sec. IV.2.5.2, $\mathcal{G}_{\text{zero}}$ is given in Eq. (IV.26), $\dot{\mathcal{F}}(\tau)$ is given in Eq. (IV.25), $\mathcal{G}(\tau)$ is given in Eq. (IV.19), and $\mathcal{G}_{2,\text{zero}}(\tau)$ is given in Eq. (IV.27). The ability of the second term to go from $\mathcal{L}_{\text{zero}}$ in the first line to $\mathcal{L}$ in the second comes from the fact that in the Condon approximation, $\mathrm{Tr}_n\{\mathcal{L}_{\text{int}}\mathcal{Q}[...]\} = \mathcal{L}_{\text{int}}\,\mathrm{Tr}_n\{\mathcal{Q}[...]\} = \mathcal{L}_{\text{int}}(\mathrm{Tr}_n\{[...]\} - \mathrm{Tr}_n\{\mathcal{P}[...]\}) = 0$, so this step is essentially adding zero in the form of $\frac{1}{\hbar^2}\,\mathrm{Tr}_n\Big\{\mathcal{L}_{\text{int}}\mathcal{Q}e^{-i\mathcal{L}(\tau-\tau')/\hbar}\mathcal{L}\hat{\rho}_n(0)\Big\}$ in order to get to the full Liouvillian operator used in $\dot{\mathcal{F}}(\tau)$. Obtaining the Volterra equation for $\mathcal{G}_{2,\text{zero}}(\tau)$ starts the same way as in the M-TE-C1 approach but stops the derivation at Eq. (IV.28), leading to

$$\begin{aligned}
\mathcal{G}_{2,\text{zero}}(\tau) &= \frac{1}{\hbar}\,\mathrm{Tr}_n\Big\{e^{-i\mathcal{L}\tau/\hbar}\mathcal{L}_{\text{zero}}\hat{\rho}_n(0)\Big\} \\
&\quad + \frac{i}{\hbar}\int_0^\tau d\tau' \, \frac{1}{\hbar}\,\mathrm{Tr}_n\Big\{e^{-i\mathcal{L}(\tau-\tau')/\hbar}\mathcal{L}\hat{\rho}_n(0)\Big\}\,\mathrm{Tr}_n\Big\{e^{-i\mathcal{L}\mathcal{Q}\tau'/\hbar}\mathcal{L}_{\text{zero}}\hat{\rho}_n(0)\Big\} \\
\mathcal{G}_{2,\text{zero}}(\tau) &= \mathcal{G}_{\text{zero}}(\tau) + i\int_0^\tau d\tau' \, \mathcal{G}(\tau-\tau')\mathcal{G}_{2,\text{zero}}(\tau') \quad .
\end{aligned} \tag{IV.31}$$

Therefore, the process of obtaining the memory kernel via the Condon M-TE approach, version 2 (M-TE-C2) requires first calculating $\mathcal{F}_1(\tau)$, $\mathcal{G}_{\text{zero}}(\tau)$, $\dot{\mathcal{F}}(\tau)$, and $\mathcal{G}(\tau)$, then calculating $\mathcal{G}_{2,\text{zero}}(\tau)$ through Eq. (IV.31), and finally calculating $\mathcal{K}(\tau)$ via Eq. (IV.30).

IV.2.6 Modified Projection-First Modified Approach (M-PF)

The modified projection-first approach (M-PF) is the same as the modified approach introduced in Sec. II.3 and is the approach that is referred to in previous and upcoming chapters as the *modified GQME (M-GQME)*. While more details are given in Sec. II.3 and Sec. II.4, some details are copied below that are important for understanding the expansions of the projection-free inputs given in Sec. IV.3 and for comparing to the other methods.

IV.2.6.1 Non-Condon Variation (M-PF-NC)

The non-Condon modified projection-first approach (M-PF-NC) uses a memory kernel of the form given in Eq. (II.23):

$$\mathcal{K}(\tau) = \frac{1}{\hbar^2}\text{Tr}_n\Big\{\mathcal{L}\, e^{-i\mathcal{Q}\mathcal{L}\tau/\hbar}\mathcal{Q}\mathcal{L}\hat{\rho}_n(0)\Big\} \quad .$$

Substituting $\mathcal{A} = \mathcal{L}$ and $\mathcal{B} = \mathcal{Q}\mathcal{L}$ into Eq. (IV.9) and plugging the identity into the memory kernel above leads to the Volterra equation given in Eq. (II.30):

$$\mathcal{K}(\tau) = i\dot{\mathcal{F}}(\tau) - \frac{1}{\hbar}\mathcal{F}(\tau)\langle\mathcal{L}\rangle_n^0 + i\int_0^\tau d\tau'\, \mathcal{F}(\tau-\tau')\mathcal{K}(\tau') \quad ,$$

where [see Eq. (II.31)]

$$\mathcal{F}(\tau) = \frac{1}{\hbar}\,\text{Tr}_n\left\{\mathcal{L}e^{-i\mathcal{L}\tau/\hbar}\hat{\rho}_n(0)\right\}$$

and $\dot{\mathcal{F}}(\tau)$ is as given in Eq. (IV.25). Therefore, the process of obtaining the memory kernel via the M-PF-NC approach requires first calculating $\mathcal{F}(\tau)$ and $\dot{\mathcal{F}}(\tau)$ and then calculating $\mathcal{K}(\tau)$ via Eq. (II.30).

IV.2.6.2 Condon Variation (M-PF-C)

The Condon modified projection-first approach (M-PF-C) uses a memory kernel of the form given in Eq. (II.28):

$$\mathcal{K}(\tau) = \frac{1}{\hbar^2}\mathrm{Tr}_n\Big\{\mathcal{L}_{\text{zero}}\, e^{-i\mathcal{Q}\mathcal{L}\tau/\hbar}\mathcal{Q}\mathcal{L}_{\text{zero}}\hat{\rho}_n(0)\Big\} \quad .$$

Substituting $\mathcal{A} = \mathcal{L}$ and $\mathcal{B} = \mathcal{Q}\mathcal{L}$ into Eq. (IV.9) and plugging the identity into the memory kernel above leads to the Volterra equation given in Eq. (II.32):

$$\mathcal{K}(\tau) = \mathcal{F}_1(\tau) - \frac{1}{\hbar}\mathcal{F}_2(\tau)\langle\mathcal{L}_{\text{zero}}\rangle_n^0 + i\int_0^\tau d\tau'\, \mathcal{F}_2(\tau-\tau')\mathcal{K}(\tau') \quad ,$$

where $\mathcal{F}_1(\tau)$ is as given in Eq. (II.33) and copied above in Sec. IV.2.5.2 and $\mathcal{F}_2(\tau)$ is as given in Eq. (II.34):

$$\mathcal{F}_2(\tau) = \frac{1}{\hbar}\,\mathrm{Tr}_n\left\{\mathcal{L}_{\text{zero}}e^{-i\mathcal{L}\tau/\hbar}\hat{\rho}_n(0)\right\} \quad .$$

Therefore, the process of obtaining the memory kernel via the M-PF-C approach requires first calculating $\mathcal{F}_1(\tau)$ and $\mathcal{F}_2(\tau)$ and then calculating $\mathcal{K}(\tau)$ via Eq. (II.32).

IV.2.7 Modified Projection-Second Modified Approach (M-PS)

IV.2.7.1 Non-Condon Variation (M-PS-NC)

The non-Condon modified projection-second approach (M-PS-NC) uses the same memory kernel as the M-TE-NC approach, Eq. (IV.16). Substituting $\mathcal{A} = \mathcal{L}\mathcal{Q}$ and $\mathcal{B} = \mathcal{L}$ into Eq. (IV.9) and plugging the identity into Eq. (IV.16) results in the Volterra equation

$$\mathcal{K}(\tau) = i\dot{\mathcal{F}}(\tau) - \frac{1}{\hbar}\langle\mathcal{L}\rangle_n^0\mathcal{G}(\tau) + i\int_0^\tau d\tau'\, \mathcal{K}(\tau-\tau')\mathcal{G}(\tau') \quad , \tag{IV.32}$$

where $\dot{\mathcal{F}}(\tau)$ is given previously in Eq. (IV.25) and $\mathcal{G}(\tau)$ is given in Eq. (IV.19). Therefore, the process of obtaining the memory kernel via the M-PS-NC approach requires first calculating $\dot{\mathcal{F}}(\tau)$ and $\mathcal{G}(\tau)$ and then calculating $\mathcal{K}(\tau)$ via Eq. (IV.32).

IV.2.7.2 Condon Variation (M-PS-C)

The Condon modified projection-second approach (M-PS-C) uses the same memory kernel as the M-TE-C1 and M-TE-C2 approaches, Eq. (IV.22). Substituting $\mathcal{A} = \mathcal{L}\mathcal{Q}$ and $\mathcal{B} = \mathcal{L}$ into Eq. (IV.9) and plugging the identity into Eq. (IV.22) results in the Volterra equation

$$\mathcal{K}(\tau) = \mathcal{F}_1(\tau) - \frac{1}{\hbar}\langle \mathcal{L}_{\text{zero}} \rangle_n^0 \mathcal{G}_{\text{zero}}(\tau) + i\int_0^\tau d\tau' \, \mathcal{K}(\tau - \tau')\mathcal{G}_{\text{zero}}(\tau') \quad , \tag{IV.33}$$

where $\mathcal{F}_1(\tau)$ is given in Eq. (II.33) and $\mathcal{G}_{\text{zero}}(\tau)$ is given in Eq. (IV.26). Therefore, the process of obtaining the memory kernel via the M-PS-C approach requires first calculating $\mathcal{F}_1(\tau)$ and $\mathcal{G}_{\text{zero}}(\tau)$ and then calculating $\mathcal{K}(\tau)$ via Eq. (IV.33).

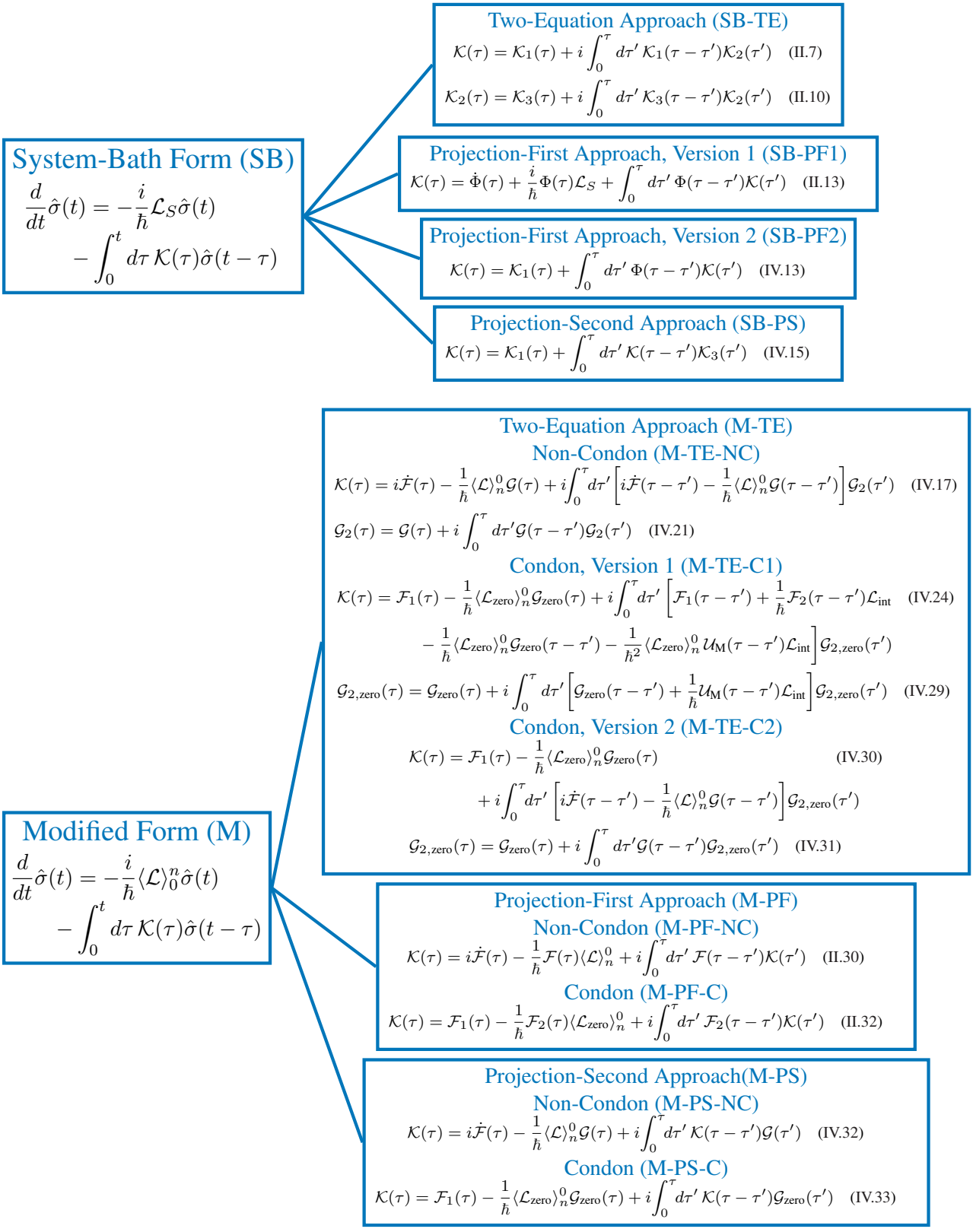

Figure IV.2: Tree diagram of the approaches to obtaining the memory kernel including equations.

IV.3 Expansions of the Projection-Free Inputs

The expansions of the projection-free inputs can be categorized based on the nature of their nuclear operators. The first type of expansion involves direct calculation of the projection-free inputs as they are given Sec. IV.2 and is therefore called the *Bare* expansion. The second type of expansion involves calculating the projection-free inputs with CFs and time-derivatives of CFs that only have nuclear operators at time $t = 0$ and is called the *Static* expansion. The third type of expansion involves calculating the projection-free inputs with CFs and time-derivatives of CFs that only have nuclear operators at time $t = \tau$ and is called the *Dynamic* expansion. The fourth type of expansion involves calculating the projection-free inputs from only the time propagation superoperator for the reduced electronic density matrix, $\mathcal{U}(\tau) = \mathrm{Tr}_n\{e^{-i\mathcal{L}\tau/\hbar}\hat{\rho}_n(0)\}$, and is called the *Propagator* expansion. The expansions of each of the projection-free inputs are summarized in Tables IV.1 and IV.2. The proofs of each expansion for each projection-free input are given in Appendix A.

Projection -Free Input	Bare Expansion	Static Expansion	Dynamic Expansion	Propagator Expansion
$\mathcal{K}_1(\tau)$	Eq. (II.8)	$i\frac{d}{d\tau}\mathcal{K}_3(\tau) - \frac{1}{\hbar}\mathcal{L}_S\mathcal{K}_3(\tau)$	$\frac{d}{d\tau}\Phi(\tau) + \frac{i}{\hbar}\Phi(\tau)\mathcal{L}_S$	$-\ddot{\mathcal{U}}(\tau) + \frac{1}{\hbar^2}\mathcal{L}_S\mathcal{U}(\tau)\mathcal{L}_S$ $-\frac{i}{\hbar}\left[\dot{\mathcal{U}}(\tau), \mathcal{L}_S\right]_+$
$\mathcal{K}_3(\tau)$	Eq. (II.11)	Eq. (II.11)	$i\dot{\mathcal{U}}(\tau) - \frac{1}{\hbar}\mathcal{U}(\tau)\mathcal{L}_S$	$i\dot{\mathcal{U}}(\tau) - \frac{1}{\hbar}\mathcal{U}(\tau)\mathcal{L}_S$
$\dot{\Phi}(\tau)$	Eq. (IV.11)	$i\frac{d}{d\tau}\mathcal{K}_3(\tau) + \frac{i}{\hbar}\dot{\mathcal{U}}(\tau)\mathcal{L}_S$ $-\frac{1}{\hbar^2}\mathcal{L}_S\mathcal{U}(\tau)\mathcal{L}_S - \frac{1}{\hbar}\mathcal{L}_S\mathcal{K}_3(\tau)$	$\frac{d}{d\tau}\Phi(\tau)$	$-\ddot{\mathcal{U}}(\tau) - \frac{i}{\hbar}\mathcal{L}_S\dot{\mathcal{U}}(\tau)$
$\Phi(\tau)$	Eq. (II.14)	$-\dot{\mathcal{U}}(\tau) - \frac{i}{\hbar}\mathcal{L}_S\mathcal{U}(\tau)$	Eq. (II.14)	$-\dot{\mathcal{U}}(\tau) - \frac{i}{\hbar}\mathcal{L}_S\mathcal{U}(\tau)$

Table IV.1: Expansions of the System-Bath Projection-Free Inputs.
In this table, numerical derivatives of projection-free inputs are indicated with $d/d\tau$ in front of them, to differentiate from projection-free inputs that have an overdot in their symbol, e.g., $\dot{\mathcal{F}}(\tau)$ and $\dot{\Phi}(\tau)$. However, the numerical derivatives of the time propagation superoperator $\mathcal{U}(\tau)$ are denoted with a single overdot for the first derivative and a double overdot for the second derivative, in order to be compact. Additionally, $[\mathcal{A}, \mathcal{B}]_+ = \mathcal{A}\mathcal{B} + \mathcal{B}\mathcal{A}$ denotes the anticommutator.

Projection -Free Input	Bare Expansion	Static Expansion	Dynamic Expansion	Propagator Expansion
$\dot{\mathcal{F}}(\tau)$	Eq. (IV.25)	$\frac{d}{d\tau}\mathcal{G}(\tau)$	$\frac{d}{d\tau}\mathcal{F}(\tau)$	$i\ddot{\mathcal{U}}(\tau)$
$\mathcal{F}(\tau)$	Eq. (II.31)	$i\dot{\mathcal{U}}(\tau)$	Eq. (II.31)	$i\dot{\mathcal{U}}(\tau)$
$\mathcal{F}_1(\tau)$	Eq. (II.33)	$i\frac{d}{d\tau}\mathcal{G}_{\text{zero}}(\tau)$ $-\frac{1}{\hbar}\mathcal{L}_{\text{int}}\mathcal{G}_{\text{zero}}(\tau)$	$i\frac{d}{d\tau}\mathcal{F}_2(\tau)-\frac{1}{\hbar}\mathcal{F}_2(\tau)\mathcal{L}_{\text{int}}$	$-\ddot{\mathcal{U}}(\tau)-\frac{i}{\hbar}\left[\dot{\mathcal{U}}(\tau),\mathcal{L}_{\text{int}}\right]_+$ $+\frac{1}{\hbar^2}\mathcal{L}_{\text{int}}\mathcal{U}(\tau)\mathcal{L}_{\text{int}}$
$\mathcal{F}_2(\tau)$	Eq. (II.34)	$i\dot{\mathcal{U}}(\tau)-\frac{1}{\hbar}\mathcal{L}_{\text{int}}\mathcal{U}(\tau)$	Eq. (II.34)	$i\dot{\mathcal{U}}(\tau)-\frac{1}{\hbar}\mathcal{L}_{\text{int}}\mathcal{U}(\tau)$
$\mathcal{G}(\tau)$	Eq. (IV.19)	Eq. (IV.19)	$i\dot{\mathcal{U}}(\tau)$	$i\dot{\mathcal{U}}(\tau)$
$\mathcal{G}_{\text{zero}}(\tau)$	Eq. (IV.26)	Eq. (IV.26)	$i\dot{\mathcal{U}}(\tau)-\frac{1}{\hbar}\mathcal{U}(\tau)\mathcal{L}_{\text{int}}$	$i\dot{\mathcal{U}}(\tau)-\frac{1}{\hbar}\mathcal{U}(\tau)\mathcal{L}_{\text{int}}$

Table IV.2: Expansions of the Modified Projection-Free Inputs.
In this table, numerical derivatives of projection-free inputs are indicated with $d/d\tau$ in front of them, to differentiate from projection-free inputs that have an overdot in their symbol, e.g., $\dot{\mathcal{F}}(\tau)$ and $\dot{\Phi}(\tau)$. However, the numerical derivatives of the time propagation superoperator $\mathcal{U}(\tau)$ are denoted with a single overdot for the first derivative and a double overdot for the second derivative, in order to be compact. Additionally, $[\mathcal{A},\mathcal{B}]_+ = \mathcal{A}\mathcal{B}+\mathcal{B}\mathcal{A}$ denotes the anticommutator.

IV.4 Results for a Spin-Boson Model

The 44 different methods of obtaining the memory kernel were tested on the spin-boson model outlined in Secs. II.6 and III.4. The parameters tested were those of model 2 in Table III.1. In this model, the energy splitting is 2ϵ with $\epsilon = 1$, the off-diagonal coupling is $\Gamma = 1$, the temperature is given via $\beta = 1/k_BT = 5$, and the number of nuclear number modes is $N_n = 400$. Calculations were carried out with 10^6 trajectories with a time step $\Delta t = 0.005\,\Gamma^{-1}$. The spectral density is the Ohmic spectral density outlined in Sec. II.6 with a Kondo parameter $\xi = 0.1$, a cutoff frequency $\omega_c = 2$, and a maximum frequency of $\omega_{\text{max}} = 10$. Exact results were adopted from Ref. 44.

The input methods used were the two QC/MH methods outlined in Chapter III, LSCI and LSCII. The Ehrenfest method was not used as an input method due to the added difficulty of tracking the impact on the dynamics of the choice of initial basis outlined in Sec. II.5.

IV.4.1 System-bath vs. Modified Form

The first comparison we will examine are the approaches based on the system-bath form of the GQME, outlined in Secs. IV.2.1 - IV.2.4, compared to those based on the modified form of the GQME, outlined in Secs. IV.2.5 - IV.2.7. All of the results in this section are with a memory time of 20 Γ^{-1}.

In Fig. IV.3, the electronic population difference results of applying each of the approaches with the bare expansion are shown, split into three graphs based on the type of approach (i.e., TE, PF, or PS), with LSCI as input method for the GQME. From this figure, it can be seen that the system-bath TE and PS approaches have much larger oscillations than their modified counterparts. The non-Condon M-TE and M-PS approaches have both damped oscillations and underestimate the dynamics while the Condon M-TE and M-PS approaches have damped oscillations but accurate estimation of the dynamics. Comparatively, the PF approaches for both system-bath and modified forms are able to obtain accurate results.

In Fig. IV.4, the electronic population difference results of applying each of the approaches with the bare expansion are shown, split into three graphs based on the type of approach, with LSCII as input method for the GQME. From this figure, it can be seen that the problems that the LSCI-GQME had with the TE and PS approaches for both system-bath and modified forms seen in Fig. IV.3 have been corrected by using LSCII as input method instead, though the SB-TE and SB-PS results still have slightly larger amplitudes than the exact results. Additionally, the PF approaches for both system-bath and modified forms are able to get accurate results with LSCII as well as LSCI.

From Figs. IV.3 and IV.4, for the bare expansion, there is slight improvement shown with the M-TE and M-PS approaches compared to the SB-TE and SB-PS approaches but the SB-PF and M-PF approaches outperform all of the other approaches and yield the same results regardless of system-bath or modified form. This indicates that the choice of type of approach (i.e., TE, PF, or PS) has more impact than system-bath v. modified form, though there are some differences seen

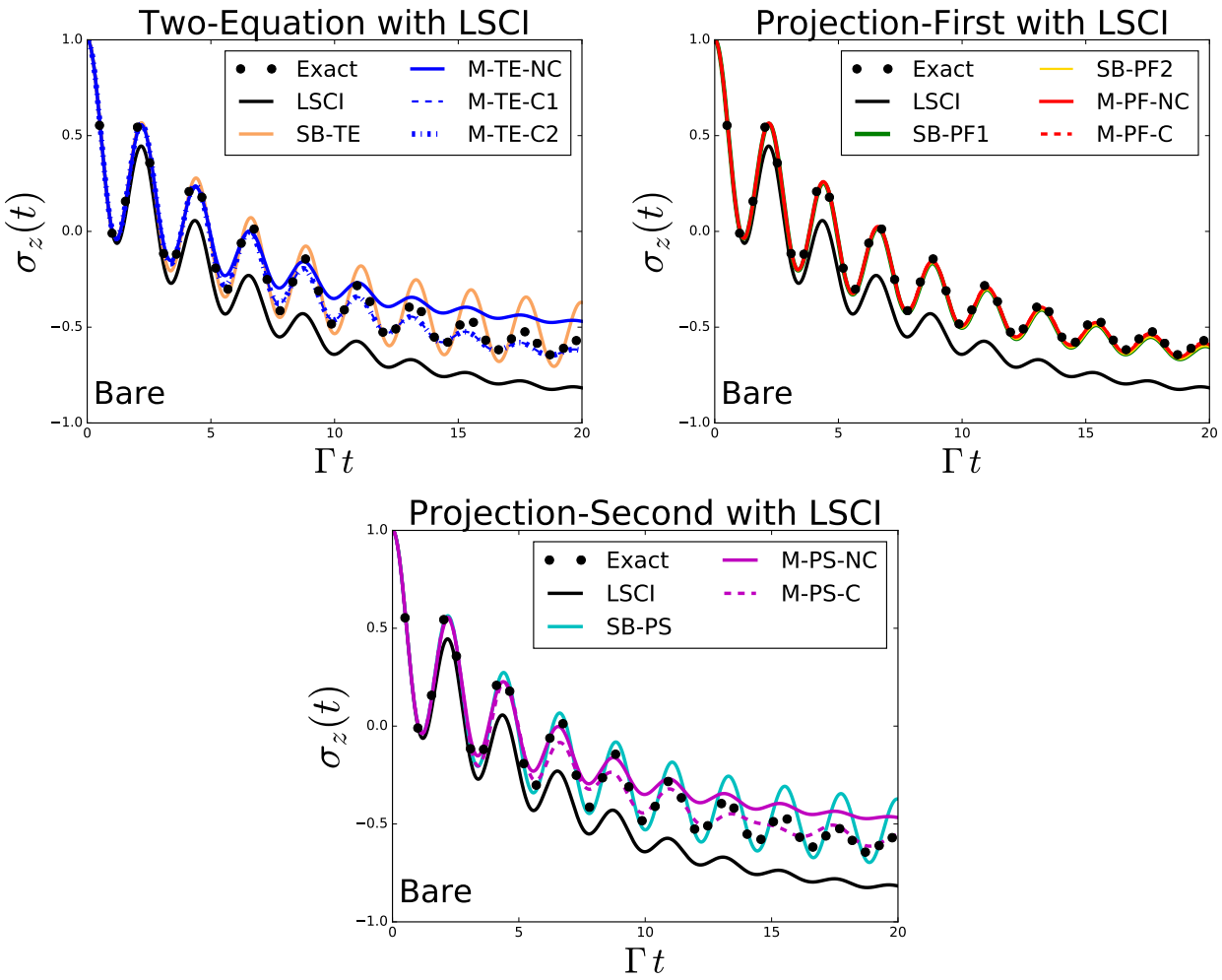

Figure IV.3: Starting from the upper left and moving clockwise, shown are the electronic population differences, $\sigma_z(t) = \sigma_{DD}(t) - \sigma_{AA}(t)$, for the bare expansion of the two-equation approaches, the projection-first approaches, and the projection-second approaches. The input method is LSCI, with the direct application of LSCI results shown on each graph as a solid black line. Exact results are shown in black circles on each graph.

there for TE and PS approaches. It is also possible that more differences would be seen between the system-bath and modified forms of the PF approaches for a model that they are unable to capture the exact results for.

Shown in Fig. IV.5 are the electronic population difference results for the propagator expansion with LSCII as input method, with the TE approaches shown in the top row and the PF approaches shown in the bottom row and the time step of the left column results is $\Delta t = 0.01\,\Gamma^{-1}$ whereas the time step of the right column results is $\Delta t = 0.005\,\Gamma^{-1}$. The results with LSCI as input method are given in Appendix B rather than this chapter because they show the same trends as

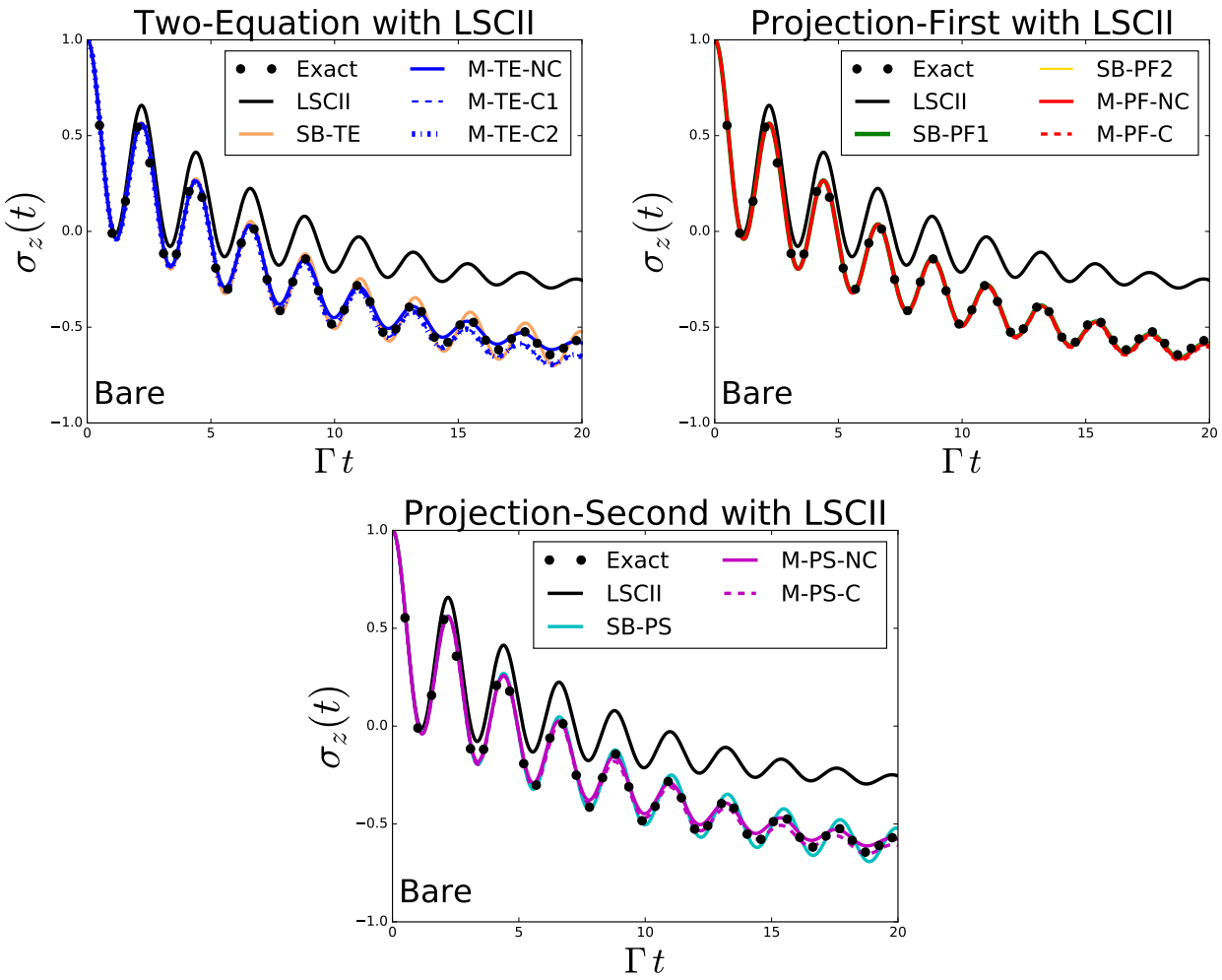

Figure IV.4: Starting from the upper left and moving clockwise, shown are the electronic population differences, $\sigma_z(t) = \sigma_{DD}(t) - \sigma_{AA}(t)$, for the bare expansion of the two-equation approaches, the projection-first approaches, and the projection-second approaches. The input method is LSCII, with the direct application of LSCII results shown on each graph as a solid black line. Exact results are shown in black circles on each graph.

the LSCII-GQME results. The results for the Condon M-TE approaches and the PS approaches are not shown because their results are still being verified. The results in Fig. IV.5 show that the propagator expansion dynamics are much more sensitive to time step for the system-bath form compared to the modified form. Results for even smaller time steps are being calculated and may allow the propagator system-bath results to converge to the modified results but at much higher computational cost than the modified form approaches. Regardless, the dynamics with the propagator expansion are much worse compared to the bare expansion shown in Fig. IV.4, with the propagator expansion giving back the dynamics of the direct application of the input method

while the bare expansion improves the results compared to the direct application as is normally seen with GQME. Ref. 71 observed this phenomenon for the SB-PF2 approach with Ehrenfest method as input and did a Fourier-Laplace transform to show that when the projection-free inputs are calculated with the time propagation operator $\mathcal{U}(\tau)$ and its time derivatives, then the results with the GQME will be equivalent to the dynamics of the direct application of the input method.

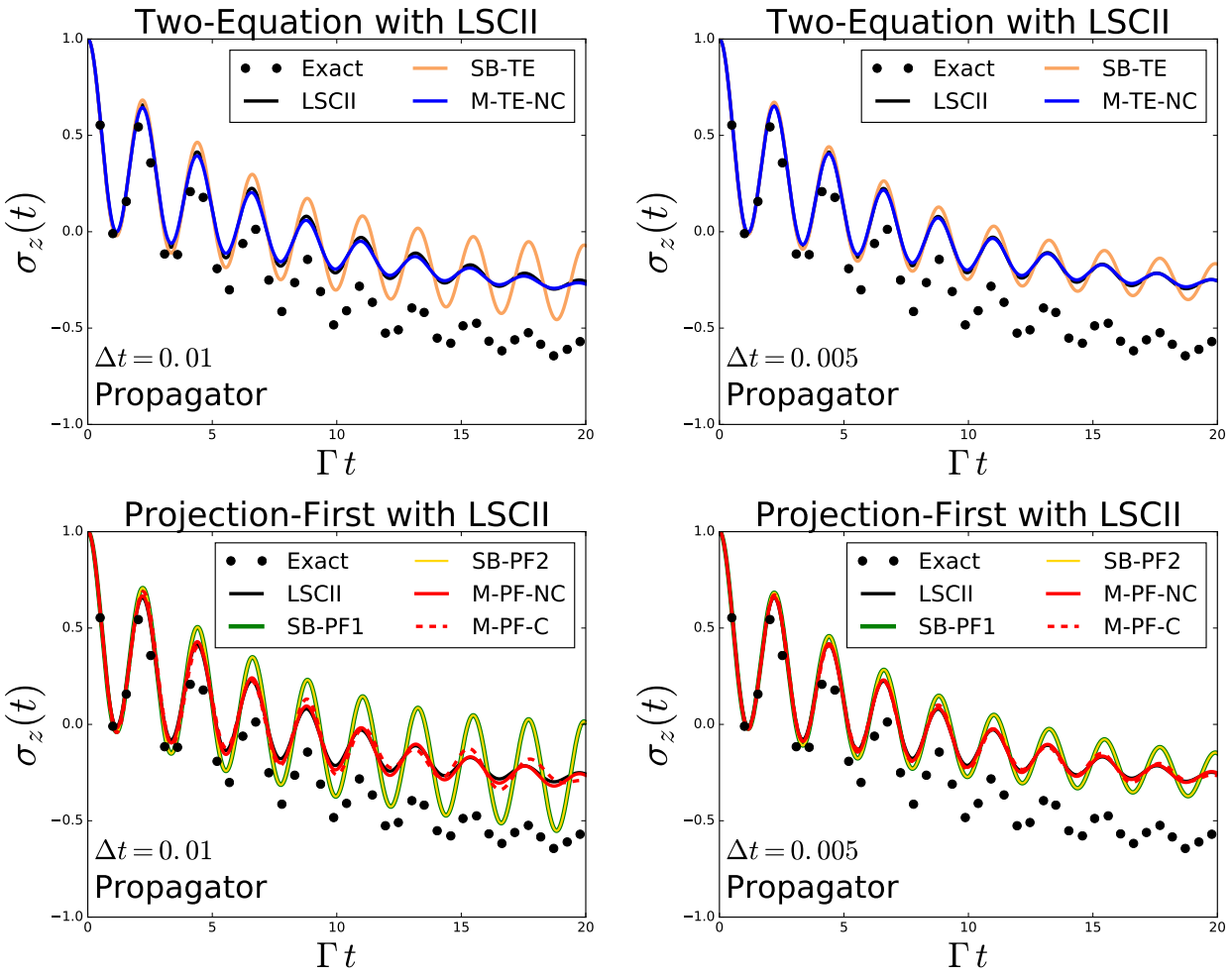

Figure IV.5: In the top row, shown are the electronic population differences, $\sigma_z(t) = \sigma_{DD}(t) - \sigma_{AA}(t)$, for the propagator expansion of the two-equation approaches with a time step of $\Delta t = 0.01\,\Gamma^{-1}$ on the left and a time step of $\Delta t = 0.005\,\Gamma^{-1}$ on the right. In the bottom row, shown are the electronic population differences for the propagator expansion of the projection-first approaches with $\Delta t = 0.01\,\Gamma^{-1}$ on the left and a time step of $\Delta t = 0.005\,\Gamma^{-1}$ on the right. The input method is LSCII, with the direct application of LSCII results shown on each graph as a solid black line. Exact results are shown in black circles on each graph.
The M-TE-C1 and M-TE-C2 results are not shown in the top row because the results are still being verified. Similarly, the projection-second results are not shown because results with the modified form are still being verified.

IV.4.2 Non-Condon vs. Condon

In Fig. IV.6, the results for the bare and static expansions of the modified two-equation and projection-second approaches with LSCI as the input method are shown. As can be seen, the non-Condon approaches slightly underestimate the dynamics while the Condon approaches are more accurate.

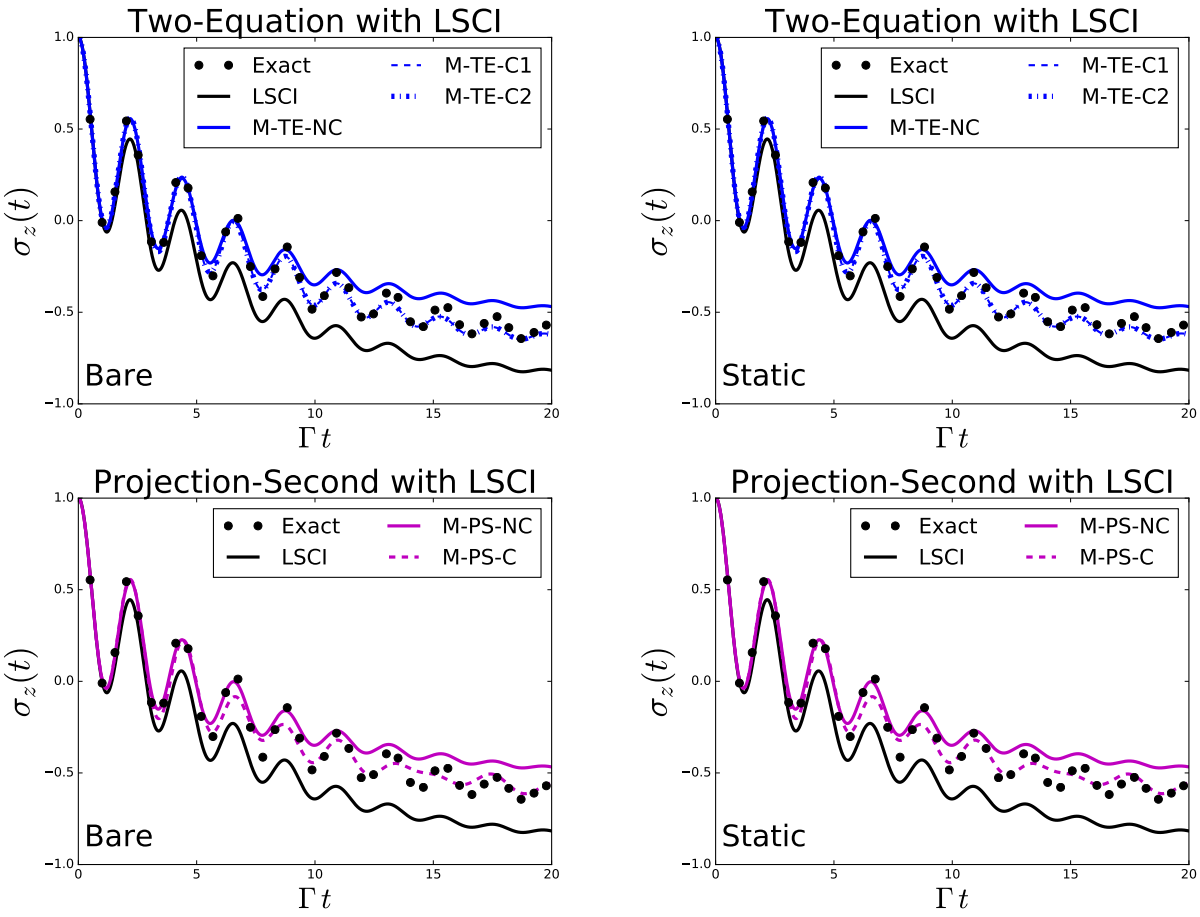

Figure IV.6: In the top row, shown are the electronic population differences, $\sigma_z(t) = \sigma_{DD}(t) - \sigma_{AA}(t)$, for the bare (left) and static (right) expansions of the modified two-equation approaches. In the bottom row, shown are the electronic population differences for the bare (left) and static (right) expansions of the modified projection-second approaches. The input method is LSCI, with the direct application of LSCI results shown on each graph as a solid black line. Exact results are shown in black circles on each graph.

Shown in Fig. IV.7 are the bare, static, dynamic, and propagator expansions for the modified projection-first approaches with LSCI as the input method. The same results with LSCII are given

in Appendix B. For the bare and static expansions, the non-Condon and Condon M-PF approaches give the same accurate results. For the dynamic and propagator expansions, results are shown for time steps of $\Delta t = 0.01\,\Gamma^{-1}$ and $\Delta t = 0.005\,\Gamma^{-1}$ to illustrate that the non-Condon projection-first approaches have not converged with respect to time step for the dynamic and propagator expansions. Additionally, the dynamic and propagator expansion results give worse results when compared to the bare and static expansions. The Condon dynamic and propagator expansion results for the M-PF approach give the same results as the direct application of LSCI and it is likely that the non-Condon results will converge to the same dynamics.

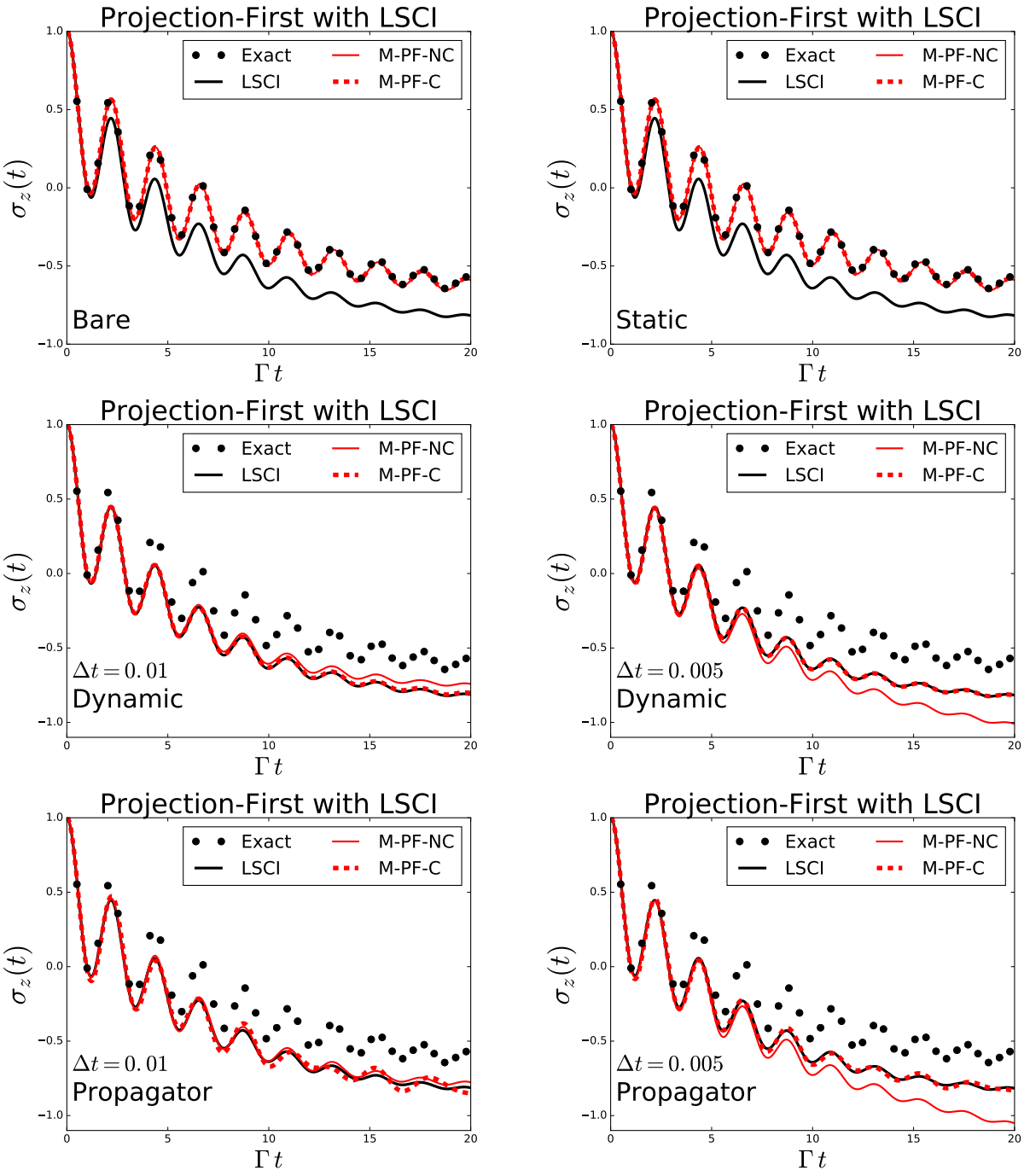

Figure IV.7: In the top row, shown are the electronic population differences, $\sigma_z(t) = \sigma_{DD}(t) - \sigma_{AA}(t)$, for the bare (left) and static (right) expansions of the modified projection-first approaches. In the middle row, shown are the electronic population differences for the dynamic expansion of the modified projection-first approaches with a time step of $\Delta t = 0.01\,\Gamma^{-1}$ (left) and a time step of $\Delta t = 0.005\,\Gamma^{-1}$ (right). In the bottom row, shown are the electronic population differences for the dynamic expansion of the modified projection-first approaches with a time step of $\Delta t = 0.01\,\Gamma^{-1}$ (left) and a time step of $\Delta t = 0.005\,\Gamma^{-1}$ (right). The input method is LSCI, with the direct application of LSCI results shown on each graph as a solid black line. Exact results are shown in black circles on each graph.

IV.4.3 Two Equations vs. One Equation for the Memory Kernel

Four approaches, one with the system-bath form and three with the modified form, have two equations to obtain the memory kernel; the first equation is a Volterra integral equation of the second type to obtain an intermediary projection-dependent input and the second an equation to obtain the memory kernel from the projection-free and projection-dependent inputs. The other seven approaches, three with system-bath form and four with the modified form, have one Volterra integral equation of the second type to obtain the memory kernel from projection-free inputs.

In Fig. IV.8, the electronic population difference results are compared for the SB approaches for the bare, static, and dynamic expansions with LSCI and LSCII as input methods. Notably, for the bare expansion with LSCI, the SB-TE and SB-PS give the same results while SB-PF1 and SB-PF2 give the same results as each other, but different from SB-TE and SB-PS. The SB-TE and SB-PS approaches have the same projection-free inputs, $\mathcal{K}_1(\tau)$ and $\mathcal{K}_3(\tau)$, while SB-PF1 has the projection-free inputs $\dot{\Phi}(\tau)$ and $\Phi(\tau)$, and SB-PF2 shares one projection-free input with each of the other approaches, with it using $\mathcal{K}_1(\tau)$ and $\Phi(\tau)$. $\mathcal{K}_1(\tau)$ and $\dot{\Phi}(\tau)$ are fairly similar projection-free inputs with nuclear operators at times $t = 0$ and $t = \tau$ but $\mathcal{K}_3(\tau)$ and $\Phi(\tau)$ are not, with $\mathcal{K}_3(\tau)$ having a nuclear operator at time $t = 0$ and with $\Phi(\tau)$ having its nuclear operator at time $t = \tau$. The greater success of the SB-PF1 and SB-PF2 approaches, which have $\Phi(\tau)$, compared to the SB-TE and SB-PS approaches, which have $\mathcal{K}_3(\tau)$, seems to run counter-intuitive to the results of the static and dynamic expansion shown in Fig. IV.8. The static expansion, where projection-free inputs are built of CFs with only nuclear operators at time $t = 0$ or time derivatives of the time propagation superoperator, gives much better results than the dynamic expansion, where the projection-free inputs are built of CFs with only nuclear operators at time $t = \tau$ or time derivatives of the time propagation superoperator. In fact, the dynamic expansion results give back the dynamics of the direct application of the input method. As seen in Figs. B.1 and IV.5 and discussed in Sec. IV.4.1, the propagator expansion of the SB approaches have larger amplitudes than the dynamics of the direct application of the input method but this is expected to decrease to the dynamics of the direct

application of the input method with smaller time step, giving the same results as the dynamics expansion.

Shown in Fig. IV.9 are the results for the bare, static, and dynamic expansions with the modified form approaches with LSCI as input method. The same results for LSCII are shown in Appendix B. The bare and static expansions behave the same while the dynamics expansion gives comparatively worse results. In the bare and static expansions, the M-TE and M-PS approaches do comparatively worse that the M-PF. The non-Condon M-TE and M-PS approaches give the same results, the two Condon M-TE approaches give the same, and better, results, and the Condon M-TE and M-PS approaches giving similar but not the same results. The M-TE-NC and M-PS-NC approaches use the same projection-free inputs, $\dot{\mathcal{F}}(\tau)$ and $\mathcal{G}(\tau)$, and the M-TE-C1 and M-PS-C approaches use the same projection-free inputs, $\mathcal{F}_1(\tau)$ and $\mathcal{G}_{\text{zero}}$ while the M-TE-C2 uses all four that the other approaches use. It is interesting then that the M-TE-C1 and M-PS-C approaches do not give the exact same results, as was seen with the other approaches that have the same projection-free inputs, M-TE-NC and M-PS-NC and, shown previously in Fig. IV.8, the SB-TE and SB-PS approaches. The M-TE-C1 approach has more complicated equations that the M-TE-NC and SB-TE approaches, with two terms in the linear and integral part of both equations, but the fact that it obtains the same results as the M-TE-C2 approach, which has simpler equations, seems to indicate that this is not the cause of the differences between M-TE-C1 and M-PS-C. In the dynamic expansion results in Fig. IV.9, the M-TE-NC and M-PF-C approaches give back the dynamics of the direct application of LSCI, gaining no accuracy from using the GQME. The M-PF-NC is more sensitive to the change in time step than the M-TE-NC and M-PF-C approaches, but it could also end up giving back the dynamics of the direct application of LSCI with a converged time step. The M-TE-C1 and M-TE-C2 approaches' results are not shown because the results are still being verified. The results for the propagator expansion are not shown in this chapter as they are similar to the dynamic expansion results, with the graphs given in Appendix B.

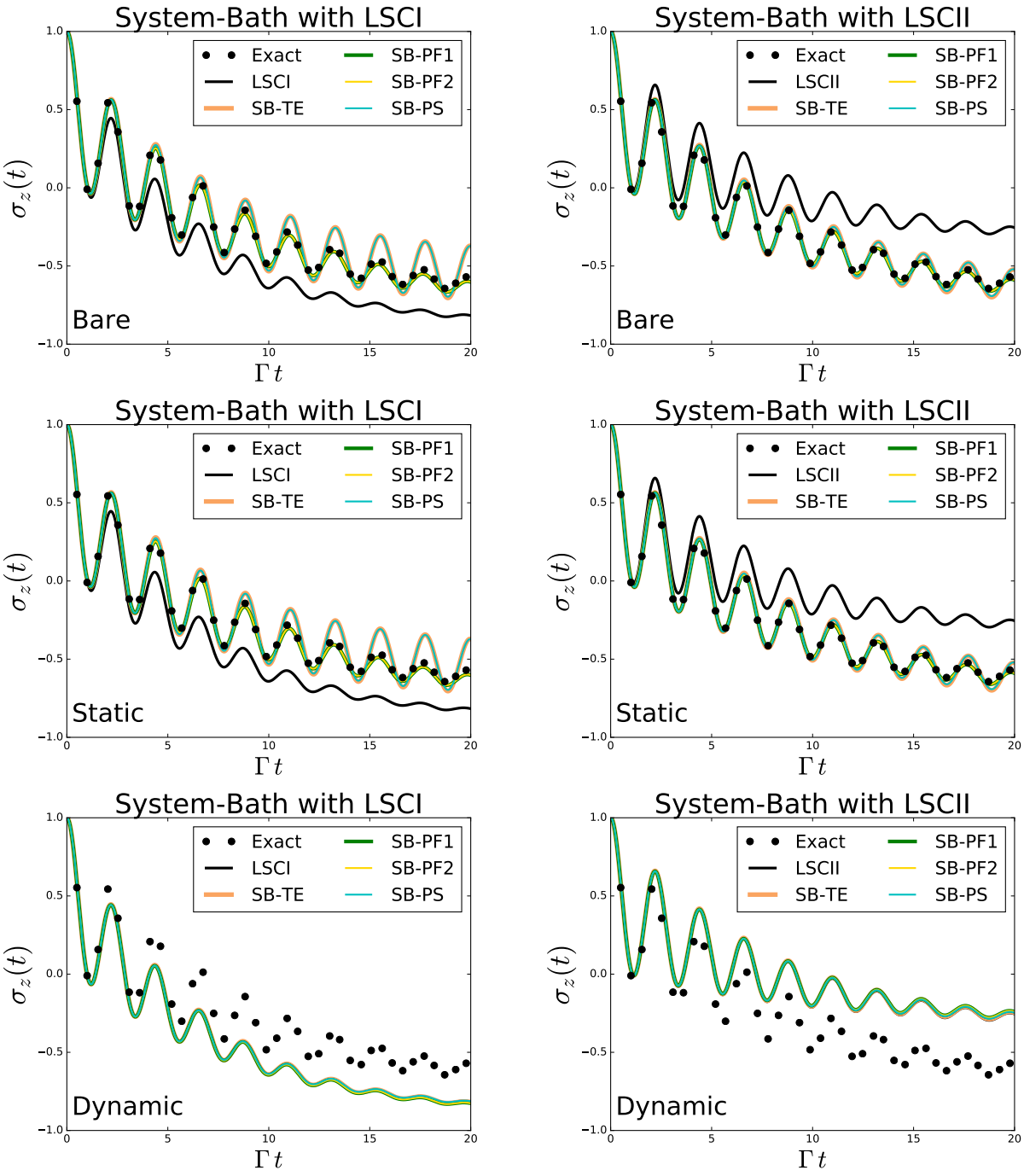

Figure IV.8: Shown are the electronic population differences, $\sigma_z(t) = \sigma_{DD}(t) - \sigma_{AA}(t)$, for the system-bath form approaches. In the top row, the bare expansion is used; in the middle row, the static expansion; and in the bottom row, the dynamic expansion. The left column is results with LSCI as input method and on the left are the results with LSCII as input method, with the direct application of each shown with a solid black line. Exact results are shown in black circles on each graph.

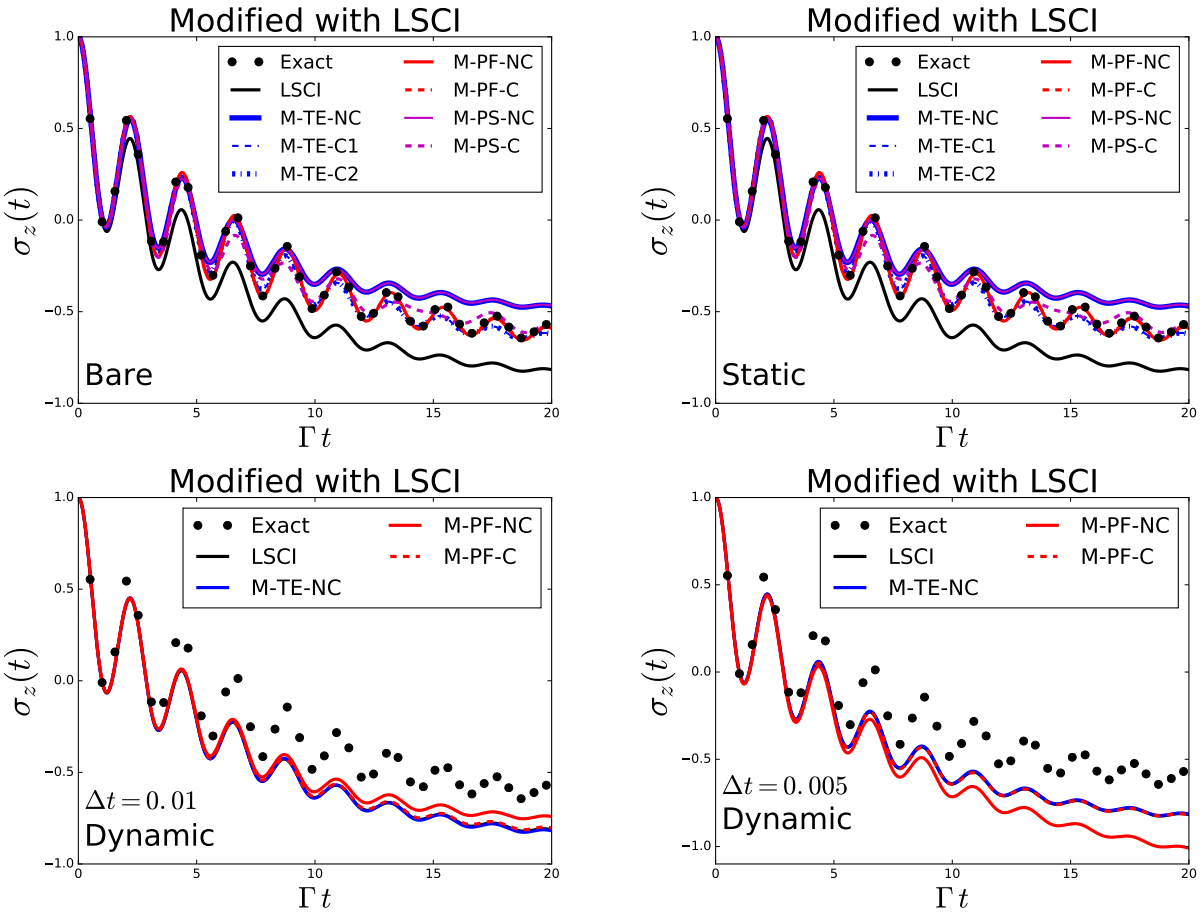

Figure IV.9: Shown are the electronic population differences, $\sigma_z(t) = \sigma_{DD}(t) - \sigma_{AA}(t)$, for the modified form approaches. Starting from the upper left and moving counter-clockwise are the results with the bare expansion, the static expansion, the dynamic expansion with $\Delta t = 0.005\,\Gamma^{-1}$, and the dynamic expansion with $\Delta t = 0.01\,\Gamma^{-1}$. The input method for the GQME is LSCI, with the dynamics of the direct application of LSCI shown with a solid black line. Exact results are shown in black circles on each graph.

IV.4.4 Memory Time Convergence

Shown in Fig. IV.10 are the five approaches, SB-TE, SB-PS, M-PS-NC, M-PS-C, and M-TE-NC, that do not converge with respect to memory time for the bare expansion with LSCI as the input method. All of the projection-second approaches and all of the two-equation approaches except the two Condon approaches fail to obtain converged results with increasing memory time. For these five approaches with LSCI as the input method, the static and propagator expansions also do not obtain converged results with increasing memory time but the dynamic expansions do. All

of the other approaches with LSCI as the input method and all of the approaches with LSCII as input method give converged results for the bare expansion with increasing memory time, with the longest memory time needed to converge being 8 Γt.

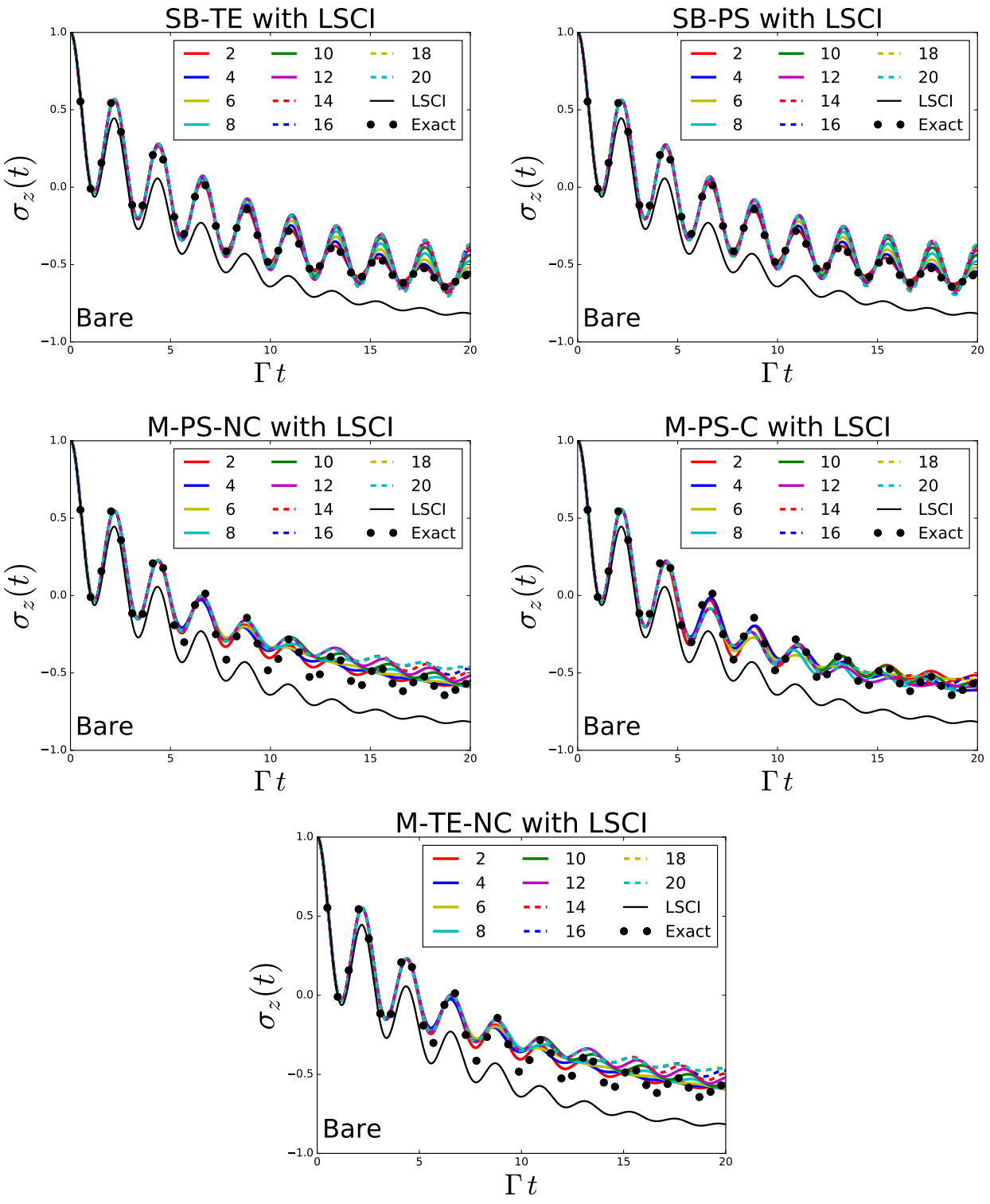

Figure IV.10: Shown are the electronic population differences, $\sigma_z(t) = \sigma_{DD}(t) - \sigma_{AA}(t)$, of the five approaches that do not obtain converged results with increasing memory time for the bare expansion with LSCI as the input method. Starting from the upper left and moving clockwise, the five approaches are SB-TE, SB-PS, M-PS-C, M-TE-NC, and M-PS-NC. The memory times are given in the legend in units of Γ^{-1}. The exact results are shown as black circles and the results from the direct application of LSCI are shown as a solid black line.

IV.5 Discussion of Results

With the many methods for calculating the memory kernel explored in this chapter, some valuable insight can be gained. These insights can be summarized as follows:

- **System-bath vs. Modified form:** While there are differences between the results of the bare expansion with LSCI for the TE and PS approaches, the more critical differences seem to stem from the type of approach (TE, PF, or PS) rather than the form of the Hamiltonian used. Considering the disadvantages of the system-bath form and the advantages of the modified form outlined in Chapter II, this makes the modified form the preferable one in general.

- **Effect of number of equations for the memory kernel:** The TE and PS approaches share the same projection-free inputs but have a different number of equations needed to obtain the memory kernel. The TE approaches require first calculating a projection-dependent input with a Volterra equation before calculating the memory kernel with an equation of the projection-free and projection-dependent inputs. In contrast, the PS approaches have a single Volterra equation for the memory kernel. As shown in the results in this chapter, this difference causes little to no difference between the results (with the only slight difference seen for the M-PC-C approach compared to the M-TE-C1 and M-TE-C2) and the more critical differences come from the different projection-free inputs and their expansions than the number of equations.

- **Effect of the projection-free inputs on the memory time convergence in the bare expansion:** For LSCI, the two-equation and projection-second approaches struggle to converge their results with respect to memory time for the bare expansion while the projection-first approaches do not. The main difference between these approaches stems from the projection-free inputs that either have nuclear operators at time $t = 0$ or time $t = \tau$ and not both. For the TE and PS approaches, these projection-free inputs have the nuclear operator at time $t = 0$ while the PF approaches have the nuclear operator at time $t = \tau$. Considering the

first point in this list, it may have been expected then that the TE and PS approaches would have given better results but instead the opposite is seen. It is possible that the time $t = \tau$ nuclear operators are stabilizing the longer time dynamics. For the model explored here, the PF approach results are too accurate to see if the memory time becomes unstable for the static expansion, which would help to prove (or disprove) this point.

- **Effect of the expansions:** As seen and discussed previously in Refs. 32 and 71, the bare and static expansions are able to give similar and accurate results while the dynamic and propagator expansions give back the same dynamics as the direct application of the input method. This result seems to add credence to the proposition that the sampling of the static nuclear operators done within the projection-free inputs improves the accuracy of the GQME compared to the direct application of the input method.

- **Overall greater success of the PF approaches:** While the TE and PS approaches were able to give accurate results and converging memory time for some expansions, the PF approaches were most consistent in giving accurate, converged results. The only area where the PF approaches struggled compared to the TE and PS approaches is in the convergence of the non-Condon dynamic and propagator expansions with LSCI. However, since the dynamic and propagator expansions have been proven to fail to give improvements compared to the direct application of the input method, this failure of the M-PF-NC approach is essentially irrelevant, since those expansions should not be used.

IV.6 Concluding Remarks

The GQME is a complex method for obtaining electronic dynamics in the condensed phase. The relative recency of the derivation of approaches to be able to calculate the GQME means that the impact of the various components of the GQME is unknown. The memory kernel in particular can be calculated in a variety of ways without obvious advantages to any particular way. For this reason, the thorough investigation of the many methods for obtaining the memory kernel explored

in this chapter adds valuable insight into the GQME.

From the results shown in this chapter and the disadvantages of the system-bath form and the advantages of the modified form outlined in Chapter II, it can be concluded that the modified projection-first approach with either the bare or static expansion is the best general method. The bare expansion of the modified projection-first approach is what has been referred to in previous chapters and will be referred to in upcoming chapters as the *modified GQME (M-GQME)*. As seen in Chapters II and III, the M-GQME was already known to perform well but the results in this chapter show that it outperforms other methods in several ways. The new insight into the success of the static expansion with the M-GQME could be of use for future systems in which the longer time dynamics are more erratic and the inclusion of nuclear operators at time $t = \tau$ could be exasperating difficulties with convergence.

CHAPTER V

Photosynthetic Systems with M-GQME

V.1 Introduction

Photosynthetic light-harvesting systems are of considerable interest due to their prevalence in nature and the efficiency of excitation energy transfer (EET) within them. Better understanding of EET in these systems can also help to yield improvements in artificial systems designed to mimic them.[109] The experimental observation of long-lived quantum coherence in some photosynthetic systems has led to interest in the importance of quantum effects on photosynthesis.[110] The Fenna-Matthews-Olson (FMO) complex was one of the first photosynthetic systems observed to have long-lived coherences. These coherences were originally designated as electronic coherences[111–114] but recent experimental and theoretical advancements indicate a significant contribution from vibrational coherences, demonstrating the importance of the nuclear DOF on the FMO dynamics.[115–117] These dynamics has been extensively studied, including with exact results for a model Hamiltonian via hierarchical equations of motion (HEOM).[118–120] This makes the FMO complex an appealing benchmark model system for testing methods for simulating nonadiabatic dynamics. In this chapter, the robustness and accuracy of the GQME methods with short-lived inputs obtained via the Ehrenfest method will be tested by applying them to FMO.

The rest of this chapter is organized as follows. The FMO complex is described in Sec. V.2. The results obtained by applying the Ehrenfest method with the GQME to the FMO complex and the discussion of these results are reported in Sec. V.3. Concluding remarks are given in Sec. V.4.

V.2 Fenna-Matthews-Olson (FMO) Complex

FMO is often described by a Frenkel exciton Hamiltonian of the following form[119,121] [see Eq. (I.3)]

$$\hat{H} = \sum_{j=1}^{N_e} \hat{H}_j |j\rangle\langle j| + \sum_{\substack{j,k=1 \\ k\neq j}}^{N_e} \hat{V}_{jk} |j\rangle\langle k| \quad . \tag{V.1}$$

Here, $\{\hat{H}_j\}$ and $\{\hat{V}_{jk}\}$ are given by

$$\begin{aligned} \hat{H}_j &= \varepsilon_j + \sum_{k=1}^{N_e} \sum_{i=1}^{N_n/N_e} \frac{\hat{P}_{k,i}^2}{2} + V_j\left(\hat{\mathbf{R}}\right) \quad , \\ V_j(\hat{\mathbf{R}}) &= \sum_{i=1}^{N_n/N_e} \frac{1}{2}\omega_i^2 \left(\hat{R}_{j,i} - \frac{c_i}{\omega_i^2}\right)^2 + \sum_{\substack{l=1 \\ l\neq j}}^{N_e} \sum_{i=1}^{N_n/N_e} \frac{1}{2}\omega_i^2 \hat{R}_{l,i}^2 \quad , \\ \hat{V}_{jk} &= \Gamma_{jk} \quad . \end{aligned} \tag{V.2}$$

Here, $N_e = 7$ is the number of electronic states; $N_n = 1400$ is the number of nuclear DOF; $\{\hat{R}_{1,1}, ..., \hat{R}_{N_e,N_n}\}$ and $\{\hat{P}_{1,1}, ..., \hat{P}_{N_e,N_n}\}$ are the mass-weighted position and momentum operators of the nuclear DOF, respectively; $\{c_1, ..., c_{N_n/N_e}\}$ and $\{\omega_1, ..., \omega_{N_n/N_e}\}$ are the mass-weighted coupling coefficients and frequencies for the nuclear normal modes, respectively; ε_j is the energy of the electronic state $|j\rangle$; and Γ_{jk} are the nonadiabatic couplings between electronic states, which are constant for FMO.

The initial state of the overall system is given by Eq. (I.4), $\hat{\rho}(0) = \hat{\rho}_n(0) \otimes \hat{\sigma}(0)$, where $\hat{\rho}_n(0)$ and $\hat{\sigma}(0)$ are the reduced density operators of the initial states of the nuclear and electronic DOF, respectively. For FMO, the initial nuclear density operator is given by

$$\hat{\rho}_n(0) = \frac{\exp\left[-\beta \sum_{j=1}^{N_e} \sum_{i=1}^{N_n/N_e} \frac{\hat{P}_{j,i}^2}{2} + \frac{1}{2}\omega_i^2 \hat{R}_{j,i}^2\right]}{\mathrm{Tr}\left\{\exp\left[-\beta \sum_{j=1}^{N_e} \sum_{i=1}^{N_n/N_e} \frac{\hat{P}_{j,i}^2}{2} + \frac{1}{2}\omega_i^2 \hat{R}_{j,i}^2\right]\right\}} \tag{V.3}$$

and the initial electronic density operator is given by $\hat{\sigma}(0) = |1\rangle\langle 1|$ or $\hat{\sigma}(0) = |6\rangle\langle 6|$ (using the usual numbering of the BChls, originally chosen by Fenna and Matthews[122]).

The energies $\{\varepsilon_j\}$ and couplings $\{\Gamma_{jk}\}$ of the electronic states are given in cm^{-1} by[119]

$$\begin{pmatrix} 12410 & -87.7 & 5.5 & -5.9 & 6.7 & -13.7 & -9.9 \\ -87.7 & 12530 & 30.8 & 8.2 & 0.7 & 11.8 & 4.3 \\ 5.5 & 30.8 & 12210 & -53.5 & -2.2 & -9.6 & 6.0 \\ -5.9 & 8.2 & -53.5 & 12320 & -70.7 & -17.0 & -63.3 \\ 6.7 & 0.7 & -2.2 & -70.7 & 12480 & 81.1 & -1.3 \\ -13.7 & 11.8 & -9.6 & -17.0 & 81.1 & 12630 & 39.7 \\ -9.9 & 4.3 & 6.0 & -63.3 & -1.3 & 39.7 & 12440 \end{pmatrix} \quad . \tag{V.4}$$

The nuclear normal modes are described by a Debye spectral density

$$J(\omega) = \frac{2\lambda\omega_c\omega}{\omega_c^2 + \omega^2} \tag{V.5}$$

where the discrete set of coupling coefficients $\{c_i\}$ and frequencies $\{\omega_i\}$ are given by

$$\begin{aligned} \omega_i &= \omega_c \tan\left[\frac{\pi N_e}{2N_n}\left(i - \frac{1}{2}\right)\right] \quad , \\ c_i &= \omega_i\sqrt{\frac{2\lambda N_e}{N_n}} \quad . \end{aligned} \tag{V.6}$$

Here, $\omega_c = 106.14\ \text{cm}^{-1}$ is the cutoff frequency and $\lambda = 35\ \text{cm}^{-1}$ is the reorganization energy.[46]

V.3 Results and Discussion

The dynamics of the FMO complex were obtained using the modified approach to the GQME (M-GQME) as outlined in Sec. II.3 with the projection-free inputs obtained with the Ehrenfest method, following the same procedure as in Sec. II.5. Since FMO is a Condon system (i.e., the electronic coupling terms are not dependent on $\hat{\mathbf{R}}$), the projection-free inputs calculated are $\mathcal{F}_1(\tau)$

and $\mathcal{F}_2(\tau)$, given in Eqs. (II.33) and (II.34), respectively. The results for the FMO complex were calculated with a time step of $\Delta t = 0.25$ fs and 35,000 trajectories per initial condition. The Volterra equation in Eq. (II.32) was solved using an iterative algorithm, outlined in Sec. II.4.1, and the GQME in Eq. (II.21) was solved using a Runge-Kutta 4th-order algorithm.

Fig. V.1 shows the populations of states 1, 2, and 3 with the dynamics starting in state 1 and Fig. V.2 shows the populations of states 3, 5, and 6 with the dynamics starting in state 6 for the direct application of the Ehrenfest method (MF) and for the MF-GQME method with a memory time of 0.4 ps. It should be noted that for several of these states, the memory time is converged at lower values (see Fig. V.3) but the memory time given is the value at which all states are converged. As seen in Figs. V.1 and V.2, the MF-GQME is able to obtain much more accurate results compared to the direct application of the Ehrenfest method.

While the FMO model has been studied previously with a GQME method in Ref. 46, it was done using a variation of the Shi-Geva approach (also called the SB-TE approach in Chapter IV).[28,46] As shown previously in Ref. 35 and Sec. IV.4.4, the Shi-Geva approach can have unstable results with regards to the memory time for the spin-boson model. For this reason, results were generated using the Shi-Geva approach following the procedure outlined in Ref. 35 for FMO, to see if the memory time converged. In Fig. V.4, we can see that these problems with the Shi-Geva approach apply also to the FMO model while in Fig. V.3 we can see that the results are very stable with regards to memory time for the M-GQME.

The ability to have stable results with regards to memory time is critical for systems in which the exact results are not known. With the Shi-Geva approach, a "plateau of stability" method was used previously, in which the memory time was determined by a memory time range in which the results were stable.[32,44,46] However, the plateau of stability can be small to non-existent and therefore difficult to determine. Additionally, without exact results, determining where to search for a plateau of stability can be difficult. With the spin-boson model, it was possible to guess what the memory time should be based on when the memory kernel elements decay to zero.[35,45] For the FMO model, many of the memory kernel elements are much more erratic, as shown in Figs. V.5

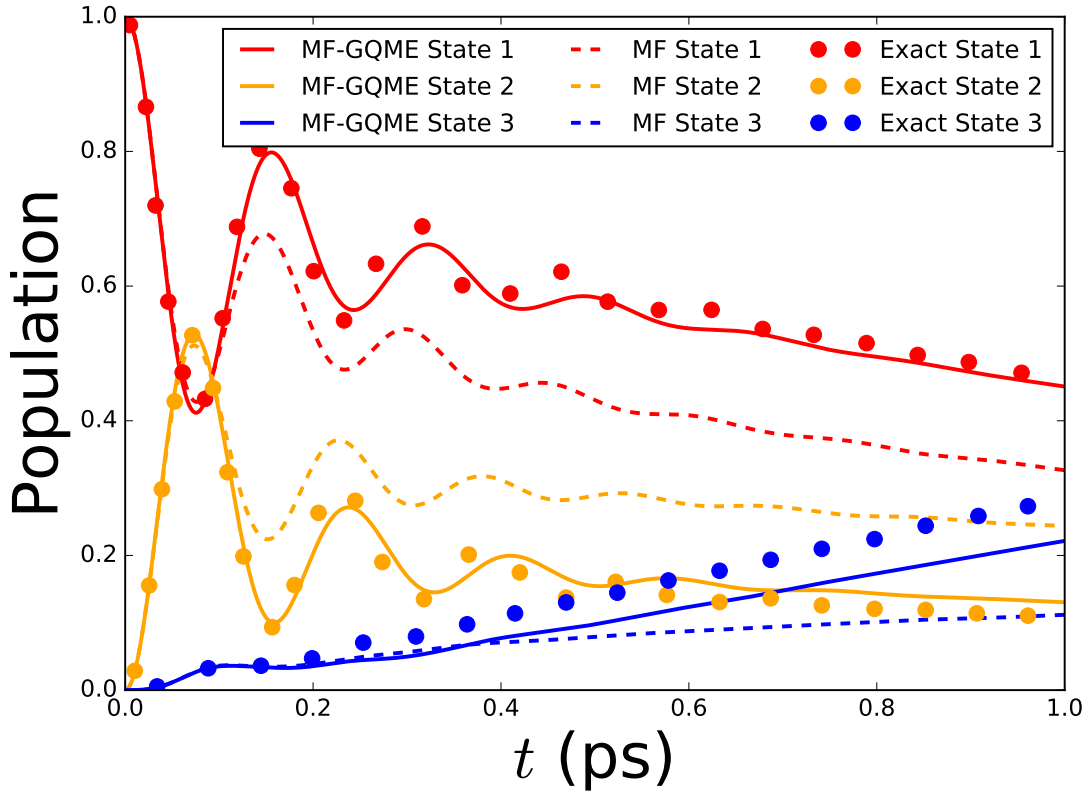

Figure V.1: Electronic population as a function of time for states 1, 2, and 3 with an initial electronic state starting in state 1. Shown are the exact results displayed with circle markers as well as the results obtained via direct application of the Ehrenfest method with dashed lines and via M-GQME with memory kernel calculated via the Ehrenfest method with solid lines. The state 1 dynamics are red for each method, state 2 results are orange, and stage 3 results are blue.

and V.6, thereby making the determination of the memory time based on the memory kernel elements less straightforward. With the modified approach to the GQME, even for large systems, the memory time converges and stays converged even with erratic memory kernel elements, allowing for greater certainty of the GQME results when the exact results are unknown.

The FMO complex is a well-studied molecular system with exact results but there are many systems of interest for which exact results have not been or cannot be determined. Therefore, a GQME approach that is not reliant on the existence of exact results and is able to give converged results with increasing memory time is critical for these systems.

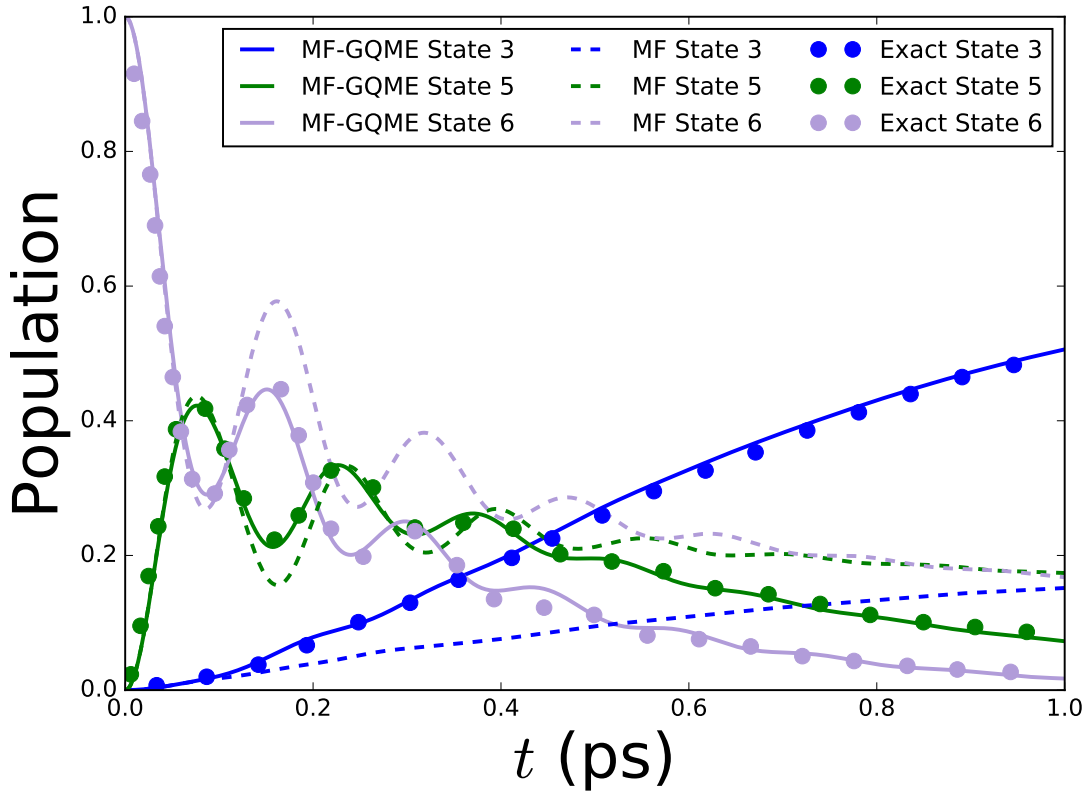

Figure V.2: Electronic population as a function of time for states 3, 5, and 6 with an initial electronic state starting in state 6. Shown are the exact results displayed with circle markers as well as the results obtained via direct application of the Ehrenfest method with dashed lines and via M-GQME with memory kernel calculated via the Ehrenfest method with solid lines. The state 3 dynamics are blue for each method, state 5 results are green, and stage 6 results are purple.

V.4 Concluding Remarks

Photosynthetic systems are of considerable interest due to their prevalence in nature and the efficiency of excitation energy transfer (EET) within them. Better understanding of this EET can help to yield improvements in artificial photosynthetic systems.[109] The observance of long-lived quantum coherence in some photosynthetic systems has led to interest in the importance of quantum effects on photosynthesis.[110] The Fenna-Matthews-Olson (FMO) complex was one of the first photosynthetic systems observed to have long-lived coherences and its dynamics has been extensively studied, including with exact results via hierarchical equations of motion (HEOM).[118–120] This makes the FMO complex an appealing system to test methods for obtaining photosynthetic

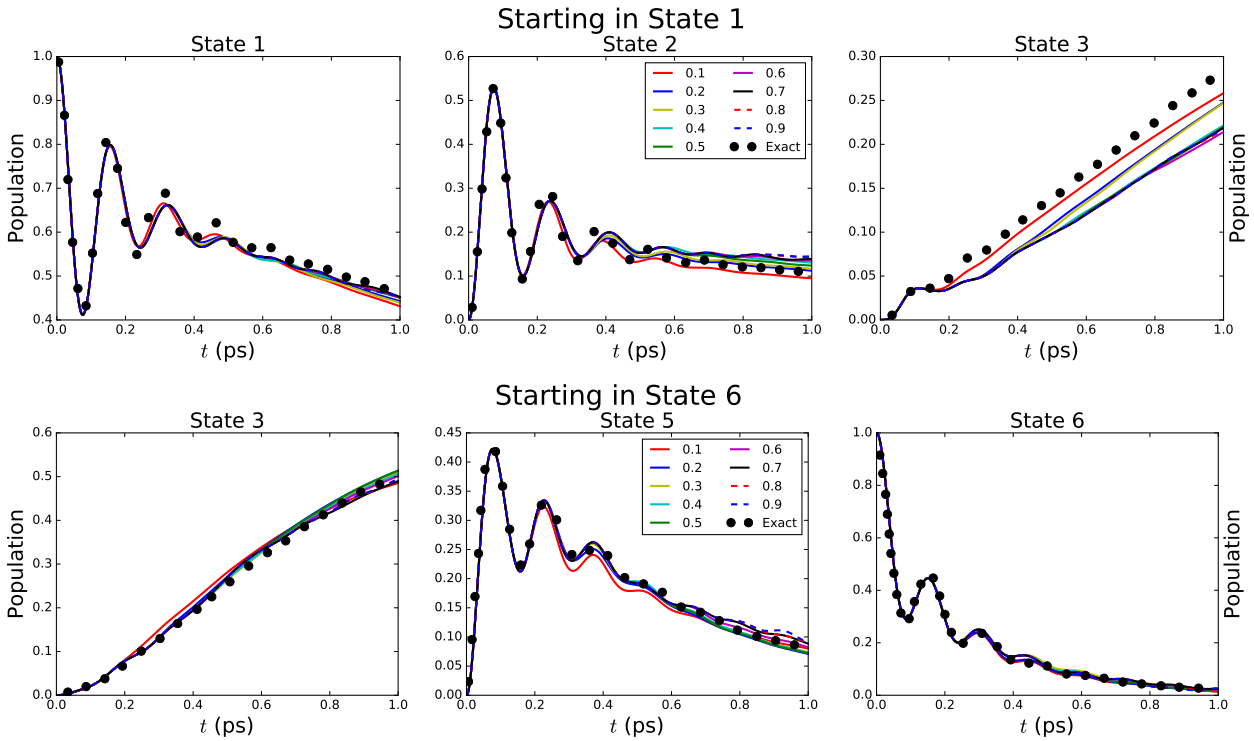

Figure V.3: Memory time convergence for the modified approach to the GQME, with memory times in ps given in the legend. We can see that by 0.4 ps at the latest, the populations for these states have converged results, regardless of increasing memory time.

dynamics on.

The M-GQME method has been found to give accurate dynamics for the spin-boson model, as seen in Chapters II, III, and IV. In this chapter, the M-GQME was shown to also be able to obtain accurate dynamics for a model of the FMO complex, which increases the complexity of the dynamics by having seven electronic states compared to only two in the spin-boson model. Additionally, the M-GQME had converged results with regards to memory time for FMO as well as the spin-boson model, which is in contrast to the Shi-Geva approach. This result is especially important moving forward in applying the GQME approach to other photosynthetic systems. Many photosynthetic systems of interest are not as extensively studied as FMO and do not or cannot obtain exact results. For these systems, it is important to have an approach that remains converged with respect to memory time, as it will be much more difficult if not impossible to find the memory time that gives the correct results if it does not.

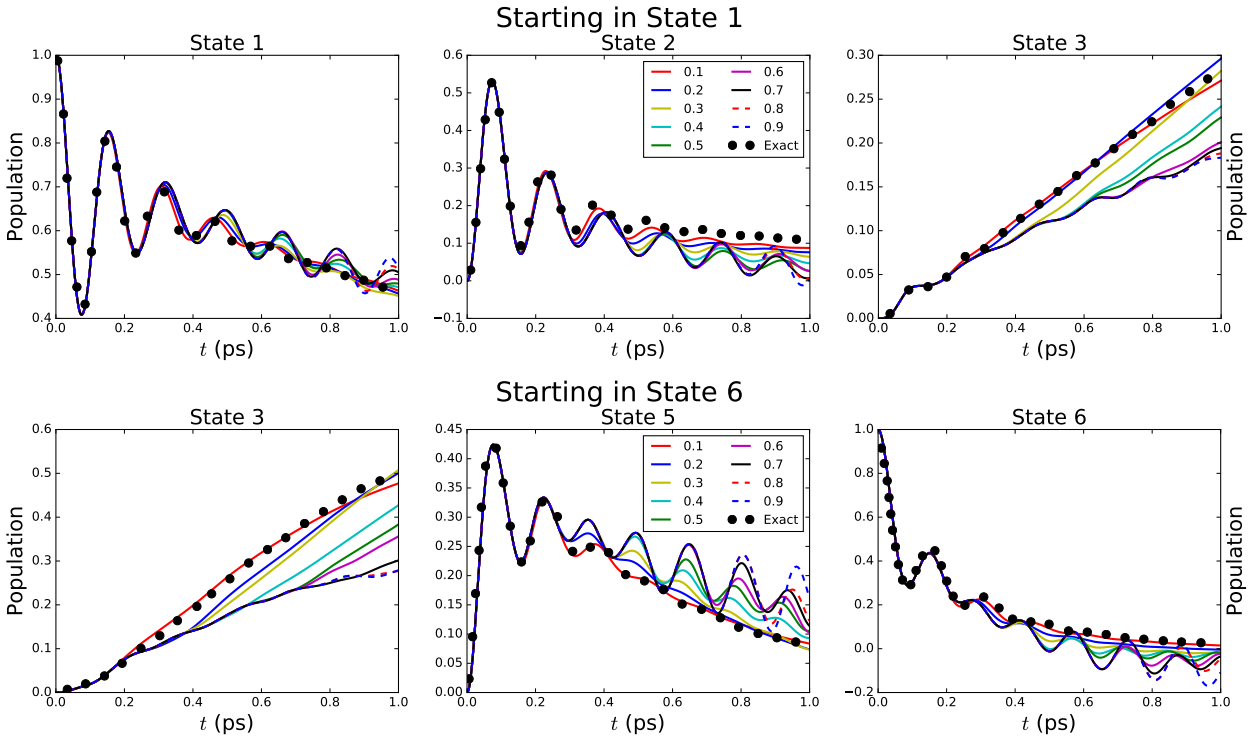

Figure V.4: Memory time convergence for the Shi-Geva approach to the GQME, with memory times in ps given in the legend. Here we see the failure of the Shi-Geva approach noted in Sec. II.5 of unstable results with increasing memory times, despite accurate results at early memory times.

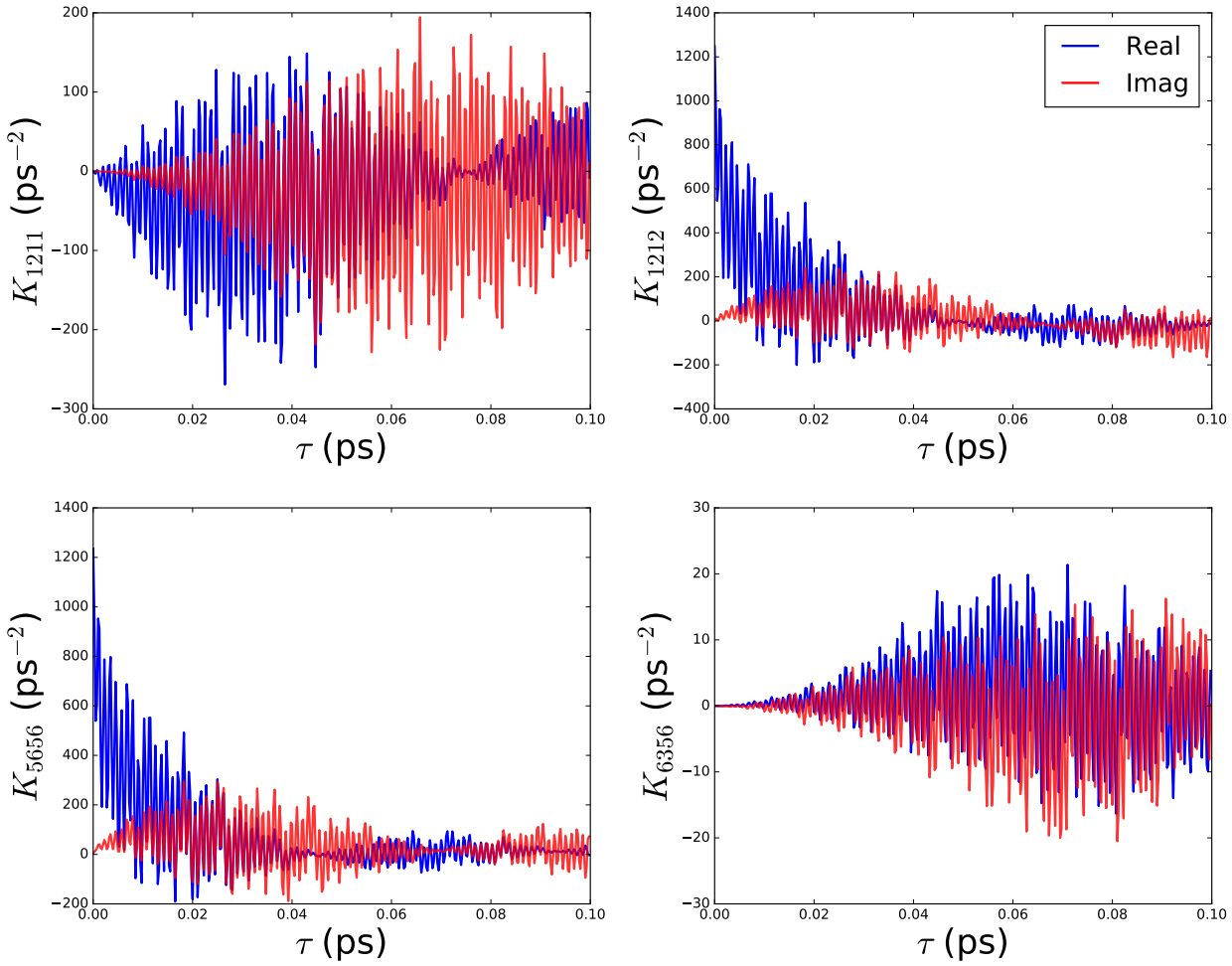

Figure V.5: Select memory kernel elements with the modified approach to the GQME. The real part of the memory kernel element is given in red and the imaginary part in blue.

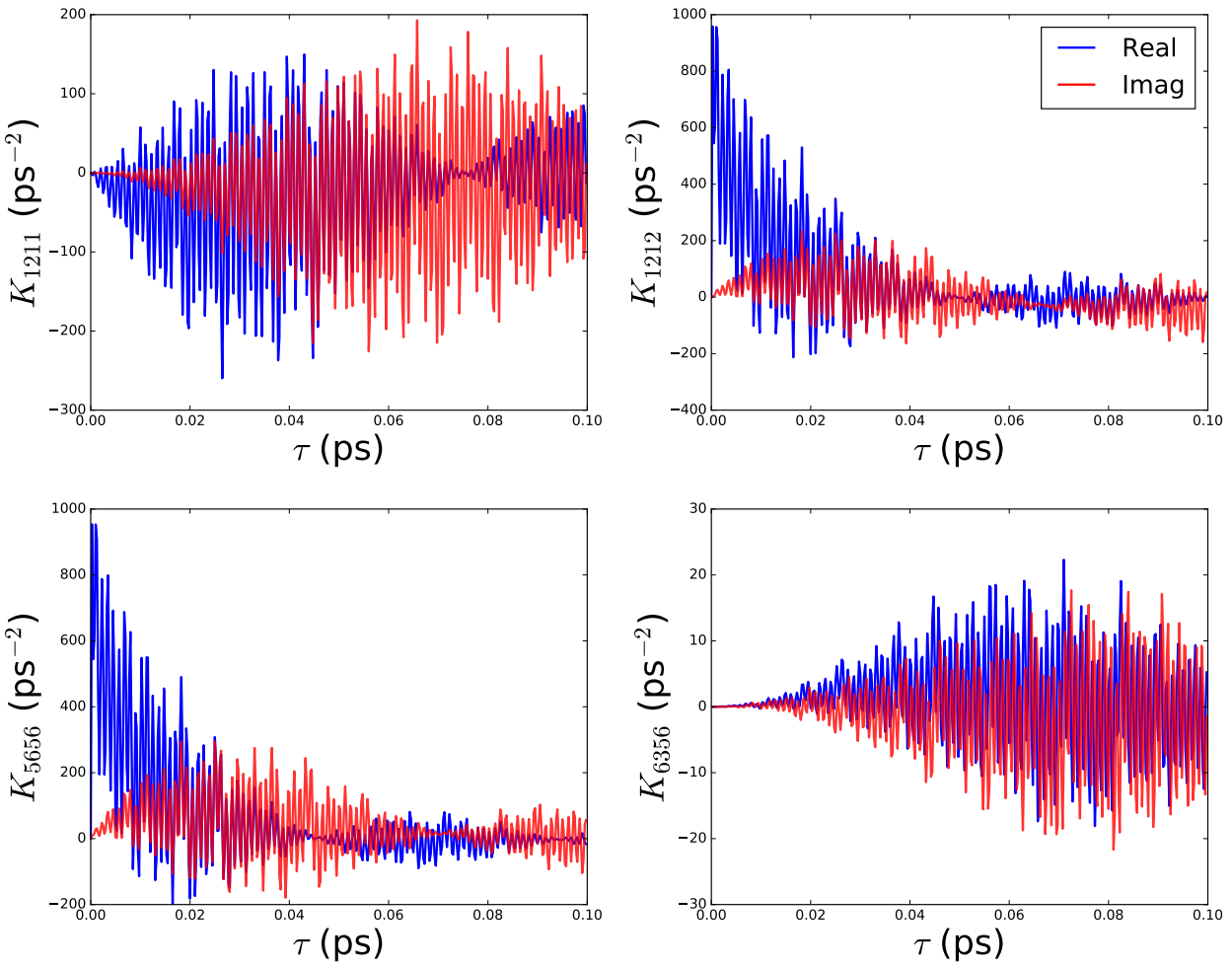

Figure V.6: Select memory kernel elements with the Shi-Geva approach to the GQME. The real part of the memory kernel element is given in red and the imaginary part in blue.

CHAPTER VI

Linearized Vibronic Coupling Systems with M-GQME

VI.1 Introduction

Conical intersections (CIs) are believed to play a central role in many photochemical processes.[13,123–133] Being able to calculate the rates of electronic transitions through CIs in a reliable and feasible manner is therefore key for understanding such processes and developing rational design principles towards controlling them. An exact fully quantum-mechanical simulation of the dynamics of electronic transitions through CIs is limited to relatively low-dimensional molecular systems and/or simple model Hamiltonians.[4,10,73,134] Thus, developing approximate methods for simulating the dynamics of electronic transitions through CIs in complex molecular systems is highly desirable.

In Chapters II, III, and V, the modified approach to the generalized quantum master equation (M-GQME) was shown to have considerable success with the spin-boson model and the Fenna-Matthews-Olson (FMO) complex. However, neither of these systems include CIs. The goal in this chapter is to extend the range of applications of the M-GQME to systems with CIs. This is done in the context of the linear vibronic coupling (LVC) model Hamiltonian.[125,135] The choice of the LVC model Hamiltonian as a benchmark for testing the ability of the M-GQME to describe the dynamics of electronic transitions through CIs is motivated by the fact that it has been reported to provide a rather accurate description of CI photophysics in many polyatomic molecules and

the ability to calculate quantum-mechanically exact electronic transition rates for it. The analysis was performed on a LVC Hamiltonian parameterized for the 2,6-bis(methylene) adamantyl (BMA) radical cation polyatomic system. Two other polyatomic systems, fulvene and and the 2-methylene-6-isopropylidene adamantyl (MIA) radical cation, are also outlined in this chapter as simulating their dynamics is a goal of future work in this area. The choice of these systems was motivated by the availability of ab-initio parameter sets and the fact that these systems were used in the past as benchmarks for equilibrium Fermi's golden rule (EQ-FGR), nonequilibrium Fermi's golden rule (NE-FGR) and LSC approximations with EQ-FGR and NE-FGR.[13,17] It should also be noted that these systems represent the inverted region (fulvene), normal region (BMA), and in the vicinity of the transition point between those two regions (MIA).

The rest of this chapter is organized as follows. The LVC model and choice of initial state are described in Sec. VI.2. The models of the aforementioned molecular systems described by the LVC Hamiltonian, the results obtained by applying the Ehrenfest method with the M-GQME to BMA, and the discussion of these results are reported in Sec. VI.3. Concluding remarks are given in Sec. VI.4.

VI.2 The Linear Vibronic Coupling (LVC) Model and Choice of Initial State

The LVC model Hamiltonian is given by[125,135]

$$\hat{H} = \hat{H}_1|1\rangle\langle 1| + \hat{H}_2|2\rangle\langle 2| + V_{12}(\hat{\mathbf{R}})|1\rangle\langle 2| + V_{21}(\hat{\mathbf{R}})|2\rangle\langle 1| \ , \tag{VI.1}$$

where

$$\begin{aligned} \hat{H}_j &= \frac{\hat{\mathbf{P}}^2}{2} + V_{jj}(\hat{\mathbf{R}}) \quad , \\ V_{jj}(\hat{\mathbf{R}}) &= \Delta_j + \sum_{i=1}^{N_n} \frac{1}{2}\omega_i^2 \hat{R}_i^2 + d_i^{(j)} \hat{R}_i \quad , \\ V_{12}(\hat{\mathbf{R}}) &= V_{21}(\hat{\mathbf{R}}) = \sum_{i=1}^{N_n} c_i \hat{R}_i \quad . \end{aligned} \tag{VI.2}$$

$\hat{H}_j$ represents the nuclear Hamiltonian when the system is in the electronic state $|j\rangle$ ($j = 1, 2$), $V_{12}(\hat{\mathbf{R}}) = V_{21}(\hat{\mathbf{R}})$ are the coupling terms between the two electronic states, and N_n is the number of nuclear DOF.

Within the LVC Hamiltonian, Eq. (VI.1), the nuclear DOF are given in terms of their mass-weighted coordinates, $\hat{\mathbf{R}} = (\hat{R}_1, \ldots, \hat{R}_{N_n})$, and momenta, $\hat{\mathbf{P}} = (\hat{P}_1, \ldots, \hat{P}_{N_n})$. Importantly, the diabatic potential energy surfaces (PESs), $V_j(\hat{\mathbf{R}}) = \sum_{i=1}^{N_n} \left[\frac{1}{2}\omega_i^2 \hat{R}_i^2 + d_i^{(j)} \hat{R}_i\right]$, are assumed harmonic and identical, except for a shift in equilibrium energy and geometry. The electronic coupling terms, $V_{12}(\hat{\mathbf{R}}) = V_{21}(\hat{\mathbf{R}})$, are assumed linear in the nuclear coordinates. The fact that the electronic coupling terms are explicitly $\hat{\mathbf{R}}$-dependent (i.e., in the non-Condon regime) is what makes it possible for the LVC Hamiltonian to account for CIs.

In what follows, the initial state of the overall system is given by Eq. (I.4), $\hat{\rho}(0) = \hat{\rho}_n(0) \otimes \hat{\sigma}(0)$, where $\hat{\rho}_n(0)$ and $\hat{\sigma}(0)$ are the reduced density operators that describe the initial states of the nuclear DOF and electronic DOF, respectively. The initial electronic state, $\hat{\sigma}(0)$, is assumed to be given by $|1\rangle\langle 1|$ or $|2\rangle\langle 2|$. The initial nuclear state, $\hat{\rho}_n(0)$, is assumed to be given by $\hat{\rho}_n(0) = e^{-\beta \hat{H}_2} \Big/ \mathrm{Tr}\Big\{e^{-\beta \hat{H}_2}\Big\}$ if $\hat{\sigma}(0) = |1\rangle\langle 1|$ or $\hat{\rho}_n(0) = e^{-\beta \hat{H}_1} \Big/ \mathrm{Tr}\Big\{e^{-\beta \hat{H}_1}\Big\}$ if $\hat{\sigma}(0) = |2\rangle\langle 2|$. Here, $\beta = 1/k_B T$ where T is the absolute temperature and k_B is the Boltzmann constant. It should be noted that this choice corresponds to a *nonequilibrium* initial state since the nuclear DOF are in equilibrium with respect to one electronic state while the electronic DOF are described by the other state.

The electronic density operator at a later time t is given by

$$\hat{\sigma}(t) = \sigma_{11}(t)|1\rangle\langle 1| + \sigma_{22}(t)|2\rangle\langle 2| + \sigma_{12}(t)|1\rangle\langle 2| + \sigma_{21}(t)|2\rangle\langle 1| \ , \tag{VI.3}$$

where

$$\sigma_{jk}(t) = \mathrm{Tr}\Big\{\hat{\rho}_n(0)|\alpha\rangle\langle\alpha|e^{i\hat{H}t/\hbar}|k\rangle\langle j|e^{-i\hat{H}t/\hbar}\Big\} \ . \tag{VI.4}$$

Here, $\hat{\rho}_n(0)|\alpha\rangle\langle\alpha|$ is the aforementioned nonequilibrium initial state. $\sigma_{jj}(t)$ corresponds to the population of the j-th electronic state and $\sigma_{jk}(t)$ (where $j \neq k$) corresponds to the electronic coherence between the j-th and the k-th electronic states.

VI.3 Results and Discussion

In this section, the preliminary results of calculations performed on the LVC model are reported for the set of parameters corresponding to the gas-phase molecules the 2,6-bis(methylene) adamantyl (BMA) radical cation. The sets of parameters corresponding to fulvene and the 2-methylene-6-isopropylidene adamantyl (MIA) radical cation are outlined as well, as they are of interest for future work. These parameters were adopted from Ref. 13, where they were obtained from electronic structure calculations and the Köppel diabatization scheme.[136–138] Several key model parameters for the three molecules are shown in Table VI.1. It should be noted that fulvene corresponds to the Marcus inverted region ($|\Delta E| > E_r$), while BMA and MIA correspond to the Marcus normal region ($|\Delta E| < E_r$). For BMA, the initial electronic state is given by $\hat{\sigma}(0) = |1\rangle\langle 1|$ and the initial nuclear state is $\hat{\rho}_n(0) = e^{-\beta\hat{H}_2}\Big/\mathrm{Tr}\Big\{e^{-\beta\hat{H}_2}\Big\}$ (the electronic states are as labeled in Ref. 13). In the case of fulvene, $\hat{\sigma}(0) = |2\rangle\langle 2|$ and $\hat{\rho}_n(0) = e^{-\beta\hat{H}_1}\Big/\mathrm{Tr}\Big\{e^{-\beta\hat{H}_1}\Big\}$ and for MIA, $\hat{\sigma}(0) = |1\rangle\langle 1|$ and $\hat{\rho}_n(0) = e^{-\beta\hat{H}_2}\Big/\mathrm{Tr}\Big\{e^{-\beta\hat{H}_2}\Big\}$.

The results obtained with the M-GQME were done using the Ehrenfest method outlined in Sec.II.5. Because BMA is a non-Condon system, the projection-free inputs calculated are $\dot{\mathcal{F}}(\tau)$ and $\mathcal{F}(\tau)$, given in Eqs. (IV.25) and (II.31), respectively. Calculations were carried out with 200,000

	fulvene	BMA	MIA
# modes	30	78	96
$\lvert\Delta E\rvert$ (a.u.)	0.0989	0.0004	0.0250
E_r (a.u.)	0.0887	0.0297	0.0274

Table VI.1: Number of nuclear modes, absolute value of the reaction free energy, $|\Delta E|$, and reorganization energy, E_r, for fulvene, BMA, and MIA.

trajectories and a variety of time steps. The preliminary results for BMA are shown in Fig. VI.1.

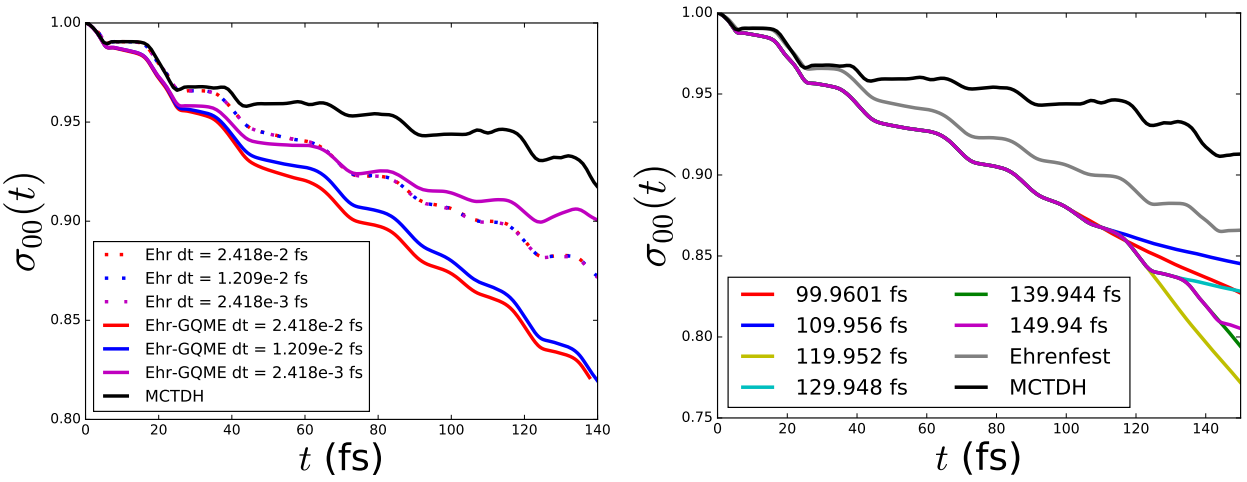

Figure VI.1: On the left is the donor population dynamics for the gas-phase BMA radical cation for time steps of 2.419×10^{-3} fs, 1.209×10^{-2} fs, and 2.419×10^{-3} fs and memory times of 137.826 fs, 149.94 fs, and 149.94 fs, respectively. The results of the direct application of Ehrenfest (Ehr) for the three time steps are shown with dashed lines while the GQME results with Ehrenfest as the input method are shown with solid lines. On the right is the donor population with a time step of 1.209×10^{-2} fs are given for the memory times listed in the legend. The dynamics for the direct application of Ehrenfest are also given with a gray line. The MCTDH results, represented by a black line, give the exact dynamics for BMA with the LVC model in both graphs.

In the left graph of Fig. VI.1, it can be seen that the M-GQME results for BMA are sensitive to the time step, much more so than the results from the direct application of Ehrenfest. In Ref. 139, it was noted that the coherence, $\sigma_{10}(t)$, is relatively small ($\sim 10^{-3}$) and oscillates rapidly for the systems under consideration in this chapter. This means getting converged results for the coherence requires a significantly larger number of trajectories and smaller time step than the populations. For Ref. 139, this was not justified because the paper was examining the direct application of QC/MH methods and the population transfer dynamics were the main quantity of interest. However, for the

GQME, the coherences need to be converged because they contribute to the projection-free inputs, meaning that a large number of trajectories and small time step will be needed to get accurate GQME results. It is possible that the computational cost of obtaining these results could reach prohibitively costly levels. An interesting option to explore would be to use the static expansion of the M-GQME described in Sec. IV.3, as the elimination of nuclear operators at time $t = \tau$ may decrease the impact of the erratic coherences and the static expansion was shown to perform as well as the bare expansion. One concern with this would be how smooth the static projection-free inputs would be, since their time derivatives could introduce errors if they are not smooth.

As seen in the right graph in Fig. VI.1, BMA also has a memory time as long as the time for which the MCTDH results are given. This is not surprising given the stepwise dynamics of BMA, indicating that there is still memory in the system from the initial excitation. For the sake of obtaining dynamics, this is problematic as the increasing memory time will be computationally costly. For the GQME, a memory time as long as the dynamics is not ideal, as it increases the time that the approximate methods used to calculate the projection-free inputs must be used, leading to higher computational costs and less accurate results.

VI.4 Concluding Remarks

While the goal of the M-GQME is to apply to molecular systems, for the systems outlined in this section, the use of the M-GQME may not be justified. Because of the rapidly oscillating coherences, the GQME requires much smaller time steps and greater number of trajectories than the population dynamics which can be obtained via the direct application of a mixed quantum-classical or exact method. Additionally, because the memory time of these systems is very long, the GQME may not give much more accurate results even when converged. This means that the GQME will be much more costly without necessarily giving much benefit.

For systems with conical intersections, more exploration is needed to determine if the GQME can provide accuracy and computational benefits as it has been shown to do for Condon systems

in the previous chapters. This is an important goal of future work with the GQME.

CHAPTER VII

Conclusion

VII.1 Summary

The simulation of electronically nonadiabatic dynamics in condensed phases is an area of considerable interest and challenge for computational chemistry. The reduced dynamics methods for simulating electronically nonadiabatic dynamics often rely on restrictive assumptions such as weak coupling between the electronic and nuclear degrees of freedom (DOF) or between electronic states. An alternative approach for simulating nonadiabatic dynamics is via mixed quantum-classical (MQC) and quasiclassical (QC) methods. These methods can handle strong coupling but their reliability and computational feasibility decrease with increasing simulation time. In comparison, the generalized quantum master equation (GQME) requires no approximation in its derivation and scales favorably with increasing simulation time.

Within the GQME, the memory kernel is the key quantity and most difficult to calculate. Two approaches were introduced in 2003 and 2006 for calculating the GQME but they were reliant on splitting the Hamiltonian into system, bath, and system-bath coupling terms, which is not natural nor convenient for many systems of interest. In Chapter II, a modified approach to the GQME (M-GQME) was introduced and compared with the two previous approaches on the spin-boson model with Ehrenfest as the input method. It was shown that the M-GQME was able to obtain either the same or better results compared to the previous approaches for all sets of parameters. An important distinction between the M-GQME and one of the commonly used previous approaches is its ability

to obtain converged results with respect to increasing memory time. This behavior is critical for systems in which tuning the memory time to achieve the exact results will not be available.

While the M-GQME with Ehrenfest as input method was able to obtain better results than the direct application of Ehrenfest for the spin-boson model in Chapter II, it was not able to obtain the exact results for all sets of parameters. In Chapter III, two mapping Hamiltonian + quasiclassical approximation (QC/MH) methods, LSCI and LSCII, were introduced and used as input for the M-GQME. For the same five sets of parameters for the spin-boson model as in Chapter II, these QC/MH methods combined with the M-GQME were able to obtain more accurate results than both the direct application of the QC/MH methods and the Ehrenfest method combined with the M-GQME. Of the three input methods, Ehrenfest, LSCI, and LSCII, LSCII with the M-GQME was able to obtain the best results with the shortest memory time for most of the sets of parameters.

The modified approach and the two previous approaches are only three of many possible ways of obtaining the memory kernel. In Chapter IV, forty-four different methods for calculating the memory kernel were explored and the results of applying these methods to one set of parameters for the spin-boson model with the two QC/MH methods from Chapter III as input methods were presented and discussed. This thorough investigation of various ways of obtaining the memory kernel helped to outline the impact of the forms of the projection-free inputs and the equations for the memory kernel on the accuracy and convergence of the GQME results. Through this investigation, it was shown that the M-GQME and one of its variants were the most accurate, stable, and generally applicable methods for obtaining the memory kernel.

In Chapter V, the M-GQME method was applied to the Fenna-Matthews-Olson (FMO) complex with Ehrenfest as the input method. It was shown that the M-GQME was able to obtain much more accurate results than the direct application of Ehrenfest for the FMO complex. Additionally, while a GQME method had previously been applied to the FMO complex, it was done with the previous approach that was shown to have non-converged results with respect to memory time for the spin-boson model in Chapter II. In Chapter V, it was shown that this issue with the previous approach also occurs with the FMO complex while the M-GQME is able to obtain converged re-

sults with respect to memory time. These results with the FMO complex establish the M-GQME as a feasible and accurate method for simulating electronically nonadiabatic dynamics in multi-state photosynthetic systems. Considering the many photosynthetic systems of interest without robust dynamics results, this is an area that the M-GQME can provide important insight into in the future.

In Chapter VI, the M-GQME was applied to a molecular system containing a conical intersection (CI). While all of the models studied in the previous chapter satisfied the Condon approximation (e.g., their electronic coupling terms were not dependent on the nuclear position), any system that contains a CI must by nature be non-Condon. Considering the importance and prevalence of systems containing CIs, this represents an area of interest for the applicability of the M-GQME. In the preliminary results for the 2,6-bis(methylene) adamantyl (BMA) radical cation polyatomic system studied in Chapter VI with the Ehrenfest method as input, it was found to require a much smaller time step than the direct application of Ehrenfest in order to obtain the population dynamics due to the osillatory nature of the coherences. The direct application of Ehrenfest is not as reliant on the convergence of these coherences in order to obtain the population dynamics but for the M-GQME, the coherences play an important role in obtaining the projection-free inputs and therefore need to be converged. Additionally, BMA was found to have a memory time at least as long as the length of the MCTDH results previously calculated. These two facts make the calculation of converged BMA results with the M-GQME computationally costly and possibly not much more accurate than the input method, due to the long memory time. Further exploration of BMA and other systems with CIs is important to determining the limitations and applicability of the M-GQME.

VII.2 Outlook

This dissertation outlined an introduction, exploration, and application of the M-GQME and provided comparison of the success of the M-GQME in relation to other methods of determining electronically nonadiabatic dynamics and other approaches to the GQME along with important

insight into systems of interest where the M-GQME is expected to succeed or fail. Moving forward, there are many areas in which the M-GQME is expected to provide benefits.

The M-GQME could be further optimized and extended by developing it for lower-dimensional quantities like electronic populations, electronic coherences, photonic correlation functions, and other such quantities. For many systems, the full electronic density matrix is not necessarily of interest and calculating lower-dimensional quantities should provide computational advantages if not also accuracy benefits. The M-GQME could also provide benefits to currently existing packages such as multi configuration time dependent Hartree (MCTDH)[4] as a multi-scale tool to get long-time outputs from inexpensive short-time inputs.

While many systems can be adequately described with model Hamiltonians, a goal of the M-GQME is to apply to truly molecular systems with on-the-fly electronic structure calculations or with electronic state-specific force fields. One such system of interest is the carotenoid-porphyrin-C_{60} molecular triad, a bioinspired molecular triad whose conformations affect its charge transfer abilities.[47] Another area of recent interest is the description of photonic DOF, such as those in quantum cavities. The M-GQME could provide useful insight into the manipulation of quantum cavities to control chemical dynamics.

Appendices

Appendix A

Proofs of the Expansions of the Projection-Free Inputs from Chapter IV

This appendix gives the mathematical proofs of the expansions of the projection-free inputs given in Sec. IV.3.

I.1 System-Bath Expansions

I.1.1 $\mathcal{K}_1(\tau)$

I.1.1.1 Static Expansion

$$\begin{aligned} i\frac{d}{d\tau}\mathcal{K}_3(\tau) &= \frac{i}{\hbar}\frac{d}{d\tau}\,\mathrm{Tr}_B\left\{e^{-i\mathcal{L}\tau/\hbar}\mathcal{L}_{BS}\hat{\rho}_B^{\mathrm{eq}}\right\} \\ &= \frac{1}{\hbar^2}\,\mathrm{Tr}_B\left\{\mathcal{L}\,e^{-i\mathcal{L}\tau/\hbar}\mathcal{L}_{BS}\hat{\rho}_B^{\mathrm{eq}}\right\} \\ &= \frac{1}{\hbar^2}\,\mathrm{Tr}_B\left\{\Big(\mathcal{L}_B+\mathcal{L}_S+\mathcal{L}_{BS}\Big)e^{-i\mathcal{L}\tau/\hbar}\mathcal{L}_{BS}\hat{\rho}_B^{\mathrm{eq}}\right\} \end{aligned}$$

- The term with $\mathcal{L}_B$ is equal to zero because, for any operator $\hat{A}=\sum_j \hat{S}_j\otimes\hat{B}_j$ where $\hat{S}_j$ and $\hat{B}_j$ are system and bath operators, respectively, because

$$\mathrm{Tr}_B\left\{\mathcal{L}_B\hat{A}\right\} = \sum_j \hat{S}_j \underbrace{\mathrm{Tr}_B\left\{[\hat{H}_B,\hat{B}_j]\right\}}_{=0} = 0 \ . \tag{A.1}$$

- Because $\mathcal{L}_S$ is a purely system superoperator, it can be pulled out of the partial trace over the bath:

$$\frac{1}{\hbar^2}\,\mathrm{Tr}_B\left\{\mathcal{L}_S\, e^{-i\mathcal{L}\tau/\hbar}\mathcal{L}_{BS}\hat{\rho}_B^{\mathrm{eq}}\right\} = \frac{1}{\hbar^2}\mathcal{L}_S\,\mathrm{Tr}_B\left\{e^{-i\mathcal{L}\tau/\hbar}\mathcal{L}_{BS}\hat{\rho}_B^{\mathrm{eq}}\right\} = \frac{1}{\hbar}\mathcal{L}_S\mathcal{K}_3(\tau) \tag{A.2}$$

Putting the terms back together,

$$\begin{aligned} i\frac{d}{d\tau}\mathcal{K}_3(\tau) = &\underbrace{\frac{1}{\hbar^2}\,\mathrm{Tr}_B\left\{\mathcal{L}_B\, e^{-i\mathcal{L}\tau/\hbar}\mathcal{L}_{BS}\hat{\rho}_B^{\mathrm{eq}}\right\}}_{0} + \underbrace{\frac{1}{\hbar^2}\,\mathrm{Tr}_B\left\{\mathcal{L}_S\, e^{-i\mathcal{L}\tau/\hbar}\mathcal{L}_{BS}\hat{\rho}_B^{\mathrm{eq}}\right\}}_{\frac{1}{\hbar}\mathcal{L}_S\mathcal{K}_3(\tau)} \\ &+ \underbrace{\frac{1}{\hbar^2}\,\mathrm{Tr}_B\left\{\mathcal{L}_{BS}\, e^{-i\mathcal{L}\tau/\hbar}\mathcal{L}_{BS}\hat{\rho}_B^{\mathrm{eq}}\right\}}_{\mathcal{K}_1(\tau)}\ , \end{aligned} \tag{A.3}$$

$$\therefore\ \mathcal{K}_1^{\mathrm{static}}(\tau) = i\frac{d}{d\tau}\mathcal{K}_3(\tau) - \frac{1}{\hbar}\mathcal{L}_S\mathcal{K}_3(\tau)\ .$$

I.1.1.2 Dynamic Expansion

$$\begin{aligned} \frac{d}{d\tau}\Phi(\tau) &= \frac{i}{\hbar}\frac{d}{d\tau}\,\mathrm{Tr}_B\left\{\mathcal{L}_{BS}\, e^{-i\mathcal{L}\tau/\hbar}\hat{\rho}_B^{\mathrm{eq}}\right\} \\ &= \frac{1}{\hbar^2}\,\mathrm{Tr}_B\left\{\mathcal{L}_{BS}\, e^{-i\mathcal{L}\tau/\hbar}\mathcal{L}\hat{\rho}_B^{\mathrm{eq}}\right\} \\ &= \frac{1}{\hbar^2}\,\mathrm{Tr}_B\left\{\mathcal{L}_{BS}\, e^{-i\mathcal{L}\tau/\hbar}\Big(\mathcal{L}_B + \mathcal{L}_S + \mathcal{L}_{BS}\Big)\hat{\rho}_B^{\mathrm{eq}}\right\} \end{aligned}$$

- The term with $\mathcal{L}_B$ is equal to zero because

$$\mathcal{L}_B\hat{\rho}_B^{\mathrm{eq}} = \left[\hat{H}_B, \hat{\rho}_B^{\mathrm{eq}}\right] = 0\ . \tag{A.4}$$

- Because $\mathcal{L}_S$ is a purely system operator, it can both commute with $\hat{\rho}_B^{\mathrm{eq}}$ and move outside of

the partial trace over the bath:

$$\frac{1}{\hbar^2}\,\mathrm{Tr}_B\left\{\mathcal{L}_{BS}\,e^{-i\mathcal{L}\tau/\hbar}\mathcal{L}_S\hat{\rho}_B^{\text{eq}}\right\} = \frac{1}{\hbar^2}\,\mathrm{Tr}_B\left\{\mathcal{L}_{BS}\,e^{-i\mathcal{L}\tau/\hbar}\hat{\rho}_B^{\text{eq}}\right\}\mathcal{L}_S = -\frac{i}{\hbar}\Phi(\tau)\mathcal{L}_S \tag{A.5}$$

Putting the terms back together,

$$\begin{aligned}\frac{d}{d\tau}\Phi(\tau) = \underbrace{\frac{1}{\hbar^2}\,\mathrm{Tr}_B\left\{\mathcal{L}_{BS}\,e^{-i\mathcal{L}\tau/\hbar}\mathcal{L}_B\hat{\rho}_B^{\text{eq}}\right\}}_{0} + \underbrace{\frac{1}{\hbar^2}\,\mathrm{Tr}_B\left\{\mathcal{L}_{BS}\,e^{-i\mathcal{L}\tau/\hbar}\mathcal{L}_S\hat{\rho}_B^{\text{eq}}\right\}}_{-\frac{i}{\hbar}\Phi(\tau)\mathcal{L}_S} \\ + \underbrace{\frac{1}{\hbar^2}\,\mathrm{Tr}_B\left\{\mathcal{L}_{BS}\,e^{-i\mathcal{L}\tau/\hbar}\mathcal{L}_{BS}\hat{\rho}_B^{\text{eq}}\right\}}_{\mathcal{K}_1(\tau)}\end{aligned}$$

$$\therefore\ \mathcal{K}_1^{\text{dynamic}}(\tau) = \frac{d}{d\tau}\Phi(\tau) + \frac{i}{\hbar}\Phi(\tau)\mathcal{L}_S$$

I.1.1.3 Propagator Expansion

$$\begin{aligned}-\ddot{\mathcal{U}}(\tau) &= -\frac{d^2}{d\tau^2}\,\mathrm{Tr}_B\left\{e^{-i\mathcal{L}\tau/\hbar}\hat{\rho}_B^{\text{eq}}\right\} \\ &= \frac{1}{\hbar^2}\,\mathrm{Tr}_B\left\{\mathcal{L}e^{-i\mathcal{L}\tau/\hbar}\mathcal{L}\hat{\rho}_B^{\text{eq}}\right\} \\ &= \frac{1}{\hbar^2}\,\mathrm{Tr}_B\left\{\mathcal{L}e^{-i\mathcal{L}\tau/\hbar}\Big(\mathcal{L}_B + \mathcal{L}_S + \mathcal{L}_{BS}\Big)\hat{\rho}_B^{\text{eq}}\right\}\end{aligned}$$

- From Eq. (A.4), we know

$$\frac{1}{\hbar^2}\,\mathrm{Tr}_B\left\{\mathcal{L}e^{-i\mathcal{L}\tau/\hbar}\mathcal{L}_B\hat{\rho}_B^{\text{eq}}\right\} = 0$$

- Since $\mathcal{L}_S$ is a purely system superoperator,

$$\frac{1}{\hbar^2}\,\mathrm{Tr}_B\left\{\mathcal{L}e^{-i\mathcal{L}\tau/\hbar}\mathcal{L}_S\hat{\rho}_B^{\text{eq}}\right\} = \frac{1}{\hbar^2}\,\mathrm{Tr}_B\left\{\mathcal{L}e^{-i\mathcal{L}\tau/\hbar}\hat{\rho}_B^{\text{eq}}\right\}\mathcal{L}_S$$

So now we have

$$
\begin{aligned}
-\ddot{\mathcal{U}}(\tau) &= \frac{1}{\hbar^2}\,\mathrm{Tr}_B\left\{\mathcal{L}e^{-i\mathcal{L}\tau/\hbar}\hat{\rho}_B^{\mathrm{eq}}\right\}\mathcal{L}_S + \frac{1}{\hbar^2}\,\mathrm{Tr}_B\left\{\mathcal{L}e^{-i\mathcal{L}\tau/\hbar}\mathcal{L}_{BS}\hat{\rho}_B^{\mathrm{eq}}\right\} \\
&= \frac{1}{\hbar^2}\,\mathrm{Tr}_B\left\{\Big(\mathcal{L}_B+\mathcal{L}_S+\mathcal{L}_{BS}\Big)e^{-i\mathcal{L}\tau/\hbar}\hat{\rho}_B^{\mathrm{eq}}\right\}\mathcal{L}_S + \frac{1}{\hbar^2}\,\mathrm{Tr}_B\left\{\Big(\mathcal{L}_B+\mathcal{L}_S+\mathcal{L}_{BS}\Big)e^{-i\mathcal{L}\tau/\hbar}\mathcal{L}_{BS}\hat{\rho}_B^{\mathrm{eq}}\right\}
\end{aligned}
$$

- From Eq. (A.1), we know

$$
\begin{aligned}
\frac{1}{\hbar^2}\,\mathrm{Tr}_B\left\{\mathcal{L}_B\,e^{-i\mathcal{L}\tau/\hbar}\hat{\rho}_B^{\mathrm{eq}}\right\}\mathcal{L}_S &= 0 \\
\frac{1}{\hbar^2}\,\mathrm{Tr}_B\left\{\mathcal{L}_B\,e^{-i\mathcal{L}\tau/\hbar}\mathcal{L}_{BS}\hat{\rho}_B^{\mathrm{eq}}\right\} &= 0
\end{aligned}
$$

- Since $\mathcal{L}_S$ is a purely system superoperator,

$$
\begin{aligned}
\frac{1}{\hbar^2}\,\mathrm{Tr}_B\left\{\mathcal{L}_S\,e^{-i\mathcal{L}\tau/\hbar}\hat{\rho}_B^{\mathrm{eq}}\right\}\mathcal{L}_S &= \frac{1}{\hbar^2}\mathcal{L}_S\,\mathrm{Tr}_B\left\{e^{-i\mathcal{L}\tau/\hbar}\hat{\rho}_B^{\mathrm{eq}}\right\}\mathcal{L}_S = \frac{1}{\hbar^2}\mathcal{L}_S\,\mathcal{U}(\tau)\mathcal{L}_S \\
\frac{1}{\hbar^2}\,\mathrm{Tr}_B\left\{\mathcal{L}_S\,e^{-i\mathcal{L}\tau/\hbar}\mathcal{L}_{BS}\hat{\rho}_B^{\mathrm{eq}}\right\} &= \frac{1}{\hbar^2}\mathcal{L}_S\,\mathrm{Tr}_B\left\{e^{-i\mathcal{L}\tau/\hbar}\mathcal{L}_{BS}\hat{\rho}_B^{\mathrm{eq}}\right\} = \frac{1}{\hbar}\mathcal{L}_S\mathcal{K}_3(\tau)
\end{aligned}
$$

Putting this all together, we get

$$
\begin{aligned}
-\ddot{\mathcal{U}}(\tau) &= \frac{1}{\hbar^2}\mathcal{L}_S\,\mathrm{Tr}_B\left\{e^{-i\mathcal{L}\tau/\hbar}\hat{\rho}_B^{\mathrm{eq}}\right\}\mathcal{L}_S + \frac{1}{\hbar^2}\,\mathrm{Tr}_B\left\{\mathcal{L}_{BS}\,e^{-i\mathcal{L}\tau/\hbar}\hat{\rho}_B^{\mathrm{eq}}\right\}\mathcal{L}_S + \frac{1}{\hbar^2}\mathcal{L}_S\,\mathrm{Tr}_B\left\{e^{-i\mathcal{L}\tau/\hbar}\mathcal{L}_{BS}\hat{\rho}_B^{\mathrm{eq}}\right\} \\
&\quad + \frac{1}{\hbar^2}\,\mathrm{Tr}_B\left\{\mathcal{L}_{BS}\,e^{-i\mathcal{L}\tau/\hbar}\mathcal{L}_{BS}\hat{\rho}_B^{\mathrm{eq}}\right\} \\
&= \frac{1}{\hbar^2}\mathcal{L}_S\,\mathcal{U}(\tau)\mathcal{L}_S - \frac{i}{\hbar}\Phi(\tau)\mathcal{L}_S + \frac{1}{\hbar}\mathcal{L}_S\mathcal{K}_3(\tau) + \mathcal{K}_1(\tau) \\
\therefore\ \mathcal{K}_1(\tau) &= -\ddot{\mathcal{U}}(\tau) - \frac{1}{\hbar^2}\mathcal{L}_S\,\mathcal{U}(\tau)\mathcal{L}_S + \frac{i}{\hbar}\Phi(\tau)\mathcal{L}_S - \frac{1}{\hbar}\mathcal{L}_S\mathcal{K}_3(\tau)
\end{aligned}
$$

Plugging in Eq. (A.6) and Eq. (A.7), we reach

$$\begin{aligned}
\mathcal{K}_1(\tau) &= -\ddot{\mathcal{U}}(\tau) - \frac{1}{\hbar^2}\mathcal{L}_S\mathcal{U}(\tau)\mathcal{L}_S + \frac{i}{\hbar}\Big(-\dot{\mathcal{U}}(\tau) - \frac{i}{\hbar}\mathcal{L}_S\mathcal{U}(\tau)\Big)\mathcal{L}_S - \frac{1}{\hbar}\mathcal{L}_S\Big(i\dot{\mathcal{U}}(\tau) - \frac{1}{\hbar}\mathcal{U}(\tau)\mathcal{L}_S\Big) \\
&= -\ddot{\mathcal{U}}(\tau) - \frac{1}{\hbar^2}\mathcal{L}_S\mathcal{U}(\tau)\mathcal{L}_S - \frac{i}{\hbar}\dot{\mathcal{U}}(\tau)\mathcal{L}_S + \frac{1}{\hbar^2}\mathcal{L}_S\mathcal{U}(\tau)\mathcal{L}_S - \frac{i}{\hbar}\mathcal{L}_S\dot{\mathcal{U}}(\tau) + \frac{1}{\hbar^2}\mathcal{L}_S\mathcal{U}(\tau)\mathcal{L}_S \\
\mathcal{K}_1^{\text{propagator}}(\tau) &= -\ddot{\mathcal{U}}(\tau) + \frac{1}{\hbar^2}\mathcal{L}_S\mathcal{U}(\tau)\mathcal{L}_S - \frac{i}{\hbar}\Big[\dot{\mathcal{U}}(\tau), \mathcal{L}_S\Big]_+
\end{aligned}$$

I.1.2 $\mathcal{K}_3(\tau)$

I.1.2.1 Dynamic and Propagator Expansion

$$\begin{aligned}
i\dot{\mathcal{U}}(\tau) &= i\frac{d}{d\tau}\,\mathrm{Tr}_B\left\{e^{-i\mathcal{L}\tau/\hbar}\hat{\rho}_B^{\text{eq}}\right\} \\
&= \frac{1}{\hbar}\,\mathrm{Tr}_B\left\{e^{-i\mathcal{L}\tau/\hbar}\mathcal{L}\hat{\rho}_B^{\text{eq}}\right\} \\
&= \frac{1}{\hbar}\,\mathrm{Tr}_B\left\{e^{-i\mathcal{L}\tau/\hbar}\Big(\mathcal{L}_B + \mathcal{L}_S + \mathcal{L}_{BS}\Big)\hat{\rho}_B^{\text{eq}}\right\}
\end{aligned}$$

From Eq. (A.4), we know the $\mathcal{L}_B$ term is equal to zero and because $\mathcal{L}_S$ is a purely system super-operator:

$$\frac{1}{\hbar}\,\mathrm{Tr}_B\left\{e^{-i\mathcal{L}\tau/\hbar}\mathcal{L}_S\hat{\rho}_B^{\text{eq}}\right\} = \frac{1}{\hbar}\,\mathrm{Tr}_B\left\{e^{-i\mathcal{L}\tau/\hbar}\hat{\rho}_B^{\text{eq}}\right\}\mathcal{L}_S = \frac{1}{\hbar}\mathcal{U}(\tau)\mathcal{L}_S$$

Plugging this back in, we get:

$$\begin{aligned}
i\dot{\mathcal{U}}(\tau) &= \underbrace{\frac{1}{\hbar}\,\mathrm{Tr}_B\left\{e^{-i\mathcal{L}\tau/\hbar}\hat{\rho}_B^{\text{eq}}\right\}\mathcal{L}_S}_{\frac{1}{\hbar}\mathcal{U}(\tau)\mathcal{L}_S} + \underbrace{\frac{1}{\hbar}\,\mathrm{Tr}_B\left\{e^{-i\mathcal{L}\tau/\hbar}\mathcal{L}_{BS}\hat{\rho}_B^{\text{eq}}\right\}}_{\mathcal{K}_3(\tau)} \\
\therefore\ \mathcal{K}_3^{\substack{\text{dynamic \&}\\ \text{propagator}}}(\tau) &= i\dot{\mathcal{U}}(\tau) - \frac{1}{\hbar}\mathcal{U}(\tau)\mathcal{L}_S
\end{aligned} \tag{A.6}$$

I.1.3 $\dot{\Phi}(\tau)$

I.1.3.1 Static Expansion

From Eq. (A.3), we know

$$
\begin{aligned}
i\frac{d}{d\tau}\mathcal{K}_3(\tau) &= \frac{1}{\hbar^2}\,\mathrm{Tr}_B\left\{\mathcal{L}_S\, e^{-i\mathcal{L}\tau/\hbar}\mathcal{L}_{BS}\hat{\rho}_B^{\mathrm{eq}}\right\} + \frac{1}{\hbar^2}\,\mathrm{Tr}_B\left\{\mathcal{L}_{BS}\, e^{-i\mathcal{L}\tau/\hbar}\mathcal{L}_{BS}\hat{\rho}_B^{\mathrm{eq}}\right\} \\
i\frac{d}{d\tau}\mathcal{K}_3(\tau) &+ \frac{1}{\hbar^2}\,\mathrm{Tr}_B\left\{\mathcal{L}_{BS}\, e^{-i\mathcal{L}\tau/\hbar}\mathcal{L}_B\hat{\rho}_B^{\mathrm{eq}}\right\} + \frac{1}{\hbar^2}\,\mathrm{Tr}_B\left\{\mathcal{L}_{BS}\, e^{-i\mathcal{L}\tau/\hbar}\mathcal{L}_S\hat{\rho}_B^{\mathrm{eq}}\right\} \\
&= \underbrace{\frac{1}{\hbar^2}\,\mathrm{Tr}_B\left\{\mathcal{L}_S\, e^{-i\mathcal{L}\tau/\hbar}\mathcal{L}_{BS}\hat{\rho}_B^{\mathrm{eq}}\right\}}_{\frac{1}{\hbar}\mathcal{L}_S\mathcal{K}_3(\tau)} + \underbrace{\frac{1}{\hbar^2}\,\mathrm{Tr}_B\left\{\mathcal{L}_{BS}\, e^{-i\mathcal{L}\tau/\hbar}\mathcal{L}\hat{\rho}_B^{\mathrm{eq}}\right\}}_{\dot{\Phi}(\tau)}
\end{aligned}
$$

From Eq. (A.4) and because $\mathcal{L}_S$ is a purely system superoperator, we know

$$
\begin{aligned}
i\frac{d}{d\tau}\mathcal{K}_3(\tau) &+ \underbrace{\frac{1}{\hbar^2}\,\mathrm{Tr}_B\left\{\mathcal{L}_{BS}\, e^{-i\mathcal{L}\tau/\hbar}\mathcal{L}_B\hat{\rho}_B^{\mathrm{eq}}\right\}}_{=0} + \underbrace{\frac{1}{\hbar^2}\,\mathrm{Tr}_B\left\{\mathcal{L}_{BS}\, e^{-i\mathcal{L}\tau/\hbar}\mathcal{L}_S\hat{\rho}_B^{\mathrm{eq}}\right\}}_{-\frac{i}{\hbar}\Phi(\tau)\mathcal{L}_S} \\
&= \underbrace{\frac{1}{\hbar^2}\,\mathrm{Tr}_B\left\{\mathcal{L}_S\, e^{-i\mathcal{L}\tau/\hbar}\mathcal{L}_{BS}\hat{\rho}_B^{\mathrm{eq}}\right\}}_{\frac{1}{\hbar}\mathcal{L}_S\mathcal{K}_3(\tau)} + \underbrace{\frac{1}{\hbar^2}\,\mathrm{Tr}_B\left\{\mathcal{L}_{BS}\, e^{-i\mathcal{L}\tau/\hbar}\mathcal{L}\hat{\rho}_B^{\mathrm{eq}}\right\}}_{\dot{\Phi}(\tau)} \\
\therefore\ \dot{\Phi}^{\text{static}}(\tau) &= i\frac{d}{d\tau}\mathcal{K}_3(\tau) - \frac{i}{\hbar}\Phi(\tau)\mathcal{L}_S - \frac{1}{\hbar}\mathcal{L}_S\mathcal{K}_3(\tau)
\end{aligned}
$$

I.1.3.2 Dynamic Expansion

The dynamic expansion is straightforward, so no proof is given.

I.1.3.3 Propagator Expansion

$$
\begin{aligned}
-\ddot{\mathcal{U}}(\tau) &= -\frac{d^2}{d\tau^2}\,\mathrm{Tr}_B\left\{e^{-i\mathcal{L}\tau/\hbar}\hat{\rho}_B^{\mathrm{eq}}\right\} \\
&= \frac{1}{\hbar^2}\,\mathrm{Tr}_B\left\{\mathcal{L}e^{-i\mathcal{L}\tau/\hbar}\mathcal{L}\hat{\rho}_B^{\mathrm{eq}}\right\} \\
&= \frac{1}{\hbar^2}\,\mathrm{Tr}_B\left\{\Big(\mathcal{L}_B+\mathcal{L}_S+\mathcal{L}_{BS}\Big)e^{-i\mathcal{L}\tau/\hbar}\mathcal{L}\hat{\rho}_B^{\mathrm{eq}}\right\}
\end{aligned}
$$

From Eq. (A.1), we know the term with $\mathcal{L}_B$ is equal to zero and because $\mathcal{L}_S$ is a purely system superoperator:

$$
\frac{1}{\hbar^2}\,\mathrm{Tr}_B\left\{\mathcal{L}_S e^{-i\mathcal{L}\tau/\hbar}\mathcal{L}\hat{\rho}_B^{\mathrm{eq}}\right\} = \frac{1}{\hbar^2}\mathcal{L}_S\,\mathrm{Tr}_B\left\{e^{-i\mathcal{L}\tau/\hbar}\mathcal{L}\hat{\rho}_B^{\mathrm{eq}}\right\}
$$

We can expand the $\mathcal{L}$ of the above RHS and use Eqs. (A.4) and the fact that $\mathcal{L}_S$ is a purely system superoperator to reach

$$
\begin{aligned}
\frac{1}{\hbar^2}\mathcal{L}_S\,\mathrm{Tr}_B\left\{e^{-i\mathcal{L}\tau/\hbar}\mathcal{L}\hat{\rho}_B^{\mathrm{eq}}\right\} &= \frac{1}{\hbar^2}\mathcal{L}_S\,\mathrm{Tr}_B\left\{e^{-i\mathcal{L}\tau/\hbar}\hat{\rho}_B^{\mathrm{eq}}\right\}\mathcal{L}_S + \frac{1}{\hbar^2}\mathcal{L}_S\,\mathrm{Tr}_B\left\{e^{-i\mathcal{L}\tau/\hbar}\mathcal{L}_{BS}\hat{\rho}_B^{\mathrm{eq}}\right\} \\
&= \frac{1}{\hbar^2}\mathcal{L}_S\mathcal{U}(\tau)\mathcal{L}_S + \frac{1}{\hbar}\mathcal{L}_S\mathcal{K}_3(\tau)
\end{aligned}
$$

Plugging this back in, we get:

$$
\begin{aligned}
-\ddot{\mathcal{U}}(\tau) &= \frac{1}{\hbar^2}\mathcal{L}_S\mathcal{U}(\tau)\mathcal{L}_S + \frac{1}{\hbar}\mathcal{L}_S\mathcal{K}_3(\tau) + \dot{\Phi}(\tau) \\
\therefore\ \dot{\Phi}(\tau) &= -\ddot{\mathcal{U}}(\tau) - \frac{1}{\hbar^2}\mathcal{L}_S\mathcal{U}(\tau)\mathcal{L}_S - \frac{1}{\hbar}\mathcal{L}_S\mathcal{K}_3(\tau)
\end{aligned}
$$

Plugging in Eq. (A.6), we get:

$$\begin{aligned}
\dot{\Phi}(\tau) &= -\ddot{\mathcal{U}}(\tau) - \frac{1}{\hbar^2}\mathcal{L}_S\mathcal{U}(\tau)\mathcal{L}_S - \frac{1}{\hbar}\mathcal{L}_S\left(i\dot{\mathcal{U}}(\tau) - \frac{1}{\hbar}\mathcal{U}(\tau)\mathcal{L}_S\right) \\
&= -\ddot{\mathcal{U}}(\tau) - \frac{1}{\hbar^2}\mathcal{L}_S\mathcal{U}(\tau)\mathcal{L}_S - \frac{i}{\hbar}\mathcal{L}_S\dot{\mathcal{U}}(\tau) + \frac{1}{\hbar^2}\mathcal{L}_S\mathcal{U}(\tau)\mathcal{L}_S \\
\dot{\Phi}^{\text{propagator}}(\tau) &= -\ddot{\mathcal{U}}(\tau) - \frac{i}{\hbar}\mathcal{L}_S\dot{\mathcal{U}}(\tau)
\end{aligned}$$

I.1.4 $\Phi(\tau)$

I.1.4.1 Static and Propagator Expansion

$$\begin{aligned}
-\dot{\mathcal{U}}(\tau) &= -\frac{d}{d\tau}\,\mathrm{Tr}_B\left\{e^{-i\mathcal{L}\tau/\hbar}\rho_B^{\text{eq}}\right\} \\
&= \frac{i}{\hbar}\,\mathrm{Tr}_B\left\{\mathcal{L}e^{-i\mathcal{L}\tau/\hbar}\rho_B^{\text{eq}}\right\} \\
&= \frac{i}{\hbar}\,\mathrm{Tr}_B\left\{\Big(\mathcal{L}_B + \mathcal{L}_S + \mathcal{L}_{BS}\Big)e^{-i\mathcal{L}\tau/\hbar}\rho_B^{\text{eq}}\right\}
\end{aligned}$$

From Eq. (A.1), we know the $\mathcal{L}_B$ term is equal to zero and because $\mathcal{L}_S$ is a purely system superoperator:

$$\frac{i}{\hbar}\,\mathrm{Tr}_B\left\{\mathcal{L}_S e^{-i\mathcal{L}\tau/\hbar}\rho_B^{\text{eq}}\right\} = \frac{i}{\hbar}\mathcal{L}_S\,\mathrm{Tr}_B\left\{e^{-i\mathcal{L}\tau/\hbar}\rho_B^{\text{eq}}\right\} = \frac{i}{\hbar}\mathcal{L}_S\mathcal{U}(\tau)$$

Plugging this back in, we get:

$$-\dot{\mathcal{U}}(\tau) = \underbrace{\frac{i}{\hbar}\mathcal{L}_S\,\mathrm{Tr}_B\left\{e^{-i\mathcal{L}\tau/\hbar}\rho_B^{\text{eq}}\right\}}_{\frac{i}{\hbar}\mathcal{L}_S\mathcal{U}(\tau)} + \underbrace{\frac{i}{\hbar}\,\mathrm{Tr}_B\left\{\mathcal{L}_{BS}e^{-i\mathcal{L}\tau/\hbar}\rho_B^{\text{eq}}\right\}}_{\Phi(\tau)}$$

$$\therefore\ \Phi^{\substack{\text{static \&}\\ \text{propagator}}}(\tau) = -\dot{\mathcal{U}}(\tau) - \frac{i}{\hbar}\mathcal{L}_S\mathcal{U}(\tau) \tag{A.7}$$

I.2 Modified Expansions

I.2.1 $\dot{\mathcal{F}}(\tau)$, $\mathcal{F}(\tau)$, and $\mathcal{G}(\tau)$

The expansions of $\dot{\mathcal{F}}(\tau)$, $\mathcal{F}(\tau)$, and $\mathcal{G}(\tau)$ are all straightforward so no proofs are given.

I.2.2 $\mathcal{F}_1(\tau)$

I.2.2.1 Static Expansion

$$\begin{aligned} i\frac{d}{d\tau}\mathcal{G}_{\text{zero}}(\tau) &= \frac{i}{\hbar}\frac{d}{d\tau}\,\mathrm{Tr}_N\left\{e^{-i\mathcal{L}\tau/\hbar}\mathcal{L}_{\text{zero}}\hat{\rho}_N(0)\right\} \\ &= \frac{1}{\hbar^2}\,\mathrm{Tr}_N\left\{\mathcal{L}e^{-i\mathcal{L}\tau/\hbar}\mathcal{L}_{\text{zero}}\hat{\rho}_N(0)\right\} \\ &= \frac{1}{\hbar^2}\,\mathrm{Tr}_N\left\{\Big(\mathcal{L}_{\text{zero}}+\mathcal{L}_{\text{int}}\Big)e^{-i\mathcal{L}\tau/\hbar}\mathcal{L}_{\text{zero}}\hat{\rho}_N(0)\right\} \end{aligned}$$

In the Condon limit, $\mathcal{L}_{\text{int}}$ is a purely electronic superoperator, so this can be written as

$$i\frac{d}{d\tau}\mathcal{G}_{\text{zero}}(\tau) = \underbrace{\frac{1}{\hbar^2}\,\mathrm{Tr}_N\left\{\mathcal{L}_{\text{zero}}e^{-i\mathcal{L}\tau/\hbar}\mathcal{L}_{\text{zero}}\hat{\rho}_N(0)\right\}}_{\mathcal{F}_1(\tau)} + \underbrace{\frac{1}{\hbar^2}\mathcal{L}_{\text{int}}\,\mathrm{Tr}_N\left\{e^{-i\mathcal{L}\tau/\hbar}\mathcal{L}_{\text{zero}}\hat{\rho}_N(0)\right\}}_{\frac{1}{\hbar}\mathcal{L}_{\text{int}}\mathcal{G}_{\text{zero}}(\tau)}$$

$$\therefore\ \mathcal{F}_1^{\text{static}}(\tau) = i\frac{d}{d\tau}\mathcal{G}_{\text{zero}}(\tau) - \frac{1}{\hbar}\mathcal{L}_{\text{int}}\mathcal{G}_{\text{zero}}(\tau)$$

I.2.2.2 Dynamic Expansion

$$\begin{aligned} i\frac{d}{d\tau}\mathcal{F}_2(\tau) &= \frac{i}{\hbar}\frac{d}{d\tau}\,\mathrm{Tr}_N\left\{\mathcal{L}_{\text{zero}}e^{-i\mathcal{L}\tau/\hbar}\hat{\rho}_N(0)\right\} \\ &= \frac{1}{\hbar^2}\,\mathrm{Tr}_N\left\{\mathcal{L}_{\text{zero}}e^{-i\mathcal{L}\tau/\hbar}\mathcal{L}\hat{\rho}_N(0)\right\} \\ &= \frac{1}{\hbar^2}\,\mathrm{Tr}_N\left\{\mathcal{L}_{\text{zero}}e^{-i\mathcal{L}\tau/\hbar}\Big(\mathcal{L}_{\text{zero}}+\mathcal{L}_{\text{int}}\Big)\hat{\rho}_N(0)\right\} \end{aligned}$$

In the Condon limit, $\mathcal{L}_{\text{int}}$ is a purely electronic superoperator, so this can be written as

$$i\frac{d}{d\tau}\mathcal{F}_2(\tau) = \underbrace{\frac{1}{\hbar^2}\,\mathrm{Tr}_N\left\{\mathcal{L}_{\text{zero}}e^{-i\mathcal{L}\tau/\hbar}\mathcal{L}_{\text{zero}}\hat{\rho}_N(0)\right\}}_{\mathcal{F}_1(\tau)} + \underbrace{\frac{1}{\hbar^2}\,\mathrm{Tr}_N\left\{\mathcal{L}_{\text{zero}}e^{-i\mathcal{L}\tau/\hbar}\hat{\rho}_N(0)\right\}\mathcal{L}_{\text{int}}}_{\frac{1}{\hbar}\mathcal{F}_2(\tau)\mathcal{L}_{\text{int}}}$$

$$\therefore\ \mathcal{F}_1^{\text{dynamic}}(\tau) = i\frac{d}{d\tau}\mathcal{F}_2(\tau) - \frac{1}{\hbar}\mathcal{F}_2(\tau)\mathcal{L}_{\text{int}}$$

I.2.2.3 Propagator Expansion

$$\begin{aligned}
-\ddot{\mathcal{U}}(\tau) &= -\frac{d^2}{d\tau^2}\,\mathrm{Tr}_N\left\{e^{-i\mathcal{L}\tau/\hbar}\hat{\rho}_N(0)\right\} \\
&= \frac{1}{\hbar^2}\,\mathrm{Tr}_N\left\{\mathcal{L}e^{-i\mathcal{L}\tau/\hbar}\mathcal{L}\hat{\rho}_N(0)\right\} \\
&= \frac{1}{\hbar^2}\,\mathrm{Tr}_N\left\{\Big(\mathcal{L}_{\text{zero}}+\mathcal{L}_{\text{int}}\Big)e^{-i\mathcal{L}\tau/\hbar}\Big(\mathcal{L}_{\text{zero}}+\mathcal{L}_{\text{int}}\Big)\hat{\rho}_N(0)\right\}
\end{aligned}$$

In the Condon limit, $\mathcal{L}_{\text{int}}$ is a purely electronic superoperator, so this can be written as

$$\begin{aligned}
-\ddot{\mathcal{U}}(\tau) = &\underbrace{\frac{1}{\hbar^2}\,\mathrm{Tr}_N\left\{\mathcal{L}_{\text{zero}}e^{-i\mathcal{L}\tau/\hbar}\mathcal{L}_{\text{zero}}\hat{\rho}_N(0)\right\}}_{\mathcal{F}_1(\tau)} + \underbrace{\frac{1}{\hbar^2}\,\mathrm{Tr}_N\left\{\mathcal{L}_{\text{zero}}e^{-i\mathcal{L}\tau/\hbar}\hat{\rho}_N(0)\right\}\mathcal{L}_{\text{int}}}_{\frac{1}{\hbar}\mathcal{F}_2(\tau)\mathcal{L}_{\text{int}}} \\
&+ \underbrace{\frac{1}{\hbar^2}\mathcal{L}_{\text{int}}\,\mathrm{Tr}_N\left\{e^{-i\mathcal{L}\tau/\hbar}\mathcal{L}_{\text{zero}}\hat{\rho}_N(0)\right\}}_{\frac{1}{\hbar}\mathcal{L}_{\text{int}}\mathcal{G}_{\text{zero}}(\tau)} + \underbrace{\frac{1}{\hbar^2}\mathcal{L}_{\text{int}}\,\mathrm{Tr}_N\left\{e^{-i\mathcal{L}\tau/\hbar}\hat{\rho}_N(0)\right\}\mathcal{L}_{\text{int}}}_{\frac{1}{\hbar^2}\mathcal{L}_{\text{int}}\mathcal{U}(\tau)\mathcal{L}_{\text{int}}}
\end{aligned}$$

$$\therefore\ \mathcal{F}_1(\tau) = -\ddot{\mathcal{U}}(\tau) - \frac{1}{\hbar}\mathcal{F}_2(\tau)\mathcal{L}_{\text{int}} - \frac{1}{\hbar}\mathcal{L}_{\text{int}}\mathcal{G}_{\text{zero}}(\tau) - \frac{1}{\hbar^2}\mathcal{L}_{\text{int}}\mathcal{U}(\tau)\mathcal{L}_{\text{int}}$$

Plugging in Eqs. (A.8) and (A.9), we reach

$$\begin{aligned}
\mathcal{F}_1(\tau) &= -\ddot{\mathcal{U}}(\tau) - \frac{1}{\hbar}\Big(i\dot{\mathcal{U}}(\tau) - \frac{1}{\hbar}\mathcal{L}_{\text{int}}\mathcal{U}(\tau)\Big)\mathcal{L}_{\text{int}} - \frac{1}{\hbar}\mathcal{L}_{\text{int}}\Big(i\dot{\mathcal{U}}(\tau) - \frac{1}{\hbar}\mathcal{U}(\tau)\mathcal{L}_{\text{int}}\Big) \\
&\quad - \frac{1}{\hbar^2}\mathcal{L}_{\text{int}}\mathcal{U}(\tau)\mathcal{L}_{\text{int}} \\
&= -\ddot{\mathcal{U}}(\tau) - \frac{i}{\hbar}\dot{\mathcal{U}}(\tau)\mathcal{L}_{\text{int}} + \frac{1}{\hbar^2}\mathcal{L}_{\text{int}}\mathcal{U}(\tau)\mathcal{L}_{\text{int}} - \frac{i}{\hbar}\mathcal{L}_{\text{int}}\dot{\mathcal{U}}(\tau) + \frac{1}{\hbar^2}\mathcal{L}_{\text{int}}\mathcal{U}(\tau)\mathcal{L}_{\text{int}} \\
&\quad - \frac{1}{\hbar^2}\mathcal{L}_{\text{int}}\mathcal{U}(\tau)\mathcal{L}_{\text{int}} \\
\mathcal{F}_1(\tau) &= -\ddot{\mathcal{U}}(\tau) - \frac{i}{\hbar}\Big[\dot{\mathcal{U}}(\tau), \mathcal{L}_{\text{int}}\Big]_+ + \frac{1}{\hbar^2}\mathcal{L}_{\text{int}}\mathcal{U}(\tau)\mathcal{L}_{\text{int}}
\end{aligned}$$

I.2.3 $\mathcal{F}_2(\tau)$

I.2.3.1 Static and Propagator Expansion

$$\begin{aligned}
i\dot{\mathcal{U}}(\tau) &= i\frac{d}{d\tau}\,\mathrm{Tr}_N\left\{e^{-i\mathcal{L}\tau/\hbar}\hat{\rho}_N(\tau)\right\} \\
&= \frac{1}{\hbar}\,\mathrm{Tr}_N\left\{\mathcal{L}e^{-i\mathcal{L}\tau/\hbar}\hat{\rho}_N(\tau)\right\} \\
&= \frac{1}{\hbar}\,\mathrm{Tr}_N\left\{\Big(\mathcal{L}_{\text{zero}} + \mathcal{L}_{\text{int}}\Big)e^{-i\mathcal{L}\tau/\hbar}\hat{\rho}_N(0)\right\}
\end{aligned}$$

In the Condon limit, $\mathcal{L}_{\text{int}}$ is a purely electronic superoperator, so this can be written as

$$i\dot{\mathcal{U}}(\tau) = \underbrace{\frac{1}{\hbar}\,\mathrm{Tr}_N\left\{\mathcal{L}_{\text{zero}}e^{-i\mathcal{L}\tau/\hbar}\hat{\rho}_N(0)\right\}}_{\mathcal{F}_2(\tau)} + \underbrace{\frac{1}{\hbar}\mathcal{L}_{\text{int}}\,\mathrm{Tr}_N\left\{e^{-i\mathcal{L}\tau/\hbar}\hat{\rho}_N(0)\right\}}_{\frac{1}{\hbar}\mathcal{L}_{\text{int}}\mathcal{U}(\tau)}$$

$$\therefore\ \mathcal{F}_2^{\substack{\text{static \&}\\ \text{propagator}}}(\tau) = i\dot{\mathcal{U}}(\tau) - \frac{1}{\hbar}\mathcal{L}_{\text{int}}\mathcal{U}(\tau) \tag{A.8}$$

I.2.4 $\mathcal{G}_{\textbf{zero}}(\tau)$

I.2.4.1 Dynamic and Propagator Expansion

$$\begin{aligned} i\dot{\mathcal{U}}(\tau) &= i\frac{d}{d\tau}\,\mathrm{Tr}_N\left\{e^{-i\mathcal{L}\tau/\hbar}\hat{\rho}_N(0)\right\} \\ &= \frac{1}{\hbar}\,\mathrm{Tr}_N\left\{e^{-i\mathcal{L}\tau/\hbar}\mathcal{L}\hat{\rho}_N(0)\right\} \\ &= \frac{1}{\hbar}\,\mathrm{Tr}_N\left\{e^{-i\mathcal{L}\tau/\hbar}\Big(\mathcal{L}_{\text{zero}}+\mathcal{L}_{\text{int}}\Big)\hat{\rho}_N(0)\right\} \end{aligned}$$

In the Condon limit, $\mathcal{L}_{\text{int}}$ is a purely electronic superoperator, so this can be written as

$$i\dot{\mathcal{U}}(\tau) = \underbrace{\frac{1}{\hbar}\,\mathrm{Tr}_N\left\{e^{-i\mathcal{L}\tau/\hbar}\mathcal{L}_{\text{zero}}\hat{\rho}_N(0)\right\}}_{\mathcal{G}_{\text{zero}}(\tau)} + \underbrace{\frac{1}{\hbar}\,\mathrm{Tr}_N\left\{e^{-i\mathcal{L}\tau/\hbar}\hat{\rho}_N(0)\right\}\mathcal{L}_{\text{int}}}_{\frac{1}{\hbar}\mathcal{U}(\tau)\mathcal{L}_{\text{int}}}$$

$$\therefore\ \overset{\text{dynamic \& propagator}}{\mathcal{G}_{\text{zero}}}(\tau) = i\dot{\mathcal{U}}(\tau) - \frac{1}{\hbar}\mathcal{U}(\tau)\mathcal{L}_{\text{int}} \tag{A.9}$$

Appendix B

Additional Results of the Various Approaches to the GQME from Chapter IV

This appendix includes additional results for the various methods to the obtain the GQME outlined in Chapter IV.

II.1 Additional Results

II.1.1 System-Bath v. Modified Form

Shown in Fig. B.1 are the electronic population difference results for the propagator expansion with LSCI as input method, with the TE approaches shown in the top row and the PF approaches shown in the bottom row and the time step of the left column results is $\Delta t = 0.01$ whereas the time step of the right column results is $\Delta t = 0.005$. The results with LSCII as input method are given in Fig. IV.5 and show the same trends as the LSCI-GQME results given here. The results for the Condon M-TE approaches and the PS approaches are not shown because their results are still being verified.

II.1.2 Non-Condon v. Condon

In Fig. B.2, the results for the bare and static expansions of the modified two-equation and projection-second approaches with LSCII as the input method are shown. Contrasting with the

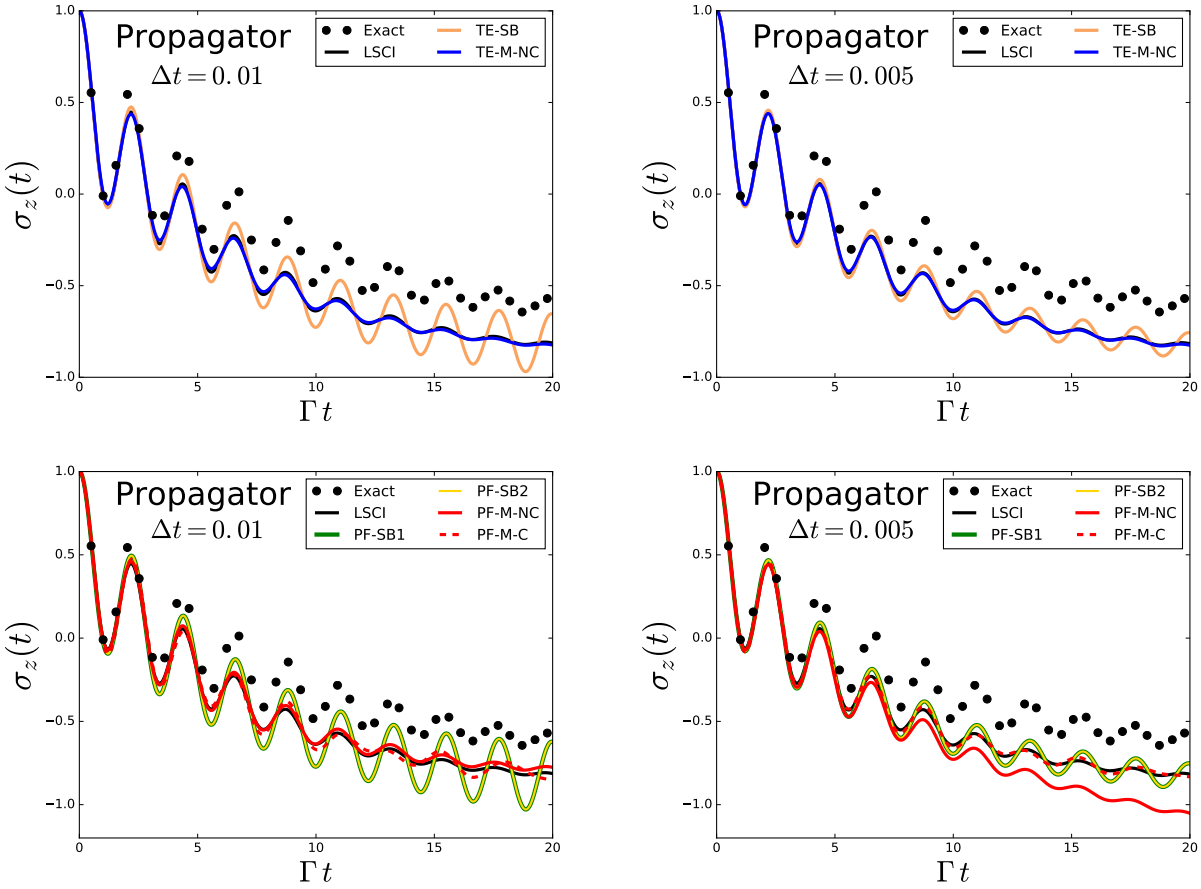

Figure B.1: In the top row, shown are the electronic population differences, $\sigma_z(t) = \sigma_{DD}(t) - \sigma_{AA}(t)$, for the propagator expansion of the two-equation approaches with a time step of $\Delta t = 0.01$ on the left and a time step of $\Delta t = 0.005$ on the right. In the bottom row, shown are the electronic population differences for the propagator expansion of the projection-first approaches with $\Delta t = 0.01$ on the left and a time step of $\Delta t = 0.005$ on the right. The parameters are those of model 2 in Table IV.1 and the input method is LSCII, with the direct application of LSCII results shown on each graph as a solid black line. Exact results are shown in black circles on each graph. The M-TE-C1 and M-TE-C2 results are not shown in the top row because the results are still being verified. Similarly, the projection-second results are not shown because results with the modified form are still verified.

results for LSCI as input method shown in Fig. IV.6, the non-Condon approaches are slightly more or as equally accurate as the Condon approaches.

Shown in Fig. B.3 are the bare, static, dynamic, and propagator expansions for the modified projection-first approaches with LSCII as the input method. Differing from the same results with LSCI as input method given in Fig. IV.7, all four expansions show very similar results for the

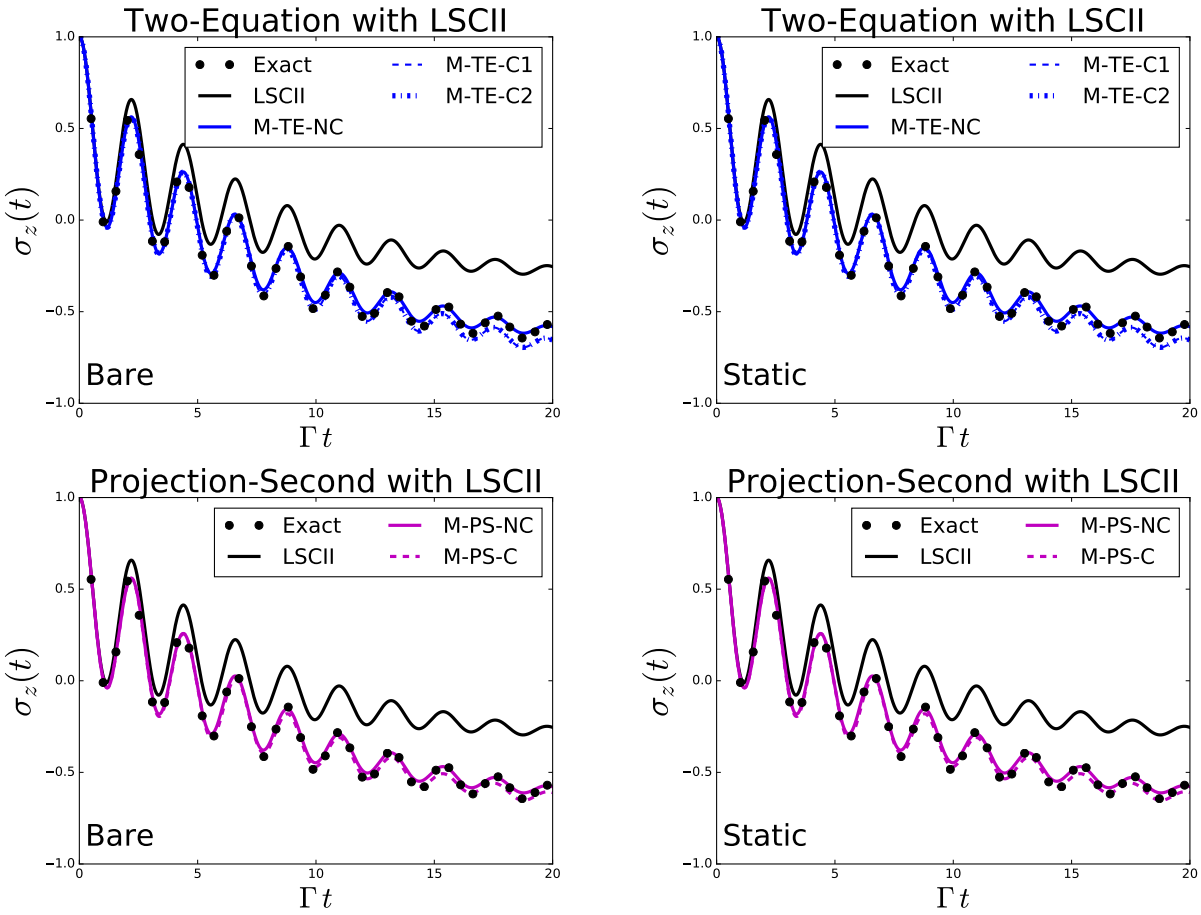

Figure B.2: In the top row, shown are the electronic population differences, $\sigma_z(t) = \sigma_{DD}(t) - \sigma_{AA}(t)$, for the bare (left) and static (right) expansions of the modified two-equation approaches. In the bottom row, shown are the electronic population differences for the bare (left) and static (right) expansions of the modified projection-second approaches. The input method is LSCI, with the direct application of LSCI results shown on each graph as a solid black line. Exact results are shown in black circles on each graph.

Condon and non-Condon M-PF approaches and the M-PF-NC approach is converged with respect to time step by a time step of $\Delta t = 0.005$. Similar to Fig. IV.7, the dynamic and propagator expansion results give worse results when compared to the bare and static expansions, giving back the same results as the direct application of LSCII.

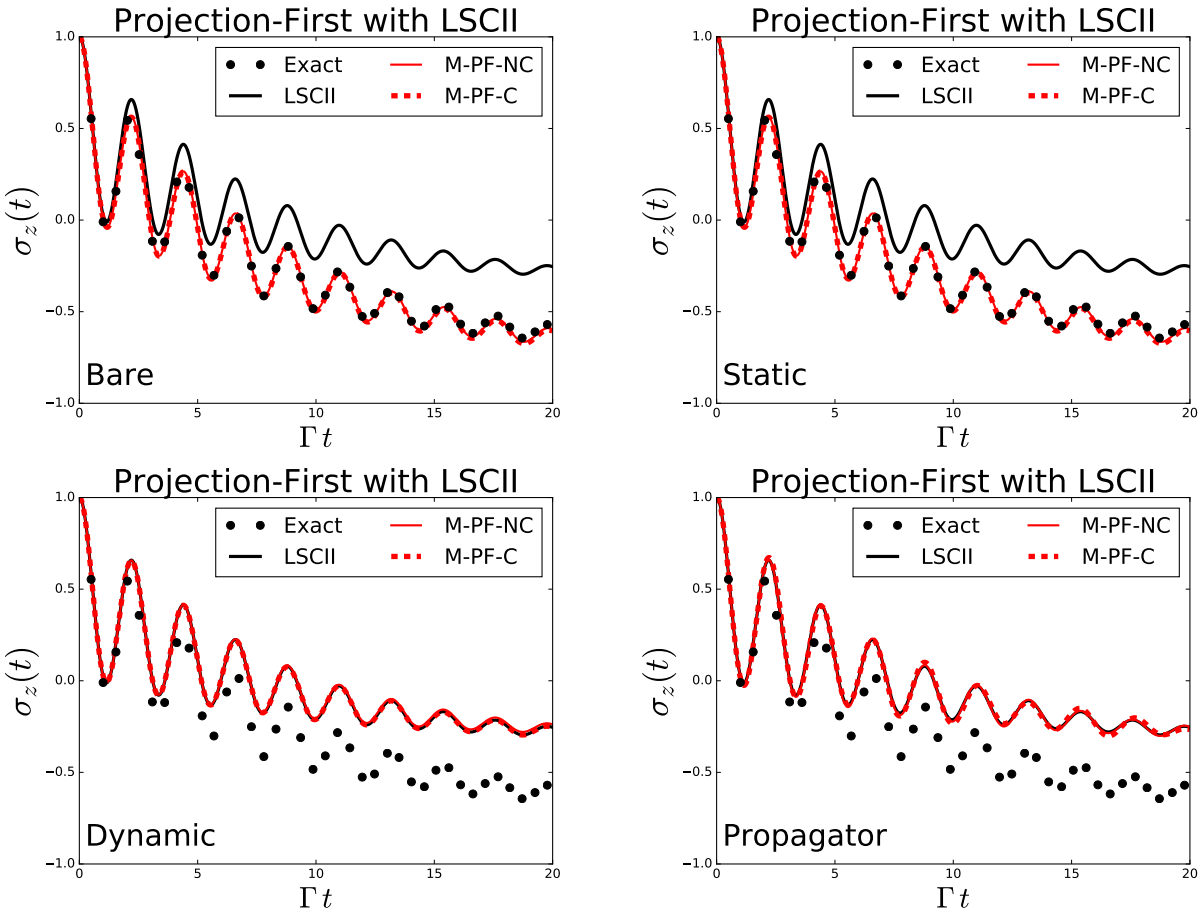

Figure B.3: In the top row, shown are the electronic population differences, $\sigma_z(t) = \sigma_{DD}(t) - \sigma_{AA}(t)$, for the bare (left) and static (right) expansions of the modified projection-first approaches. In the middle row, shown are the electronic population differences for the dynamic (left) and propagator (right) expansions of the modified projection-first approaches. The parameters are those of model 2 in Table IV.1 and the input method is LSCI, with the direct application of LSCI results shown on each graph as a solid black line. Exact results are shown in black circles on each graph.

II.1.3 Two Equations v. One Equation for the Memory Kernel

Shown in Fig. B.4 are the results for the bare, static, and dynamic expansions with the modified form approaches with LSCII as input method. Compared to the same results for LSCI shown in Fig. IV.9, it can be seen that the bare and static expansions again behave the same while the dynamics expansion gives comparatively worse results. However, within each expansion, the approaches behave very similarly, which can be contrasted with the results shown in Fig. IV.9.

In Fig. B.5, the electronic population difference results for the modified form approaches

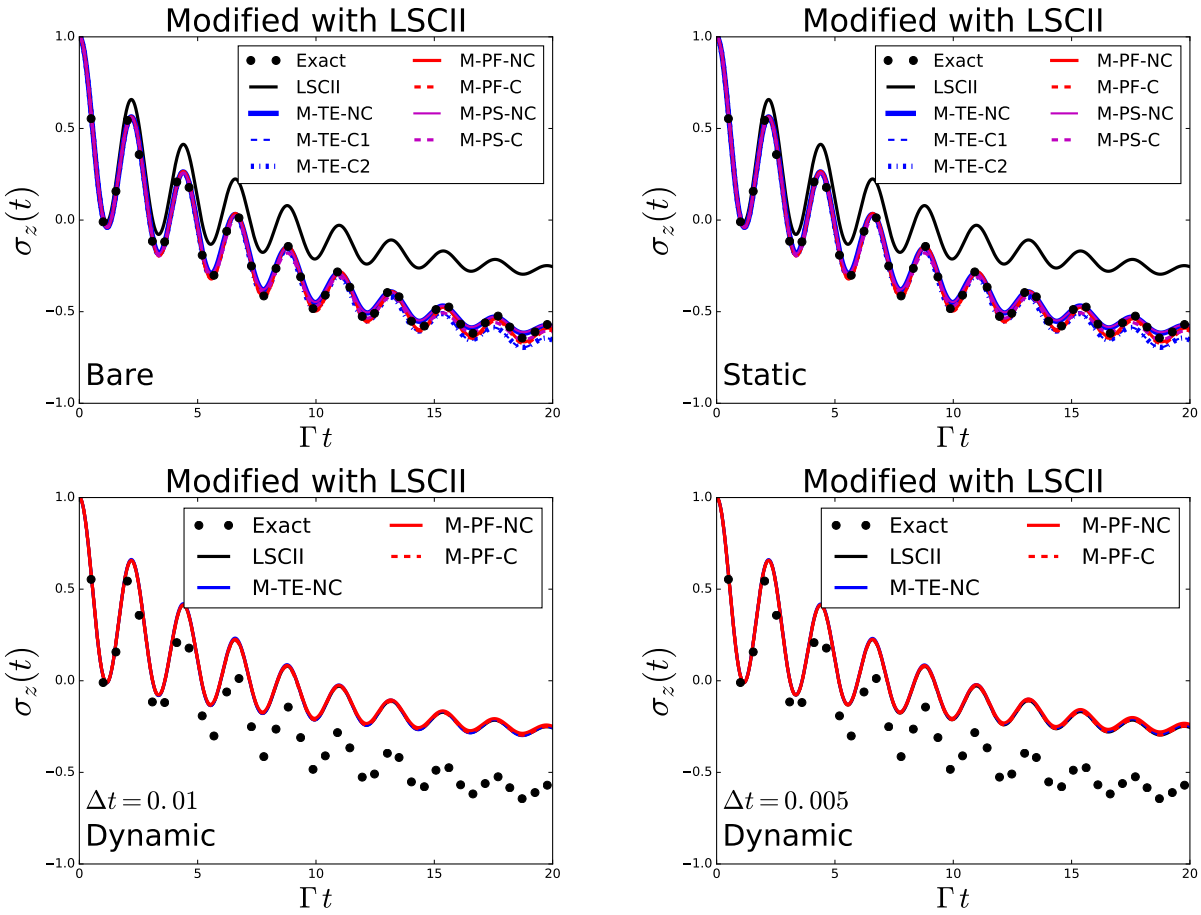

Figure B.4: Shown are the electronic population differences, $\sigma_z(t) = \sigma_{DD}(t) - \sigma_{AA}(t)$, for the modified form approaches. Starting from the upper left and moving counter-clockwise are the results with the bare expansion, the static expansion, the dynamic expansion with $\Delta t = 0.005$, and the dynamic expansion with $\Delta t = 0.01$. The input method for the GQME is LSCII, with the dynamics of the direct application of LSCII shown with a solid black line. The parameters are those of model 2 in Table IV.1 and exact results are shown in black circles on each graph.

with the propagator expansion with LSCI and LSCII as input method and time steps of $\Delta t = 0.01$ and $\Delta t = 0.005$ are shown. Similar to the dynamic expansion results shown in Fig. IV.9, with LSCI as input, the M-TE-NC and M-PF-C approaches give the same dynamics as the direct application of LSCI and the M-PF-NC approach has not converged by a time step of $\Delta t = 0.005$. For LSCII, all three approaches give the same dynamics as the direct application of LSCII, with the results converged for the time step $\Delta t = 0.005$.

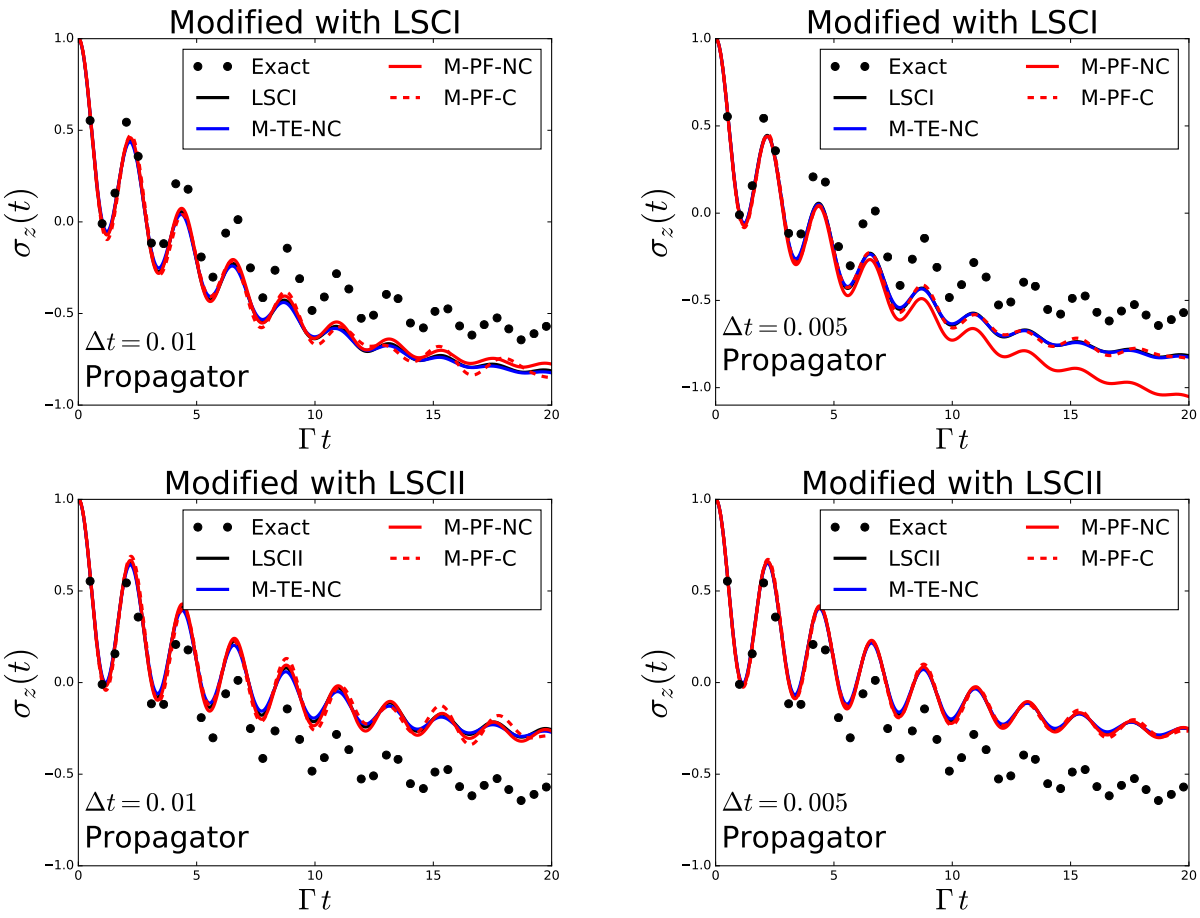

Figure B.5: Shown are the electronic population differences, $\sigma_z(t) = \sigma_{DD}(t) - \sigma_{AA}(t)$, for the system-bath form approaches. In the top row, the bare expansion is used; in the middle row, the static expansion; and in the bottom row, the dynamic expansion. The left column is results with LSCI as input method and on the left are the results with LSCII as input method, with the direct application of each shown with a solid black line. The parameters are those of model 2 in Table IV.1 and exact results are shown in black circles on each graph.

BIBLIOGRAPHY

[1] A. Nitzan, *Chemical Dynamics in Condensed Phases* (Oxford University Press, New York, 2006).

[2] S. Mukamel, *Principles of Nonlinear Optical Spectroscopy* (Oxford, New York, 1995).

[3] V. May, O. Kühn, *Charge and energy transfer dynamics in molecular systems* (Willey-VCH, Berlin, 2000).

[4] H.-D. Meyer, F. Gatti, G. A. Worth, *Multidimensional Quantum Dynamics*, MCTDH Theory and Applications (John Wiley & Sons, 2009).

[5] N. Makri, *Annu. Rev. Phys. Chem.* **50**, 167 (1999).

[6] J. Jin, X. Zheng, Y. Yan, *The Journal of chemical physics* **128**, 234703 (2008).

[7] Y. Tanimura, R. K. Kubo, *J. Phys. Soc. Jap.* **58**, 101 (1989).

[8] Y. Tanimura, *Phys.˜Rev.˜A* **41**, 6676 (1990).

[9] Y. Tanimura, *J. Phys. Soc. Jpn.* **75**, 082001 (2006).

[10] S. M. Greene, V. S. Batista, *Journal of Chemical Theory and Computation* **13**, 4034 (2017).

[11] R. A. Marcus, *J. Chem. Phys.* **24**, 966 (1956).

[12] R. D. Coalson, D. G. Evans, A. Nitzan, *J. Chem. Phys.* **101**, 436 (1994).

[13] A. F. Izmaylov, *et al.*, *J. Chem. Phys.* **135**, 234106 (2011).

[14] X. Sun, E. Geva, *J. Phys. Chem. A* **120**, 2976 (2016).

[15] X. Sun, E. Geva, *J. Chem. Theory Comput.* **12**, 2926 (2016).

[16] X. Sun, E. Geva, *J. Chem. Phys.* **144**, 244105 (2016).

[17] X. Sun, E. Geva, *J. Chem. Phys.* **145**, 064109 (2016).

[18] X. Sun, *et al.*, *Journal of Physical Chemistry C* **122**, 11288 (2018).

[19] A. Pereverzev, E. R. Bittner, *J. Chem. Phys.* **125**, 104906 (2006).

[20] P. de Bree, D. A. Wiersma, *J. Chem. Phys.* **70**, 790 (1979).

[21] D. Egorova, A. Kühl, W. Domcke, *Chem. Phys.* **268**, 105 (2001).

[22] A. Ishizaki, G. R. Fleming, *The Journal of chemical physics* **130**, 234110 (2009).

[23] A. Kühl, W. Domcke, *J. Chem. Phys.* **116**, 263 (2002).

[24] V. I. Novoderezhkin, A. G. Yakovlev, R. van Grondelle, V. A. Shuvalov, *J. Phys. Chem. B* **108**, 7445 (2004).

[25] W. T. Pollard, R. A. Friesner, *J. Chem. Phys.* **100**, 5054 (1994).

[26] S. Nakajima, *Prog. Theor. Phys.* **20**, 948 (1958).

[27] R. Zwanzig, *J. Chem. Phys.* **33**, 1338 (1960).

[28] Q. Shi, E. Geva, *J. Chem. Phys.* **119**, 12063 (2003).

[29] M.-L. Zhang, B. J. Ka, E. Geva, *J. Chem. Phys.* **125**, 044106 (2006).

[30] A. Kelly, T. E. Markland, *J. Chem. Phys.* **139**, 014104 (2013).

[31] L. Kidon, E. Y. Wilner, E. Rabani, *The Journal of chemical physics* **143**, 234110 (2015).

[32] A. Montoya-Castillo, D. R. Reichman, *J. Chem. Phys.* **144**, 184104 (2016).

[33] J. Cerrillo, J. Cao, *Phys. Rev. Lett.* **112**, 110401 (2014).

[34] A. A. Kananenka, C.-Y. Hsieh, J. Cao, E. Geva, *J. Phys. Chem. Lett.* **7**, 4809 (2016).

[35] E. Mulvihill, A. Schubert, X. Sun, B. D. Dunietz, E. Geva, *J. Chem. Phys.* **150**, 034101 (2019).

[36] A. McLachlan, *Mol. Phys.* **8**, 39 (1964).

[37] C. C. Martens, J. Fang, *J. Chem. Phys.* **106**, 4918 (1997).

[38] A. Donoso, C. C. Martens, *J. Chem. Phys. A* **102**, 4291 (1998).

[39] R. Kapral, G. Ciccotti, *J. Chem. Phys.* **110**, 8919 (1999).

[40] S. Nielsen, R. Kapral, G. Ciccotti, *J. Chem. Phys.* **112**, 6543 (2000).

[41] Q. Shi, E. Geva, *J. Chem. Phys.* **121**, 3393 (2004).

[42] D. MacKernan, R. Kapral, G. Ciccotti, *J. Phys: Cond. Matter* **14**, 9069 (2002).

[43] D. Mac Kernan, G. Ciccotti, R. Kapral, *J. Phys. Chem. B* **112**, 424 (2008).

[44] A. Kelly, N. Brackbill, T. E. Markland, *J. Chem. Phys.* **142**, 094110 (2015).

[45] E. Mulvihill, *et al.*, *The Journal of Chemical Physics* **151**, 074103 (2019).

[46] W. C. Pfalzgraff, A. Montoya-Castillo, A. Kelly, T. E. Markland, *The Journal of Chemical Physics* **150**, 244109 (2019).

[47] A. K. Manna, D. Balamurugan, M. S. Cheung, B. D. Dunietz, *J. Phys. Chem. Lett.* **6**, 1231 (2015).

[48] J. Tinnin, *et al.*, *Phys. Rev. Applied* **13**, 054075 (2020).

[49] S. Chandrasekaran, M. Aghtar, S. Valleau, A. Aspuru-Guzik, U. Kleinekathöfer, *J. Phys. Chem. B* **119**, 9995 (2015).

[50] C. Olbrich, J. Strümpfer, K. Schulten, U. Kleinekathöfer, *The Journal of Physical Chemistry Letters* **2**, 1771 (2011).

[51] A. Gelzinis, D. Abramavicius, J. P. Ogilvie, L. Valkunas, *The Journal of Chemical Physics* **147**, 115102 (2017).

[52] D. J. Tannor, *Introduction to quantum Mechanics - A time dependent perspective* (University Science Books, Sausalito, CA, 2006).

[53] Q. Shi, E. Geva, *J. Chem. Phys.* **120**, 10647 (2004).

[54] R. Zwanzig, *Physica* **30**, 1109 (1964).

[55] F. Haake, *Springer Tracts Mod. Phys.* **66**, 98 (1973).

[56] H. Grabert, *Projection Operator Techniques in Nonequilibrium Statistical Mechanics* (Springer-Verlag, Berlin, 1982).

[57] R. Alicki, K. Lendi, *Quantum Dynamical Semigroups and Applications* (Springer-Verlag, Berlin, 1987).

[58] B. Yoon, J. M. Deutch, J. H. Freed, *J. Chem. Phys.* **62**, 4687 (1975).

[59] I. Oppenheim, K. E. Shuler, G. H. Weiss, *Stochastic Processes in Chemical Physics: The Master Equation* (MIT Press, Cambridge MA, 1977).

[60] S. Mukamel, I. Oppenheim, J. Ross, *Phys. Rev. A* **17**, 1988 (1978).

[61] V. Romero-Rochin, A. Orsky, I. Oppenheim, *Physica A* **156**, 244 (1989).

[62] R. Zwanzig, *Nonequilibrium statistical mechanics* (Oxford University Press, New York, 2001).

[63] H.-P. Breuer, F. Petruccione, *The Theory of Open Quantum Systems* (Oxford Press, Oxford, 2002).

[64] M. Sparpaglione, S. Mukamel, *J. Chem. Phys.* **88**, 3263 (1988).

[65] A. Montoya-Castillo, D. R. Reichman, *The Journal of chemical physics* **146**, 084110 (2017).

[66] M. E. Tuckerman, *Statistical Mechanics: Theory and Molecular Simulation* (Oxford, London, 2010).

[67] S. A. Sato, A. Kelly, A. Rubio, *Phys. Rev. B* **97**, 134308 (2018).

[68] N. Makri, *J. Phys. Chem. B* **103**, 2823 (1999).

[69] K. Thompson, N. Makri, *J. Chem. Phys.* **110**, 1343 (1999).

[70] G. Cohen, E. Y. Wilner, E. Rabani, *New Journal of Physics* **15**, 073018 (2013).

[71] A. Kelly, A. Montoya-Castillo, L. Wang, T. E. Markland, *The Journal of Chemical Physics* **144**, 184105 (2016).

[72] A. Kelly, R. van Zon, J. Schofield, R. Kapral, *J. Chem. Phys.* **136**, 084101 (2012).

[73] H. D. Meyer, W. H. Miller, *J. Chem. Phys.* **70**, 3214 (1979).

[74] G. Stock, M. Thoss, *Phys. Rev. Lett.* **78**, 578 (1997).

[75] S. J. Cotton, W. H. Miller, *J. Phys. Chem. A* **117**, 7190 (2013).

[76] S. J. Cotton, W. H. Miller, *J. Chem. Phys.* **139**, 234112 (2013).

[77] S. J. Cotton, K. Igumenshchev, W. H. Miller, *J. Chem. Phys.* **141**, 084104 (2014).

[78] S. J. Cotton, W. H. Miller, *J. Phys. Chem. A* **119**, 12138 (2015).

[79] S. J. Cotton, W. H. Miller, *J. Chem. Theory Comput.* **12**, 983 (2016).

[80] S. J. Cotton, W. H. Miller, *J. Chem. Phys.* **145**, 144108 (2016).

[81] Q. Shi, E. Geva, *J. Phys. Chem. A* **107**, 9059 (2003).

[82] Q. Shi, E. Geva, *J. Phys. Chem. A* **107**, 9070 (2003).

[83] Q. Shi, E. Geva, *J. Phys. Chem. A* **108**, 6109 (2004).

[84] Q. Shi, E. Geva, *J. Chem. Phys.* **122**, 064506 (2005).

[85] B. J. Ka, Q. Shi, E. Geva, *J. Phys. Chem. A* **109**, 5527 (2005).

[86] B. J. Ka, E. Geva, *J. Phys. Chem. A* **110**, 9555 (2006).

[87] Q. Shi, E. Geva, *J. Chem. Phys.* **129**, 124505 (2008).

[88] F. X. Vazquez, I. Navrotskaya, E. Geva, *J. Phys. Chem. A* **114**, 5682 (2010).

[89] F. X. Vazquez, S. Talapatra, E. Geva, *J. Phys. Chem. A* **115**, 9775 (2011).

[90] P. L. McRobbie, E. Geva, *J. Phys. Chem. A* **113**, 10425 (2009).

[91] M. Thoss, G. Stock, *Phys. Rev. A* **59**, 64 (1999).

[92] G. Stock, U. Müller, *The Journal of chemical physics* **111**, 65 (1999).

[93] W. H. Miller, *J. Phys. Chem. A* **105**, 2942 (2001).

[94] N. Ananth, C. Venkataraman, W. H. Miller, *J. Chem. Phys.* **127**, 084114 (2007).

[95] W. H. Miller, S. J. Cotton, *J. Chem. Phys.* **145**, 081102 (2016).

[96] W. H. Miller, S. J. Cotton, *Farad. Discuss.* **195**, 9 (2016).

[97] S. J. Cotton, R. Liang, W. H. Miller, *J. Chem. Phys.* **147**, 064112 (2017).

[98] J. Liu, *J. Chem. Phys.* **145**, 204105 (2016).

[99] J. E. Subotnik, *et al.*, *Annu. Rev. Phys. Chem.* **67**, 387 (2016).

[100] L. Wang, A. Akimov, O. V. Prezhdo, *Faraday* **7**, 2100 (2016).

[101] H. Kim, A. Nassimi, R. Kapral, *J. Chem. Phys.* **129**, 084102 (2008).

[102] X. Sun, H. Wang, W. H. Miller, *J. Chem. Phys.* **109**, 7064 (1998).

[103] C. Cohen-Tannoudji, B. Diu, F. Laloë, *Quantum Mechanics* (Wiley, New York, 1977).

[104] M. A. C. Saller, A. Kelly, J. O. Richardson, *J. Chem. Phys.* **150**, 071101 (2019).

[105] M. A. C. Saller, A. Kelly, J. O. Richardson, *Faraday Discuss.* **221**, 150 (2020).

[106] P. Huo, D. F. Coker, *J. Chem. Phys.* **135**, 201101 (2011).

[107] C.-Y. Hsieh, R. Kapral, *J. Chem. Phys.* **137**, 22A507 (2012).

[108] R. Kubo, M. Toda, N. Hashitsume, *Statistical Physics II: Nonequilibrium Statistical Mechanics* (Springer-Verlag, New York, 1985).

[109] J. Strümpfer, M. Şener, K. Schulten, *The Journal of Physical Chemistry Letters* **3**, 536 (2012). PMID: 22844553.

[110] G. D. Scholes, G. R. Fleming, A. Olaya-Castro, R. van Grondelle, *Nature Chem* **3**, 763 (2011).

[111] S. Savikhin, D. R. Buck, W. S. Struve, *Chem. Phys.* **223**, 303 (1997).

[112] S. I. E. Vulto, *et al.*, *J. Phys. Chem. B* **103**, 8153 (1999).

[113] G. S. Engel, *et al.*, *Nature* **446**, 782 (2007).

[114] G. Panitchayangkoon, *et al.*, *Proc. Natl. Acad. Sci. USA* **107**, 12766 (2010).

[115] X. Liu, O. Kühn, *Chemical Physics* **481**, 272 (2016). Quantum Dynamics and Femtosecond Spectroscopy dedicated to Prof. Vladimir Y. Chernyak on the occasion of his 60th birthday.

[116] E. Thyrhaug, *et al.*, *Nature Chemistry* **10**, 780 (2018).

[117] S. Irgen-Gioro, K. Gururangan, R. G. Saer, R. E. Blankenship, E. Harel, *Chem. Sci.* **10**, 10503 (2019).

[118] T. Brixner, *et al.*, *Nature* **434**, 625 (2005).

[119] A. Ishizaki, G. R. Fleming, *Proc. Natl. Acad. Sci. USA* **106**, 17255 (2009).

[120] D. M. Wilkins, N. S. Dattani, *Journal of Chemical Theory and Computation* **11**, 3411 (2015). PMID: 26575775.

[121] J. Adolphs, T. Renger, *Biophysical Journal* **91**, 2778 (2006).

[122] R. E. Fenna, B. W. Matthews, *Nature* **258**, 573 (1975).

[123] W. Domcke, D. R. Yarkony, H. Köppel, *Conical Intersections* (World Scientific, 2004).

[124] G. A. Worth, L. S. Cederbaum, *Annu. Rev. Phys. Chem.* **55**, 127 (2004).

[125] H. Köppel, W. Domcke, L. S. Cederbaum, *The Multi-Mode Vibronic-Coupling Approach* (World Scientific, 2004), pp. 323–367.

[126] B. G. Levine, T. J. Martínez, *Annu. Rev. Phys. Chem.* **58**, 613 (2007).

[127] S. Deb, P. M. Weber, *Annu. Rev. Phys. Chem.* **62**, 19 (2011).

[128] S. Matsika, P. Krause, *Annu. Rev. Phys. Chem.* **62**, 621 (2011).

[129] W. Domcke and D.R. Yarkony and H. Köppel, *Conical Intersections: Theory, Computation and Experiment* (World Scientific, Singapore, 2011).

[130] W. Domcke, D. R. Yarkony, *Ann. Rev. Phys. Chem.* **63**, 325 (2012).

[131] J. S. Endicott, L. Joubert-Doriol, A. F. Izmaylov, *J. Chem. Phys.* **141**, 034104 (2014).

[132] Y. Shu, B. G. Levine, *Journal of Physical Chemistry C* **119**, 1737 (2015).

[133] R. Gherib, I. G. Ryabinkin, A. F. Izmaylov, *Journal of Chemical Theory and Computation* **11**, 1375 (2015).

[134] R. Kosloff, *Ann. Rev. Phys. Chem.* **45**, 145 (1994).

[135] H. Köppel, W. Domcke, L. S. Cederbaum, *Multimode Molecular Dynamics Beyond the Born-Oppenheimer Approximation* (John Wiley & Sons, Ltd, 2007), pp. 59–246.

[136] H. Köppel, J. Gronki, S. Mahapatra, *jcp* **115**, 2377 (2001).

[137] H. Köppel, B. Schubert, *Mol. Phys.* **104**, 1069 (2006).

[138] C. S. M. Allan, B. Lasorne, G. A. Worth, M. A. Robb, *jpca* **114**, 8713 (2010).

[139] Y. Liu, X. Gao, Y. Lai, E. Mulvihill, E. Geva, *Journal of Chemical Theory and Computation* **16**, 4479 (2020). PMID: 32421321.